

Greener on the Other Side: Inequity and Tax Compliance*

Michael Carlos Best[†] Luigi Caloi[‡] François Gerard[§] Evan Plous Kresch[¶]
Joana Naritomi^{||} Laura Zoratto^{**}

This version: June 20, 2025

Abstract

Governments frequently use proxies for deservingness—tags—to implement progressive tax and transfer policies. These proxies are often imperfect, leading to misclassification and inequities among equally deserving individuals. This paper studies the efficiency effects of such misclassification in the context of the property tax system in Manaus, Brazil. We leverage quasi-experimental variation in inequity generated by the boundaries of geographic sectors used to compute tax liabilities and a large tax reform in a series of augmented boundary discontinuity designs. We find that inequities significantly reduce tax compliance. The elasticity of compliance with respect to inequity is between 0.12 and 0.25, accounting for half of the overall change in compliance at the boundaries. A simple model of presumptive property taxation shows how mistagging affects the optimal tax schedule, highlighting the opposite implications of responses to the level of taxation and to inequity for optimal tax progressivity. Interpreting our findings through the lens of the model implies that optimal progressivity is around 50% lower than it would be absent inequity responses. These results underscore the importance of inequity for public policy design, especially in contexts with low fiscal capacity.

*We are grateful to Katarzyna Bilicka, Nadja Dwenger, Bill Hoyt, Henrik Kleven, Wojciech Kopczuk, Ilyana Kuziemko, Horacio Larreguy, Ben Lockwood, Karthik Muralidharan, Victor Pouliquen, Joel Slemrod, Johannes Spinnewijn, Jonathan Weigel and numerous seminar and conference participants at Berkeley, the CEPR Public Economics Symposium, Duke, FGV-EESP, Fordham, Georgetown, IFS-STICERD, INSPER, ITAM, University of Kentucky, Mannheim, Munich, the National Tax Association Conference, Northwestern, Oxford, Princeton, PUC-Rio, SITE, UFPE, UC Chile, Universitat Pompeu Fabra, and Wharton. We are grateful to Amanda Awadey, Carlota Loran Lopez, Malavika Mani, Samira Noronha, Maggie Shi, and Thaissa Sousa for excellent research assistance. We thank Zaheer Abbas, Angela Bayarmaa, Jonathan Chan, Cali Marie Dutta, Tingjun Huang, Nicole Li, Christian Lippmann, Lizzie Melashvili, Yunfeng Wu, Dongyang Zhang, Giovanni Ramos, and Sungjin Kim for their help with the Viva Real data. We thank *Secretaria Municipal de Finanças e Tecnologia da Informação* (SEMEF), who provided access anonymized administrative data. This study has been funded by JPAL and the World Bank. All remaining errors are ours.

[†]michael.best@columbia.edu. Columbia University, BREAD, CEPR, IFS & NBER.

[‡]luigi.caloi@columbia.edu. Columbia University.

[§]f.gerard@ucl.ac.uk. University College London, BREAD, CEPR, & IFS.

[¶]ekresch@oberlin.edu. Oberlin College.

^{||}J.Naritomi@lse.ac.uk. London School of Economics, BREAD, CEPR, & IFS.

^{**}lzoratto@worldbank.org. World Bank.

1 Introduction

One of the most basic functions of the state is the measurement of its tax base. This requires investments in the capacity to “read” the rich complexity of taxpayers’ economic activities and reduce them to standardized measures of the size of the tax base (Scott, 1998). Doing so successfully allows the modern state to differentiate between taxpayers with higher or lower ability to pay, and to target transfers at citizens with the greatest need. However, welfare-relevant attributes such as earning ability are hard, if not impossible, to observe directly. Thus, governments often rely on proxies: observable attributes that are correlated with individuals’ unobserved types. These (often coarse) tags can facilitate the implementation of policies intended to be progressive (Akerlof, 1978).

However, relying on imperfect proxies leads to misclassification: Individuals with the same welfare-relevant types, but different levels of a government policy’s proxies may be treated differently, creating (horizontal) inequity.¹ Citizens have strong views on this type of inequity, it has been shown to influence economic decisions such as labor supply (Card *et al.*, 2012), policy preferences (Hvidberg *et al.*, 2023), and even political stability (Keen & Slemrod, 2021). In low- and middle-income countries, these challenges are further exacerbated by a lack of reliable data to differentiate between individuals.

This paper studies the direct efficiency effects of this misclassification, and how policy should respond. Misclassification may generate resentment among those treated less favorably than others with the same welfare-relevant type, causing them to reduce their voluntary compliance with a policy’s mandates.² In particular, we focus on the effects of inequities among equally deserving taxpayers, caused by the use of tags in property taxation, on tax compliance. We argue that inequities induced by mistagging reduce tax morale and generate strong decreases in voluntary tax compliance. The effects exist over and above the more standard responses of compliance to the overall size of the taxes/transfers individuals receive. Moreover, inequity responses have implications for public policy’s optimal design which are strikingly different from those of individuals’ responses to the overall size of the taxes/transfers they receive.

We study these issues in the context of the property tax in the city of Manaus, Brazil. Like

¹With imperfect tags, individuals with differing welfare-relevant types, but who share the same policy-relevant attributes will be treated equally, and individuals who have the same welfare-relevance but differing levels of the policy-relevant attributes will be treated differently. Adam Smith (Smith 1776) invokes this inequity in objection to the “Window Tax,” an English presumptive property tax:

“The principal objection to all such taxes is their inequality, an inequality of the worst kind, as they must frequently fall much heavier upon the poor than upon the rich. A house of ten pounds rent in a country town may sometimes have more windows than a house of five hundred pounds rent in London; and though the inhabitant of the former is likely to be a much poorer man than that of the latter, yet so far as his contribution is regulated by the window-tax, he must contribute more to the support of the state.”

²In principle, those treated more advantageously than intended may feel impelled to reciprocate, but as we show in section 6.3, we see no evidence for this response in our setting. Similarly, Dube *et al.* (2019a) show that responses to peer wages are driven by comparisons with higher-paid peers.

most cities', Manaus' property tax is presumptive, based on properties' observable characteristics rather than a direct assessment of their market values.³ As is common, the presumptive tax formula features an assessed price of land that is different in different sectors of the city.⁴ As a result, at the boundaries of these sectors, tax liabilities jump discretely.

The boundaries of these sectors also generate inequity: houses on one side of the boundary would have discretely different tax liabilities if they had happened to be located on the other side of the boundary they face. However, since the assessed land price is only one of several inputs into the property tax formula, properties composed of relatively large amounts of land and relatively small amounts of built structure are more *exposed* to this source of inequity. As a result, the discontinuities at the tax sector boundaries provide sources of quasi-experimental variation in both tax liabilities and the extent of mistagging.

The overall change in compliance at tax sector boundaries is large: We estimate that compliance is 8% lower on the side with the higher assessed land price. However, this combines responses to the higher tax liability with responses to greater inequity. Using a range of extensions to the Boundary Discontinuity Design (BDD) (Black, 1999; Bayer *et al.*, 2007), we show that behavioral responses to inequity are strong. We augment the BDD to leverage cross-sectional variation in exposure to inequity and variation from a 2011 reform, estimating that the elasticity of compliance with respect to inequity is between 0.12 and 0.25, accounting for around half of the total effect at the boundary. Comparing responses to reductions in overtagging (in our context, being located on the high-price side of a boundary) to responses to reductions in undertagging suggests that responses to inequity are driven entirely by resentment of overtagging.

To draw out the implications of these results, we develop a simple model of the optimal design of a presumptive property tax. The model highlights the different implications of responses to the overall tax liability and responses to inequity for the degree to which the optimal policy differentiates between taxpayers. Responses to inequity push towards less differentiation, while responses to the size of the tax liability suggest greater differentiation. Distinguishing between these responses is, therefore, a crucial input into policy design. Our results suggest that optimal policy is 50% less progressive than if behavioral responses were driven solely by the level of the tax liability. Conversely, this suggests that the returns to investment in the fiscal capacity with which to accurately differentiate between properties are sizable, both in terms of raising additional revenue, and for reducing inequity.

Manaus, the relatively prosperous capital city of the state of Amazonas in Brazil, is divided into 63 tax sectors *exclusively* for the purposes of property taxation.⁵ Each of these sectors is associated with a sector-specific assessed land price, a key input into the presumptive formula that determines each property's tax liability. These sector-specific assessed land prices are coarse

³Table 1 shows a majority of the global population lives under this type of presumptive property tax scheme, as opposed to one based on market value.

⁴73% (16 /22) of the cities listed in table 1 with presumptive property taxes use geographic sectors in their assessment formulae.

⁵That is, access to and delivery of public goods and services are not dependent on which sector a property is located in.

tags for the value of properties in different parts of the city. However, this also means that at the boundaries of the tax sectors there are geographic discontinuities in tax bills. Two identical properties on the same street face different tax bills if they fall in different tax sectors.

This provides us with an opportunity to construct our measure of inequity: For each property, our measure of the inequity they face takes the ratio of their tax liability to the counterfactual tax liability their property would have had if it been located across the street in a different tax sector—and hence been tagged with a different land price. Our empirical measure of inequity has the advantages of capturing inequity at the individual household level rather than at the group level, thus not requiring the analyst to take a position on what the reference group is that taxpayers compare themselves to in forming opinions about the (in)equity of their taxes. Moreover, these sharp differences in tax burdens are unlikely to be damped by capitalization into house prices. Manaus has a thin property market, and using data on property listings we see no evidence that there is meaningful capitalization of the property tax into house prices. This sharp variation in inequity at the tax sector boundaries undergirds our empirical approach to studying the behavioral responses to inequity.

We develop a simple model of presumptive property tax design to frame our analysis and draw out policy implications. In the model, properties are of two types (market values), but the government cannot observe a property's true type. Instead, the government observes a *tag* that proxies for the property's type and uses these tags as the basis for its presumptive tax. Taxpayers, however, know their property type. When they receive the incorrect tag, this creates inequity, affecting their tax compliance decisions and creating a novel source of efficiency costs of taxation.

We derive sufficient statistics expressions characterizing the optimal tax schedule. Mistagging affects the optimal tax schedule through three channels. First, mistagging affects the composition of taxpayers. Some of the taxpayers paying the high-tag tax have low-type houses. Second, behavioral responses to inequity increase the efficiency costs of raising revenue. Third, mistagging raises the marginal utility of consumption of mistagged households, aggravating the welfare costs of taxation.

Importantly, the two channels of behavioral responses—to the size of the tax liability, and to inequity—have opposite implications for the degree of progressivity of the optimal tax schedule. The standard elasticity of compliance with respect to the tax liability pushes in favor of more progressive taxes. By contrast, the more elastic compliance is with respect to inequity, the less progressive the optimal tax schedule is. As a result, it is critical to disentangle the sources of behavioral responses in order to draw welfare and policy conclusions. Our analysis provides a number of empirical strategies with which to achieve this.

We begin our empirical analysis by documenting a large change in compliance at the tax sector boundaries. Using a Boundary Discontinuity Design (BDD) ([Black, 1999](#); [Bayer *et al.*, 2007](#)), we estimate that compliance is 8% lower on the side of the boundary with the higher land-price tag than on the side with the lower tag. However, this compliance change combines

the responses to two changes at the boundary. First, tax liabilities are on average 13% higher. Second, inequity is 62% higher.

To disentangle these two effects, we develop a series of augmented BDD strategies that complement the BDD with two additional sources of variation. Our first approach exploits the fact that some properties are more exposed to inequity than others: The inequity we study is driven by mistagging of land prices, while the presumptive tax formula depends on proxies for both land prices and the value of the built structure on the property. As a result, properties with a lot of land and relatively little built structure are more exposed to this source of inequity. This is true even conditional on a property's tax liability, allowing us to hold tax liabilities fixed and exploit the variation in exposure to mistagging to estimate the effects of inequity.

We present two augmented BDD strategies that leverage this variation in exposure to mistagging. Our most restrictive strategy amounts to assuming that holding constant taxpayers' tax liabilities and their properties' exposure to mistagging, the BDD identifies the effect of inequity on compliance. Under these assumptions, augmenting the BDD with flexible controls for the tax liability and exposure, we can recover the average elasticity of compliance with respect to inequity. Implementing this design, we estimate the elasticity of compliance to be between 0.19 and 0.23. We also show that the results are driven by households for whom the inequity is likely to be the most salient: those whose neighbors across the tax sector border are most similar to them.

Our second strategy relaxes the assumptions required for identification. We allow for the possibility that taxpayers on the high-tax side of the boundaries may be less compliant than taxpayers on the low-tax side of the boundaries for reasons that are not related to their tax liabilities and their properties' exposure to mistagging. For example, this may arise if households with dimmer views of government and lower tax morale systematically sort into properties on the high-tax side of the boundary. We assume that the resulting selection bias is uncorrelated with exposure to mistagging. This is analogous to the parallel trends assumption used in difference in differences designs that changes over time in the outcome of interest are uncorrelated with selection into treatment but applied to changes across tax sector boundaries. This allows us to pursue a difference in boundary discontinuity design that compares discontinuities in compliance at the tax sector boundaries across properties with differing levels of exposure to mistagging. Implementing this strategy, we estimate that the elasticity of compliance with respect to inequity is between 0.23 and 0.28.

Our second approach leverages a large reform to the property tax implemented in 2011. The reform made many changes to the tax sectors' assessed land prices and to the other parameters of the presumptive tax formula, but left the map of the tax sectors unchanged. As a result, households experienced large changes in their tax liabilities—the average taxpayer's property tax liability doubled—but also in their counterfactual tax liabilities had they lived in their neighboring tax sector, and hence in the degree of inequity they face. This provides us with a powerful additional source of quasi-experimental variation in both tax liabilities and inequity allowing us

to hold any time-invariant determinants of property tax compliance fixed and relate *changes* in compliance to changes in the tax liability and changes in inequity.

We incorporate this additional variation in two augmented BDD designs that mirror the two previous research designs. A first approach assumes that holding constant the changes in taxpayers' tax liabilities and their properties' exposure to mistagging, the BDD identifies the effect of changes in inequity on changes in compliance. This approach requires changes in compliance over time on the high-tax side of the tax sector boundaries to be parallel to changes over time on the low-tax side of the boundaries. With these assumptions, an augmented BDD that controls flexibly for the change in the tax liability and exposure identifies the average elasticity of compliance with respect to inequity.

Finally, our least restrictive approach allows the low-tax and high-tax sides of the boundaries to have different time trends, provided that the difference in the trends is uncorrelated with exposure to mistagging. Combining the reform with variation in exposure, we show that an augmented BDD akin to a triple-differences design is able to recover the elasticity of compliance with respect to inequity. This design makes the weakest assumptions of all of our designs, allowing for arbitrary patterns of sorting on time-invariant determinants of compliance, and differences in trends in compliance between the high-tax and low-tax sides of the boundaries. Our results here suggest that the elasticity of compliance with respect to inequity is around 0.12, and robust to a battery of different controls.

The final part of our empirical analysis develops an approach that allows us to separately identify the impacts of overtagging on the high-tax side of the tax sector boundaries and the impacts of undertagging on the low-tax side of the boundaries. We invoke a “strong parallel trends” assumption ([Callaway et al., 2024](#)) on either side of the tax sector boundaries. Among properties on the high-tax side of the boundary, we require changes over time in compliance to be uncorrelated with properties’ exposure to mistagging, and similarly on the low-tax side of the boundaries. With these assumptions, we show that the responses to inequity are driven exclusively by households resenting being overtaxed on the high-tax side of the boundaries. We are unable to reject a null effect of undertagging on the low-tax side of the boundaries.

Our empirical analysis deploys a number of distinct strategies to estimate the impacts of inequity on tax compliance. They uniformly suggest that these responses are strong, with an elasticity of compliance with respect to inequity between 0.11 and 0.28, driven entirely by households’ responses to over-taxation. This suggests that around half of the 8% drop in compliance we observe at the tax sector boundaries is driven by the increase in inequity at the boundaries rather than the increase in tax liabilities.

Viewed through the lens of a calibration of our model, the findings suggest that the optimal property tax schedule is around 50% less progressive than would be the case if behavioral responses operated exclusively through the level of the tax liability, as is commonly presumed. The findings also suggest that there are large returns to investments in improving the fiscal capacity to differentiate properties of different values. We consider the potential for data on

property listings, now widely available on the internet, to undergird this additional capacity. Back-of-the-envelope calculations suggest that using this data to recalibrate Manaus' existing property tax formula can yield a 21% reduction in mistagging and hence allow 9% more progressivity. Additionally incorporating additional property attributes available in property listings, and using standard machine-learning tools, can reduce mistagging further by as much as 73%, allowing for 36% greater progressivity.

Our paper contributes to four strands of literature. First, we contribute to the literature on presumptive taxation and tagging in public finance. [Akerlof \(1978\)](#) and [Nichols & Zeckhauser \(1982\)](#) made seminal contributions showing how tagging can relax the incentive-compatibility constraints faced by redistributive policies. Despite these powerful theoretical arguments, [Mankiw & Weinzierl \(2010\)](#) argue that tagging is not as prevalent a feature of real-world policy as one might expect, possibly due to equity considerations ([Saez & Stantcheva, 2016](#)). Subsequent literature incorporates moral hazard considerations into the standard tagging framework ([Besley & Coate, 1992](#); [Gaubert et al., 2021](#)). We explore an additional channel: efficiency effects of inequity from imperfect tagging.

Second, we contribute to the literature on fairness and tax compliance, and tax morale. Recent contributions include [Cruces et al. \(2013\)](#); [Giaccobasso et al. \(2022\)](#); [Kuziemko et al. \(2015\)](#); [Hvidberg et al. \(2023\)](#).⁶ In the context of property taxes, [Cabral & Hoxby \(2012\)](#) show that the more salient property taxes are, the lower governments set rates and limits. [Nathan et al. \(2023, 2025\)](#) study property tax appeals in Texas, showing experimentally that hassle costs and perceptions of the property tax system's fairness affect appeal behavior. In a related paper, [Ajzenman et al. \(2025\)](#) study the impacts of a different type of inequity. Through an information experiment, [Ajzenman et al. \(2025\)](#) study the effects of inequity that comes from the fact that taxpayers may care directly about how the tax system treats property types distinct from their own. By contrast, we study inequity that arises from the fact that the system features misclassification: it creates arbitrary differences in tax burdens between taxpayers with the same type. We contribute quasi-experimental estimates of the impact of inequity on compliance behavior and draw out the implications for policy design. Naturally, the two are highly complementary.

Third, we contribute to a growing literature on property taxation in low- and middle-income countries ([Castro & Scartascini, 2015](#); [Del Carpio, 2016](#); [Weigel, 2020](#); [Balan et al., 2022](#); [Okunogbe, 2023](#); [Bergeron et al., 2024a](#); [Dzansi et al., 2024](#); [Bergeron et al., 2024b](#); [Kapon et al., 2024](#)). [Brockmeyer et al. \(2023\)](#) provide evidence on the impact of enforcement activities and tax rates on compliance with Mexico City's property tax, and explore the implications for how policy should trade off between the two instruments. Building on their work, we study a distinct channel: inequity, and draw out its implications for optimal policy.

Fourth, we contribute to the literature using boundary discontinuity designs to study public policy. Foundational contributions in this literature include [Black \(1999\)](#) and [Bayer et al. \(2007\)](#). More recent work has used augmented boundary discontinuity designs to study the valuation of

⁶see [Luttmer & Singhal \(2014\)](#); [Slemrod \(2019\)](#) for surveys.

local jurisdictions (Schönholzer, 2022) and the impacts of wealth taxation on saving (Ring, 2024). We show how the boundary discontinuity design can be augmented to incorporate cross-section differences in the intensity of treatment and changes over time in treatment.

Our paper proceeds as follows. Section 2 presents the context we study in Manaus, the data we use, and how we use it to measure inequity. Section 3 develops our presumptive property tax model, showing conceptually how mistagging and inequity affect the optimal tax schedule. Section 4 presents our Boundary Discontinuity Design (BDD) to study the overall changes in compliance that we see at the boundaries of Manaus' tax sectors, documenting an 8% overall reduction in compliance. Section 5 presents our identification arguments and results for our augmented BDD leveraging variation in the exposure to mistagging. Section 6 presents our identification arguments and results for the augmented BDD leveraging Manaus' 2011 reform, and our strategy to separately estimate the effects of overtagging and undertagging. Section 7 sketches the implications of our findings for tax design, and finally, section 8 concludes.

2 Context & Data

2.1 Property Tax (IPTU) in Manaus

The property tax (IPTU: *Imposto Predial e Territorial Urbano*) is one of the two main tax instruments assessed by municipal governments in Brazil.⁷ The tax authority of Manaus (SEMEF; *Secretaria Municipal de Finanças e Tecnologia da Informação*) informs households of their liability by letter in mid-January of the relevant tax year. Taxpayers can choose between making a single payment or paying their tax bill in installments and can do so either online or in person by visiting SEMEF's offices or an affiliated bank.⁸ Failure to pay the IPTU bill, however, results in fines, interest, and ultimately, legal recourse. The imposition of fines and interest is automatically triggered on any household delinquent in their payment on January 1 of the year after the IPTU issuance, with no discretion by SEMEF to levy fines on particular households.⁹

Like all municipalities in Brazil, Manaus employs a presumptive formula to calculate the property tax liability. This differs from the market value-based assessment used in the United States but is in line with how property tax is calculated in most large urban centers around the world (see table 1). As with many cities employing a presumptive formula, the calculation of property tax in Manaus is in part a function of geography, with rates differing depending on where the property is located within the city. Table 1 compares Manaus' property tax to 40 of the world's largest cities; 22 of the 38 cities with a property tax have presumptive systems, of which 16 use geography as an input to the tax formula.¹⁰

⁷The other being the *Imposto Sobre Serviços* (ISS), a tax on services.

⁸For more information, see <https://semefatende.manaus.am.gov.br/inventario.php?id=3663>

⁹See <https://www.manaus.am.gov.br/pgm/divida-ativa-servico/>. A detailed discussion on enforcement and an empirical test examining differential enforcement across boundaries is provided in Appendix I.

¹⁰Beijing and Shanghai do not have a recurring property tax.

The statutory property tax rate—defined as the IPTU bill’s percentage of a property’s assessed value—is set at 0.9%.¹¹ However, average IPTU bills as a fraction of asking prices imply an effective tax rate closer to 0.46%.¹² Using the 2010 census, we estimate that the average residential IPTU bill in Manaus for a given year represents roughly 2.6% of annual household income.¹³ This property tax burden as a share of annual income is similar to property taxes in the United States, which range from 1.5% to 5%, and is nearly identical to the burden faced by residents of California.¹⁴ The estimated effective tax rate places Manaus among the lowest effective rates in the United States, which range from 0.4% to 3% (Twait & Langley, 2024).

The IPTU liability for property i in year y , T_{iy} , is calculated based on an estimate of the property’s value (*valor venal*), which is the sum of the estimated value of the property’s land (*valor do terreno*) and the value of the built structure (b_{isy} ; *valor da edificação*). These are multiplied by the statutory tax rate (*aliquota*) according to a schedule (α_y) based on the type of property. The land value is, in turn, the product of the adjusted land area a_{iy} and a sector-specific price per unit of land $p_{s(i)}$ to account for differences in property values across the city (figure 1 shows the map of the sectors):

$$T_{iy} = \alpha_y [b_{iy} + p_{s(i)}a_{iy}] = \alpha_y [f_{by}(\mathbf{B}'_{iy}\xi_y^B) + p_{s(i)}f_{ay}(\mathbf{A}'_{iy}\xi_y^A)] \quad (1)$$

The value a_{iy} is based on four observable land characteristics for the property (\mathbf{A}_{iy}), each with an associated corrective factor ξ_y^A . Similarly, b_{iy} is based on characteristics of the building or house (with associated factors ξ_y^B): the type of construction, the materials used in the construction, the size of the property, among other characteristics.

Crucially for our identification, the tax sectors are not used for other policy or administrative purposes beyond property tax, and only a few of the sector boundaries overlap with neighborhood boundaries (see appendix A, figure A.1). The use of geography is ubiquitous in presumptive property taxes around the world (see table 1), and Manaus is not unique in having tax sectors that do not align with municipal administrative divisions. All properties within a sector are assigned the same square meter value (General Plan for Standardize Property Value; *Planta Genérica de Valores*), which was set when the tax authority first created the city-wide tax sectors in 1983. Despite the rapid growth of the city, the boundaries of these sectors have not changed (and the prices were unchanged for almost 30 years until the reform described in section 2.2), leading to arbitrary changes in the square-meter values for very similar properties in close proximity to each other but across a tax sector boundary (see figure 2).

The IPTU is a salient and much discussed tax in Manaus for several reasons. First, the IPTU—like all property taxes—is a direct tax on households that makes it inherently more salient to

¹¹Lei No 1.628/2011, article 2

¹²In appendix J, we present a dataset of asking prices scraped from Viva Real, a Brazilian real estate platform, and matched to our cadaster, from which we draw this statistic.

¹³This figure is calculated using the average household income in Manaus from the 2010 census tracts. Note that this figure is likely to be an upper bound, as we are likely underestimating household income.

¹⁴Source: USAFacts. <https://usafacts.org/articles/where-do-people-pay-the-most-and-least-in-property-taxes/>

taxpayers (Cabral & Hoxby, 2012). Google search activity in Manaus show a cyclical interest in the IPTU, which peaks in late January just after residents first receive their IPTU bills (see appendix A, figure A.5). This is in stark contrast to the other main municipal tax, which is an indirect tax on services (ISS), and has virtually no search activity (despite it being levied on many more transactions). Second, articles related to the IPTU appear frequently in the local newspaper, including an annual announcement in January outlining how and when residents can pay their bills.¹⁵ IPTU is also a feature in many real estate listings on popular sites used in Manaus to search for houses and apartments (see appendix A, figure A.6).¹⁶

2.2 2011 Tax Reform

In an effort to reflect the significant changes in the city over nearly three decades, Manaus passed a major reform to its property tax system (Law 1.628/2011) that came into force in 2012. One of the main goals of the reform was to update the policy parameters used to estimate land and house values. In 1983, a government committee divided Manaus into 62 sectors (see figure 1), with the square-meter values ($p_{s(i)}$) based on property valuations in the city in 1983. These values did not change in subsequent decades and by 2011 these policy parameters were drastically out of date as Manaus experienced substantial sprawl of the city outward from the historic core (see appendix B, figure B.1). The population in 1983 was only 30 percent of the current population of Manaus, and its remarkable growth led to entirely new housing developments in previously uninhabited forest. However, these uninhabited areas were still assigned a tax sector in 1983, resulting in areas of the city with house values that were unrelated to the established sector rates.

As a result of not updating the tax code, property taxes became less progressive over time. Although households in wealthier census tracts still had a larger tax bill in 2010, the difference across census tracts with different household incomes flattened considerably (see appendix B, figure B.3a). Insofar as the parameters for a_{iy} and b_{iy} were set in 1983 to target wealthier households, an inability to revise the city's General Plan for Standardize Property Value to reflect the shifting socioeconomic geography of the city led to a deterioration in the usefulness of the tags.

To address these concerns about progressivity, the 2011 reform adjusted rates across the city, with the amount resulting from the additional IPTU phased in over five years. Each year, 20% of the additional amount was added to the tax bill (from 2012 to 2016).¹⁷ The reform raised tax liabilities for almost every property with striking heterogeneity in size of the tax increase to address the inequities in the previous system (see appendix B, figure B.2).

Although the 2012 property tax system was still based on presumptive estimates of the value

¹⁵For example, the 2014 announcement in the Diário do Amazonas [found here](#).

¹⁶It is also possible for residents to look up the IPTU of any property throughout the city via the government's open access geodata portal: <https://wsgeo.manaus.am.gov.br/ConsultaPreviaCidadao/>.

¹⁷This phase-in was meant to avoid backlash from the sharp increases in the IPTU bill. The first attempt to update IPTU's tax rates and revise the Municipal General Plan for Standardize Property Value was made in 2006, but the reform failed and was never implemented.

of the property, it was considered more fair by the municipal government as it was more aligned with the actual current property values than the previous estimates from 1983.¹⁸ Panel B of figure B.3 shows the improvement in targeting as a result of the reform; not only did the reform increase the average IPTU across census tracts, it also led to a larger change in tax bills for richer households (see appendix B, figure B.3b). It should be noted that while the 2011 reform led to an improvement in targeting, the system was still based on a presumptive formula that did not eliminate the potential for mistagging - especially for otherwise identical households on sector boundaries - which we use as our main source of identification throughout the rest of the paper.

2.3 Data

In collaboration with SEMEF, we have access to de-identified property registry information (cadaster) for 613,131 properties that includes a recent snapshot of the building characteristics, lot size and land characteristics. This data is geo-referenced and matched to the road network of the city. We also have GIS maps for all relevant boundaries (tax sector, neighborhood, city block, parcel), which we use to measure a household's distance to a tax sector boundary, and hence to the discontinuity in the per-square meter rate.

In addition to the cadaster, we have data on IPTU liabilities from 2004–2019 and IPTU payments from 2004–2019 for the universe of taxpayers in Manaus, including fines and legal follow-up due to delinquency. This allows us to directly observe both the household's tax liability in a given year and whether a given property was compliant with IPTU payments. We also have data on property transfers and sales from the property transfer tax system (ITBI; *Imposto sobre transmissão de bens imóveis*).

Our main outcome of interest for studying the behavioral response to mistagging is compliance—share of a household's IPTU bill that they pay within 18 months of receiving their bill. Since a household's property tax bill is mechanically determined by its characteristics in the cadaster, there is no self-declaration of the tax base.¹⁹ Thus, we do not measure the moral hazard response of households attempting to change their “tags”, but rather the response of households *after* receiving their tax bill. In Appendix F we repeat the main exercises using alternative definitions of compliance and find the same results.²⁰

Compliance with the property tax in Manaus is relatively low and stable over time (see appendix A, figure A.3). Two features of tax compliance in Manaus are worth noting. First, compliance is driven almost entirely by the extensive margin: The vast majority of households either pay their IPTU bill in full or do not pay it at all (see appendix A, figure A.3). Second, compared

¹⁸The online portal of one of the main Brazilian newspaper *O Globo* (*G1*) highlighted that the updated property value estimates were more fair given how outdated the 1983 values were [link to article](#).

¹⁹There is a mechanism by which a household can petition SEFAZ to update the cadaster, but this is almost never used. SEFAZ can update the cadaster (and did so in 2011), but this is generally done on the city-wide stock of housing inventory and is exogenous from the point of view of households.

²⁰Appendix F.1 studies the extensive margin response to mistagging, while Appendix F.2 varies the time horizon that we consider for payments in the definition of compliance.

to other large cities in Brazil, Manaus has a markedly lower collection rate, although this is consistent with the fact that poorer cities throughout the country tend to have lower collection rates (see appendix A, figure A.4).

2.4 Boundary Sample

Our identification strategy relies in part on the discontinuous changes in the square-meter rate across the tax sector boundaries in a boundary discontinuity design. We restrict our sample of interest to properties within 300 meters of a tax sector boundary. The distance from the boundary is measured as the closest point of a given lot to the boundary line, where properties on the boundary are defined as having a distance of zero. Appendix C provides additional details on the construction of the distance measure. We define households as being on the “high-tax” side of the boundary if the square-meter price $p_{s(i)}$ in their sector is higher than the sector rate $p_{\hat{s}(i)}$ on the other side of the boundary they face.

To refine our dataset for the boundary discontinuity analysis, we narrowed our focus to properties within 300 meters of the tax sector boundaries, excluding those exempt from tax, without construction, or not designated as residential. Properties on sector boundaries that overlap with neighborhood (“bairro”) boundaries were also excluded from the boundary discontinuity design since these boundaries may have additional salience, even if nothing about the provision of public goods or the enforcement of taxes varies across neighborhoods. After these adjustments, our analysis centers on 27,356 properties, resulting in 415,546 property-year observations from 2004 to 2019. Appendix E presents the full details on the sample selection process.

2.5 Measuring Inequity

The inequity in the IPTU that we study arises from the discrepancy between properties’ assessed property values and their market values. While the IPTU formula described in section 2.1 is complex, it is only a rough proxy for properties’ market values.²¹ Misspecification of all of the components of the formula creates misclassification of properties and hence potential inequity. However, this misclassification varies sharply at the boundaries of the tax sectors, and so we construct a measure of inequity based on the jumps in tax liabilities at the tax sector boundaries.

For a given property i in tax sector $s(i)$, we identify the nearest neighboring tax sector $\hat{s}(i)$ and define our inequity measure σ_{iy} as

$$\sigma_{iy} = \frac{T_{iy}}{\hat{T}_{iy}}$$

²¹In Appendix J, we detail our exercise to gather data on housing market asking prices. Figure J.1 presents a scatter plot comparing properties’ log tax liabilities to their log asking prices. While they are correlated, the R^2 is only 0.20, demonstrating that assessed values only roughly approximate true market values.

where T_{iy} is property i 's tax liability while the counterfactual tax liability \hat{T}_{iy} is the tax liability property i would have received had it been located on the other side of the tax sector boundary, with all other land (a_{iy}) and building (b_{iy}) characteristics held fixed: $\hat{T}_{iy} := \alpha [b_{iy} + p_{\$}(i)a_{iy}]$.

Defining inequity in this way has two key advantages. First, since we are computing the counterfactual tax bill using the household's own characteristics, we are able to construct our measure of inequity for every property in our data at the individual property level. Second, our measure is based only on how the taxpayer is treated relative to how they would have been treated had they lived in their neighboring tax sector, allowing us to be agnostic about what peer group(s) taxpayers compare themselves to in forming their opinions about inequity. This is in contrast to papers such as [Dube et al. \(2019b\)](#), [Card et al. \(2012\)](#), [Hvidberg et al. \(2023\)](#) and [Ajzenman et al. \(2025\)](#) that define the peer group needed for comparisons of inequity. Our measure of inequity is therefore a "selfish" measure, where the household's response is driven by whether they feel that they have been treated by the system, and does not capture whether a household cares about whether other people are treated fairly.²² We further investigate the salience of our inequity measure in appendix G.

Two attributes of our measure of σ make it useful for studying the behavioral response to inequity inherent in the tax system, as discussed in more detail in appendix D. First, there is significant variation in σ for households across the city (see appendix D, figure D.5), implying that individuals respond to a markedly different counterfactual of what their IPTU would have been if taxed on the other side of the sector boundary. Second, the counterfactual tax liabilities and true tax liability (τ) are not collinear (see appendix D, figure D.6). This allows us to separately estimate the behavioral response to changes in both the direct effect (changes in τ) and the effect driven by changes in the relative inequity of imperfect tagging in the system.

Nevertheless, to the extent that property taxes are capitalized into house prices, this may dampen the inequity felt by taxpayers when making tax compliance decisions. However, house price capitalization is unlikely to be a meaningful factor in our context. First, Manaus' property market is relatively thin. Using data from the property transaction tax, the *Imposto Sobre Transmissão de Bens Imóveis* (ITBI), we estimate that only around 1.4% of properties in Manaus are sold per year, compared to around 3.1–5.6% in US cities and 4% in the UK.²³ Second, as described in appendix J, we gathered data from a large online property listing platform, and linked it to the property tax cadaster. With this data we run both hedonic regressions and a version of our boundary discontinuity design, neither of which show evidence for any meaningful capitalization of the IPTU into listing prices. In section 3.3.2 we develop an extension of our conceptual model incorporating house price capitalization to make precise how any capitalization affects the optimal policy design.

²²This can be seen in residents' posts on social media complaining about their increase in IPTU relative to their neighbors (appendix D, table D.7), and the government's response that highlights how the IPTU is calculated and how the 2011 reform was implemented (appendix D, table D.8).

²³Statistics for the United States are calculated by taking the ratio of [existing home sales](#) to the [number of housing units](#) nationally. The numbers for the whole country are similar to the estimated 3.2–6.5% of residential homes for sale annually in the Chicago metropolitan area ([Institute for Housing Studies](#)).

3 Conceptual Framework

This section presents a simple model of the welfare effects of property taxation. There are a mass 1 of each of two *types* of houses: $\theta \in \{H, L\}$. These houses generate flows of housing consumption $y_H > y_L$. Actual house types θ are not observable to the government. Instead, the government observes a *tag* ϕ : either h or l for each house. When houses are correctly tagged, the H -type houses receive the tag $\phi = \phi(H) = h$ and the L -type houses receive the tag $\phi = \phi(L) = l$. However, when a house receives the incorrect tag ($\phi \neq \phi(\theta)$) this generates inequity for the occupant. We model this inequity as $\sigma_{\theta\phi} = T_\phi / T_{\phi(\theta)}$. Whenever $\sigma_{\theta\phi} > 1$ the house is said to be *overtagged*, while if $\sigma_{\theta\phi} < 1$ the house is *undertagged*. Households have a distaste for paying an inequitable tax $d(\sigma_{\theta\phi})$. We assume that when they are correctly tagged they have no distaste for inequity: $d(1) = 0$ and that $d(\cdot)$ is continuous, but place no additional restrictions on $d(\cdot)$.²⁴

Households decide whether to pay their property tax T_ϕ . If they pay, this reduces their consumption and they bear the disutility of inequity. If they don't pay, they face a cost of being a tax delinquent γ . This cost is idiosyncratic in the population with a distribution $F(\gamma)$. A household will pay its taxes whenever their cost of delinquency is high enough:

$$u_{\theta\phi}^{\text{pay}} > u_{\theta\phi}^{\text{evade}} \leftrightarrow u(y_\theta - T_\phi) - d(\sigma_{\theta\phi}) > u(y_\theta) - \gamma \leftrightarrow \gamma > u(y_\theta) - u(y_\theta - T_\phi) + d(\sigma_{\theta\phi}) = \gamma_{\theta\phi}^*$$

and as a result, compliance among households of type θ with tag ϕ is $c_{\theta\phi} = 1 - F(\gamma_{\theta\phi}^*)$.

For simplicity, we will assume that there is only overtagging: All H -type houses are correctly tagged with $\phi = h$, but a fraction ψ of the L -type houses are incorrectly given the $\phi = h$ tag. In section 3.3.1 and appendix O we present the extension to incorporate undertagging, but in section 6.3 we provide empirical evidence that there is no behavioral response to undertagging in our setting, so this simplification is warranted in our context.

Tax revenue $r = \psi c_{Lh} T_h + (1 - \psi) c_{Ll} T_l + c_{Hh} T_h$ is used to finance the provision of local public goods with social benefits of $B(r)$ and marginal benefits $b(r)$. Social welfare combines the welfare of a unit mass of each type of household and the benefits of the public good:

$$W = \psi \omega_L V_{Lh} + (1 - \psi) \omega_L V_{Ll} + \omega_H V_{Hh} + B(r)$$

where ω_θ are Pareto weights on the welfare of the two types of households, and

$$V_{\theta\phi} = \int_{-\infty}^{\gamma_{\theta\phi}^*} [u(y_\theta) - \gamma] dF(\gamma) + \int_{\gamma_{\theta\phi}^*}^{\infty} [u(y_\theta - T_\phi) - d(\sigma_{\theta\phi})] dF(\gamma)$$

is the private welfare of θ -type houses with the ϕ tag.

²⁴Households may have different distaste for inequity depending on whether they are undertagged ($\sigma_{\theta\phi} < 1$) or overtaged ($\sigma_{\theta\phi} > 1$), analogously to Dube *et al.* (2019b). For example, we might use a piecewise linear function $d(\sigma_{\theta\phi}) = (\sigma_{\theta\phi} - 1)(d_1 + (\delta - d_1)\mathbf{1}[\sigma_{\theta\phi} > 1])$ where $\delta > d_1 \geq 0$.

3.1 Benchmark: Perfect Tagging, No Inequity

As a benchmark, first consider the case in which tagging is perfect ($\psi = 0$ and so $\phi = \phi(\theta)$ for all houses). In this case, there is no inequity and so households' compliance behavior is driven only by the level of taxation they face. Changes in compliance in response to marginal changes in taxes generate fiscal externalities so that the increase in tax revenue from marginal increases in the l -tag tax is $dr/dT_l = c_{Ll}(1 - \varepsilon)$, where $\varepsilon \equiv -\frac{\partial c}{\partial T} \frac{T}{c}$ is the elasticity of compliance with respect to the tax liability. Analogously, the effect of a marginal increase in the h -tag tax is $dr/dT_h = c_{Hh}(1 - \varepsilon)$.

The optimal property tax trades off the benefits of additional revenue for public goods against the costs of reducing private welfare and the fiscal externality from changes in compliance. The following lemma characterizes this optimal balance.

Proposition 1 (Property Taxes Under Perfect Tagging). *With perfect tagging ($\phi = \phi(\theta)$ for all houses), the optimal property tax satisfies*

$$\frac{T_l}{y_L} = \frac{1 - \varepsilon - g_L}{\rho g_L} \quad (2)$$

$$\frac{T_h}{y_H} = \frac{1 - \varepsilon - g_H}{\rho g_H} \quad (3)$$

where $g_\theta = \omega_\theta u'(y_\theta)/b(r)$ is the generalized social marginal welfare weight of type θ (Saez & Stantcheva, 2016) and $\rho \equiv -u''(y)/u'(y)$ is the coefficient of relative risk aversion.

The level of taxation is lower the stronger are behavioral responses to the tax liability: $\partial T_\phi / \partial \varepsilon < 0$. Moreover, the optimal property tax is more progressive the stronger society's preference for redistribution g_L/g_H , and the larger the elasticity of compliance with respect to the tax liability ε :

$$\frac{\partial}{\partial g_L/g_H} \left(\frac{T_h/y_H}{T_l/y_L} \right) > 0 \quad \& \quad \frac{\partial}{\partial \varepsilon} \left(\frac{T_h/y_H}{T_l/y_L} \right) > 0$$

Proof. See appendix M □

These simple expressions relate taxes to the parameters in intuitive ways. The larger are the utility costs of reducing consumption (governed by the g_θ and the curvature of utility ρ), the lower are taxes; and similarly the larger are the behavioral responses and the corresponding fiscal externalities (governed by the elasticity of compliance ε) the lower are taxes. Perhaps less obviously, the progressivity of the tax is steeper the stronger are behavioral responses. While both taxes are decreasing in ε , the proportional decrease in T_l/y_L is larger, leading to higher progressivity.²⁵

²⁵This effect is also present in the classic many-person Ramsey rule (Feldstein, 1972; Diamond, 1975). When the demand elasticity is small, the sensitivity of commodity tax rates to the covariance between consumption of the good and social marginal welfare weights is stronger when the price elasticity of demand is larger.

3.2 Imperfect Tagging and Inequity Aversion

We now consider a model that also features the key force that our empirical analysis seeks to study: Households are mistagged ($\psi > 0$) and they have a distaste for the resulting inequity ($d(\sigma)$). This creates a third group of households: L -type houses incorrectly tagged with the h tag. These households face inequity $\sigma_{Lh} > 1$, adding two new channels to the optimal policy tradeoff.

First, the disutility from inequity creates first-order welfare losses for Lh households. Second, Lh households' compliance decisions depend both on their tax liability T_h and on the inequity they face $\sigma_{Lh} = T_h/T_l$. This creates a new source of fiscal externalities of both the high tax T_h and the low tax T_l governed by the strength of the elasticity of compliance with respect to inequity $\eta \equiv -\frac{\partial c}{\partial \sigma} \frac{\sigma}{c}$. As a result, the elasticity of compliance by Lh households with respect to the h tax is $\frac{dc_{Lh}}{dT_h} \frac{T_h}{c_{Lh}} = -\varepsilon - \eta < 0$ and with respect to the l tax (which they do not face but which affects inequity) is $\frac{dc_{Lh}}{dT_l} \frac{T_l}{c_{Lh}} = \eta > 0$.²⁶

The following proposition characterizes the optimal tax schedule and how the presence of mistagging and inequity aversion affect the optimal policy:

Proposition 2 (Property Taxes with Imperfect Tagging and Inequity Aversion). *The optimal property tax schedule satisfies*

$$\frac{T_l}{y_L} = \frac{1 - g_L - \varepsilon + \varphi_l \frac{\eta}{\varepsilon} \sigma (g_L + \varepsilon)}{g_L \rho (1 - \varphi_l \frac{\eta}{\varepsilon} \sigma^2)} \quad (4)$$

$$\frac{T_h}{y_H} = \frac{1 - \bar{g}_h - \varepsilon - \varphi_h \frac{\eta}{\varepsilon} (g_L + \varepsilon)}{\rho \left[\bar{g}_h + \varphi_h g_L \left(\frac{y_H}{y_L} (1 + \frac{\eta}{\varepsilon}) - 1 \right) \right]} \quad (5)$$

where $\sigma = \sigma_{Lh} = T_h/T_l$; $\varphi_l = \psi c_{Lh}/(1 - \psi)c_{Ll}$ is the number of mistagged L taxpayers relative to the number of l -tax taxpayers; $\varphi_h = \psi c_{Lh}/(\psi c_{Lh} + c_{Hh})$ is the number of mistagged L taxpayers relative to the number of h -tax taxpayers, and $\bar{g}_h = \varphi_h g_L + (1 - \varphi_h) g_H$ is the average social marginal welfare weight of h -tax taxpayers.

Relative to a benchmark with perfect tagging, imperfect tagging reduces optimal property tax revenues. In particular,

1. The greater the extent of mistagging ψ the lower optimal property tax revenues;
2. The stronger the behavioral response to inequity η the lower optimal property tax revenues;
3. The stronger the behavioral response to the tax liability ε , the lower optimal property tax revenues.

Relative to a benchmark with perfect tagging, imperfect tagging lessens the optimal degree of progressivity of the property tax. In particular,

²⁶To see these, note that $\frac{dc_{Lh}}{dT_h} \frac{T_h}{c_{Lh}} = \left(\frac{\partial c_{Lh}}{\partial T_h} + \frac{\partial c_{Lh}}{\partial \sigma} \frac{\partial \sigma}{\partial T_h} \right) \frac{T_h}{c_{Lh}} = \frac{\partial c_{Lh}}{\partial T_h} \frac{T_h}{c_{Lh}} + \frac{\partial c_{Lh}}{\partial \sigma} \frac{\sigma}{c_{Lh}} \frac{\partial \sigma}{\partial T_h} \frac{T_h}{\sigma} = -\varepsilon - \eta$ and, analogously, that $\frac{dc_{Lh}}{dT_l} \frac{T_l}{c_{Lh}} = \frac{\partial c_{Lh}}{\partial \sigma} \frac{\sigma}{c_{Lh}} \frac{\partial \sigma}{\partial T_l} \frac{T_l}{\sigma} = \eta$.

1. *The greater the extent of mistagging ψ the less progressive the property tax;*
2. *The stronger the behavioral response to inequity η the less progressive the property tax;*
3. *The stronger the behavioral response to the tax liability ε , the more progressive the property tax.*

Proof. See appendix N □

Comparing the characterization of the optimal property tax schedule in (4) & (5) to the benchmark with perfect tagging characterized in (2) & (3), the presence of imperfect tagging and inequity aversion adds three new effects. First, a fraction φ_h of the households paying the h tax are not H -types (the tax's intended targets) but rather mistagged L -types. This raises the average social marginal welfare weight of the h -taxpayers from g_H to \bar{g}_h , lowering the h tax.

Second, inequity aversion $d(\sigma)$ directly reduces the utility of mistagged types and increases the fiscal externality of compliance responses to T_h . Conversely, increasing T_l reduces inequity, increasing the utility of mistagged types and reducing the fiscal externality of their compliance responses. The $\varphi_\phi \frac{\eta}{\varepsilon}$ terms in the numerators of (4) & (5) account for these effects. They increase T_l and reduce T_h , making the tax system less progressive.

Third, mistagged L households pay a higher tax than their correctly tagged counterparts, raising the marginal utility at which their consumption losses are evaluated. The φ_ϕ terms in the denominators of (4) & (5) account for these effects. They also increase T_l and reduce T_h , making the tax system less progressive.

While these additional effects push in the intuitive directions, proposition 2 highlights the importance of understanding the mechanisms behind behavioral responses to property taxes. In particular, the proposition shows that ε and η can have opposite implications for optimal tax progressivity. In general, empirical estimates of behavioral responses to taxes will contain a mixture of the two channels (in section 4 we show how this issue affects the interpretation of estimates from our reduced-form boundary discontinuity design), with unclear implications for policy. In sections 5 and 6 we show how to disentangle the two channels empirically. Before turning to these empirical challenges, however, we present some extensions of the model to highlight the robustness of the qualitative conclusions in proposition 2.

3.3 Extensions

3.3.1 Mistagging of Both House Types

Appendix O presents an extension to the model in which both L - and H -type houses can be mistagged. It incorporates two changes to the baseline model. First, a fraction $\psi_{Hl} \geq 0$ of H -type houses is mistagged with the l tag (in addition to a fraction $\psi_{Lh} \geq 0$ of mistagged L -types as in the baseline model in section 3.2). Second, the elasticity of compliance with respect to inequity of the undertagged, η_{Hl} need not equal the elasticity of the overtaged η_{Lh} . With these

additions, we can characterize the optimal tax schedule:

$$\frac{T_l}{y_L} = \frac{1 - \varepsilon - \bar{g}_l + \varphi_{Ll} \frac{\eta_{Lh}}{\varepsilon} \sigma (g_L + \varepsilon) - \varphi_{Hl} \frac{\eta_{Hl}}{\varepsilon} (g_H + \varepsilon)}{\rho \left(\bar{g}_l + g_H \varphi_{Hl} \left[\left(1 + \frac{\eta_{Hl}}{\varepsilon} \right) \frac{y_L}{y_H} - 1 \right] - g_L \varphi_{Ll} \frac{\eta_{Lh}}{\varepsilon} \sigma^2 \right)} \quad (6)$$

$$\frac{T_h}{y_H} = \frac{1 - \varepsilon - \bar{g}_h + \varphi_{Hh} \frac{\eta_{Hl}}{\varepsilon} \frac{1}{\sigma} (g_H + \varepsilon) - \varphi_{Lh} \frac{\eta_{Lh}}{\varepsilon} (g_L + \varepsilon)}{\rho \left(\bar{g}_h + g_L \varphi_{Lh} \left[\left(1 + \frac{\eta_{Lh}}{\varepsilon} \right) \frac{y_H}{y_L} - 1 \right] - g_H \varphi_{Hh} \frac{\eta_{Hl}}{\varepsilon} \frac{1}{\sigma^2} \right)} \quad (7)$$

where $\sigma = T_h/T_l$; $\bar{g}_l = \frac{(1-\psi_{Lh})c_{Ll}g_L + \psi_{Hl}c_{Hl}g_H}{(1-\psi_{Lh})c_{Ll} + \psi_{Hl}c_{Hl}}$ is the average social marginal welfare weight of l -tax taxpayers, and analogously $\bar{g}_h = \frac{\psi_{Lh}c_{Lh}g_L + (1-\psi_{Hl})c_{Hh}g_H}{\psi_{Lh}c_{Lh} + (1-\psi_{Hl})c_{Hh}}$ is the average social marginal welfare weight of h -tax taxpayers; and the $\varphi_{\theta\phi}$ terms are the number of mistagged θ -types as a fraction of the number of ϕ -tax taxpayers (e.g. $\varphi_{Lh} = \frac{\psi_{Lh}c_{Lh}}{\psi_{Lh}c_{Lh} + (1-\psi_{Hl})c_{Hh}}$).

The three forces discussed in proposition in the context of the baseline model with only mistagging of L -types are present now also for the mistagged H -types. The lower social marginal welfare weight of the l -tax taxpayers ($\bar{g}_l < g_L$) also pushes towards more progressive taxes, but the two effects due to the behavioral response to inequity now have opposite signs: they push towards more progressive taxes.²⁷ This suggests that the overall effect on the tax schedule is ambiguous and depends on the magnitudes of the parameters (the extent of mistagging of the two types $\psi_{\theta\phi}$, the elasticities $\eta_{\theta\phi}$, and the property values y_θ). However, for given parameter values, all three forces are weaker for the mistagged H -types than for the mistagged L -types, suggesting that the net effects will still be in the directions highlighted by proposition 2.²⁸ Moreover, as we show in section 6.3, our empirical evidence suggests that the elasticity of compliance with respect to undertagging, η_{Lh} is zero, so these additional terms are not empirically relevant in our context.

3.3.2 Location Choice and House-Price Capitalization

Appendix P presents a modified model in which L -type households can choose to move between L -type houses in locations with l and h tags.²⁹ As is common in spatial models (Redding & Rossi-Hansberg, 2017), households have idiosyncratic preferences for houses in each location ξ_ϕ . Households take house prices $p_{L\phi}$ and property taxes T_ϕ as given and choose where to live,

²⁷These are: First, the $\varphi_{\theta\phi}$ terms in the numerators to account for direct utility losses and the fiscal externality. The $\varphi_{L\phi}$ terms push towards less progressive taxes while the $\varphi_{H\phi}$ terms suggest more progressive taxes. Second, the $\varphi_{\theta\phi}$ terms in the denominators to account for the higher marginal utility of consumption of mistagged households. Again, the $\varphi_{L\phi}$ terms push towards less progressive taxes while the $\varphi_{H\phi}$ terms suggest more progressive taxes.

²⁸To see this, consider the case of the $\varphi_{\theta\phi}$ terms in the numerator of equation (6) for T_l . These push towards a less progressive tax (as in the baseline case in proposition 2) whenever the φ_{Lh} term is larger than the φ_{Hl} term. This is likely because first, the positive φ_{Lh} term is multiplied by $\sigma \geq 1$ while the negative φ_{Hl} term is not; and second, because the φ_{Lh} term depends on the social marginal welfare weight of the L -types, g_L , which is larger than the social marginal welfare weight of the H -types, g_H , appearing in the negative φ_{Hl} . As a result, for the force from the mistagged H -types to dominate, it would need to be the case that they are a large group (large φ_{Hl}) and/or that they are much more sensitive to inequity than the mistagged L -types ($\eta_{Hl} > \eta_{Lh}$). In section 6.3 we show that our evidence suggests that $\eta_{Hl} = 0$, suggesting that the forces from the mistagged L -types will dominate. Analogous reasoning applies to the numerator of (7) and to the $\varphi_{\theta\phi}$ terms in the denominators of (6) and (7).

²⁹For simplicity, we assume that the H -type households all live in houses with h tags and do not move.

anticipating whether or not they will pay their property tax. Given house prices and taxes, these household choices determine which households live in which location and which ones pay their property taxes. House prices then adjust to equilibrate housing demand and an exogenous supply of houses in each sector.

In this model, households' distaste for tax inequities is net of the extent to which tax differences are capitalized into house prices. To capture this we model the disutility of inequity as $d(\tilde{\sigma})$ where $\tilde{\sigma} = (T_h + p_{Lh} - p_{Ll}) / T_l$, where $p_{L\phi}$ is the price of an L -type house taxed at T_ϕ . In the extreme, when tax differences are fully capitalized into house prices, households no longer experience inequity ($\tilde{\sigma} = 1$) and the impacts of mistagging on optimal policy described in section O disappear. However, whenever tax differences are less than fully capitalized into house prices, misclassification still generates inequity and affects tax compliance decisions, shaping the optimal policy schedule.

L -type households will choose to live in the sector with the h tax whenever $V_h(\gamma, \xi_h; p_{Lh}, T_h) > V_l(\gamma, \xi_l; p_{Ll}, T_l)$, where $V_\phi = \max\{u(v_L - p_{L\phi} - T_\phi) - d(\tilde{\sigma}) + \xi_\phi, u(v_L - p_{L\phi}) - \gamma + \xi_\phi\}$ is their value from living in the sector with the ϕ tax, incorporating their optimal choice of whether to pay the corresponding property tax. Whenever households all share the same tastes for the two sectors ($\text{Var}(\xi_\phi) = 0$), households must be indifferent between living in the two sectors and tax differences are fully capitalized in to prices.³⁰ But whenever there are idiosyncratic tastes for living in each sector, this will lead to incomplete capitalization of property taxes, and hence inequity.

Marginal changes in property taxes now also cause households to move. However, by the envelope theorem, these moves have no first-order effect on movers' utility. Nevertheless, moves affect house-prices, with first-order effects on home buyers' welfare.³¹ Moreover, the compliance elasticities now also incorporate a composition effect as some households move between sectors. These compliance elasticities are still, however, the relevant sufficient statistics for welfare and optimal policy, alongside an additional sufficient statistic: $\kappa \equiv -\partial p_{L\phi} / \partial T_\phi$ governing the extent to which property taxes are capitalized into house prices. In Appendix J, we empirically examine the response of property market asking prices to changes in property taxes and find evidence against significant and complete capitalization.

³⁰To see this, let $\xi_h = \xi_l = 0$ for all households and consider compliant households. Whenever they are not indifferent between the two sectors, they all choose the same sector and the aggregate demand for houses in the sectors will not equal supply. For them to be indifferent it must be the case that $v_L - p_{Ll} - T_l = v_L - p_{Lh} - T_h - d(\tilde{\sigma})$. If $T_h > T_l$ and this is not fully capitalized into house prices, $d(\tilde{\sigma}) > 0$ so households cannot be indifferent. They can only be indifferent when taxes are fully capitalized into house prices: $p_{Lh} = p_{Ll} - T_h + T_l$. p_{Ll} then adjusts such that the aggregate demand for houses in each sector equals supply.

³¹There are no sellers in the model. If there were and they had the same welfare weights as the buyers, changes in house prices would merely be transfers between the buyer and the seller with no welfare impact

The modified optimal tax formulas incorporating house price changes are:

$$\frac{T_l}{\tilde{y}_{Ll}} = \frac{1 - \varepsilon - g_L + \varphi_l \frac{\eta}{\varepsilon} \sigma (g_L + \varepsilon) + \kappa \frac{g_L}{c_{Ll}}}{\rho g_L (1 - \kappa) [1 - \varphi_l \frac{\eta}{\varepsilon} \sigma^2 (1 - \tilde{\kappa})]} \quad (8)$$

$$\frac{T_h}{\tilde{y}_{Hh}} = \frac{1 - \varepsilon - \bar{g}_h - \varphi_h \frac{\eta}{\varepsilon} (g_L + \varepsilon) + \kappa \frac{\tilde{g}_h}{c_h}}{\rho (1 - \kappa) [\bar{g}_h + \varphi_h g_L \left(\frac{\tilde{y}_{Hh}}{\tilde{y}_{Ll}} (1 + \frac{\eta}{\varepsilon}) (1 - \tilde{\kappa}) - 1 \right) + \varphi_h g_L \frac{\kappa}{c_{Lh}} \tilde{\kappa} \frac{\tilde{y}_{Hh}}{\tilde{y}_{Ll}}]} \quad (9)$$

where $\tilde{\kappa} = \frac{\kappa}{1-\kappa} (1 - \frac{1}{\sigma})$ governs the increase in marginal utility from the loss in house value from being taxed at T_h rather than T_l ; $\tilde{g}_h = (g_H + \psi g_L) / (1 + \psi)$ is the average marginal social welfare weight of those asked to pay the h tax (note this is not the same as the average social marginal welfare weight of those who *do* pay the h -tax \bar{g}_h); $\tilde{c}_h = (c_{Hh} + \psi c_{Lh}) / (1 + \psi)$ is the fraction of those asked to pay the h tax who comply; and $\tilde{y}_{\theta\phi} = v_\theta - p_{\theta\phi}$ is the value of living in a θ -type house with unpaid tax liability T_ϕ .

The equations look much as before, but with some new terms. In the numerators we have the $\kappa g/c$ terms. These account for the fact that when taxes reduce property prices, all households benefit from access to cheaper housing.³² The $(1 - \kappa)$ term in the denominators is similarly there to account for the decrease in marginal utility of consumption coming from the lower house prices. The $(1 - \tilde{\kappa})$ terms in the denominators account for the dampening of the effects of tax differences on the disutility from inequity. Finally, the final term in the denominator in (9) accounts for the lower marginal utility of all overtagged households from their lower house prices.

Notably, these effects interact with only one of the channels highlighted for mistagging: The $(1 - \tilde{\kappa})$ terms dampen (but do not eliminate) the fact that mistagged L households pay higher taxes than their correctly tagged counterparts, softening that forces towards less progressivity. However, the other two channels are unaffected. House price changes have first-order welfare effects of their own, and so the quantitative impacts will depend on the compliance elasticities and the extent of house price capitalization, but the qualitative impacts of mistagging remain as in the baseline model in section 3.2.

4 Overall Compliance Responses: Boundary Discontinuity Evidence

We begin our empirical exploration of the forces highlighted by the conceptual framework in section 3 by studying differences in compliance behavior around the boundaries of Manaus' tax sectors (described in section 2). To do this, we develop a Boundary Discontinuity Design (BDD) (Black, 1999; Bayer *et al.*, 2007) that captures the overall effect of facing a tax schedule with a high price of land rather than the a schedule with a lower price. Naturally, this combines both the fact that taxes are higher on the high-tax side of the boundary, and the fact that those on the

³²As noted above, the model does not account for the welfare of the incumbent owners of the properties. If their welfare weights are the same as the houses' new occupants, these terms represent transfers between households with equal welfare weights and so they disappear from the expressions.

high-tax side face greater inequity. As the framework in section 3 shows, the welfare and policy implications of mistagging are very different depending on whether this reduced form effect is driven by responses to inequity or responses to the level of property's tax liabilities. Sections 5 and 6 then take up the identification challenge of separately identifying behavioral responses to inequity and to the tax liability.

4.1 Boundary Discontinuity Design

Figure 2 sets the stage for our BDD approach. It shows a street view of one of the roads forming the boundary between two tax sectors, with little apparent difference between the properties on either side. The introduction of sector-specific prices per square meter in the tax formula (1) leads to differential taxation of identical properties across the boundary. This creates quasi-experimental variation allowing us to study the impacts of this differential taxation on tax compliance.

To do this, we use our BDD approach to measure discontinuous changes in compliance at the tax sector boundaries, which we interpret to be behavioral responses to the discontinuity in the tax schedule. Note that the presence of a discontinuity in the tax schedule at the boundaries may induce sorting around the boundaries. To the extent that this sorting is driven by the property tax, it is a component of the compliance elasticities we seek to estimate, since they contribute to the fiscal externality of behavioral responses to the property tax, as discussed in section 3.3.2. However, as shown in Bayer *et al.* (2007), when sorting is driven by other forces, this can meaningfully change the interpretation of the BDD.³³ As discussed in section 2, in our setting, the boundaries that we study are used exclusively for taxation. They do not determine access to public goods or which part of the government delivers them. Moreover, to ensure that there are no other meaningful changes at the boundaries, we remove any boundaries that overlap with neighborhood ("bairro") boundaries from our analysis. Notwithstanding this, both the tax liability and inequity change discontinuously at the boundaries, and so our results should be interpreted as the causal effects of the change in the combination of the two tax-induced incentives.

Using our boundary sample as described in section 2.4, we focus on compliance in 2010, the year immediately preceding the 2011 tax reform, when the inequities in the tax system were at their most pronounced.³⁴ For each taxpayer, we compute their compliance as the fraction of their tax liability they have paid by 18 months after they receive their tax bill (e.g. for compliance in 2010 we use the amount they have paid by July 31 2011), and in appendix F we show that our results do not change when we use alternative definitions of compliance using longer time

³³In their context, sorting is driven not only by differences in school quality (their object of interest) but by preferences for neighbors' attributes. In our context, the interpretation of the BDD could also be meaningfully different if the tax authority internalized the inequity concern and provided lower enforcement of payments to the high tax side. Appendix I discusses the enforcement of tax liabilities and shows that provides evidence against lower enforcement on the high tax side of the boundary.

³⁴In appendix E we provide evidence that the estimates are robust to our sample selection decisions.

windows or looking at whether taxpayers made any tax payment. For each tax sector boundary, we split the street into 500-meter long segments, $r(i)$, which are used to ensure we are comparing properties close to each other. To study the impact of the discontinuous change in taxation on compliance, we estimate the following equation for compliance c_i by taxpayer i :

$$c_i = \lambda_{r(i)} + f_0(d_i) + \beta_0 HTS_i + f_1(d_i) \times HTS_i + \varepsilon_i \quad (10)$$

where $\lambda_{r(i)}$ are boundary-segment fixed effects, HTS_i is an indicator for being on the high-tax side of the boundary ($d_i > 0$); $f_0(d_i)$ and $f_1(d_i)$ control for distance to the boundary on the low- and high-tax sides of the boundary, respectively; and ε_i is the residual.

4.2 Results

Figure 3 shows the results of estimating (10) in the subsample of our boundary sample where properties face a non-trivial degree of inequity ($|\sigma_i| > 0.05$).³⁵ The figure shows our point estimate of the change in compliance at the boundary, computed using local linear controls for distance, the MSE-minimizing bandwidth, and triangular weighting kernels (Calonico *et al.*, 2014, 2018, 2019, 2020). To help visualize the design, the figure also shows the conditional expectation of compliance using decile-spaced bins of distance from the boundary weighted with the same triangular kernel used to compute the point estimate, but censoring the kernel at its tenth percentile to give positive weights to observations outside the MSE-optimal bandwidth. Bins containing the optimal bandwidth are shown in blue while bins outside the optimal bandwidth are shown in gray. We also plot an estimate of (10) with cubic distance controls f_0 and f_1 estimated over the full ± 300 -meter window with the same triangular kernel weights.

Three key findings emerge. First, there is a sharp drop in compliance precisely at the boundary, suggesting that compliance behavior is responsive to the tax system. Second, the drop in compliance is economically meaningful. Compliance is 6 percentage-points lower on the high-tax side of the boundary. Since average compliance is 0.75 just on the low-tax side of the boundary, this is an 8% drop in compliance. Figure 4 is constructed analogously to figure 3 but shows the corresponding first stages for the tax liability and inequity. It shows that the discontinuity in the tax liability increases tax liabilities by 13%. If all behavior is driven by the tax liability, combining this with the 8% drop in compliance implies an elasticity of compliance with respect to the tax liability of 0.62. This elasticity is large. For example Brockmeyer *et al.* (2023) employ a range of difference-in-differences and regression discontinuity approaches in Mexico City and estimate compliance elasticities between 0.24 and 0.46.

Third, as figure 4 makes clear, the tax sector boundaries generate quasi-experimental variation in two distinct first-stages: Tax liabilities are 13% higher on the high-tax side of the tax sector boundaries, but inequity is also 62% higher. The compliance effect we see in figure 3 potentially

³⁵In appendix figure E.29 we show that the results are unchanged if we use thresholds for non-triviality between 0.02 and 0.2

combines responses to both incentives. As we showed in the model in section 3, the behavioral responses to the two incentives have opposite implications for the progressivity of the optimal tax schedule, and so our next sections turn to disentangling the two mechanisms.

5 Exposure to Mistagging and Behavioral Responses to Inequity

As discussed in section 4, at the tax sector boundaries both the tax liability and inequity change discontinuously. This poses an identification challenge in recovering the elasticity of compliance with respect to inequity alone. The insight that allows us to disentangle the two is that properties vary in their *exposure* to mistagging, even holding fixed their tax liability. The inequity we seek to isolate is driven by mistagging of land prices, whereas properties' tax liabilities depend on both assessed land prices and the assessed value of the built structure on the property. A property featuring a small house on a large lot has a tax liability that is primarily due to the land it encompasses, and hence faces a high degree of inequity. Conversely, a property with the same tax liability, but a large house on a small lot has a tax liability that is primary due to the built structure on the property, and hence faces a smaller degree of inequity.

To see this formally, note that we can use the presumptive tax formula (1) to express the counterfactual tax liability for a property in sector $s(i)$ had it been on the other side of the boundary in sector $\hat{s}(i)$ as

$$\hat{T}_i = \frac{1 + p_{\hat{s}(i)}e_i}{1 + p_{s(i)}e_i} \times T_i$$

where $e_i = a_i/b_i$ is the ratio of property's IPTU contribution from land characteristics to building characteristics, $p_{s(i)}$ is the land price faced by the property in its own sector, and $p_{\hat{s}(i)}$ is the counterfactual assessed land price they would face across the boundary.³⁶ As a result, the ratio e_i governs a property's *exposure* to mistagging: properties with high e_i will be more exposed to the inequity coming from the difference in assessed land prices $p_s - p_{\hat{s}}$ than properties with low e_i , even if they share the same tax liability.

To leverage this source of quasi-experimental variation in inequity, we need to augment our boundary discontinuity design in two ways. First, we need to incorporate conditioning on the properties' tax liability to be able to isolate the discontinuous change in inequity at the boundary. To do this, we adapt the methods in Frölich & Huber (2019) who show how to incorporate conditioning covariates into a standard regression discontinuity design. Second, the classic regression discontinuity design studies the causal effect of a binary treatment, but in our setting, inequity is a continuous function of exposure to mistagging, complicating the interpretation of the regression discontinuity estimates. Here we follow the approach in Dong *et al.* (2023) who show how to achieve identification of Local Average Treatment Effects (LATEs) at quantiles of the distribution of exposure and how to aggregate them to weighted (local) average treatment

³⁶In our discussion we implicitly condition, without any loss in generality, on properties located at a particular boundary so that we can hold $p_{s(i)}$ and $p_{\hat{s}(i)}$ fixed.

effects.

In section 5.1 we begin by providing a set of strong assumptions under which we can identify and estimate the causal effect of inequity on compliance. These amount to assuming that after conditioning on the tax liability and a property's exposure to mistagging, the boundary discontinuity design identifies the causal effect of inequity on compliance.

In section 5.2 we provide much weaker assumptions that do not require that controlling for tax liability and exposure achieves identification. Instead, we require that the differences in compliance between properties on the low- and the high-tax side of the boundaries are orthogonal to exposure to mistagging conditional on tax liability and exposure. This is akin to a parallel trends assumption in a difference in differences design and allows us to pursue a difference in boundary discontinuities design comparing discontinuities in compliance at the boundaries between high- and low-exposure properties. In section 6, we relax the required assumptions further still by incorporating Manaus' 2011 property tax reform, allowing us to hold all time-varying unobservable determinants of compliance fixed, and allowing for differential time-trends in compliance on the low- and high-tax sides of the boundary.

5.1 Augmented Boundary Discontinuity Design

As a first exercise, in this section we provide a set of assumptions under which a Boundary Discontinuity Design (BDD) augmented to control flexibly for the tax liability achieves identification of the causal effect of inequity on compliance. These assumptions effectively require that the BDD identifies the causal effect of inequity at every level of exposure to mistagging, conditional on the tax liability. These are strong assumptions, but they provide transparent conditions for identification and allow us to be precise about which Local Average Treatment Effect (LATE) we can identify. Subsequent sections show that identification is preserved under more palatable assumptions, and our results are similar under all of these designs.

5.1.1 Identification

Our approach builds on the advances in Frölich & Huber (2019) and Dong *et al.* (2023) who adapt the regression discontinuity design to settings with controls, and continuous treatments, respectively. We denote our compliance outcome $C \in [0, 1]$ as the fraction of a taxpayer's liability that they pay in response to the treatment we are interested in: inequity $\sigma \in \mathbb{R}^+$. The running variable in our regression discontinuity design is distance to the boundary of a tax sector $D \in \mathcal{D} \subset \mathbb{R}$. Compliance is determined by potential outcomes given by $C = G(\sigma, \tau, D, \nu)$ where τ is the (log) tax liability, and ν are other, potentially unobserved, determinants of compliance.³⁷

It is useful to think of crossing the boundary as an instrument $Z = 1[D > 0]$ giving properties potential treatments when Z is exogenously set to z of $\sigma_z \equiv q_z(E_z) = (-1)^{1-z} \log\left(\frac{1+p_H E_z}{1+p_L E_z}\right)$, where E_z is a property's potential exposure when the instrument is $Z = z$. Since we will invoke

³⁷We allow these determinants $\nu \in \mathcal{V} \subset \mathbb{R}^{\dim \nu}$ to have arbitrary dimension.

a rank invariance assumption, it is convenient to study quantiles of the treatment distribution.³⁸ Our first assumption allows us to map 1-to-1 between quantiles of exposure to mistagging and inequity:

Assumption 1 (Quantile representation). *The conditional distribution of E_z given distance $D = d$ and tax liability $\tau = t$ is continuous with a strictly increasing CDF $F_{E_z|\tau,D}(e, t, d)$.*

This assumption allows us to define the inequity faced by the property at the u th conditional quantile of exposure as³⁹

$$q_z(d, u, t) = (-1)^{1-z} \log \left(\frac{1 + p_H F_{E_z|t,d}^{-1}(u)}{1 + p_L F_{E_z|t,d}^{-1}(u)} \right)$$

More substantively, we make a set of four smoothness assumptions:

Assumption 2 (Smoothness). *$q_z(d, u, t)$, $z = 0, 1$, is continuous in $d \in \mathcal{D}$ for any $u \in [0, 1]$ and $t \in \mathcal{T} \subset \mathbb{R}^+$. Either $G(\sigma, \tau, D, \nu)$ is continuous in all its arguments, or it is a.e. continuous and bounded. $f_{\nu|U_z, \tau, D}(v, u, t, d)$ is continuous in $d \in \mathcal{D}$ for any $u \in [0, 1]$, $t \in \mathcal{T}$, and $v \in \mathcal{V}$, where \mathcal{V} is compact. $f_{D|\tau}(d, t)$ is continuous and strictly positive around $d = 0$.*

This assumption requires that inequity, taxes, distance, and unobservables all generate smooth impacts on compliance. It also assumes that for a given rank in the exposure distribution, the distribution of unobservables is smooth near the boundaries. These are strong assumptions, and in sections 5.2 and 6 we show how we can relax both of them while still achieving identification. The assumption that distance has a smooth effect on potential treatments is easily satisfied as long as assumption 2 holds. The assumption that distance is continuous and has positive density at the boundary is standard in BDD designs.

Our final assumption requires that properties stay at approximately the same rank in the potential exposure distribution on either side of the tax sector boundaries.⁴⁰ Formally,

Assumption 3 (Local exposure rank invariance or similarity). *Conditional on $D = 0$ and $\tau = t \in \mathcal{T}$, 1. $U_0 = U_1$; or, more generally, 2. $U_0|\nu \sim U_1|\nu$*

Assumption 3 implies that crossing the boundary (our instrument) does not affect properties' rank in the distribution of exposure to mistagging.⁴¹ Notably, this assumption does not require properties to have the same potential exposure to mistagging on either side of the boundary. The relative, after-tax price of land a is higher on the high-tax side of the boundary and so we might expect property owners to substitute towards built structure. Assumption 3 allows

³⁸This is also convenient since it offers a natural way to pool across tax sector boundaries.

³⁹Note that while the reduced form only depends on e_i , it now depends on τ also because the distribution of e_i we are using to normalize with is conditional on distance and τ .

⁴⁰Note that this does not require properties to have the same exposure to mistagging, only that their rank is similar.

⁴¹The more general formulation of the assumption permits random slippages from a property's rank in the exposure distribution just on either side of the boundary (Chenozhukov & Hansen, 2005; Dong *et al.*, 2023).

this, but requires that the unobservables are not correlated with the elasticity of substitution between land a and built structure b in such a way that it would reverse the ranks in the potential distribution.

Together with the smoothness of the distribution of ν in assumption 2, assumption 3 means that at the boundary, we can use U as a control variable (Imbens & Newey, 2009) — conditional on U , the change in inequity at the tax sector boundary is exogenous (unrelated to ν) (Dong *et al.*, 2023).⁴²

With these assumptions we can show that a boundary regression discontinuity design that conditions on tax liability identifies the treatment effect of inequity:

Proposition 3 (Identification of LATEs conditional on U and τ). *Define the $Q\tau$ -LATE:*

$$\begin{aligned}\eta(u, t) &\equiv \int \frac{G(\sigma_1(u, t), t, 0, v) - G(\sigma_0(u, t), t, 0, v)}{\sigma_1(u, t) - \sigma_0(u, t)} F_{\nu|U, \tau, D}(dv, u, t, 0) \\ &= \mathbb{E} \left[\frac{C_{\sigma_1(u, t)} - C_{\sigma_0(u, t)}}{\sigma_1(u, t) - \sigma_0(u, t)} \middle| U = u, \tau = t, D = 0 \right]\end{aligned}$$

This is the average causal effect of inequity for taxpayers with exposure to mistagging rank $U = u$ and tax liability $\tau = t$.

Under Assumptions 1, 2 & 3, for any $u \in \mathcal{U}$, the set of u for which there is a first stage (non-zero exposure), and for any $t \in \mathcal{T}$, $Q\tau$ -LATE $\eta(u, t)$ is identified and is given by

$$\eta(u, t) = \frac{m^+(u, t) - m^-(u, t)}{q^+(u, t) - q^-(u, t)} \quad (11)$$

where the limits in the denominator are defined by $q^+(u, t) \equiv \lim_{d \rightarrow 0^+} q(d, u, t)$ and $q^-(u, t) \equiv \lim_{d \rightarrow 0^-} q(d, u, t)$. Also let $m(s, t, d) \equiv \mathbb{E}[C | \sigma = s, \tau = t, D = d]$, and define $m^+(u, t) \equiv \lim_{d \rightarrow 0^+} m(q^+(u, t), t, d)$ and $m^-(u, t) \equiv \lim_{d \rightarrow 0^-} m(q^-(u, t), t, d)$. All of these can be consistently estimated from the data.

Further, the W-LATE $\bar{\eta}(w) = \int_{\mathcal{U}} \int_{\mathcal{T}} \eta(u, t) w(t, u) dt du$ is identified for any known or estimable weighting function $w(t, u)$ such that $w(t, u) \geq 0$ and $\int_{\mathcal{U}} \int_{\mathcal{T}} w(t, u) dt du = 1$.

Proof. See appendix Q □

The proposition shows that under assumptions 1–3, we have a valid BDD for every exposure rank and every tax liability. A property's tax liability and exposure rank pin down its dose of the treatment, the denominator in the LATE. The smoothness assumptions allow us to identify the reduced form effect in the numerator. Assumptions 1–3 are strong, but proposition 3 shows transparently how identification is achieved and which LATEs can be estimated, and so we think of it as a good starting point in analyzing the effects of inequity on compliance.

Proposition 3 also shows that we can estimate weighted averages of the causal effects of inequity on compliance at different exposure quantiles and tax liabilities. To implement this in practice, we use regression weights and estimate the following regression:

⁴²See the proof of proposition 3 in appendix Q for details.

$$c_i = \lambda_{r(i)} + g(\tau_i, e_i) + f_0(d_i) + \beta_0 HTS_i + f_1(d_i) \times HTS_i + \varepsilon_i \quad (12)$$

where $\lambda_{r(i)}$ are fixed effects for 500-meter segments along the boundaries to ensure we are comparing properties who are nearby each other; $g(\tau_i, e_i)$ are flexible controls for property i 's (log) tax liability τ_i and exposure to mistagging e_i (our baseline estimates use τ splines and exposure deciles); $f_0(d_i)$ and $f_1(d_i)$ control flexibly for distance to the boundary on the low- and high-tax sides of the boundary respectively; and HTS_i is an indicator for properties on the high-tax side of the boundary ($d_i > 0$). We estimate the equation using our main sample as described in 2.4. In appendices E and F we provide evidence that the estimates are robust to sample selection decisions and definitions of compliance, respectively.

5.1.2 Results

Figure 5 shows the results of estimating equation (12) with (log) inequity σ as the outcome. The figure is constructed analogously to the baseline BDD in figure 3 discussed in section 4. It shows that we have a strong first-stage impact on inequity of 0.519 (down from 0.618 in figure 4) even after controlling flexibly for the tax liability and exposure to mistagging (using cubic splines of the tax liability and fixed effects for deciles of exposure). Similarly, figure 6 shows the results of estimating equation (12) with compliance as the outcome. It shows that there is a strong impact of inequity on compliance. Compliance is 7.5 percentage points lower on the high-tax side of the boundaries even after controlling flexibly for the tax liability and exposure to mistagging.

Table 2 shows the results of estimating equation (12) using a variety of approaches to controlling flexibly for the tax liability and exposure. In column (1) we control for cubic splines of the tax liability and fixed effects for deciles of exposure to mistagging. In column (2) we replace the exposure deciles with cubic splines of exposure while column (3) replaces the splines of the tax liability with deciles. Columns (4)–(6) additionally interact the tax liability controls with the exposure controls. At the bottom of the table, we also present the first stage results and the compliance elasticity the results imply. The table shows remarkably consistent results: the implied elasticity of compliance with respect to inequity ranges from 0.19 to 0.23.

5.1.3 Salience

We interpret these results as evidence that taxpayers respond to inequity by reducing their compliance. However, for this to be the case, taxpayers need to be at least somewhat aware of what their tax liability would be had their property been located in the adjoining tax sector. As we discussed in section 2.5 and appendix D, the IPTU is, in general, a highly salient tax and citizens are aware of the presumptive tax formula. The formula for the IPTU is publicly available to all citizens, and citizens can also learn about their counterfactual tax liability \hat{T}_i by comparing their

tax bill to the ones levied on similar properties on the other side of the boundary.⁴³

Moreover, the results presented above are driven by properties for whom this comparison would be particularly easy because their neighbors across the boundary have similar properties. We build a measure of similarity between a property and its neighbors across the boundary building on Auerbach & Hassett (2002).⁴⁴ We then split our sample into five disjoint groups using the quintiles of our salience measure and estimate equation (12) in each group. The inequity elasticities implied by these estimates are displayed in figure 7.

The figure shows that our results are overwhelmingly driven by taxpayers who have similar neighbors across the boundary. In the bottom quintile the estimated effect is zero, but then the elasticity of compliance with respect to inequity is positive in the higher quintiles of salience. To the extent that there are taxpayers who do not perceive the inequity they face and do not respond to it, our results should be interpreted as lower bounds on the responsiveness of behavior to salient inequity.

5.2 Difference in Boundary Discontinuities Design

Our second strategy relaxes the assumptions required for identification. A disadvantage of the approach in section 5.1 is that we have to assume that taxpayers on the high-tax side of the boundary are not differentially compliant than taxpayers on the low-tax side of a boundary for reasons that are not related to their tax liabilities or their properties' exposure to mistagging.⁴⁵ In this section we allow for the possibility that taxpayers on the high-tax side of the boundaries may be less compliant than taxpayers on the low-tax side of the boundaries for reasons that are not related to their tax liabilities and their properties' exposure to mistagging. For example, this may arise if households with dimmer views of government and lower tax morale systematically sort into properties on the high-tax sides of the boundaries. Or, it may arise if properties on the lower taxes on land on the low-tax side of the boundary attract different types of households and/or affect incentives to invest in property improvements.

Instead, we assume that the resulting selection bias is uncorrelated with exposure to mistagging. This is analogous to the parallel trends assumption used in difference in differences designs that changes over time in the outcome of interest are uncorrelated with selection into treatment but applied to changes across tax sector boundaries. This allows us to pursue a difference in boundary discontinuity design that compares discontinuities in compliance at the tax sector boundaries across properties with differing levels of mistagging exposure. Implementing this strategy, we estimate that the elasticity of compliance with respect to inequity is between 0.23 and 0.28. In section 6 we relax this assumption as well by introducing the reform to the property

⁴³The amount of the tax bill is commonly displayed in real estate websites such as [Viva Real](#) as discussed in appendix J.

⁴⁴See Appendix G for details of the construction of the measure.

⁴⁵Specifically, we assume that potential outcomes $G(\sigma, \tau, D, \nu)$ are continuous in all arguments (including distance D), and that the distribution of the unobserved determinants of compliance ν conditional on exposure rank U , tax liability τ and distance D is continuous at the boundary $D = 0$.

tax in 2011.

5.2.1 Identification

In our modified approach, we separate the potential outcomes into an untreated component G_0 capturing potential compliance in the absence of inequity, and a treatment effect G_1 capturing the impact of compliance on inequity. We also partition the unobserved determinants of compliance ν into those that influence the treatment effect ν_1 and those that only affect the untreated potential outcomes ν_0 .

$$C = G(\sigma, \tau, D, \nu) = G_0(\tau, D, \nu_0) + G_1(\sigma, \tau, D, \nu_1) \quad (13)$$

The difference in boundary discontinuity design allows for discontinuities in the untreated potential outcomes G_0 at the boundaries, and for the distribution of ν_0 to be discontinuous at the boundary, substantially relaxing the smoothness assumption (Assumption 2) required in section 5.1. Instead, we assume that

Assumption 4 (Smoothness). $q_z(d, u, t)$, $z = 0, 1$, is continuous in $d \in \mathcal{D}$ for any $u \in [0, 1]$ and $t \in \mathcal{T} \subset \mathbb{R}^+$. Either $G_1(\sigma, \tau, D, \nu_1)$ is continuous in all its arguments or it is a.e. continuous and bounded. $G_0(\tau, D, \nu_0)$ is right and left continuous in D at $D = 0$ for any $t \in \mathcal{T}$ and $\nu_0 \in \mathcal{V}_0$. $f_{\nu_1|U_z, \tau, D}(v_1, u, t, d)$ is continuous in D for any $u \in [0, 1]$, $t \in \mathcal{T}$ and $v_1 \in \mathcal{V}_1$ where \mathcal{V}_1 is compact. $f_{\nu_0|U_z, \tau, D}(v_0, u, t, d) = f_{\nu_0|\tau, D}(v_1, t, d)$ for any $u \in [0, 1]$. $f_{\nu_0|\tau, D}(v_1, t, d)$ is left and right continuous at $D = 0$ for any $t \in \mathcal{T}$ and $v_0 \in \mathcal{V}_0$ where \mathcal{V}_0 is compact. $f_{D|\tau}(d, t)$ is continuous and strictly positive around $d = 0$.

This is akin to a parallel trends assumption, but modified to allow for a continuous treatment (Callaway *et al.*, 2024). We allow for selection at the boundary in the untreated potential outcomes such that the right- and left limits of $\mathbb{E}[G_0(t, d, \nu_0) | \tau = t, D = d]$ at $D = 0$ need not be the same. However, we require that the gap be constant across potential treatment levels σ_z .

We can also weaken our assumption about the exposure ranks to condition only on the sub-component of ν that affects the treatment effects:

Assumption 5 (Local exposure rank invariance or similarity). Conditional on $D = 0, 1$. $U_0 = U_1$; or more generally, 2. $U_0|\nu_1 \sim U_1|\nu_1$

With these modified assumptions, we can show that the difference in the LATEs between any pair of levels of exposure are identified:

Proposition 4 (Identification of Differences in LATEs). Define the $Q\tau DD$ -LATE:

$$\begin{aligned}\eta(\underline{u}, \bar{u}, t) &\equiv \frac{\int G(\sigma_1(\bar{u}, t), t, 0, v) - G(\sigma_0(\bar{u}, t), t, 0, v) F_{\nu|U,\tau,D}(dv, \bar{u}, t, 0)}{-\int G(\sigma_1(\underline{u}, t), t, 0, v) - G(\sigma_0(\underline{u}, t), t, 0, v) F_{\nu|U,\tau,D}(dv, \underline{u}, t, 0)} \\ &= \frac{\mathbb{E}[C_{\sigma_1(\bar{u}, t)} - C_{\sigma_0(\bar{u}, t)} | U = \bar{u}, \tau = t, D = 0] - \mathbb{E}[C_{\sigma_1(\underline{u}, t)} - C_{\sigma_0(\underline{u}, t)} | U = \underline{u}, \tau = t, D = 0]}{[\sigma_1(\bar{u}, t) - \sigma_0(\bar{u}, t)] - [\sigma_1(\underline{u}, t) - \sigma_0(\underline{u}, t)]}\end{aligned}\tag{14}$$

This is the difference in the average causal effect of inequity for taxpayers with tax liability $\tau = t$ between taxpayers with exposure rank $U = \bar{u}$ and taxpayers with exposure rank $U = \underline{u}$. Under Assumptions 1, 4 & 5, for any $\bar{u}, \underline{u} \in \mathcal{U}$, and for any $t \in \mathcal{T}$, $Q\tau DD$ -LATE $\eta(\underline{u}, \bar{u}, t)$ is identified and is given by

$$\eta(\underline{u}, \bar{u}, t) = \frac{[m^+(\bar{u}, t) - m^-(\bar{u}, t)] - [m^+(\underline{u}, t) - m^-(\underline{u}, t)]}{[q^+(\bar{u}, t) - q^-(\bar{u}, t)] - [q^+(\underline{u}, t) - q^-(\underline{u}, t)]}\tag{15}$$

where the limits are as defined in proposition 3, all of which can be consistently estimated from the data.

Further, the weighted WDD-LATE $\bar{\eta}_{QDD}(w) = \int_{\mathcal{U}} \int_{\mathcal{U}} \int_{\mathcal{T}} \eta(\underline{u}, \bar{u}, t) w(\underline{u}, \bar{u}, t) dt d\bar{u} du$ is identified for any known or estimable weighting function $w(\underline{u}, \bar{u}, t)$ such that $w(\underline{u}, \bar{u}, t) \geq 0$ and $\int_{\mathcal{U}} \int_{\mathcal{U}} \int_{\mathcal{T}} w(\underline{u}, \bar{u}, t) dt d\bar{u} du = 1$.

Proof. See appendix R □

Proposition 4 shows that we can identify the difference in the treatment effects of crossing the boundary experienced by properties at any pair of levels of exposure to mistagging ranks \underline{u} and \bar{u} (and hence between any pair of levels of inequity since by assumption 1 there is a one-to-one mapping between exposure ranks u and potential treatments $q_z(d, u, t)$). Since we permit discontinuities in compliance at the boundary, neither the treatment effect experienced by properties with exposure rank \underline{u} nor the treatment effect at \bar{u} is identified. However, the difference between the two, and hence the shape of the relationship between inequity and treatment effects, is identified.

The second part of the proposition shows that any weighted average of the pairwise differences in the treatment effects is also identified. In our empirical analysis, we estimate such a weighted LATE through linear regression, whose weights are estimable and hence identified by proposition 4. Specifically, we estimate

$$c_i = \lambda_{r(i)} + g_0(\tau_i, e_i) + f_0(d_i) + HTS_i \times [\beta_0 + \eta \log(\sigma) + f_1(d_i) + g_1(\tau_i, e_i)] + \varepsilon_i\tag{16}$$

where terms are as defined above for equation (12) and now we also permit the controls for the tax liability τ and exposure to mistagging e_i to be different on each side of the boundary. We estimate the equation using our main sample as described in 2.4. In appendices E and F we provide evidence that the estimates are robust to sample selection decisions and definitions of compliance, respectively.

One of the main advantages of this identification strategy is that it allows for selection at the boundary in the untreated potential outcomes. However, we still require that this selection be uncorrelated with properties' exposure e_i . We are able to test this assumption by using sector boundaries at which the assessed land price does not change. We construct placebo boundaries where observations on the high-tax sides come from boundaries where assessed land prices don't change but are high, and the low-tax sides come from nearby boundaries where assessed land prices don't change but are lower. If our assumption is correct, then any differences in compliance across these placebo boundaries should be uncorrelated with the inequity they would have faced if the placebo boundary had been real when we run a placebo version of 16. Details of the dataset construction are in Appendix H, and the results are shown in Table H.1. Reassuringly, we see no evidence that compliance gaps are correlated with exposure to mistagging as measured through the placebo tax-rate differences, providing support for our identifying assumption.

5.2.2 Results

We begin by demonstrating how the impact of inequity on compliance differs across subgroups of the sample determined by the extent of inequity they face. In figure 8 we show the first-stage discontinuity in inequity estimated using (12) in two groups. The top quartile of $|\sigma|$ (high inequity) and all other properties (low inequity). Figure 9 then turns to estimating compliance effects in these two groups. Consistent with our strategy, we see no significant change in compliance at the boundary in the low inequity group in panel A. However, we see a very strong effect in the top quartile of inequity in panel B.

To quantify the relationship in a single parameter, we estimate η using equation (16), varying the controls for τ and e_i . The results, presented in Table 3, consistently confirm the negative relationship between compliance and inequity. In column (1), we control for cubic splines of the tax liability and fixed effects for deciles of the exposure distribution. In column (2) we control separately for the tax liability and exposure to mistagging on either side of the boundary. Column (3) replaces the exposure deciles with cubic splines in exposure while column (4) replaces the tax liability deciles with cubic splines. Columns (5)–(7) control for these separately on either side of the boundary. Importantly, the estimated elasticities remain robust across specifications and closely align with the findings discussed in section 5.1. In this case, we estimate elasticities of compliance with respect to inequity between 0.23 and 0.28, strikingly similar to those obtained under the stronger assumptions in section 5.1.

6 Changes in Inequity Due to the 2011 Property Tax Reform

The analysis in section 5 exploited purely cross-sectional variation in inequity using data from 2010: We augmented the boundary discontinuity design to control for the tax liability and to leverage variation in inequity induced by differences in properties' exposure to mistagging.

While our Difference in BDD design in section 5.2 required significantly weaker assumptions, concerns may remain about unobserved determinants of compliance such as household incomes or views of government that vary discontinuously around the boundaries and that are correlated with mistagging exposure.

However, these unobservables are likely to be fixed over time, at least in the short-to-medium run, and so in this section we show how to augment the BDD to incorporate Manaus' 2011 property tax reform discussed in section 2.2 and in the process hold fixed all time-invariant determinants of compliance. Our approach in section 6.1 studies the causal effect of changes in inequity on changes in compliance, while controlling for changes in taxes. This approach requires a parallel trends assumption at the tax sector boundaries: changes over time in compliance on the high-tax side of the boundaries are assumed to be the same as on the low-tax side, analogously to the assumption in section 5.1 that unobserved determinants of compliance vary smoothly at the boundaries.

The approach we develop in section 6.2 relaxes this assumption and allows for differences in trends across the boundary, but requires that the difference in the trends be uncorrelated with exposure to mistagging. Under this assumption we develop a triple-differences design to estimate the impact of changes in inequity on changes in compliance. Finally, in section 6.3, we make a "strong parallel trends" assumption (Callaway *et al.*, 2024), requiring changes over time in compliance to be uncorrelated with exposure, separately on either side of the boundaries, which permits us to separately identify the impacts of undertagging ($\sigma < 1$) and overtagging ($\sigma > 1$).

6.1 Dynamic Boundary Discontinuity Design

As discussed in section 2.2, the 2011 tax reform created large increases in households' property tax liabilities, and also in the counterfactual property tax liabilities they would face if their properties were located in the tax sector adjoining theirs. This allows us to compare changes over time in compliance on the high-tax and low-tax sides of the tax sector boundaries and relate them to changes in inequity, holding fixed the changes in tax liability they experience as well as any time-invariant determinants of compliance. Our identification arguments here mirror the augmented boundary discontinuity design in 5.1 except that the outcomes we are interested in now are *changes* in compliance over time, which we relate to changes in inequity over time.

Formally, we assume that potential compliance outcomes in year y are given by $C_y = G(\sigma_y, \tau_y, D, \mu, \nu_y, y)$. As before, compliance depends on inequity σ , the tax liability τ , and distance to the boundary D . We augment the potential outcomes to depend on a set of time-invariant unobservables μ , time-varying unobservables ν_y , and time y . We assume that the difference between potential compliance in 2010 (before the reform) and 2016 (after the reform is fully phased in) can be written as $\Delta C = \Delta G(\Delta\sigma, \Delta\tau, D, \Delta\nu)$ where, critically, by taking differences over time, we eliminate the dependence of the potential outcomes on the time-invariant unobservables μ .⁴⁶

⁴⁶Moreover, the change in compliance depends on the *change* in the tax liability $\Delta\tau$ not on the levels of taxes in

From here, we proceed as in section 5.1, but replacing the level of compliance C with the change in compliance ΔC everywhere, and the levels of tax τ and inequity σ with their time-changes $\Delta\tau$ and $\Delta\sigma$. Applying proposition 3, we are able to identify the causal effect of changes in inequity $\Delta\sigma$ on changes in compliance ΔC at all levels of the change in tax liability $\Delta\tau$ and exposure rank U , and we can also identify weighted averages of these causal effects. We do so by estimating the regression-weighted causal effect through the following equation:

$$\Delta c_i = \lambda_{r(i)} + g(\Delta\tau_i, e_i) + f_0(d_i) + HTS_i \times [\beta_0 + f_1(d_i)] + \varepsilon_i \quad (17)$$

Figure 10 shows the first stage change in inequity in two groups. First, the group of properties for whom the reform meaningfully reduced inequity (either by reducing overtagging or by reducing undertagging), and second, the remaining properties who did not experience a reduction in inequity.⁴⁷ For the analysis in this section, we re-incorporate tax sector boundaries that overlap with neighborhood boundaries since our design is able to hold fixed any changes at the boundaries that don't change over time, such as the difference between neighborhoods. We see that for the former group, overtagging decreased by 34% at the high-tax side of the boundary, while undertagging decreased by 14% at the low-tax side of the boundary. By contrast, the properties who did not experience a meaningful reduction in inequity experienced approximately equal, and small (under 10%) changes in inequity.

Figure 11 shows the effects of changes in inequity on changes in compliance in these two groups. In panel A, we see that in the group experiencing a meaningful reduction in inequity, the change in compliance is 5.7 percentage-points higher on the high-tax side than the low-tax side, and precisely estimated, suggesting that households respond strongly to the removal of inequity. Meanwhile, in panel B, we see that in the group that did not experience a reduction in inequity, the discontinuity in the change in compliance is a precisely estimated zero, providing confidence in the validity of the design.

6.2 Dynamic Difference in Boundary Discontinuity Design

Our most robust design allows compliance on the low-tax and high-tax sides of the boundaries to be on different trends, which would invalidate our dynamic boundary discontinuity design in section 6.1 as the discontinuity in changes in compliance at the boundary conflates differences in trends and the causal effect of changes in inequity we seek to estimate. Analogously to the approach in section 5.2, we require that whatever difference in trends there is between the two sides of the boundary, it is orthogonal to properties' exposure to mistagging, akin to a triple-differences design.

Applying proposition 4, replacing compliance, taxes, and inequity with their changes before either year,

⁴⁷We first defined a divergence variable as $\Delta\sigma$ for properties on the high tax side and $-1 \times \Delta\sigma$ for properties on the low tax side. We then defined the group that the reform meaningfully reduced inequity as the first quartile of "divergence."

tween 2010 and 2016, we are able to identify the differences in the causal effects of changes in inequity on changes in compliance between any two pairs of exposure ranks. Moreover, we can identify any weighted average of these differences in causal effects. We do so by estimating the following regression-weighted average causal effect η :

$$\Delta c_i = \lambda_{r(i)} + g_0(\Delta\tau_i, e_i) + f_0(d_i) + HTS_i \times [\delta_0 + \eta\Delta \log(\sigma_i) + g_1(\Delta\tau_i, e_i) + f_1(d_i)] + \varepsilon_i \quad (18)$$

where all terms are as defined previously.

Table 4 shows the results of estimating equation (18) with different specifications of the controls for the change in the tax liability and mistagging exposure. Column (1) uses splines of the tax liability and fixed effects for deciles of exposure. Column (2) adds interactions of these with the high-tax side indicator and with each other. Column (3) replaces the exposure decile fixed effects with exposure splines, while column (4) instead replaces the tax liability splines with fixed effects for deciles of the tax liability.

We see that the estimated coefficient on the interaction between the high-tax side indicator and the size of the change in inequity is strongly negative and highly statistically significant at around -0.1. Converting this to an elasticity of compliance with respect to inequity yields an elasticity of 0.15 in column (1). Moreover, the results are highly robust to alternative specifications of the controls, with the elasticity only varying between 0.105 and 0.117. In Appendices E and F we provide evidence that the estimates are robust to sample selection decisions and definitions of compliance, respectively. This design requires the weakest assumptions and so we interpret it as our most robust, and hence preferred, estimate of the elasticity of compliance with respect to inequity.

6.3 Responses to Undertagging vs Overtagging

Our final design is aimed at distinguishing between the effects of overttagging $\sigma > 1$ and the effects of undertagging $\sigma < 1$. It also permits us to evaluate the dynamics of the causal effects and evaluate the plausibility of our parallel trends assumptions by studying trends in compliance leading up to the 2011 reform.

Formally, we make a “strong” parallel trends assumption (Callaway *et al.*, 2024) to allow us to estimate the impact of changes in inequity separately for those on the high-tax side of the boundary (who were predominantly overtaged before the reform and for whom this overtaging was reduced) and those on the low tax side of the boundary (who were undertagged before the reform and for whom this undertagging was reduced through the reform):

Assumption 6 (Strong Parallel Trends).

$$\begin{aligned} & \mathbb{E}[G(s_y, t_y, d, \mu, \nu_y, y) - G(s_0, t_0, d, \mu, \nu_0, 0) | \sigma_y = s_y, \sigma_0 = s_0, \tau_y = t_y, \tau_0 = t_0, D = d] \\ &= \mathbb{E}[G(s_y, t_y, d, \mu, \nu_y, y) - G(s_0, t_0, d, \mu, \nu_0, 0) | \tau_y = t_y, \tau_0 = t_0, D = d] \quad \forall y \end{aligned} \quad (19)$$

where $G(\sigma_y, \tau_y, D, \mu, \nu_y, y)$ are the compliance potential outcomes, and we choose the base year $y = 0$ to be 2010.

Assumption 6 requires parallel trends in compliance between any pair of inequity levels σ_y and σ_0 such that we can estimate effects of changes in inequity using dynamic difference in differences designs. Specifically, we are interested in estimating the effects of changes in inequity for the undertagged households on the low-tax side of tax sector boundaries and the undertagged households on the high-tax side. We do so by estimating the following equation:

$$c_{iy} = \alpha_i + \lambda_{r(i)y} + \sum_{j \neq 2010} D_{jy} \times \left[f_{0j}(d_i) + \beta_{0j}\Delta\tau_i + \eta_{0j}\Delta\sigma_i + HTS_i \times (\delta_j + f_{1j}(d_i) + \beta_{1j}\Delta\tau_i + \eta_{1j}\Delta\sigma_i) \right] + \varepsilon_{iy} \quad (20)$$

where $\lambda_{r(i)y}$ are segment-year fixed effects, $D_{jy} \equiv \mathbf{1}[y = j]$ are year dummies, and we include year-specific distance controls $f_{0j}(d_i)$ and $f_{1j}(d_i)$; and year-specific controls for property i 's tax liability change due to the reform. We estimate the equation using our main sample as described in 2.4. In Appendices E and F we provide evidence that the estimates are robust to sample selection decisions and definitions of compliance, respectively.

Figure 12 shows the impacts of the reform. Panel A shows the impacts on the high-tax side. It plots the η_{1j} coefficients from equation (20) along with their 95% confidence intervals. We see that the estimated coefficients in years before the reform are all indistinguishable from zero, consistent with our strong parallel trends assumption on the high-tax side. We also see that the coefficients become negative after the reform, indicating that compliance by properties receiving larger cuts to inequity improves relative to properties receiving smaller cuts to inequity. This suggests that the inequity generated by overtagging has strong effects on compliance. Somewhat surprisingly, the effects emerge immediately following the reform's enactment in 2011 despite the fact that the reform was phased in over 5 years. This is likely due to the high salience of the reform as it was being implemented.

Panel B shows the impacts on the low-tax side. It plots the η_{0j} coefficients along with their 95% confidence intervals. Again, we see no evidence against our strong parallel trends assumption on the low-tax side of the boundary. If the effects of undertagging were symmetric to the effects of overtagging, we would expect that as undertagging is removed, households become relatively *less* compliant, and we would expect to see a similar pattern in panel B as we see in panel A. However, we see that the post-reform coefficients in panel B are consistently indistinguishable from zero, suggesting no impact of undertagging and that all of the responses to inequity come from taxpayers resenting being overtagged. This is consistent with the findings in Dube *et al.* (2019a) studying labor market behavior in the US. They find that workers' quit behavior is responsive to wage rises for their higher-paid peers (the analog of overtagging in our setting) but not to wage increases for their lower-paid peers.

In summary, across a range of augmented BDD designs, we find consistent evidence of the importance of inequity for tax compliance. The estimated elasticity of compliance with respect to inequity ranges from 0.11 to 0.28. Moreover, these responses are driven exclusively by resentment of overtagging. We cannot reject the hypothesis that undertagging has no effect on compliance.

7 Implications for Tax Design

Our empirical analysis in sections 5 and 6 above shows compelling evidence for the presence of behavioral responses to the presence of mistagging. We use a range of empirical designs to quantify the size of the responses, yielding estimates of the elasticity of compliance with respect to inequity η between 0.11 and 0.28. In this section we use our stylized conceptual framework introduced in section 3 to sketch the implications of our findings for tax design.

As discussed in section 3, the presence of behavioral responses to inequity has drastically different implications than behavioral responses to the dollar value of the tax liability. Figure 13 performs a simple calibration of our theoretical model to illustrate this point. The overall compliance change can be decomposed between the two behavioral mechanisms according to $-dc/c = \eta d\sigma/\sigma + \varepsilon dT/T$. In figure 13, we hold fixed the size of the overall response, but vary the share of the response that we attribute to the inequity elasticity η .⁴⁸

In figure 3, we estimate that the overall change in compliance at the sector boundaries is eight percent.⁴⁹ But as figure 4 shows, this is the response to a combination of a 13% increase in the tax liability and a 62% increase in inequity. Since our results (e.g. the analysis in figure 12) suggest that there is no response to undertagging, we treat the effective change in inequity as only the removal of overtagging — a change of 31% in σ . With these in place, we simulate the optimal tax schedule in proposition 2 for an inequity response that accounts for between 0 and 75% of the overall response.⁵⁰

Panel A of figure 13 shows the optimal tax burdens T_l/y_L in blue, and T_h/y_H in pink. The heavy, green line shows the progressivity of the tax schedule $\frac{T_h}{y_H}/\frac{T_l}{y_L}$. We can see that the source of the behavioral responses to taxation matters dramatically for the implications for the optimal tax schedule. The optimal tax rates on high-value properties is 2.6 times larger when inequity responses account for 75% of the overall response than when inequity responses are absent. For low-value properties, the tax rate is nine times larger, such that the progressivity of the tax schedule ranges between 1 and 3.7.

This comes about because the comparative statics of the optimal tax schedule with respect to the response to the tax liability (governed by the elasticity ε) and with respect to the response to inequity (governed by the elasticity η) have opposite signs: More responsiveness to the tax

⁴⁸Specifically, we vary the fraction of the overall response coming from behavioral responses to inequity $\eta \frac{d\sigma}{\sigma} / -\frac{dc}{c}$.

⁴⁹The point estimate is a reduction of six percentage points from a base of 75% compliance.

⁵⁰We set the parameters as follows: $\psi = 0.1$, $\rho = 3$, $y_H = Rs.6,630$, $y_L = Rs.4,911.5$, $b(r) = 1$, $g_H/g_L = 1.6$. See Appendix K for full details.

liability implies a *more* progressive tax schedule, while more responsiveness to inequity implies a *less* progressive tax schedule.

Our baseline estimates are $\eta = 0.12$ and $\varepsilon = 0.33$, implying that responses to inequity account for 46% of the overall change in compliance, demarcated by the dashed vertical line in the figure. These estimates imply a markedly less progressive tax schedule than would be the case if the compliance change were attributed fully to the response to the tax liability change. Absent responses to inequity, the optimal tax schedule sets the rate on high-value properties 3.7 times larger than the rate on low-value properties. But at our baseline estimates, this drops to 1.6, only 44% of the progressivity without inequity responses. In appendix K we show that this conclusion ranges from 41% to 48% when we consider optimal tax schedules under redistributive preferences g_H/g_L ranging from 1.4 to 1.8.⁵¹

Our findings that taxpayers respond strongly to the presence of inequity in the tax schedule also imply that there are large returns to investments in improving the fiscal capacity with which to differentiate between high- and low-value properties. Improving this requires the state to invest in the capacity to compute more accurate assessments of properties' values. One promising avenue for such improvements could be to leverage the fact that as the property market thickens and moves online, there are large datasets of property asking prices available on the internet. To explore this, we bring to bear a dataset of property listings from Viva Real, a property listing platform, as discussed in appendix J.

We begin by computing the effective tax rate for each property in our merged dataset. These rates vary dramatically, with a coefficient of variation of 2.5. The Root Mean Squared Error (RMSE) of the assessed values as predictions of the asking prices is large, at $RMSE_1 = 1.36$ million Reais.⁵² Second, we consider a simple possible improvement: How much better would it be possible to do by using data on asking prices to recalibrate the coefficients in the existing property tax formula? By optimizing these coefficients we estimate that the RMSE can be brought down from 1.36 million to $RMSE_2 = 1.08$ million. This simple exercise has the advantage of being transparent and not requiring wholesale legislative changes to the existing formula, but has the disadvantage of not exploiting the richness of the data available in the government's cadaster fully since the formula is likely to be misspecified.

As a third exercise, we consider how much better it might be possible to do by using only the data in the cadaster already available to the government, but with a more complex estimation of properties' assessed values. In particular, we train a random forest model to predict properties' asking values using the property features contained in the government's cadaster. This brings the RMSE down to $RMSE_3 = 805$ thousand. The significant improvement in the MSE suggests that the government's current property assessment formula is, indeed, significantly misspecified as well as featuring sub-optimal coefficients. Finally, we consider what could be done if we also incorporate additional property attributes available in the Viva Real data but not in the

⁵¹The appendix also presents comparative statics with respect to the model's other parameters as well as simulations of the extensions to the model presented in sections 3.3.1 and 3.3.2.

⁵²Appendix L contains the full details of this calculation and the exercises that follow.

cadaster.⁵³ This yields a further reduction in the RMSE, bringing it down to $RMSE_4 = 374$ thousand. In summary, these exercises suggest that by leveraging more recently available property listing data and standard machine-learning tools, the government may be able to reduce misclassification by 21–73%.

In our model, the government’s ability to correctly differentiate between property types is captured by ψ , the fraction of L -type houses that are erroneously given the h tag. In our baseline simulations, we set this probability to 10%. In panel B of figure 13 we explore how changing the extent of mistagging ψ affects the optimal tax policy. We see that completely eliminating mistagging would allow for the progressivity of the tax schedule to increase by 54% from 1.99 to 3.06. More circumspectly, the reductions in misclassification suggested by our simple exercises recalibrating the existing property assessment formula, would allow the government to reduce misclassification (which we model as a proportional reduction in ψ of the same size as the reduction in the RMSE) by 21% and increase progressivity by 9% to 2.17.

Reducing misclassification further by using machine-learning tools to use the attributes in the cadaster to predict property values would reduce misclassification by 41% and allow the government to increase progressivity by 19% to 2.36. Finally, reaching the reductions in misclassification implied by fully leveraging the property listings data would allow the government to reduce misclassification by as much as 73% and increase progressivity by 36% to 2.7. These striking results highlight the large returns to investments in the fiscal capacity to improve differentiation between properties with different market values.

8 Conclusion

Property taxes are an important source of government revenues, particularly for local governments, but they are seldom based on direct evaluations of market prices. Rather, they are overwhelmingly based on presumptive formulas that approximate properties’ values using a limited set of observable characteristics. Indeed, observable tags are used throughout tax codes, especially in low- and middle-income taxes where presumptive taxes are ubiquitous and eligibility for benefits is commonly based on proxy-means tests. A large literature has emphasized the consequences of the limited statistical precision of imperfect tags for eligibility (Besley & Kanbur, 1988) and the moral hazard presumptive taxes induce (Oates & Schwab, 2015; Gaubert *et al.*, 2021). We introduce a novel force into this discussion — direct behavioral responses to the inevitable inequity that imperfect tagging generates.

Our conceptual framework shows how imperfect tagging leads to both lower tax revenues overall, and less progressive taxation. In our empirical analysis of Manaus’ presumptive property tax we provide evidence that these behavioral responses are strong. Using a range of research designs extending the Boundary Discontinuity Design (BDD), we estimate that the elasticity of compliance is in the range of 0.11–0.28. These estimates suggest that responses to in-

⁵³These features are detailed in Appendix L.

equity account for half of the overall reduction in compliance observed at the boundaries of tax sectors.⁵⁴

Given the ubiquity of presumptive taxes throughout the world, these findings have profound implications for the design of tax systems. Imperfect tagging places severe constraints on governments' ability to raise revenues, and on their ability to redistribute through the tax code. And as a result, our findings suggest that there are large returns to investments in fiscal capacity that can allow governments to use more precise tags, reducing the extent of mistagging, the resulting inequity, and the consequent behavioral responses that raise the efficiency cost of taxation.

Our measure of inequity is a “selfish” notion of inequity. That is, our measure captures the extent to which an individual taxpayer may feel that they themselves are over/under-taxed. This has the great advantage of being easily and precisely operationalized, but does not capture the extent to which taxpayers may care about how much *others* have to pay in taxes. In particular, it cannot capture traditional notions of vertical equity regarding preferences over how the burden of taxation is distributed across groups of taxpayers with different abilities to pay. This suggests that a more comprehensive evaluation of these effects, incorporating both horizontal and vertical elements of inequity is a promising direction for future research.

⁵⁴To see this, note that the drop in compliance dc/c in figure 3 is $-0.06/0.75 = -0.08$. In figure 4 we see that $dT/T = 0.13$ and $d\sigma/\sigma = 0.62$. However, as we show in section 6.3, inequity responses are driven exclusively by overtagging, and so the effective $d\sigma/\sigma$ is only half of this: 0.31. Combining these through the relationship $-dc/c = \varepsilon dT/T + \eta d\sigma/\sigma$, the responses to inequity account for half of the overall response.

References

- AJZENMAN, NICOLAS, CRUCES, GUILLERMO, PEREZ-TRUGLIA, RICARDO, TORTAROLO, DARÍO, & VAZQUEZ-BARE, GONZALO. 2025. *From Flat to Fair? The Effects of a Progressive Tax Reform*. NBER working paper # 33286. 6, 12
- AKERLOF, GEORGE A. 1978. The economics of "tagging" as applied to the optimal income tax, welfare programs, and manpower planning. *The American economic review*, 68(1), 8–19. 1, 6
- ALLCOTT, HUNT, & TAUBINSKY, DMITRY. 2015. Evaluating Behaviorally Motivated Policy: Experimental Evidence from the Lightbulb Market. *American Economic Review*, 105, 2501–2538. 91
- AUERBACH, ALAN J., & HASSETT, KEVIN A. 2002. A New Measure of Horizontal Equity. *American Economic Review*, 92(4), 1116–1125. 27, 69
- BALAN, PABLO, BERGERON, AUGUSTIN, TOUREK, GABRIEL, & WEIGEL, JONATHAN. 2022. Local Elites as State Capacity: How City Chiefs use Local Information to Increase Tax Compliance in D.R. Congo. *American Economic Review*, 112, 1–36. 6
- BAYER, PATRICK, FERREIRA, FERNANDO, & McMILLAN, ROBERT. 2007. A Unified Framework for Measuring Preferences for Schools and Neighborhoods. *Journal of Political Economy*, 115(4). 2, 3, 6, 19, 20, 9
- BERGERON, AUGUSTIN, TOUREK, GABRIEL, & WEIGEL, JONATHAN. 2024a. The State Capacity Ceiling on Tax Rates: Evidence from Randomized Tax Abatements in the DRC. *Econometrica*, 92, 1163–1193. 6
- BERGERON, AUGUSTIN, BESSONE, P, KABEYA, JK, TOUREK, GABRIEL, & WEIGEL, JONATHAN. 2024b. *Supermodular Bureaucrats: Evidence from Randomly Assigned Tax Collectors in the DRC*. forthcoming, American Economic Review. 6
- BESLEY, TIMOTHY, & COATE, STEPHEN. 1992. Workfare versus Welfare: Incentive Arguments for Work Requirements in Poverty-Alleviation Programs. *American Economic Review*, 82, 249–261. 6
- BESLEY, TIMOTHY, & KANBUR, RAVI. 1988. Food Subsidies and Poverty Alleviation. *The Economic Journal*, 98, 701–719. 37
- BLACK, SANDRA E. 1999. Do Better Schools Matter? Parental Valuation of Elementary Education. *The Quarterly Journal of Economics*, 114(2), 577–599. 2, 3, 6, 19, 9
- BROCKMEYER, ANNE, ESTEFAN, ALEJANDRO, ARRAS, KARINA RAMÍREZ, & SERRATO, JUAN CARLOS SUÁREZ. 2023. *Taxing property in developing countries: theory and evidence from Mexico*. National Bureau of Economic Research Working Paper. 6, 21, 91
- CABRAL, MARIKA, & HOXBY, CAROLINE. 2012. *The hated property tax: salience, tax rates, and tax revolts*. Tech. rept. National Bureau of Economic Research. 6, 9, 5
- CALLAWAY, BRANTLY, GOODMAN-BACON, ANDREW, & SANT'ANNA, PEDRO H.C. 2024. *Difference-in-Differences with a Continuous Treatment*. Mimeo: Emory University: <https://doi.org/10.48550/arXiv.2107.02637>. 5, 28, 31, 33

- CALONICO, SEBASTIAN, CATTANEO, MATIAS D., & TITIUNIK, ROCIO. 2014. Robust Nonparametric Confidence Intervals for Regression-Discontinuity Designs. *Econometrica*, **82**(6), 2295–2326. [21](#), [74](#), [77](#)
- CALONICO, SEBASTIAN, CATTANEO, MATIAS D., & FARRELL, MAX H. 2018. On the Effect of Bias Estimation on Coverage Accuracy in Nonparametric Inference. *Journal of the American Statistical Association*, **113**(522), 767–779. [21](#), [74](#), [77](#)
- CALONICO, SEBASTIAN, CATTANEO, MATIAS D., FARRELL, MAX H., & TITIUNIK, ROCÍO. 2019. Regression Discontinuity Designs Using Covariates. *The Review of Economics and Statistics*, **101**(3), 442–451. [21](#), [74](#), [77](#)
- CALONICO, SEBASTIAN, CATTANEO, MATIAS D., & FARRELL, MAX H. 2020. Optimal Bandwidth Choice for Robust Bias-Corrected Inference in Regression Discontinuity Designs. *Econometrics Journal*, **23**, 192–210. [21](#), [74](#), [77](#)
- CARD, DAVID, MAS, ALEXANDRE, MORETTI, ENRICO, & SAEZ, EMMANUEL. 2012. Inequality at work: The effect of peer salaries on job satisfaction. *American Economic Review*, **102**(6), 2981–3003. [1](#), [12](#)
- CARVALHO JUNIOR, PEDRO HUMBERTO BRUNO. 2017. *Property tax performance and potential in Brazil*. Ph.D. thesis, University of Pretoria. [4](#)
- CASTRO, LUCIA, & SCARTASCINI, CARLOS. 2015. Tax Compliance and Enforcement in the Pam-pas: Evidence from a Field Experiment. *Journal of Economic Behavior & Organization*, 65–82. [6](#)
- CHENOZHUKOV, VICTOR, & HANSEN, CHRISTIAN. 2005. An IV Model of Quantile Treatment Effects. *Econometrica*, **73**, 245–261. [24](#)
- CHETTY, RAJ. 2006. A General Formula for the Optimal Level of Social Insurance. *Journal of Public Economics*, **90**, 1879–1901. [89](#)
- CRUCES, GUILLERMO, PEREZ-TRUGLIA, RICARDO, & TETAZ, MARTIN. 2013. Biased perceptions of income distribution and preferences for redistribution: Evidence from a survey experiment. *Journal of Public Economics*, **98**, 100 – 112. [6](#)
- DEL CARPIO, LUCIA. 2016. *Are the Neighbors Cheating? Evidence from a Social Norm Experiment on Property Taxes in Peru*. mimeo: INSEAD. [6](#)
- DIAMOND, PETER A. 1975. A Many-person Ramsey Tax Rule. *Journal of Public Economics*, **4**, 335–342. [14](#)
- DONG, YINGYING, LEE, YING-YING, & GOU, MICHAEL. 2023. Regression Discontinuity Designs With a Continuous Treatment. *Journal of the American Statistical Association*, **118**, 208–221. [22](#), [23](#), [24](#), [25](#), [102](#)
- DUBE, ARINDRAJIT, GIULIANO, LAURA, & LEONARD, JONATHAN. 2019a. Fairness and Fric-tions: The Impact of Unequal Raises on Quit Behavior. *American Economic Review*, **109**, 620–663. [1](#), [34](#)
- DUBE, ARINDRAJIT, GIULIANO, LAURA, & LEONARD, JONATHAN. 2019b. Fairness and fric-tions: The impact of unequal raises on quit behavior. *American Economic Review*, **109**(2), 620–663. [12](#), [13](#)

DZANSI, JAMES, JENSEN, ANDERS, LAGAKOS, DAVID, & TELLI, HENRY. 2024. *Technology and Tax Capacity: Evidence from Local Governments in Ghana*. NBER working paper number 29923. 6

ELMINEJAD, ALI, HAVRANEK, TOMAS, & IRSOVA, ZUZANA. 2025. Relative Risk Aversion: A Meta-Analysis. *Journal of Economic Surveys*, n/a(n/a). 82

FACK, GABRIELLE, & GRENET, JULIEN. 2010. When do better schools raise housing prices? Evidence from Paris public and private schools. *Journal of public Economics*, 94(1-2), 59–77. 9

FELDSTEIN, MARTIN S. 1972. Distributional Equity and the Optimal Structure of Public Prices. *American Economic Review*, 62, 32–36. 14

FRÖLICH, MARKUS, & HUBER, MARTIN. 2019. Including Covariates in the Regression Discontinuity Design. *Journal of Business & Economic Statistics*, 37, 736–748. 22, 23

GAUBERT, CECILE, KLINE, PATRICK, VERGARA, DAMIEN, & YAGAN, DANNY. 2021. *Place-Based Redistribution*. Mimeo: UC Berkeley. 6, 37

GIACCOBASSO, MATIAS, NATHAN, BRAD, PEREZ-TRUGLIA, RICARDO, & ZENTNER, ALEJANDRO. 2022. Where Do My Tax Dollars Go? Tax Morale Effects of Perceived Government Spending. *NBER Working Paper No. 29789*. 6

GIBBONS, STEPHEN, MACHIN, STEPHEN, & SILVA, OLMO. 2013. Valuing school quality using boundary discontinuities. *Journal of Urban Economics*, 75, 15–28. 9

HVIDBERG, KRISTOFFER B, KREINER, CLAUS T, & STANTCHEVA, STEFANIE. 2023. Social positions and fairness views on inequality. *Review of Economic Studies*, 90(6), 3083–3118. 1, 6, 12

IMBENS, GUIDO, & NEWHEY, WHITNEY. 2009. Identification and Estimation of Triangular Simultaneous Equations Models Without Additivity. *Econometrica*, 77, 1481–1512. 25

KAPON, SAMUEL, DEL CARPIO, LUCIA, & CHASSANG, SYLVAIN. 2024. *Using Divide-and-Conquer to Improve Tax Collection*. forthcoming, Quarterly Journal of Economics. 6

KEELE, LUKE J, & TITIUNIK, ROCIO. 2015. Geographic boundaries as regression discontinuities. *Political Analysis*, 23(1), 127–155. 9

KEEN, MICHAEL, & SLEMROD, JOEL. 2021. *Rebellion, Rascals, and Revenue: Tax Follies and Wisdom Through the Ages*. Princeton University Press. 1

KUZIEMKO, ILYANA, NORTON, MICHAEL, SAEZ, EMMANUEL, & STANTCHEVA, STEFANIE. 2015. How Elastic are Preferences for Redistribution? Evidence from Randomized Survey Experiments. *American Economic Review*, 105, 1478–1508. 6

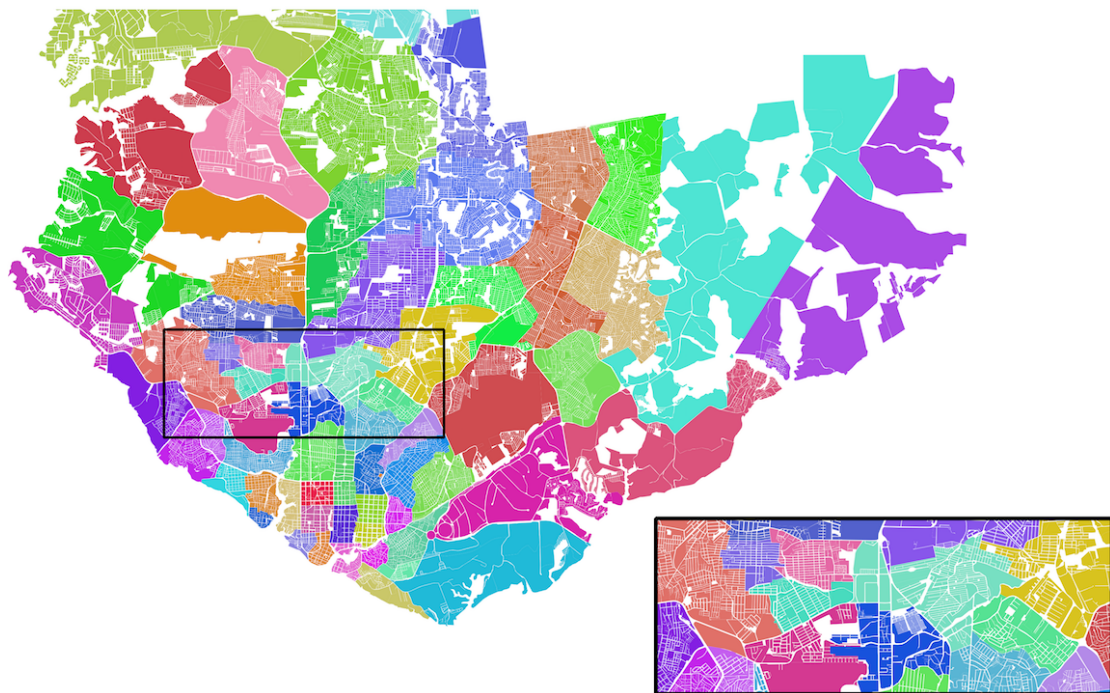
LIVY, MITCHELL R. 2018. Intra-school district capitalization of property tax rates. *Journal of Housing Economics*, 41, 227–236. 9

LUTTMER, ERZO, & SINGHAL, MONICA. 2014. Tax Morale. *Journal of Economic Perspectives*, 28, 149–168. 6

- MANKIW, N GREGORY, & WEINZIERL, MATTHEW. 2010. The optimal taxation of height: A case study of utilitarian income redistribution. *American Economic Journal: Economic Policy*, **2**(1), 155–176. [6](#)
- NATHAN, BRAD, PEREZ-TRUGLIA, RICARDO, & ZENTNER, ALEJANDRO. 2023. Paying Your Fair Share: Perceived Fairness and Tax Compliance. *NBER Working Paper No. 32588*. [6](#)
- NATHAN, BRAD, PEREZ-TRUGLIA, RICARDO, & ZENTNER, ALEJANDRO. 2025. My Taxes Are Too Darn High: Why Do Households Protest Their Taxes? *American Economic Journal: Economic Policy*, **17**(1), 273–310. [6](#)
- NICHOLS, ALBERT L, & ZECKHAUSER, RICHARD J. 1982. Targeting Transfers through Restrictions on Recipients. *American Economic Review*, **72**, 372–377. [6](#)
- OATES, WALLACE E, & SCHWAB, ROBERT M. 2015. The window tax: A case study in excess burden. *Journal of Economic Perspectives*, **29**(1), 163–180. [37](#)
- OKUNOGBE, OYEBOLA. 2023. *Becoming Legible to the State: The Role of Detection and Enforcement Capacity on Tax Compliance*. mimeo: World Bank. [6](#)
- REDDING, STEPHEN J., & ROSSI-HANSBERG, ESTEBAN. 2017. Quantitative Spatial Economics. *Annual Review of Economics*, **9**, 21–58. [17](#)
- RING, MARIUS AK. 2024. Wealth taxation and household saving: Evidence from assessment discontinuities in Norway. *Review of Economic Studies*, rdae100. [7](#), [9](#)
- SAEZ, EMMANUEL, & STANTCHEVA, STEFANIE. 2016. Generalized Social Marginal Welfare Weights for Optimal Tax Theory. *American Economic Review*, **106**, 24–45. [6](#), [14](#)
- SCHÖNHOLZER, DAVID. 2022. *Measuring Preferences for Local Governments*. Working Paper. [7](#), [9](#)
- SCOTT, JAMES C. 1998. *Seeing Like a State*. Yale University Press. [1](#)
- SLEMROD, JOEL. 2019. Tax Compliance and Enforcement. *Journal of Economic Literature*, **57**, 904–954. [6](#)
- SMITH, ADAM. 1776. *An Inquiry into the Nature and Causes of the Wealth of Nations*. London: W. Strahan and T. Cadell. Chap. Book V, Chapter 2: Of the Sources of the General or Public Revenue of the Society. [1](#)
- TURNER, MATTHEW A, HAUGHWOUT, ANDREW, & VAN DER KLAUW, WILBERT. 2014. Land use regulation and welfare. *Econometrica*, **82**(4), 1341–1403. [9](#)
- TWAIT, AARON, & LANGLEY, ADAM. 2024. *50-State Property Tax Comparison Study*. Lincoln Institute of Land Policy. [8](#)
- WEIGEL, JONATHAN. 2020. The Participation Dividend of Taxation: How Citizens in Congo Engage More with the State When it Tries to Tax Them. *Quarterly Journal of Economics*, **135**, 1849–1903. [6](#)

Figures & Tables

FIGURE 1: TAX SECTOR BOUNDARIES



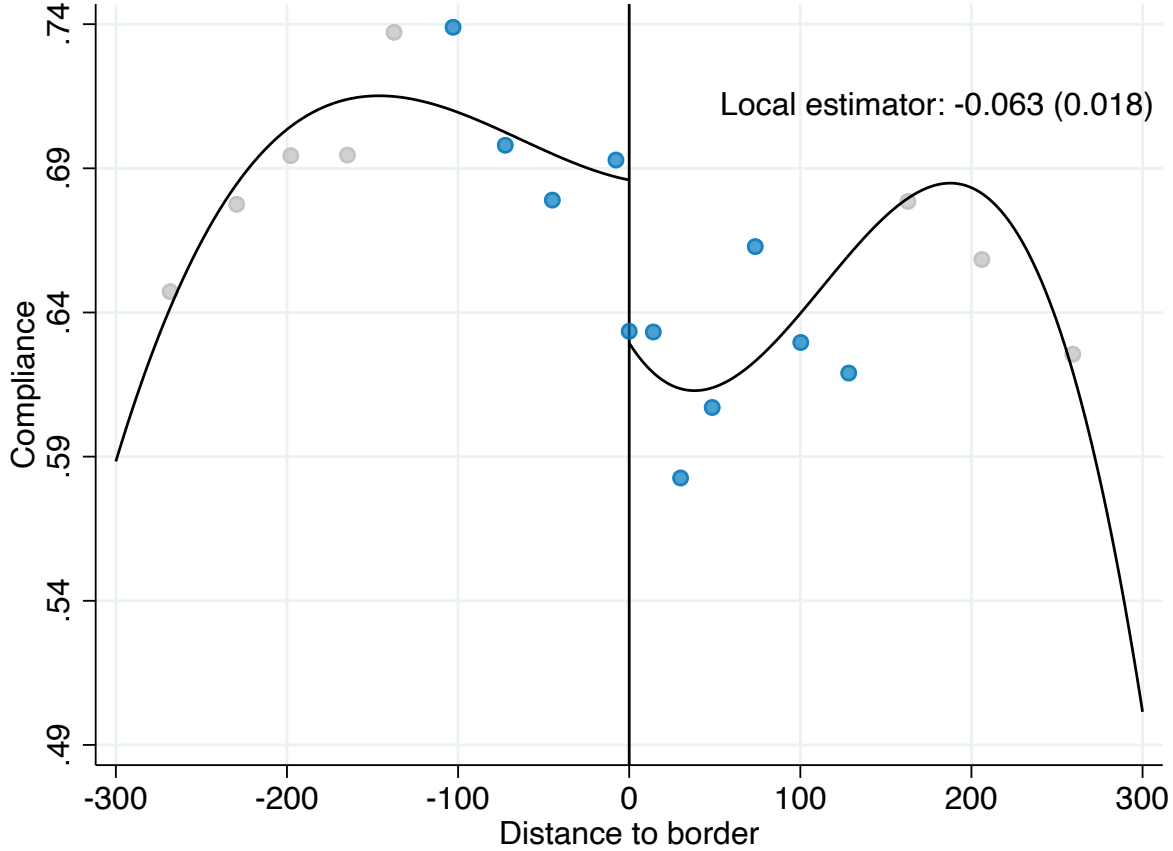
Notes: The figure shows a map of the city of Manaus, with colors highlighting the different tax sectors created by SEMEF in 1983. Within each sector, properties are assigned the same square meter land value. The rectangle zooms in on an area of the city to show more clearly the tax sector boundaries.

FIGURE 2: SECTORS CREATE ARBITRARY BOUNDARIES



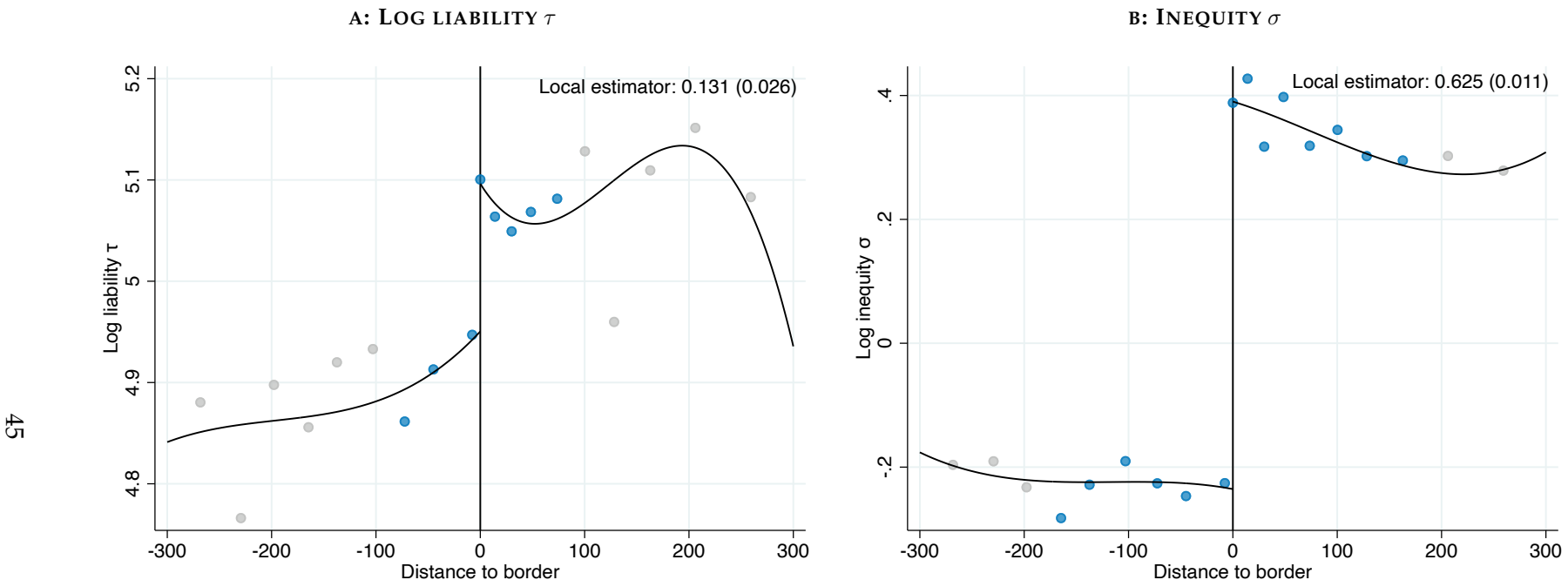
Notes: The tax sectors can create arbitrary boundaries where very similar houses are assigned different tax bills. This photo shows one of the boundaries highlighted in Figure 1. Map data: © 2018 Google.

FIGURE 3: OVERALL CHANGE IN COMPLIANCE AT TAX SECTOR BOUNDARIES



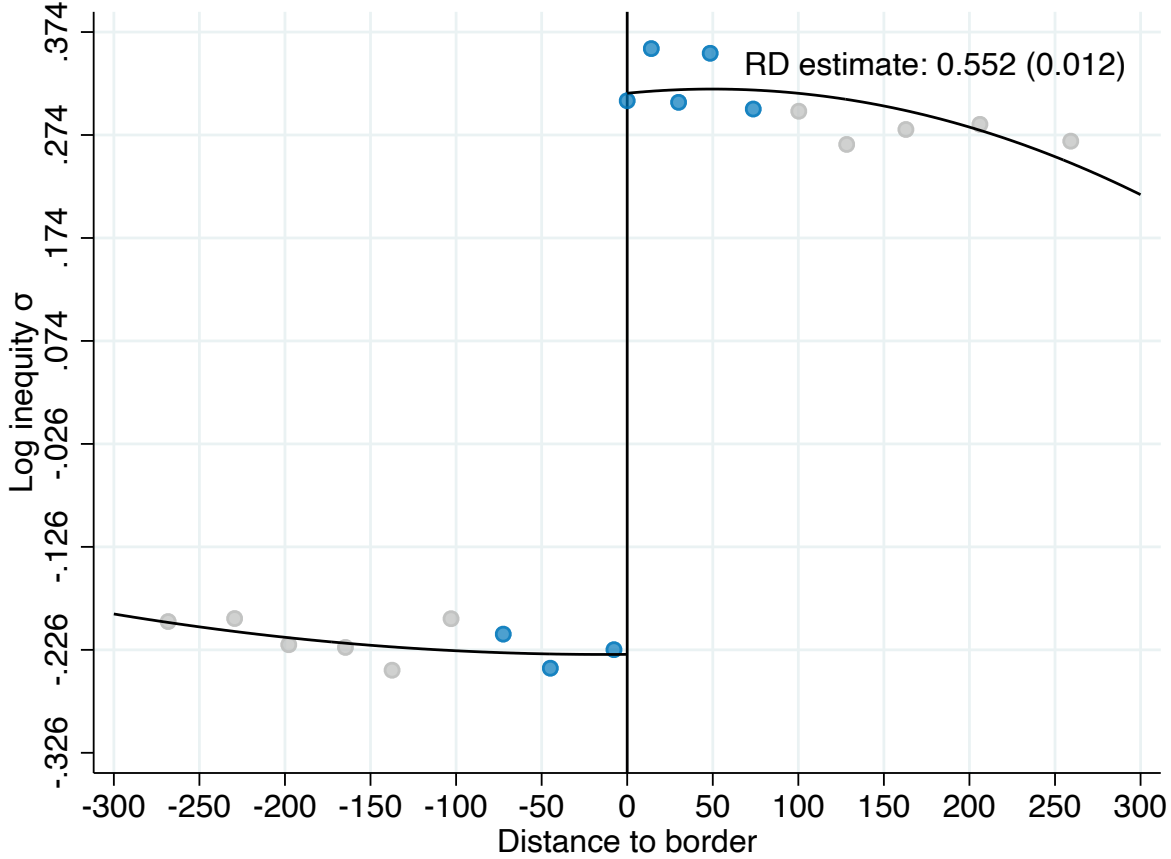
Notes: The figure shows the overall change in compliance at tax sector boundaries discussed in section 4.1. Specifically, we show the results of estimating equation (10) for compliance c_i by taxpayer i : $c_i = \lambda_{r(i)} + f_0(d_i) + \beta_0 HTS_i + f_1(d_i) \times HTS_i + \varepsilon_i$ where $\lambda_{r(i)}$ are boundary-segment fixed effects, HTS_i is an indicator for being on the high-tax side of the boundary ($d_i > 0$); $f_0(d_i)$ and $f_1(d_i)$ control for distance to the boundary on the low- and high-tax sides of the boundary, respectively; and ε_i is the residual. Overlaid on the figure, we show the point estimate of the discontinuity in compliance estimated using local linear distance controls, the MSE-minimizing bandwidth, and triangular kernel weights in distance. The dots in the figure show the coefficients from estimating (10) with fixed effects for decile-spaced bins of distance, using the same triangular kernel weights but censoring them at their tenth percentile to give non-zero weights to distances outside the optimal bandwidth. The bins in the optimal bandwidth are shown in blue while those outside are shown in gray. The black line is a global cubic polynomial fit in the same way.

FIGURE 4: OVERALL CHANGE IN INEQUITY AND LIABILITY AT TAX SECTOR BOUNDARIES



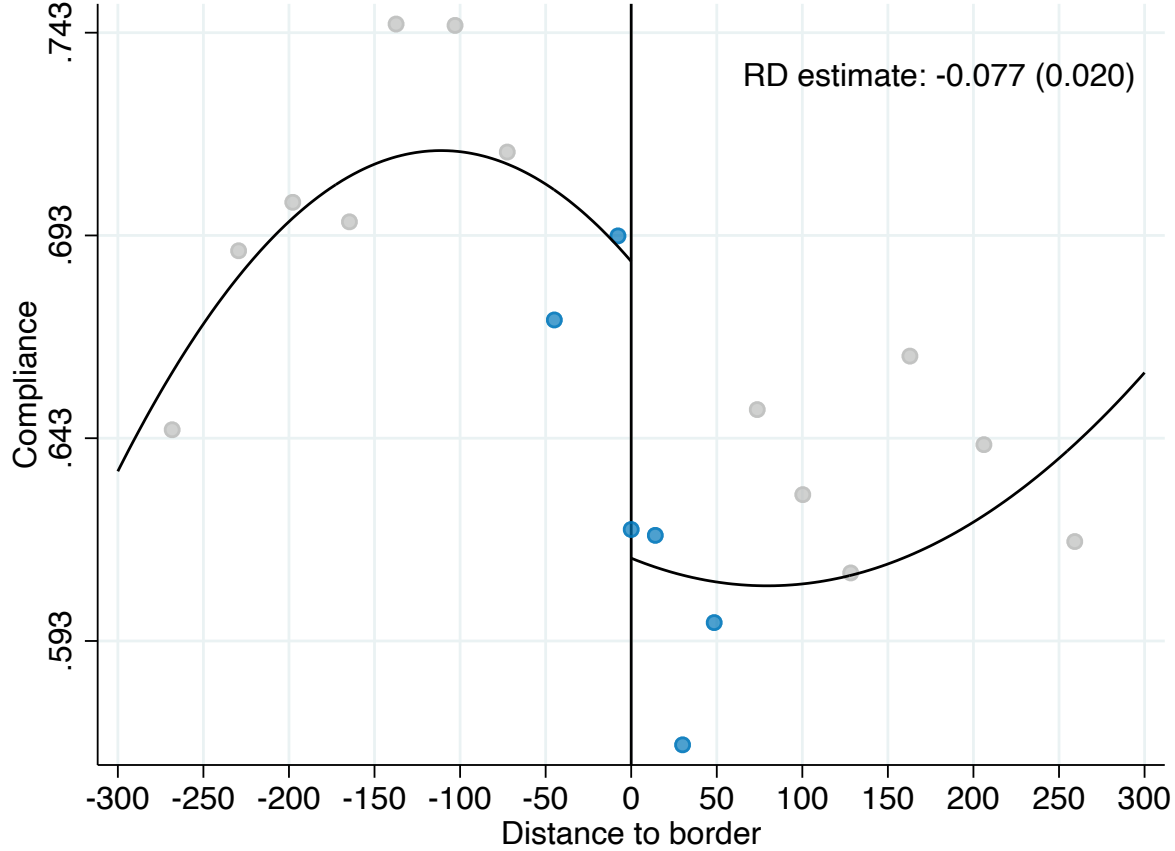
Notes: The figure shows the overall change in compliance at tax sector boundaries discussed in section 4. Specifically, we show the results of estimating the following equation (10) for log liability and inequity y_i by taxpayer i : $y_i = \lambda_{r(i)} + f_0(d_i) + \beta_0 HTS_i + f_1(d_i) \times HTS_i + \varepsilon_i$ where $\lambda_{r(i)}$ are boundary-segment fixed effects, HTS_i is an indicator for being on the high-tax side of the boundary ($d_i > 0$); $f_0(d_i)$ and $f_1(d_i)$ control for distance to the boundary on the low- and high-tax sides of the boundary, respectively; and ε_i is the residual. The outcome variable y_i is log liability τ in panel A and inequity σ in panel B. Overlaid on the figure, we show the point estimate of the discontinuity in the outcome variable estimated using local linear distance controls, the MSE-minimizing bandwidth, and triangular kernel weights in distance. The dots in the figure show the coefficients from estimating (10) with fixed effects for decile-spaced bins of distance, using the same triangular kernel weights but censoring them at their tenth percentile to give non-zero weights to distances outside the optimal bandwidth. The bins in the optimal bandwidth are shown in blue while those outside are shown in gray. The black line is a global cubic polynomial fit in the same way.

FIGURE 5: AUGMENTED BOUNDARY DISCONTINUITY DESIGN: FIRST STAGE



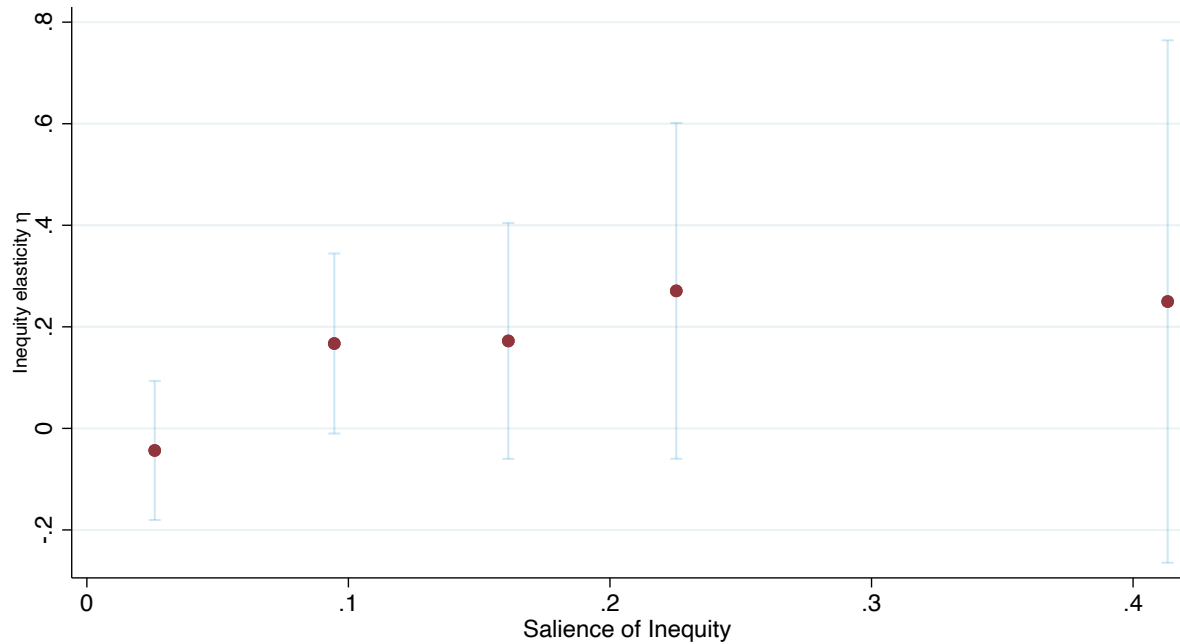
Notes: The figure shows the first stage impact on inequity in the augmented BDD discussed in section 5.1. Specifically, we show the results of estimation of equation (12): $\log(\sigma_i) = \lambda_{r(i)} + g(\tau_i, e_i) + f_0(d_i) + \beta_0 HTS_i + f_1(d_i) \times HTS_i + \varepsilon_i$ using log-inequity σ as the outcome variable, where $\lambda_{r(i)}$ are fixed effects for 500-meter segments along the boundaries to ensure we are comparing properties who are nearby each other; $g(\tau_i, e_i)$ are flexible controls for property i 's (log) tax liability τ_i and exposure to mistagging e_i (our baseline estimates use τ splines and exposure deciles); $f_0(d_i)$ and $f_1(d_i)$ control flexibly for distance to the boundary on the low- and high-tax sides of the boundary respectively; and HTS_i is an indicator for properties on the high-tax side of the boundary ($d_i > 0$). Overlaid on the figure, we show the point estimate of the discontinuity in inequity estimated using local linear distance controls, the MSE-minimizing bandwidth, and triangular kernel weights in distance. The dots in the figure show the coefficients from estimating (12) with fixed effects for decile-spaced bins of distance, using the same triangular kernel weights but censoring them at their tenth percentile to give non-zero weights to distances outside the optimal bandwidth. The bins in the optimal bandwidth are shown in blue while those outside are shown in gray. The black line is a global cubic polynomial fit in the same way.

FIGURE 6: AUGMENTED BOUNDARY DISCONTINUITY DESIGN: COMPLIANCE EFFECTS



Notes: The figure shows the first stage impact on inequity in the augmented BDD discussed in section 5.1. Specifically, we show the results of estimation of equation (12): $c_i = \lambda_{r(i)} + g(\tau_i, e_i) + f_0(d_i) + \beta_0 HTS_i + f_1(d_i) \times HTS_i + \varepsilon_i$ using compliance as the outcome variable, where $\lambda_{r(i)}$ are fixed effects for 500-meter segments along the boundaries to ensure we are comparing properties who are nearby each other; $g(\tau_i, e_i)$ are flexible controls for property i 's (log) tax liability τ_i and exposure to mistagging e_i (our baseline estimates use τ splines and exposure deciles); $f_0(d_i)$ and $f_1(d_i)$ control flexibly for distance to the boundary on the low- and high-tax sides of the boundary respectively; and HTS_i is an indicator for properties on the high-tax side of the boundary ($d_i > 0$). Overlaid on the figure, we show the point estimate of the discontinuity in inequity estimated using local linear distance controls, the MSE-minimizing bandwidth, and triangular kernel weights in distance. The dots in the figure show the coefficients from estimating (12) with fixed effects for decile-spaced bins of distance, using the same triangular kernel weights but censoring them at their tenth percentile to give non-zero weights to distances outside the optimal bandwidth. The bins in the optimal bandwidth are shown in blue while those outside are shown in gray. The black line is a global cubic polynomial fit in the same way.

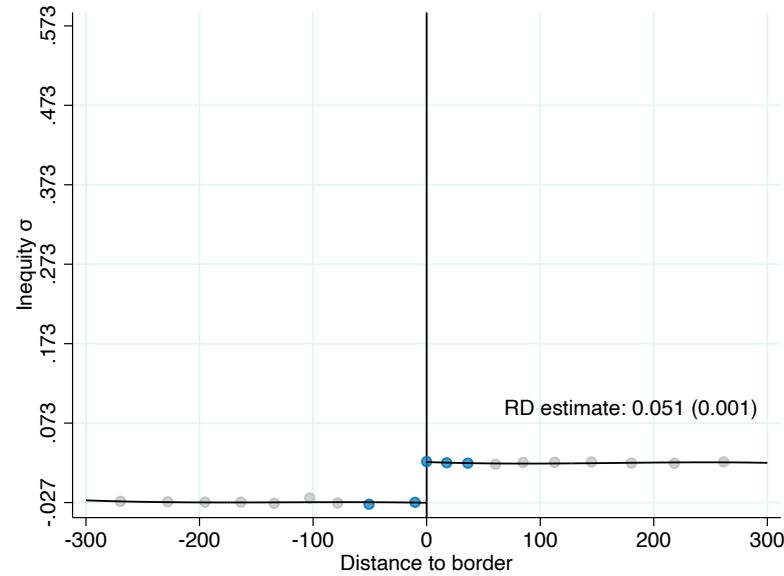
FIGURE 7: HETEROGENEITY OF THE COMPLIANCE ELASTICITY BY SALIENCE OF INEQUITY



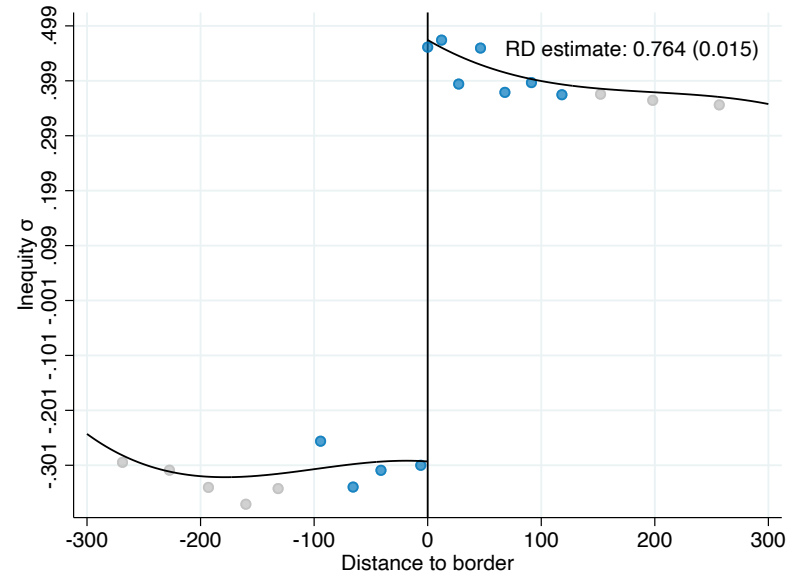
Notes: The figure shows the compliance elasticity at tax sector boundaries by groups of our salience measure. Specifically, we split our sample into five disjoint groups using the quintiles of our salience measure described in Appendix G. For each group, we show on the y-axis the inequity elasticity implied by estimating equation (12). On the x-axis, we show the average salience for each group. The figure shows that our results are strongly increasing in the salience of the property tax. In the bottom quintile the estimated effect is zero, but then the elasticity is positive in the higher quintiles of salience.

FIGURE 8: DIFFERENCE IN BOUNDARY DISCONTINUITY DESIGN: FIRST STAGE

PANEL A: LOW INEQUITY

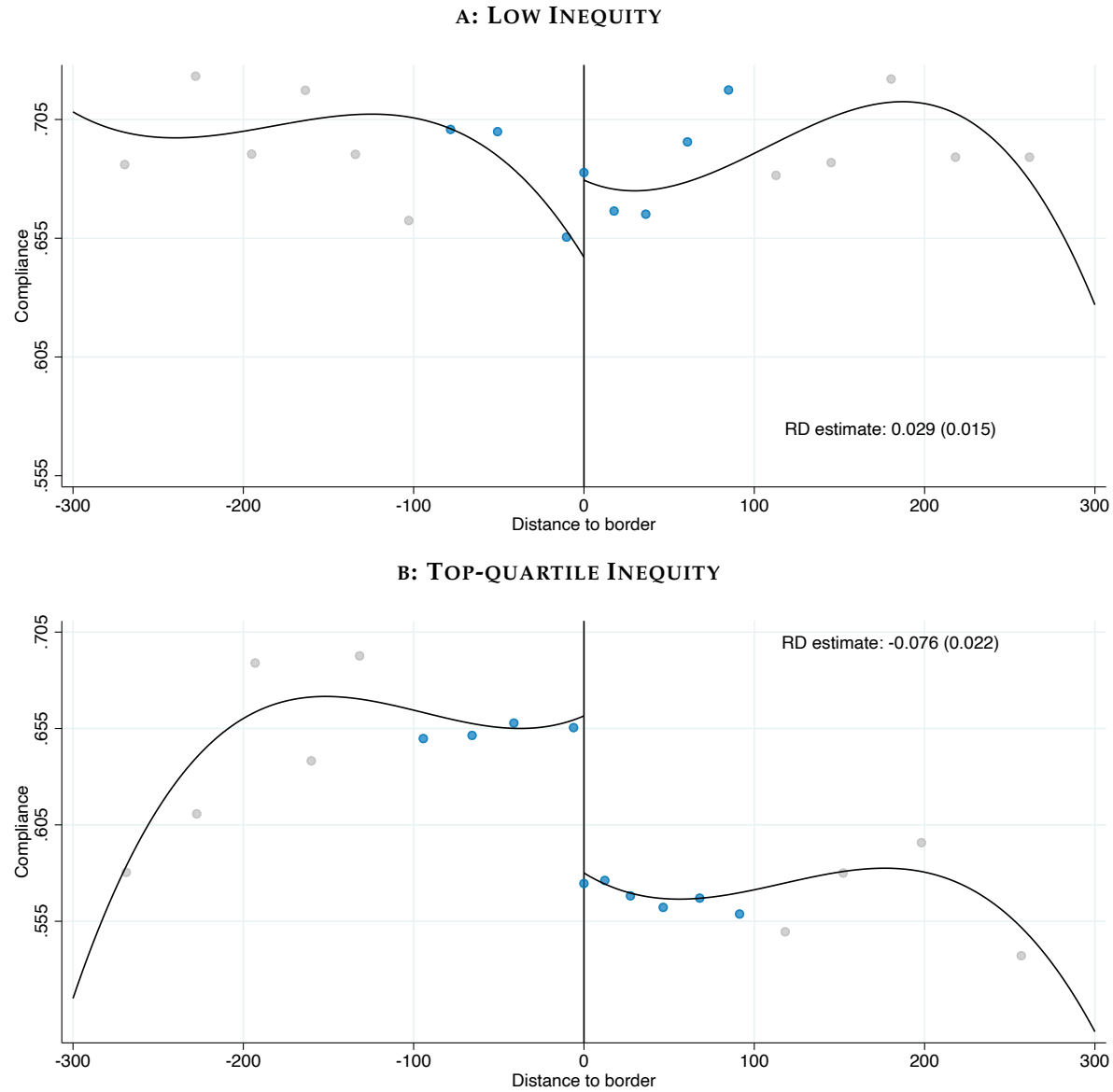


PANEL B: TOP-QUARTILE INEQUITY



Notes: The figure shows the results of estimating equation (12): $\log(\sigma_i) = \lambda_{r(i)} + g(\tau_i, e_i) + f_0(d_i) + \beta_0 HTS_i + f_1(d_i) \times HTS_i + \varepsilon_i$ with inequity as the outcome variable, where terms are as defined in the notes to figure 6. Panel A shows the estimates in the subsample of properties facing low inequity (defined as being in the bottom 3 quartiles of inequity). Panel B shows the estimates in the subsample of properties facing top-quartile inequity.

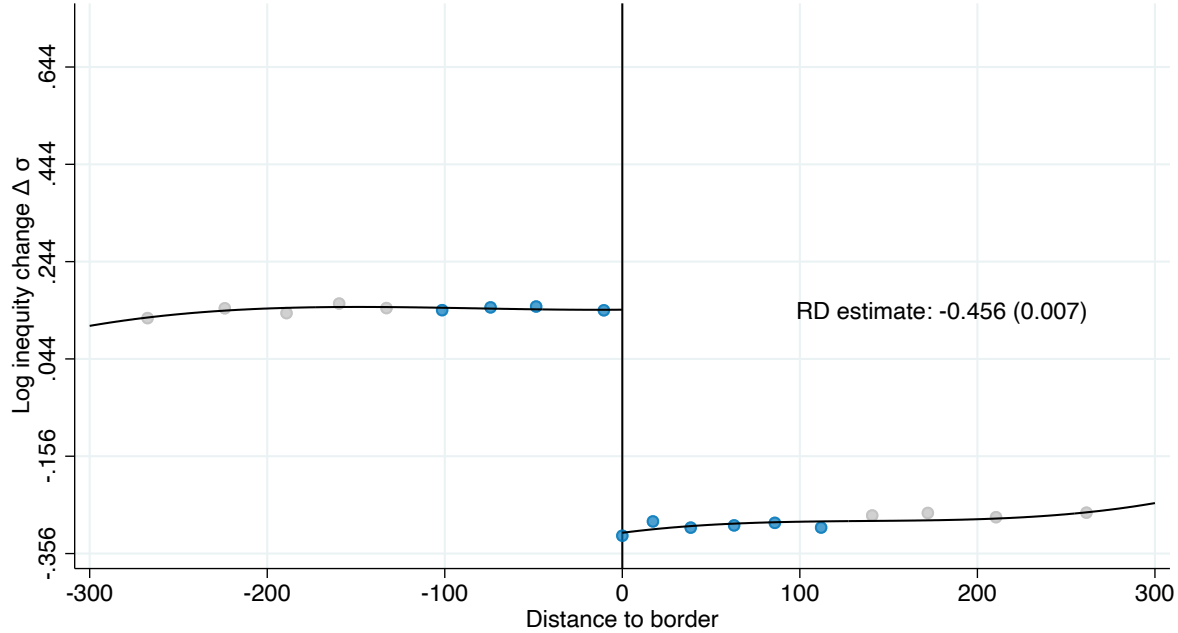
FIGURE 9: DIFFERENCE IN BOUNDARY DISCONTINUITY DESIGN: COMPLIANCE EFFECTS



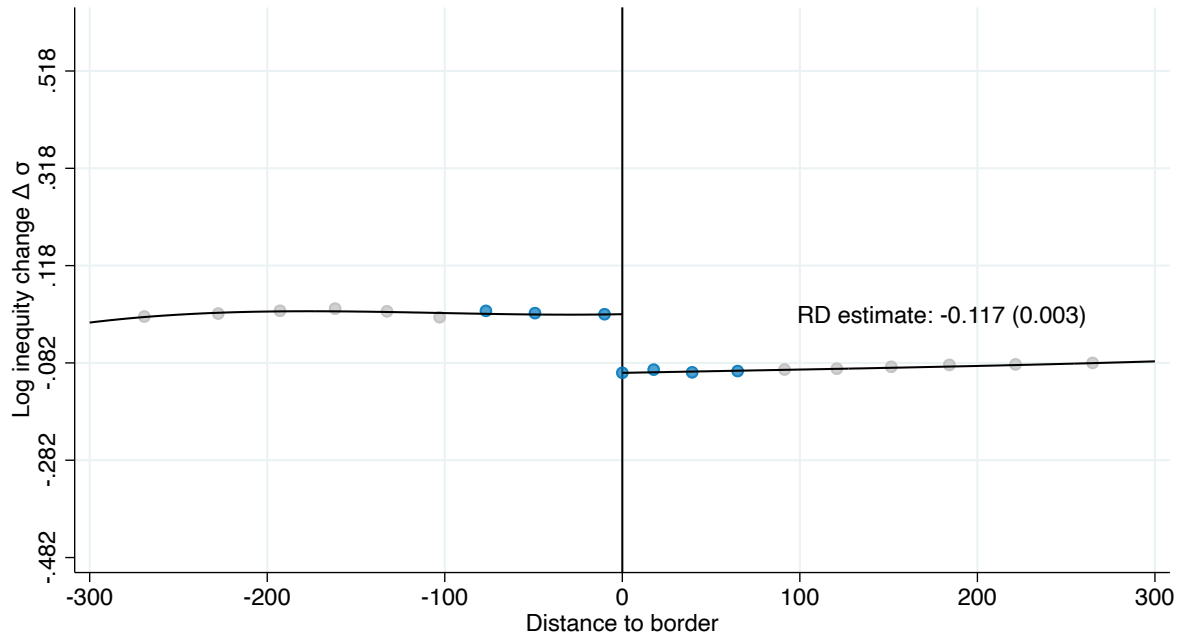
Notes: The figure shows the results of estimating equation (12): $c_i = \lambda_{r(i)} + g(\tau_i, e_i) + f_0(d_i) + \beta_0 HTS_i + f_1(d_i) \times HTS_i + \varepsilon_i$ with compliance as the outcome variable, where terms are as defined in the notes to figure 6. Panel A shows the estimates in the subsample of properties facing low inequity (defined as being in the bottom 3 quartiles of inequity). Panel B shows the estimates in the subsample of properties facing top-quartile inequity.

FIGURE 10: DYNAMIC BOUNDARY DISCONTINUITY DESIGN: FIRST STAGE

A: REMOVAL OF INEQUITY



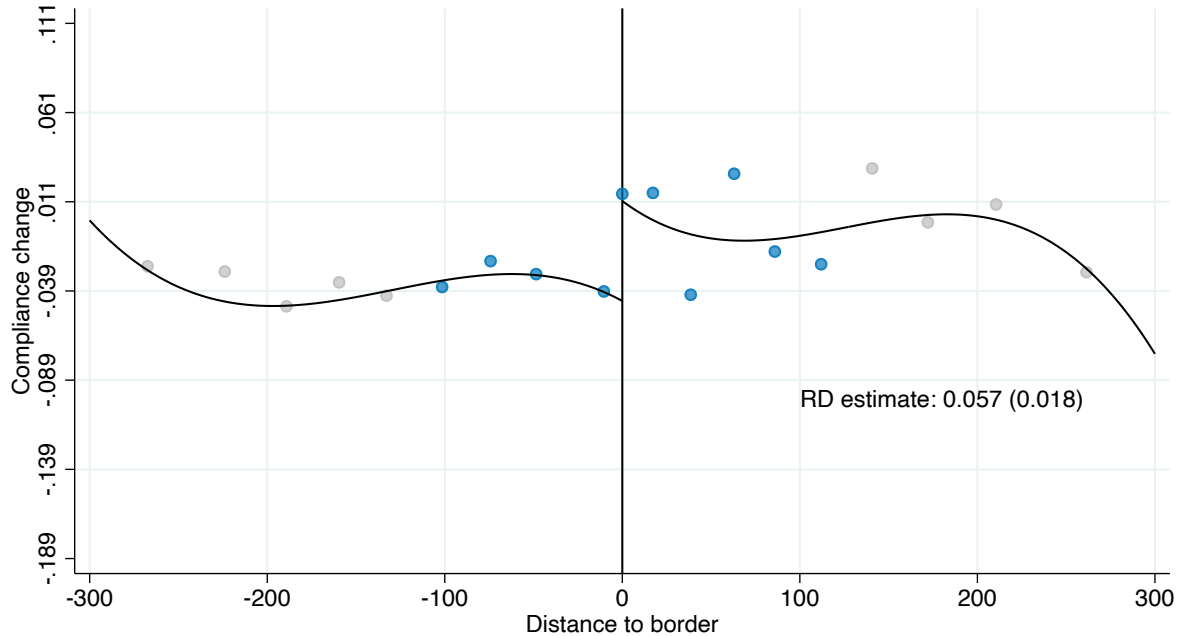
B: NO IMPROVEMENT



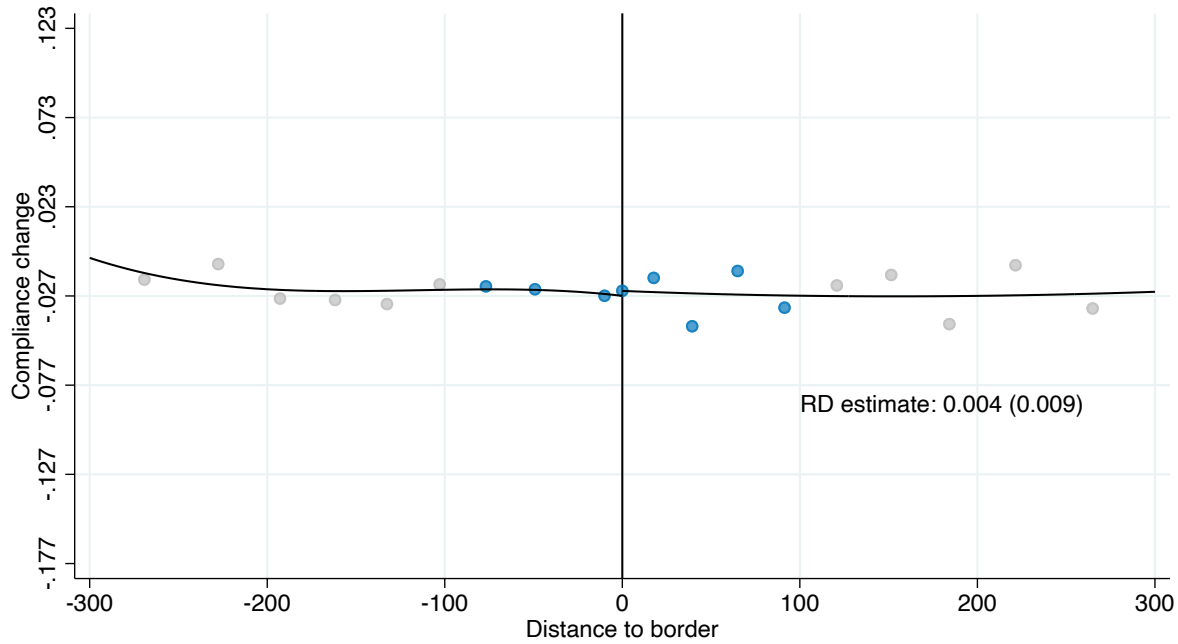
Notes: The figure shows the results of estimating equation (17) $\Delta\sigma_i = \lambda_{r(i)} + g(\Delta\tau_i) + f_0(d_i) + HTS_i \times [\beta_0 + f_1(d_i)] + \varepsilon_i$ where the outcome variable is the change in inequity, $\lambda_{r(i)}$ are boundary-segment fixed effects, HTS_i is an indicator for being on the high-tax side of the boundary ($d_i > 0$); $f_0(d_i)$ and $f_1(d_i)$ control for distance to the boundary on the low- and high-tax sides of the boundary, respectively; and ε_i is the residual. $g(\Delta\tau_i)$ controls flexibly for changes in log tax liability, τ_i . Specifically, we control for splines of $\Delta\tau_i$. Panel A shows the estimates in the subsample of properties for whom the reform meaningfully reduced inequity. Panel B shows the estimates in the remaining subsample of properties.

FIGURE 11: DYNAMIC BOUNDARY DISCONTINUITY DESIGN: COMPLIANCE EFFECTS

A: REMOVAL OF INEQUITY

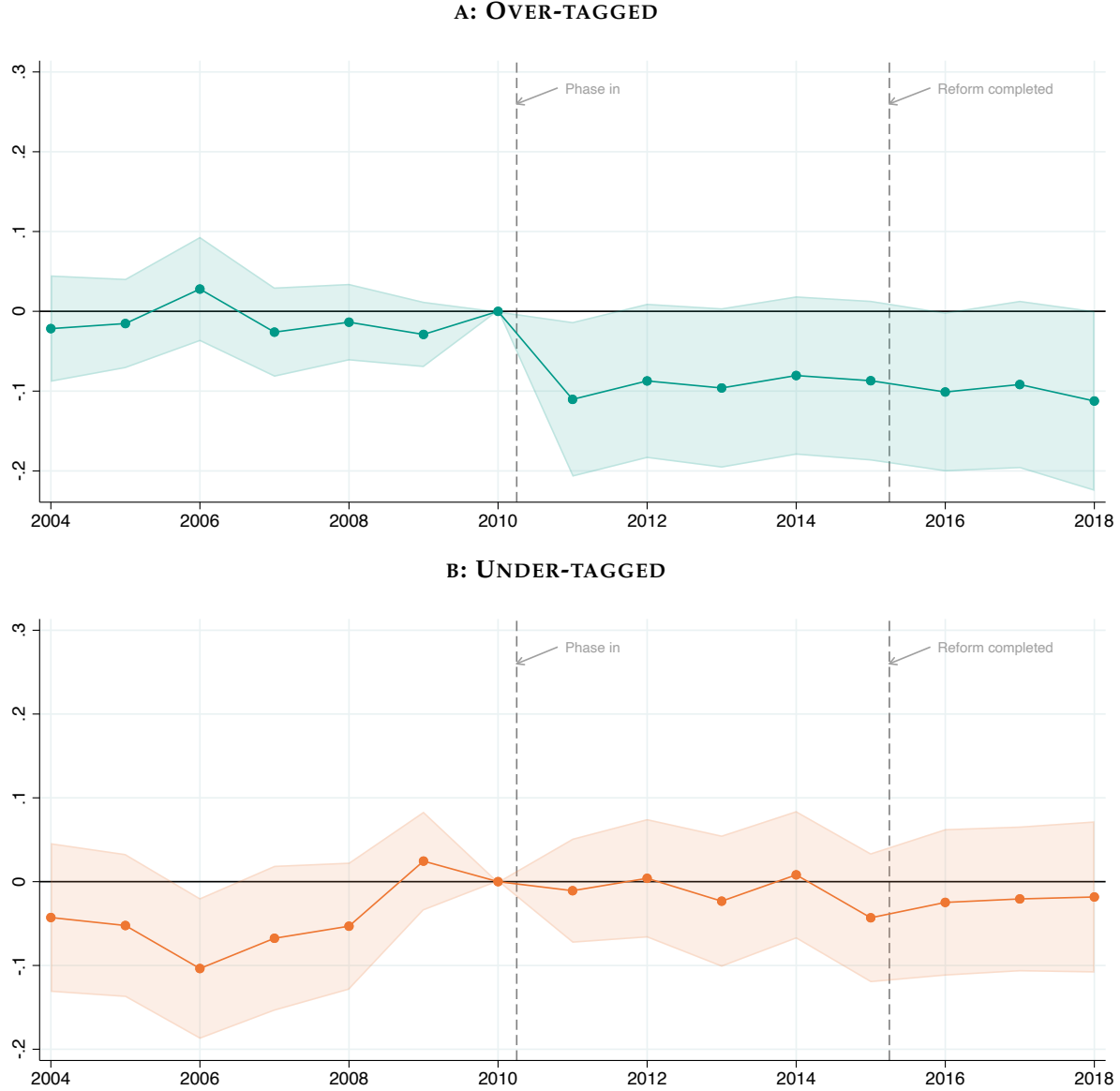


B: NO IMPROVEMENT



Notes: The figure shows the results of estimating equation (17) $\Delta c_i = \lambda_{r(i)} + g(\Delta\tau_i) + f_0(d_i) + HTS_i \times [\beta_0 + f_1(d_i)] + \varepsilon_i$ where the outcome variable is the change in compliance, $\lambda_{r(i)}$ are boundary-segment fixed effects, HTS_i is an indicator for being on the high-tax side of the boundary ($d_i > 0$); $f_0(d_i)$ and $f_1(d_i)$ control for distance to the boundary on the low- and high-tax sides of the boundary, respectively; and ε_i is the residual. $g(\Delta\tau_i)$ controls flexibly for changes in log tax liability, τ_i . Specifically, we control for splines of $\Delta\tau_i$. Panel A shows the estimates in the subsample of properties for whom the reform meaningfully reduced inequity. Panel B shows the estimates in the remaining subsample of properties.

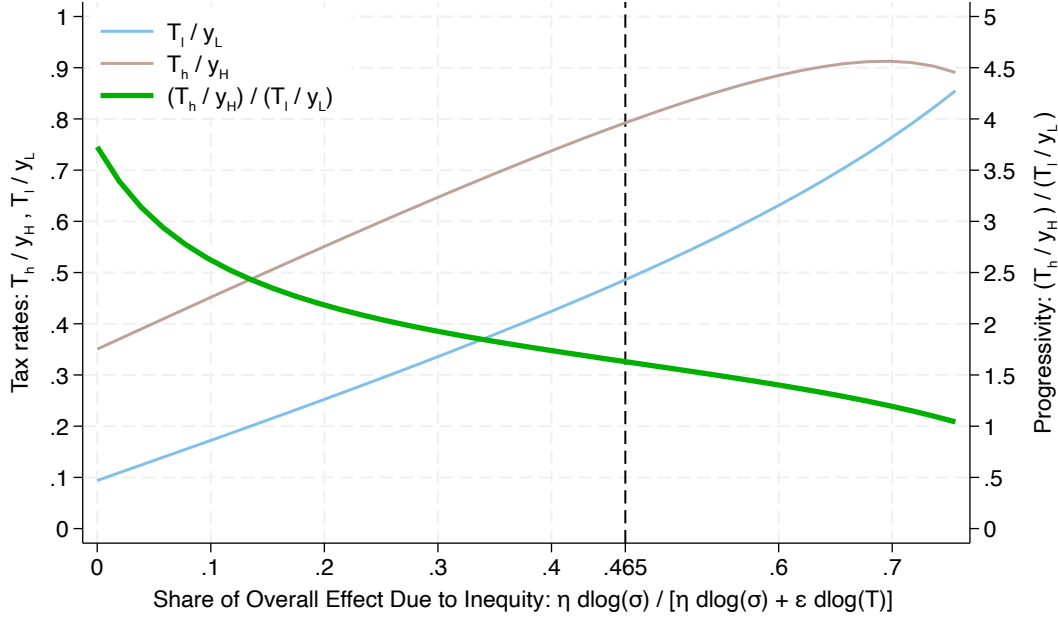
FIGURE 12: DIFFERENCE IN DIFFERENCE ESTIMATES OF OVERTAGGING AND UNDERTAGGING EFFECTS



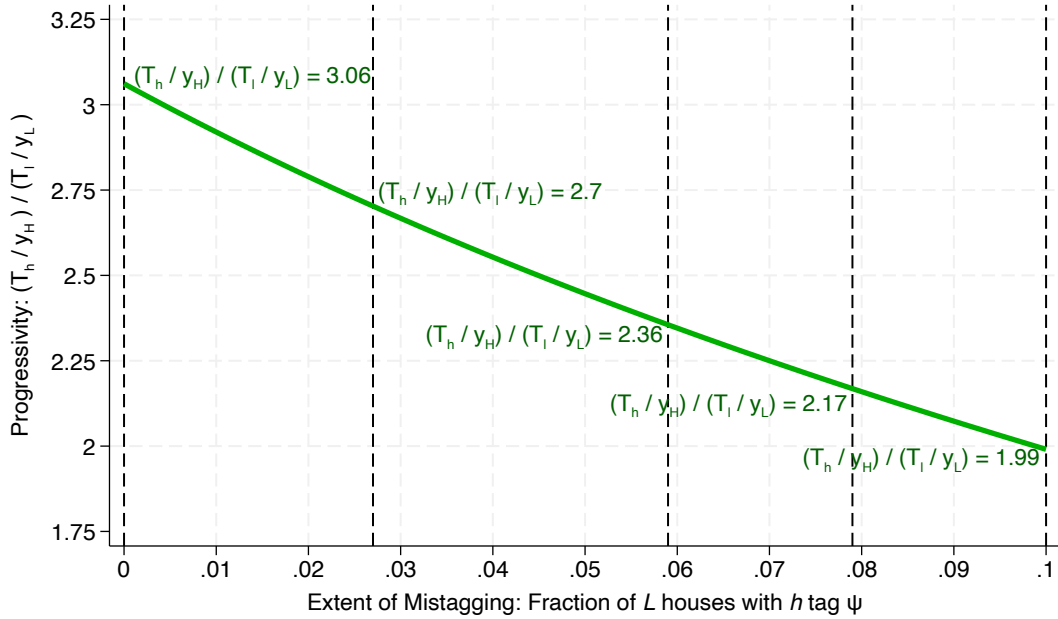
Notes: The figure shows the results of the estimation of equation (20) as discussed in section 6.3: $c_{iy} = \alpha_i + \lambda_{r(i)y} + \sum_{j \neq 2010} D_{jy} \times [f_{0j}(d_i) + \beta_{0j}\Delta\tau_i + \eta_{0j}\Delta\sigma_i + HTS_i \times (\delta_j + f_{1j}(d_i) + \beta_{1j}\Delta\tau_i + \eta_{1j}\Delta\sigma_i)] + \varepsilon_{iy}$, where $\lambda_{r(i)y}$ are segment-year fixed effects, $D_{jy} \equiv \mathbf{1}[y = j]$ are year dummies, and we include year-specific distance controls $f_{0j}(d_i)$ and $f_{1j}(d_i)$; and year-specific controls for property i 's tax liability change due to the reform. Panel A shows the estimated η_{1j} coefficients along with their 95% confidence intervals. Panel B shows the estimated η_{0j} coefficients along with their 95% confidence intervals.

FIGURE 13: OPTIMAL TAX CALIBRATION AND FISCAL CAPACITY COUNTERFACTUALS

PANEL A: SHARE OF OVERALL RESPONSE DUE TO INEQUITY RESPONSES



PANEL B: FISCAL CAPACITY COUNTERFACTUALS



Notes: The figure shows calibrations of the optimal tax schedule discussed in section 3.2. We set the parameters as follows: $\psi = 0.1$, $\rho = 3$, $y_H = Rs.6,630$, $y_L = Rs.4,911.5$, $b(r) = 1$, $g_H/g_L = 1.6$. In panel A, we hold the overall compliance response at the tax sector boundaries fixed and vary the share we attribute to responses to inequity. We show the two optimal tax rates and the ratio of the two: the progressivity of the tax schedule. Our preferred estimates imply $\eta = 0.12$ and hence 46.5% of the overall response coming from inequity. See section 7 and Appendix K for full details. In Panel B we perform counterfactual reductions in the extent of mistagging due to investments in fiscal capacity as described in section 7 and show the implications for the progressivity of the optimal tax schedule.

TABLE 1: PROPERTY TAXES AROUND THE WORLD

City	Property Tax Assessment	Does geography enter into the assessment?	Do assessment zones align with administrative divisions?
Addis Ababa (ET)	Presumptive	No	-
Amsterdam (NL)	Market value	No	-
Bangkok (TH)	Presumptive	Yes	Yes
Beijing (CN)	No property tax	-	-
Berlin (DE)	Presumptive	No	-
Bogota (CO)	Market value	-	-
Buenos Aires (AR)	Market value	No	-
Cairo (EG)	Presumptive	Yes	Yes
Chicago (US)	Market value	No	-
Delhi (IN)	Presumptive	No	-
Dhaka (BD)	Presumptive	Yes	No
Hong Kong (HK)	Market value	No	-
Istanbul (TR)	Presumptive	Yes	No
Jakarta (ID)	Market value	Yes	No
Johannesburg (ZA)	Market value	No	-
Karachi (PK)	Presumptive	Yes	No
Lagos (NG)	Market value	No	-
Lahore (PK)	Presumptive	Yes	No
Lima (PE)	Presumptive	Yes	No
London (UK)	Market value	No	-
Los Angeles (US)	Market value	No	-
Madrid (ES)	Presumptive	Yes	Yes
Manaus (BR)	Presumptive	Yes	No
Manilla (PH)	Market Value	No	-
Maputo (MZ)	Presumptive	Yes	No
Mexico City (MX)	Presumptive	Yes	Yes
Moscow (RU)	Presumptive	No	-
Mumbai (IN)	Presumptive	Yes	No
New York City (US)	Market value	No	-
Paris (FR)	Presumptive	Yes	Yes
Rio de Janeiro (BR)	Presumptive	Yes	No
Rome (IT)	Presumptive	No	-
Sao Paulo (BR)	Presumptive	Yes	No
Seoul (KR)	Presumptive	Yes	Yes
Shanghai (CN)	No property tax	-	-
Singapore (SG)	Market value	No	-
Sydney (AU)	Market value	No	-
Taipei (TW)	Presumptive	Yes	No
Tehran (IR)	Market value	No	-
Tokyo (JP)	Presumptive	No	No
Toronto (CA)	Market value	No	-

Notes: This table shows the method of property tax valuation for large urban areas across the world. Presumptive assessment uses a formula that takes observable characteristics of the property as its inputs. Market value assessment assigns a property tax based proportionally on the estimated value of the property in the real estate market. Note that China does not impose a property tax.

TABLE 2: AUGMENTED BOUNDARY DISCONTINUITY DESIGN: COMPLIANCE EFFECTS

	(1)	(2)	(3)	(4)	(5)	(6)
RD estimate	-0.08*** (0.02)	-0.07*** (0.02)	-0.08*** (0.02)	-0.07*** (0.02)	-0.08*** (0.02)	-0.09*** (0.02)
R^2						
Distance controls	✓	✓	✓	✓	✓	✓
Segment FEs	✓	✓	✓	✓	✓	✓
τ splines	✓	✓	✓	✓	✗	✗
exp dec FEs	✓	✗	✓	✗	✗	✓
τ decile FEs	✗	✗	✗	✗	✓	✓
exp splines	✗	✓	✗	✓	✗	✗
τ splines \times exp dec FEs	✗	✗	✓	✗	✗	✗
τ splines \times exp splines	✗	✗	✗	✓	✗	✗
τ dec FEs \times exp dec FEs	✗	✗	✗	✗	✗	✓
First-stage	0.538*** (0.010)	0.507*** (0.010)	0.551*** (0.010)	0.524*** (0.010)	0.537*** (0.010)	0.551*** (0.010)
Elasticity	0.216*** (0.050)	0.194*** (0.055)	0.222*** (0.049)	0.196*** (0.055)	0.220*** (0.052)	0.227*** (0.051)
N	9236	9235	9236	9235	9236	9236

Notes: The table shows the results of estimating the augmented BDD equation (12): $c_i = \lambda_{r(i)} + g(\tau_i, e_i) + f_0(d_i) + \beta_0 HTS_i + f_1(d_i) \times HTS_i + \varepsilon_i$, where $\lambda_{r(i)}$ are fixed effects for 500-meter segments along the boundaries to ensure we are comparing properties who are nearby each other; $g(\tau_i, e_i)$ are flexible controls for property i 's (log) tax liability τ_i and exposure to mistagging e_i ; $f_0(d_i)$ and $f_1(d_i)$ control flexibly for distance to the boundary on the low- and high-tax sides of the boundary respectively; and HTS_i is an indicator for properties on the high-tax side of the boundary ($d_i > 0$). The columns use a variety of approaches to controlling flexibly for the tax liability and exposure to mistagging. In column (1) we control for cubic splines of the tax liability and fixed effects for deciles of exposure. In column (2) we replace the exposure deciles with cubic splines of exposure while column (3) replaces the splines of the tax liability with deciles. Columns (4)–(6) additionally interact the tax liability controls with the exposure controls. The table shows remarkably consistent results: the implied elasticity of compliance with respect to inequity ranges from 0.25 to 0.27.

TABLE 3: DIFFERENCE IN BOUNDARY DISCONTINUITY DESIGN: COMPLIANCE EFFECTS

	(1)	(2)	(3)	(4)	(5)	(6)	(7)
1(high tax side)	0.01 (0.02)	0.00 (.)	0.00 (.)	0.00 (.)	0.27 (0.36)	0.23 (0.36)	0.00 (.)
1(high tax side) $\times \sigma $	-0.17*** (0.02)	-0.17*** (0.02)	-0.18*** (0.02)	-0.17*** (0.02)	-0.15*** (0.03)	-0.18*** (0.03)	-0.15*** (0.03)
R^2	0.130	0.130	0.130	0.130	0.133	0.132	0.137
Distance controls	✓	✓	✓	✓	✓	✓	✓
Segment fixed effects	✓	✓	✓	✓	✓	✓	✓
τ splines	✓	✓	✓	✗	✓	✓	✗
τ deciles	✗	✗	✗	✓	✗	✗	✓
Expansiveness splines	✗	✗	✓	✗	✗	✓	✗
Expansiveness deciles	✓	✓	✗	✓	✓	✗	✓
τ splines \times HTS	✗	✓	✓	✗	✓	✓	✗
τ deciles \times HTS	✗	✗	✗	✓	✗	✗	✓
τ splines \times exp deciles	✗	✗	✗	✗	✓	✗	✗
τ splines \times exp splines	✗	✗	✗	✗	✗	✓	✗
τ deciles \times exp deciles	✗	✗	✗	✗	✗	✗	✓
τ splines \times HTS \times exp deciles	✗	✗	✗	✗	✓	✗	✗
τ splines \times HTS \times exp splines	✗	✗	✗	✗	✗	✓	✗
τ deciles \times HTS \times exp deciles	✗	✗	✗	✗	✗	✗	✓
Elasticity	0.260*** (0.037)	0.261*** (0.037)	0.274*** (0.038)	0.263*** (0.037)	0.234*** (0.041)	0.280*** (0.043)	0.234*** (0.041)
N	25061	25061	25061	25061	25061	25061	25061

Notes: The table shows the results of estimation of equation (16): $c_i = \lambda_{r(i)} + g_0(\tau_i, e_i) + f_0(d_i) + HTS_i \times [\beta_0 + \eta \log(\sigma) + f_1(d_i) + g_1(\tau_i, e_i)] + \varepsilon_i$ where terms are as defined above in the notes to table 2. In column (1), we control for cubic splines of the tax liability and fixed effects for deciles of the exposure distribution. In column (2) we control separately for the tax liability and exposure to mistagging on either side of the boundary. Column (3) replaces the exposure deciles with cubic splines in exposure while column (4) replaces the tax liability deciles with cubic splines. Columns (5)–(7) control for these separately on either side of the boundary.

TABLE 4: DYNAMIC DIFFERENCE IN BOUNDARY DISCONTINUITY DESIGN

	(1) Δ Compliance	(2) Δ Compliance	(3) Δ Compliance	(4) Δ Compliance	(5) Δ Compliance	(6) Δ Compliance	(7) Δ Compliance
1(high tax side)	-0.004 (0.008)	-0.003 (0.020)	-0.003 (0.020)	0.005 (0.015)	0.008 (0.020)	0.004 (0.020)	-0.012 (0.021)
1(high tax side) \times change in σ	-0.069*** (0.025)	-0.068*** (0.025)	-0.067*** (0.025)	-0.071*** (0.025)	-0.074*** (0.026)	-0.071*** (0.028)	-0.075*** (0.026)
Distance controls	✓	✓	✓	✓	✓	✓	✓
Segment FEs	✓	✓	✓	✓	✓	✓	✓
$\Delta\tau$ splines	✓	✓	✓	✗	✓	✓	✗
$\Delta\tau$ deciles	✗	✗	✗	✓	✗	✗	✓
Expansiveness splines	✗	✗	✓	✗	✗	✓	✗
Expansiveness deciles	✓	✓	✗	✓	✓	✗	✓
$\Delta\tau$ splines \times HTS	✗	✓	✓	✗	✓	✓	✗
$\Delta\tau$ deciles \times HTS	✗	✗	✗	✓	✗	✗	✓
$\Delta\tau$ splines \times exp deciles	✗	✗	✗	✗	✓	✗	✗
$\Delta\tau$ splines \times exp splines	✗	✗	✗	✗	✗	✓	✗
$\Delta\tau$ deciles \times exp deciles	✗	✗	✗	✗	✗	✗	✓
$\Delta\tau$ splines \times HTS \times exp deciles	✗	✗	✗	✗	✓	✗	✗
$\Delta\tau$ splines \times HTS \times exp splines	✗	✗	✗	✗	✗	✓	✗
$\Delta\tau$ deciles \times HTS \times exp deciles	✗	✗	✗	✗	✗	✗	✓
Elasticity	0.108** (0.039)	0.107** (0.039)	0.105** (0.039)	0.111** (0.039)	0.115** (0.041)	0.112** (0.043)	0.117** (0.041)

Notes: This table shows the results of estimating equation (18) discussed in section 6.2: $\Delta c_i = \lambda_{r(i)} + g_0(\Delta\tau_i, e_i) + f_0(d_i) + HTS_i \times [\delta_0 + \eta\Delta \log(\sigma_i) + g_1(\Delta\tau_i, e_i) + f_1(d_i)] + \varepsilon_i$ where all terms are as defined above in the notes to table 2. Column (1) controls for cubic splines of the tax liability and fixed effects for deciles of the exposure distribution. Column (2) adds interactions between these controls and estimates them separately on either side of the boundary. Column (3) replaces the exposure deciles with splines, while column (4) replaces the tax liability splines with deciles of the tax liability distribution.

Appendices

A Additional Background on IPTU in Manaus	2
B Additional Background on the 2011 IPTU Reform	6
C Creation of Distance Measure	9
D Additional Background on Inequity Measure (σ)	11
E Sample Selection and Robustness Checks	13
E.1 Sample including properties on neighborhood borders	14
E.2 Sample excluding properties on neighborhood borders	20
E.3 Sample with non-residential properties	25
E.4 Relaxed “large lots” Definition: Drop the top 0.1% in terms of land area	34
E.5 Stringent “large lots” Definition: Drop the top 1% in terms of land area	44
E.6 Alternative Definitions of Non-Trivial Degree of Inequity	56
F Robustness to Alternative Definitions of Compliance	59
F.1 Extensive Margin Response	59
F.2 Timeframe for Payments in the Definition of Compliance	65
G Salience of inequity	69
H Placebo Test for Difference in Boundary Discontinuities Design	71
I Tax Enforcement	74
J House Prices and IPTU: Evidence from Property Listings	77
K Optimal Tax Simulations	80
K.1 Comparative Statics	80
K.2 Share of Overall Response from Inequity	80
K.3 Simulations of Extensions to the Model	80
L Fiscal Capacity Counterfactuals	87
M Proof of Proposition 1	89
N Proof of Proposition 2	91
O Model with Undertagging and Overtagging	93
P Model with Location Choice and Endogenous House Prices	95
P.1 Location Choice	95
P.2 Welfare and Optimal Policy	98
Q Proof of Proposition 3	102
R Proof of Proposition 4	104

A Additional Background on IPTU in Manaus

SEMEF calculates a property's tax bill (IPTU) as a function of a small number of easily observable characteristics of the land and any built structures on the property. Table A.1 lists the categories for each characteristic used in the calculation of the land value (VT) and building value (VE).

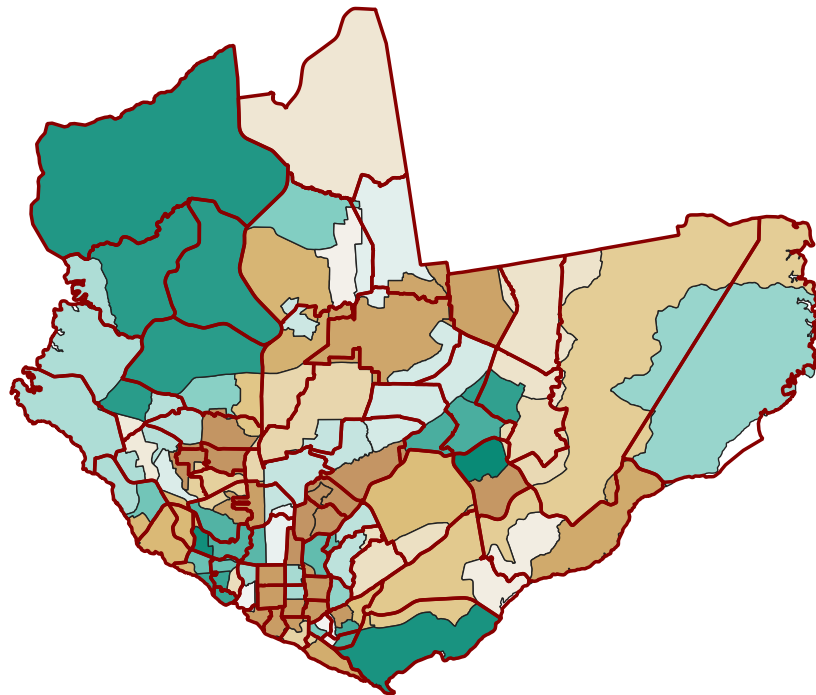
TABLE A.1: IPTU CALCULATION FACTORS

$IPTU = (VE + VT) \times \text{aliquot}$						
$VE = \text{Value}(m^2) \times \text{Area} \times (CAT/100) \times \text{Alignment} \times \text{Construction} \times \text{Position}$			$VT = \text{Value}(m^2) \times \text{Area} \times \text{Situation} \times \text{Topography} \times \text{Pedology}$			
Alignment	Construction	Position	Situation	Topography	Pedology	
<ul style="list-style-type: none"> • Aligned • Backtracked 	<ul style="list-style-type: none"> • Isolated • Combined • Detached 	<ul style="list-style-type: none"> • Front • Back • Superimposed Front • Superimposed Back • Mezzanine • Gallery • Village 	<ul style="list-style-type: none"> • Corner • Middle of Block • Village • Enclave • Horizontal Condo • Favela/Stilt 	<ul style="list-style-type: none"> • Flat • Uphill • Downhill • Irregular 	<ul style="list-style-type: none"> • Floodable + 50% • Floodable - 50% • Firm 	

Notes: This table shows the equation used by SEMEF to calculate a household's property tax bill. CAT is defined as the sum of building components points, and factors in the construction material used in a household's roof, exterior walls, structure, and building height.

To calculate the per-square meter rate in the IPTU calculation, SEMEF divided Manaus into 65 tax sectors in 1983. Importantly, this division is only used in the IPTU calculation, as the smallest official administrative division of the city is the neighborhood (*Bairro*). As the tax sectors were created in 1983, before much of the city was built out, it is not conterminous with the bairro boundaries. Figure A.1 shows the overlay between the tax sector boundaries and the bairro boundaries (in red).

FIGURE A.1: TAX SECTOR AND NEIGHBORHOOD BOUNDARY OVERLAYS



Note: This figure shows the boundaries of tax sectors (in red) overlaid on the neighborhoods (*bairros*) in Manaus.

After a household receives its IPTU bill in January (see figure A.2), it has the option to pay it in one installment by March (at a discounted rate) or to pay the bill in ten equal monthly installments. Failure to pay the complete IPTU bill by December 31 results in automatic interest and fines applied in the next billing cycle, with the property being placed on the *divida ativa* registry until the remaining balance is paid off. Despite the penalty for nonpayment, we find that compliance rates in Manaus are relatively low. Figure A.3 shows the compliance rate from 2004 through 2019 for three definitions of compliance. The series in orange circles shows the fraction of properties that make any tax payment. The series in green squares computes the ratio of tax paid to tax owed for each property and then averages it across taxpayers. The series in purple triangles shows the fraction of properties that pay their tax in full. Despite a slight increase in compliance after 2008, the fraction of (nonexempt) households in the city that pay their IPTU bill in a given year is between 60 and 65 percent. However, as seen in the figure, compliance appears to be driven at the extensive margin, with the large majority of households who pay their IPTU choosing to pay the full amount owed to SEMEF that year.

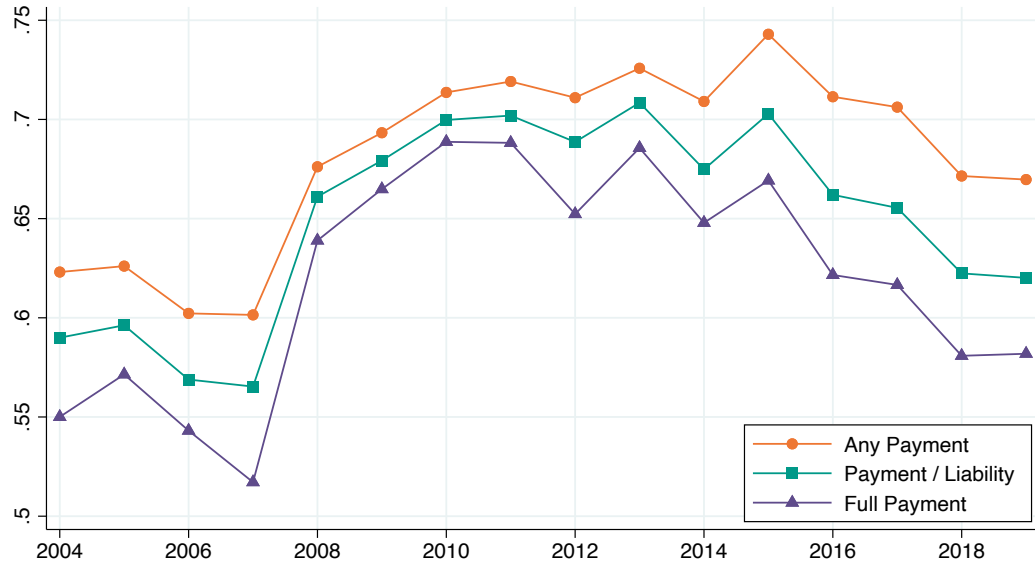
FIGURE A.2: EXAMPLE OF A 2018 IPTU BILL

PREFEITURA DE MANAUS SEMEF DOCUMENTO DE ARRECADAÇÃO MUNICIPAL - D.A.M					
Contribuinte			D.A.M.		
CPF/CNPJ	Matrícula/CMC	Tributos I.P.T.U. 2018	Referência 4/10	Vencimento 15/06/2018	Nosso Número 11000XXXXXX
Endereço de Localização					
Logradouro:	AVENTDA - JURJINAS	Complemento:	QD 25, CJ ETAPA I	Número:	1 <input checked="" type="checkbox"/>
Bairro:	CIDADE NOVA	Quadra Lot.:	25	Lote:	0200
Lotreamento:		Quadra Lot.:	25	Quadra:	0025
Imóvel:	PREDTAT,				
Área Terreno:	900,00	Área Total Construída:	623,55	Área Construída Unidade:	623,55
Valor Venal Terreno:	40.304,88	Valor Venal Construção:	271.983,90		
Valor Venal Imóvel:	312.188,78	Base de Cálculo:	312.188,78	Aliquota:	0,9000
IPU PREDIAL	R\$ 280,91	Valor R\$ 280,91			
TSA:	R\$ 0,00	Emissão: 12/06/2018 Usuário:CIDADAO			
Total:	R\$ 280,91	Autenticação:			

Note: This is an example of an IPTU bill received by a household in 2018.

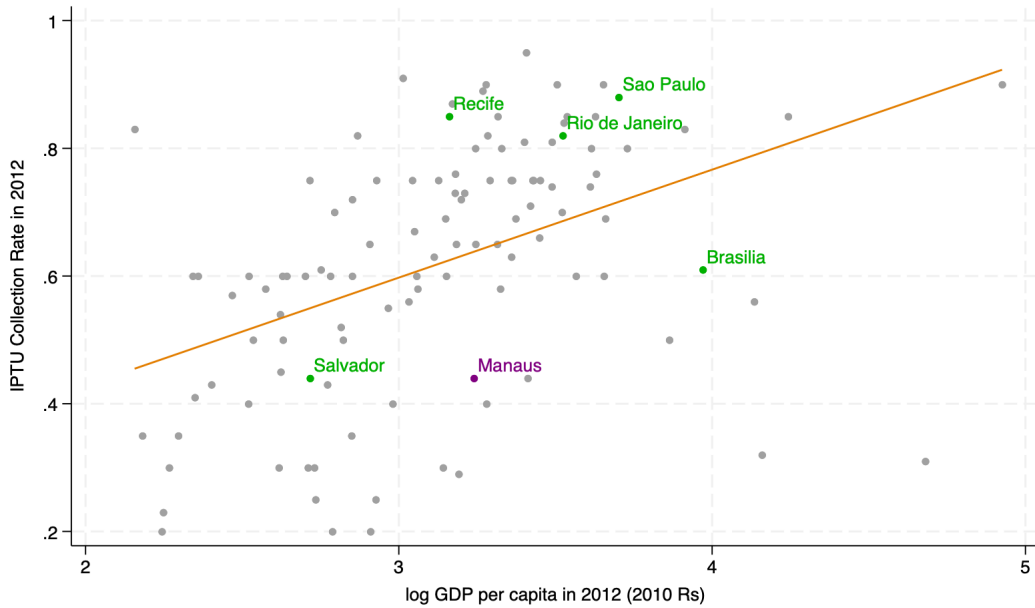
Although we do not have the data necessary to compute the compliance rate in other Brazilian municipalities, we can use publicly available data on municipal finances to calculate the property tax collection rate. This rate is defined as the ratio of total revenue collected to the total amount of IPTU bills issued in a given city in a given year and can be used as a proxy for the compliance rate assuming that the distribution of property values is similar across Brazil. Figure A.4 shows the collection rates for IPTU bills in large Brazilian municipalities in 2021. Two features of the figure stand out: relative to other large cities-particularly in the south-Manaus has a relatively low collection rate. However, its low collection rate is consistent with lower collection rates in much of the northern states of Brazil.

FIGURE A.3: COMPLIANCE IS DRIVEN BY THE EXTENSIVE MARGIN



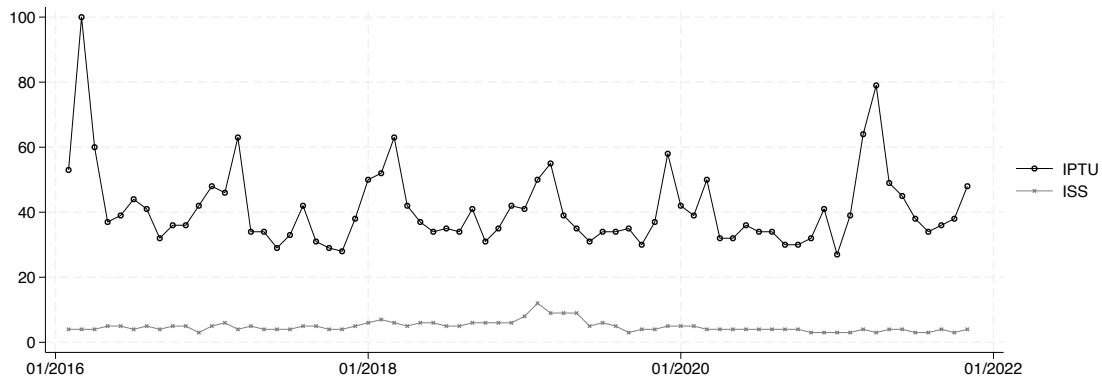
Notes: The figure shows the compliance rate by all non-exempt residential households in Manaus. The orange line depicts the fraction of households in a given year that paid at least a portion of their IPTU bill. The purple line shows the fraction of households that paid the full amount of their IPTU bill in a given year.

FIGURE A.4: IPTU COLLECTION RATE AMONG LARGE BRAZILIAN CITIES



Notes: The figure shows the 2012 IPTU collection rate for cities in Brazil with more than 200,000 residents. The collection rate is defined as the ratio of collected tax revenue to total IPTU bills issued that year. Data on municipal GDP comes from the IBGE, and data on collection rates is from [Carvalho Junior \(2017\)](#).

FIGURE A.5: GOOGLE SEARCHES IN MANAUS - PROPERTY VERSUS SERVICE TAX



Note: This figure shows the Google searched for two municipal tax: property tax (IPTU) and service tax (ISS). Data is restricted between two dates that have consistent measurement according to Google trends. Data query is from the state of Amazonas, Brazil, with 100% of searches from the city of Manaus.

Like the property tax in other settings,⁵⁵ the IPTU is very salient to residents of Manaus. Of the two main taxes that can be levied by municipalities in Brazil, there is a stark contrast in citizen interest, as proxied by Google searches (see figure A.5). Whereas searches for the property tax (IPTU) are cyclical, with searches peaking at the beginning of the year when bills are sent out, there is very little search activity on the municipal tax on services (ISS). The high salience of the IPTU can also be seen in its inclusion in many real estate listings on Viva Real, which is a popular site for people seeking to buy and rent houses in Manaus (see figure A.6).

FIGURE A.6: EXAMPLE OF A VIVA REAL LISTING

Venda / AM / Casas à venda em Manaus / Lírio do Vale / Rua Sapeaçu

R\$ 380.000 Condomínio **R\$ 1.268**

Preço abaixo do mercado

400 m² 3 quartos 2 banheiros
3 vagas 1 suíte Quintal

Todas as características

Endereço: Rua Sapeaçu, 1 - Lírio do Vale, Manaus - AM

Casa com 3 Quartos e 2 banheiros à Venda, 400 m² por R\$ 380.000

Obrigado, gostaria de ter mais informações para comprar casa, Rua Sapeaçu, 1 - Lírio do Vale, Manaus - AM

Enviar mensagem

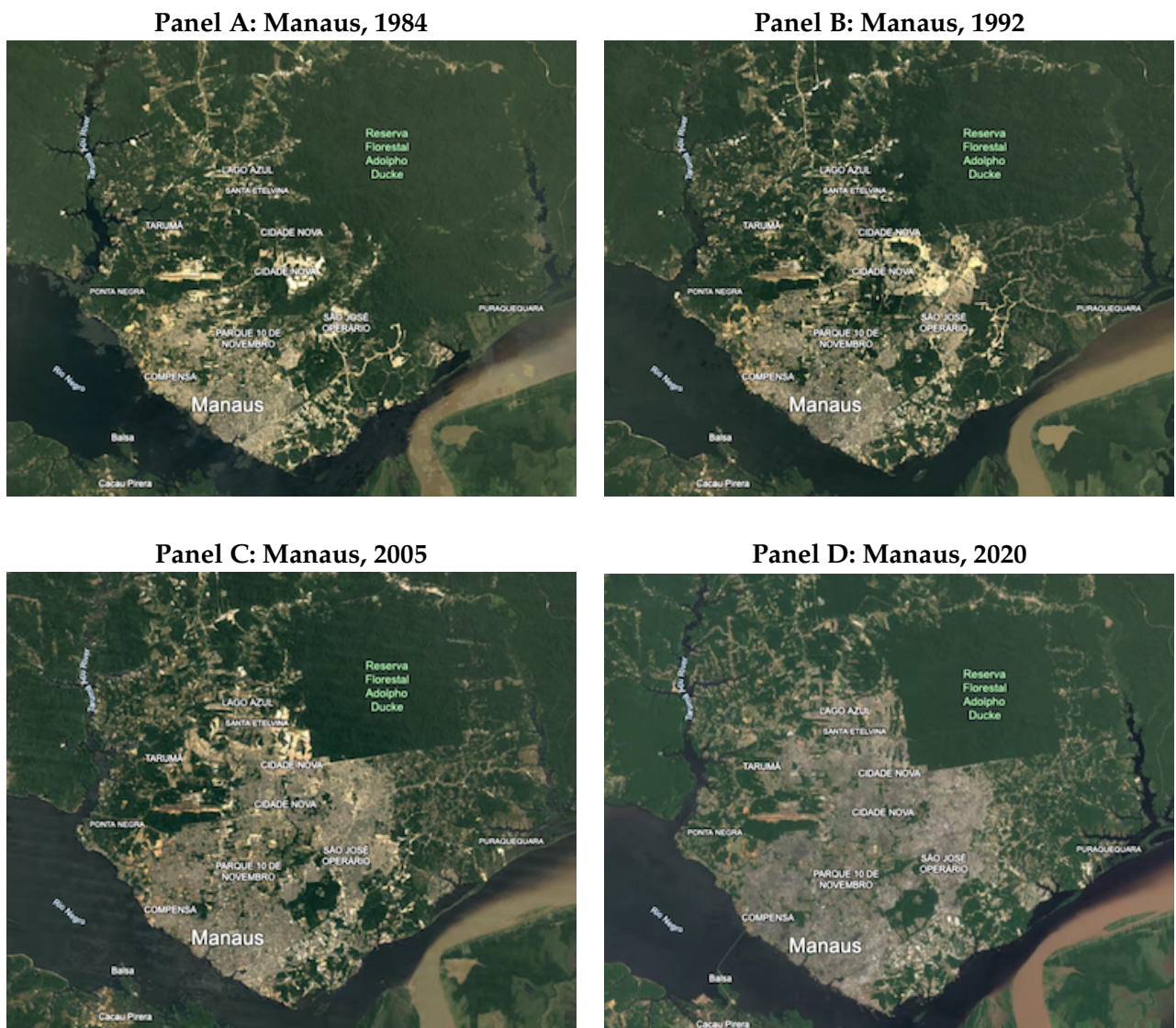
Note: This is an example of a [listing](#) for a house sale on Viva Real, with the listed IPTU highlighted in yellow.

⁵⁵For example, Cabral & Hoxby (2012)

B Additional Background on the 2011 IPTU Reform

In 2011 the government of Manaus passed Law 1.628/2011, which implemented a reform to the property tax system by altering the calculation of both the building and land value for a given property. The impetus of this reform was to better reflect the (presumptive) property values in light of the significant growth in Manaus since the IPTU was first implemented in 1983. Figure B.1 shows a timeline of satellite images of Manaus since 1984. Although the downtown core was already developed when the IPTU was created, much of the growth in the city during the past 40 years took place in the northern section of the city. Many of the tax sectors that determine the square-meter rate were sparsely populated until the late 1990s, with rates that did not reflect the increasing real estate density, activity, and value.

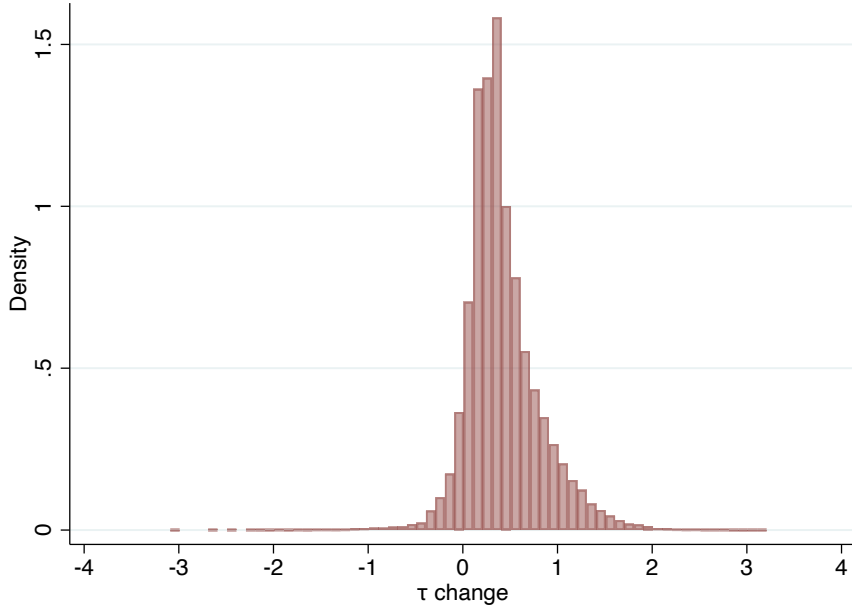
FIGURE B.1: GROWTH OF MANAUS OVER 40 YEARS THROUGH SATELLITE IMAGERY



Notes: This figure shows the growth of Manaus from 1984 to 2020 using a time lapse of satellite images. Map data: © 2023 Google / Maxar Technologies, AirbusCNES, Airbus.

The reform was not designed to be a complete overhaul of the system, but rather an update to the existing presumptive formula. The formula used to calculate the IPTU (equation 1) was unchanged, but the values for the land factors (ξ_y^A) and building factors (ξ_y^B) were changed across the different characteristics. Importantly for our empirical strategies, the reform included updates to the square-meter prices (p_s), with changes in the difference in rates across sector boundaries. Figure B.2 shows that for most residential properties in the city, the reform led to an increase in their tax bill.

FIGURE B.2: DISTRIBUTION OF CHANGES IN LOG TAX BILLS DUE TO THE 2011 REFORM



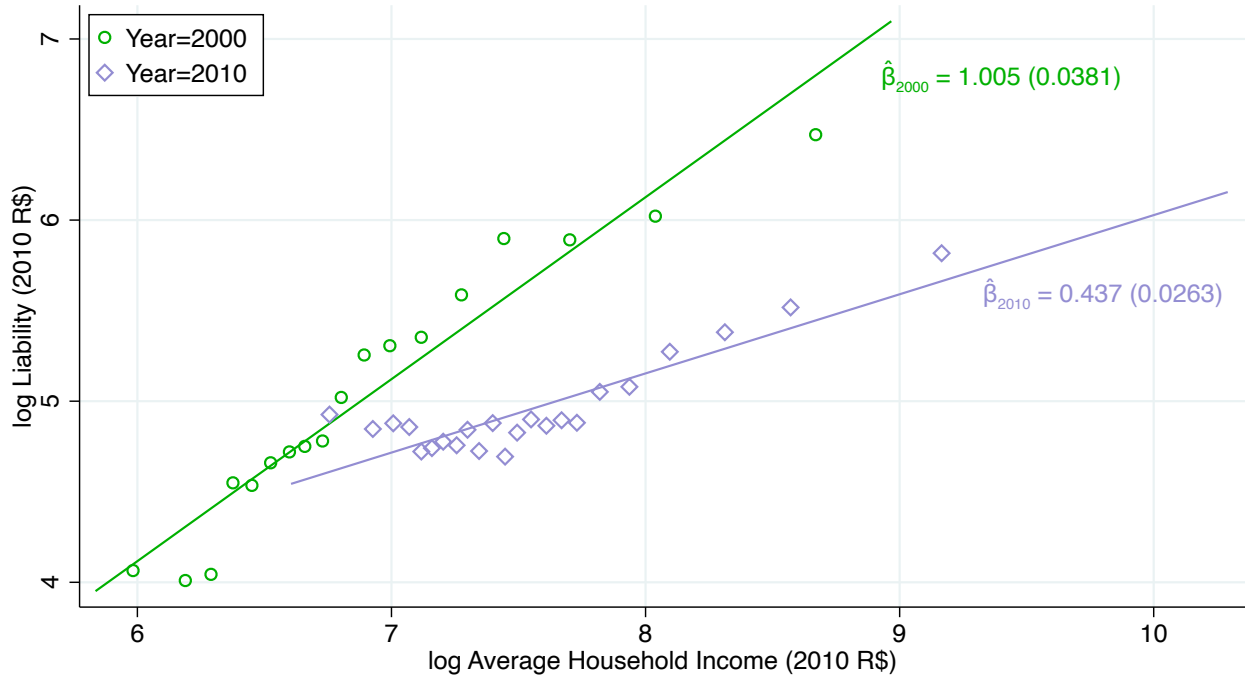
Notes: This figure shows the distribution of changes in the IPTU bill for households in our study sample.

In addition to reflecting the growth of the city since 1983, the changes implemented through the reform were meant to improve progressivity in property taxes. Without updates to the relative rates paid by households across the city, richer households would face increasingly smaller tax burdens as their property values increased, but they did not face higher IPTU bills. Figure B.3 panel A shows a weakening of tax progressivity in Manaus between the 2000 and 2010 census rounds, with a significant weakening of the relationship between the average tax bill and household income in a census tract.

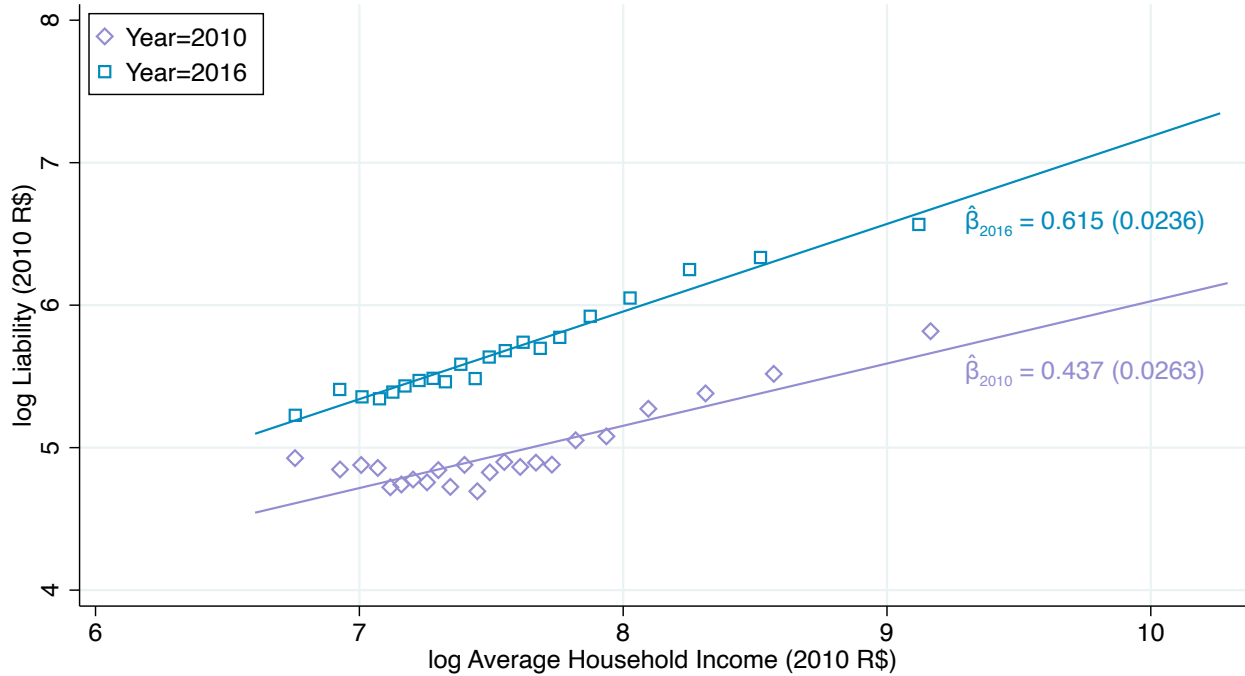
However, the 2011 reform was partially successful in strengthening the progressivity of the property tax system. Panel B of figure B.3 shows the relationship between the tax bill and average household income across census tracts in Manaus for the last pre-reform tax year (2010) and the first year when the new tax bills were fully implemented (2016). Two features are worth noting: there is an upward shift in the curves, implying that tax bills increased for almost all households in the city. However, there is also a rotation of the curve, with a steeper relationship between income and the IPTU in 2016, meaning that richer households faced a greater increase in their property taxes as a result of the reform.

FIGURE B.3: 2011 REFORM IMPROVES TARGETING OF PROPERTY TAX

Panel A: Change in Liabilities Pre-Reform



Panel B: Change in Liabilities Post-Reform



Notes: This figure plots the property tax bill against household income at the census-tract level. Data on census tracts for 2010 and 2016 comes from the 2010 census, with data on 2000 household income coming from tracts from the 2000 census. Property tax bills are shown in logs of the respective year, normalized to 2010 Reals.

C Creation of Distance Measure

In this section, we provide additional details on the construction of the distance measure employed in our Boundary Discontinuity Designs (BDD). Despite the numerous recent studies employing spatial discontinuities (Ring, 2024; Bayer *et al.*, 2007; Black, 1999; Livy, 2018; Gibbons *et al.*, 2013; Fack & Grenet, 2010; Turner *et al.*, 2014; Schönholzer, 2022; Keele & Titiunik, 2015), there is no consensus on the creation of the running variable (e.g. distance), especially in an urban setting.

Several features of our setting inform our decisions about the calculation of the distance measure. First, our level of observation is the property lot, which is often quite small relative to the tax sectors and Manaus as a whole. Second, property lots vary in size and are not uniform in their orientation to the sector boundaries; some sectors have lots that are oriented so that the short side of the lot is closest to the boundary, while other sectors have the long side of the lots running parallel to the boundary. Therefore, if one were to measure the distance of the lot to the boundary by taking the distance from the centroid of the lot polygon, there would be variation in the running variable that is not caused by the “true” distance of the property to the sector boundary, but is rather an artifact of the irregular shape and orientation of the lots relative to the street grid.

In addition to issues related to lot sizes across the city, the creation of the tax sector boundary requires careful consideration in our distance calculation. SEMEF defined the sector boundaries as (almost always) running through various streets in Manaus. However, street width varies throughout the city, with some streets used in the sector boundaries being wide avenues and others quite narrow side streets or alleys. Using the full width of the street would result in borders with varying thicknesses. Moreover, the shapefiles provided by SEMEF do not place the sector boundaries in the middle of the street, which means that the distance to households on different sides of the sector will depend on how accurately the government “drew” the polygons for the tax sectors.

To address these issues, we take the approach of constructing many transects along the sector boundaries to simulate an individual “walking” into a given sector. For each of these “walks” we record both which properties we run in to, as well as its distance along the walk. Given the shapefiles identifying the property lots and tax sector polygons, we take the following steps to estimate the distance to the boundary:

1. Remove all corners where three or more tax sectors intersect (*Note: this ensures that the transects are not generated at the edge case of a boundary*)
2. Divide sector boundaries into 500 meter long segments
3. Along the entire boundary, seed “nodes” every 10 meters
4. From each node, create a transect that is perpendicular to the boundary and has a distance of 300 meters into each sector
5. Identify points where a transect intersects the polygon of a lot (*Note: this usually generates two points per lot per transect – where the transect “enters” the lot, and where it “exits” the lot*)
6. Calculate the distance of each of these intersections to the transect node

FIGURE C.4: TRANSECT CREATION ACROSS SECTOR BOUNDARIES



Notes: This figure depicts the calculation of the distance measure to the boundary used in our regression discontinuity analysis for a small section of Manaus. The red line denotes the tax sector boundary, the blue lines denote the transects generated perpendicular to the boundary, and the green polygons depict the lot lines for the properties. Transect lines are generated along the sector boundary in 10 meter intervals, with each transect extending perpendicularly into each side of the boundary for 300 meters. The yellow dots denote places where the transect intersect a lot—either through “entering” or “exiting” the lot.

Figure C.4 shows a small portion of the SEMEF shapefile after the above process is completed. It is important to note that since the transects were seeded every 10 meters along the boundary, there may be multiple transects that intersect a given property lot. Moreover, the sector boundary on the left side of the figure is drawn very close to one side of the (wide) street; without correcting this in the distance calculation, we would interpret the properties in the left sector as being farther away from the boundary, even though the properties on both sides of the boundary are on the street. To correct for this, we make the following post-calculation adjustments:

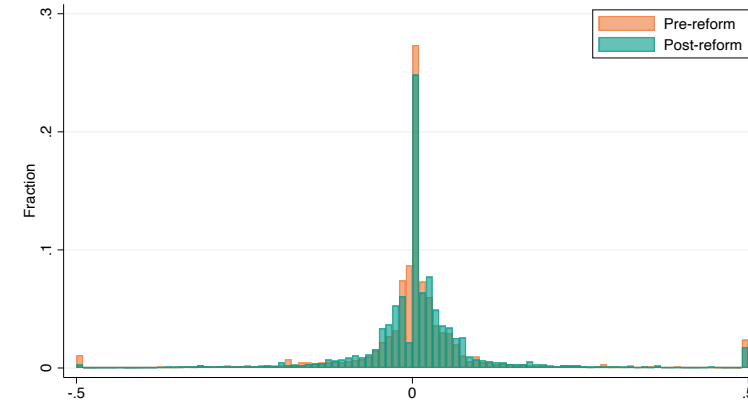
1. For each intersection point along the transect, remove the distance from the transect node to the first intersection point (*Note: this will “force” all properties nearest to the boundary to have a distance of zero to the boundary*)
2. For each lot, keep the smallest distance to the boundary

This creates a file of distances for 178,767 properties that are within 300 meters of a tax sector boundary, which we use as the base for our sample selection outlined in appendix E.

D Additional Background on Inequity Measure (σ)

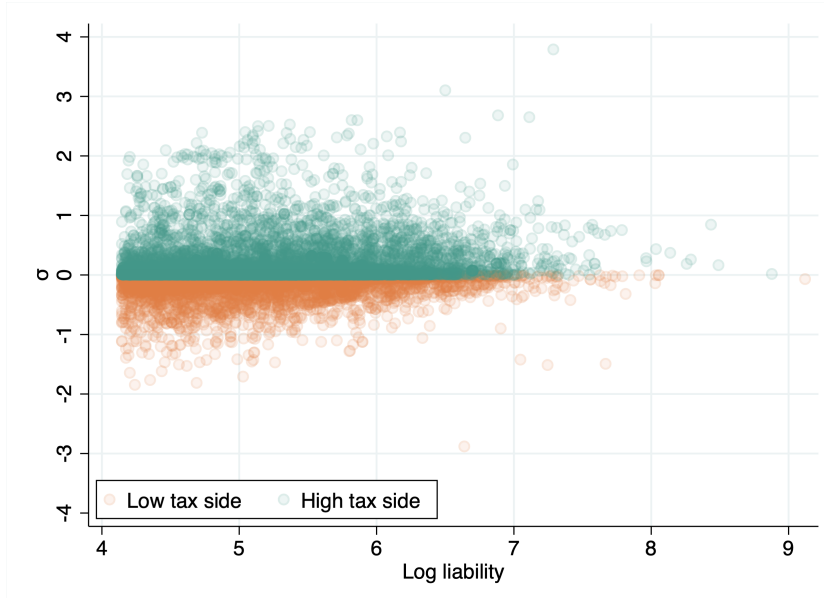
In this appendix, we provide additional evidence for our measurement of inequity (σ) and its relationship to the direct tax paid by the household (τ). Figure D.5 shows the distribution of the inequity measure for households in our sample. The histogram shows a large amount of variation in the level of inequity faced by households of different sides of the tax sectors.

FIGURE D.5: DISTRIBUTION OF σ_i



Although our measure of inequity is relative to a household's own tax liability, it is not collinear with it (figure D.6). The fact that households with the same tax liability face different levels of inequity allows us to disentangle the effect on compliance separately in section 5.

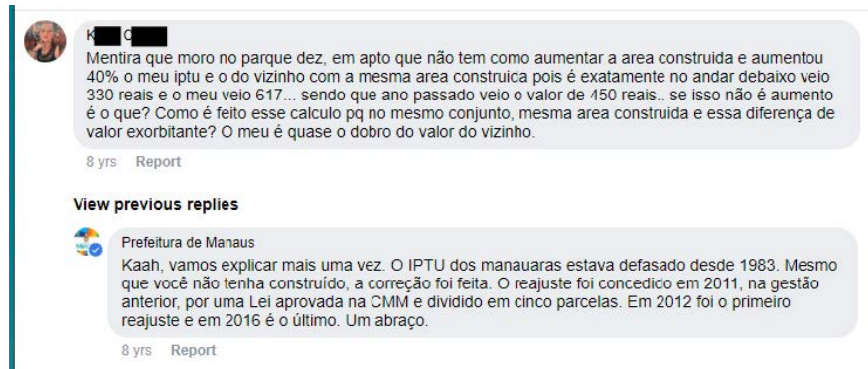
FIGURE D.6: τ_i AND σ_i ARE NOT COLLINEAR



Note: This figure plots a household's (log) tax liability against its inequity value (σ). Properties in a sector with a higher square-meter price than the neighboring sector are defined as being on the "high tax side".

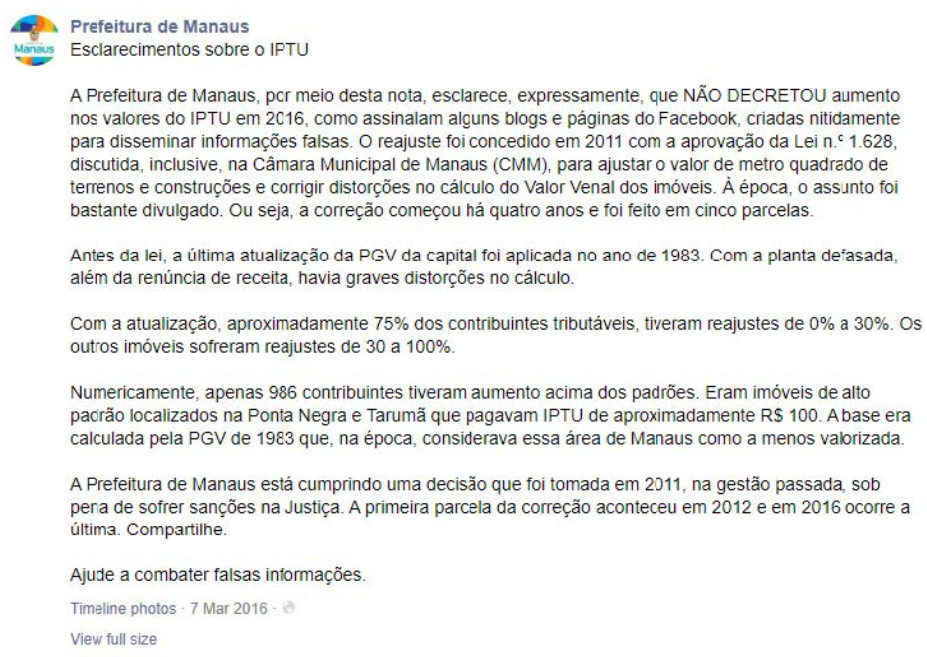
Our measure of inequity is partly driven by the observation that a household's response to the IPTU is driven by whether it feels like they have been treated by the system, and does not capture whether a household cares about whether other people are treated fairly. Figure D.7 shows a typical post on social media of a household complaining about their tax bill. In the post, the resident highlights the inequity of the system in that she pays nearly double the IPTU than her downstairs neighbor, even though they have similar apartments. This elicits a response from the government explaining that the 2011 reform caused IPTU bills to increase throughout the city, and it is not targeted at specific individuals.

FIGURE D.7: EXAMPLE OF SOCIAL MEDIA POST HIGHLIGHTING INEQUITY IN IPTU BILLS



The reform generated so many disinformation posts that the government felt it necessary to make a post clarifying the rationale and implementation of the reform (figure D.8). It highlights that the increase in 2016 was part of the 2011 reform and was not targeted at individuals.

FIGURE D.8: EXAMPLE OF SOCIAL MEDIA RESPONSE BY THE GOVERNMENT



E Sample Selection and Robustness Checks

In this appendix, we detail the sampling procedures undertaken to construct the final datasets used in our empirical analyses. Specifically, we outline each subsampling step and document the number of properties excluded at each stage.

For our cross-sectional boundary discontinuity analysis, we focus on properties located within 300 meters of the tax sector boundaries. Additionally, we exclude properties exempt from taxation, properties without construction, and those not designated as residential. Properties located on sector boundaries overlapping neighborhood boundaries were also excluded to prevent potential differences in municipal public goods provision. Table E.1 summarizes these sequential subsampling steps and provides the resulting sample sizes at every stage:

TABLE E.1: SUBSAMPLING STEPS - CROSS SECTIONAL SAMPLE

Subsampling step	N left in 2010	N left 04-18
Initial data	368,824	6,595,279
Drop properties beyond 300 meters from boundaries	178,767	3,011,054
Drop exempted properties	104,746	2,343,319
Drop properties on neighborhood borders	51,041	1,132,079
Drop non-residential properties	41,536	927,390
Drop lots without properties in 2010	41,536	626,076
Drop very large lots	33,500	509,486
Drop properties with no high tax side in 2010	25,097	382,229

We applied similar subsampling steps to construct the sample used for analyzing responses to the tax reform. The primary difference is that we reincorporate tax sector boundaries overlapping neighborhood boundaries, since our empirical design can control for boundary-specific characteristics that remain constant over time, such as differences between neighborhoods.

Table E.2 summarizes these steps and shows the corresponding sample sizes at each stage:

TABLE E.2: SUBSAMPLING STEPS - TAX REFORM SAMPLE

Subsampling step	N left in 2010	N left 04-18
Initial data	368,824	6,595,279
Drop properties beyond 300 meters from boundaries	178,767	3,011,054
Drop exempted properties	104,746	2,343,319
Drop non-residential properties	84,869	1,915,943
Drop lots without properties in 2010	84,869	1,284,321
Drop very large lots	68,735	1,055,587
Drop properties with no high tax side in 2010	53,685	825,853

To assess the robustness of our results to different sampling decisions, the following subsections replicate the main analyses under alternative subsampling criteria. Each figure and table explicitly references the corresponding results presented in the main sections of the paper.

Specifically, we check the robustness of our findings in the following alternative samples:

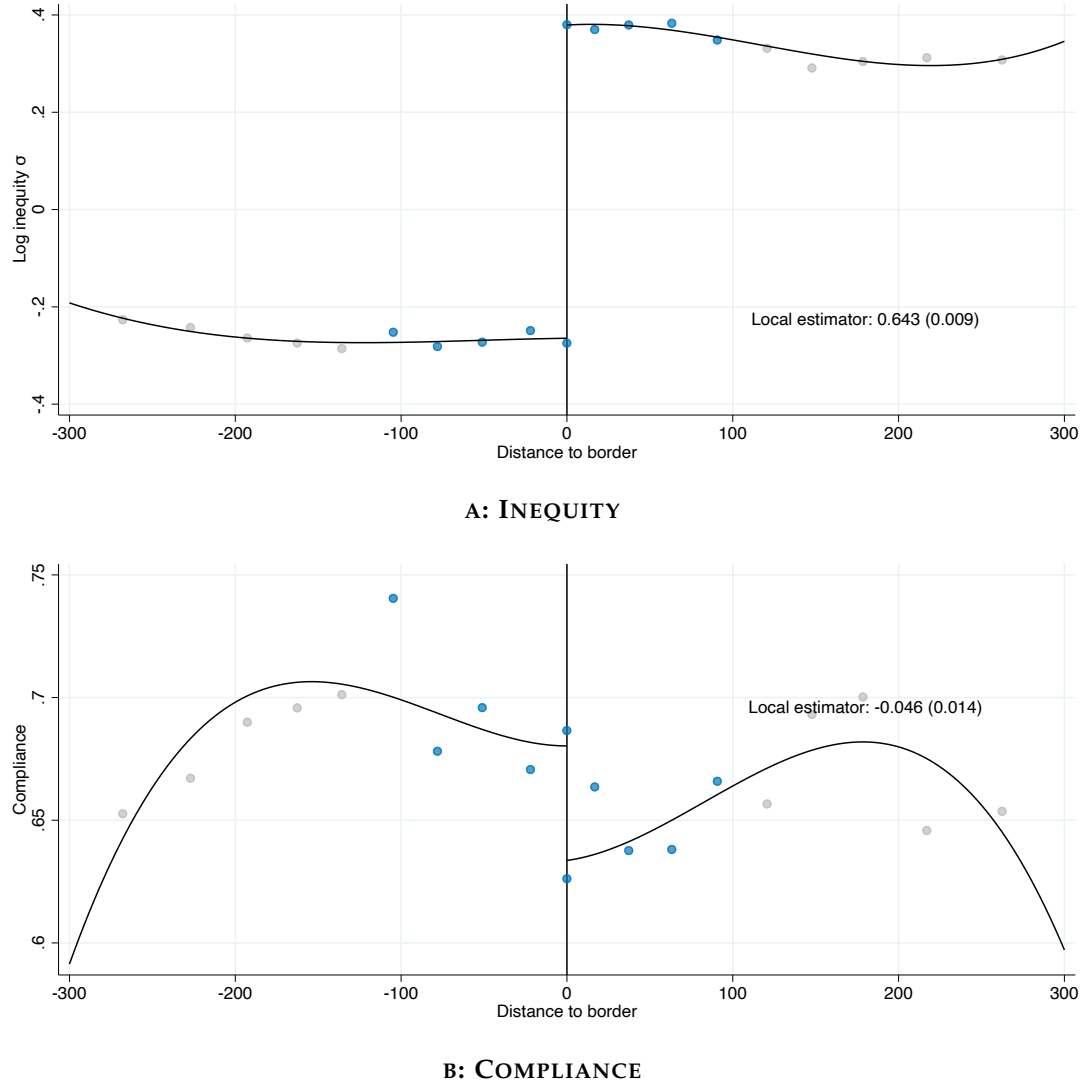
1. The sample including properties on neighborhood borders in section E.1

2. The sample excluding properties on neighborhood borders in our analysis of the 2011 reform in section [E.2](#)
3. The sample including non-residential properties in section [E.3](#)
4. The sample using a relaxed “large lots” definition in [E.4](#)
5. The sample using a stringent “large lots” definition in [E.5](#)
6. Using alternative definitions of a non-trivial degree of inequity in section [E.6](#)

E.1 Sample including properties on neighborhood borders

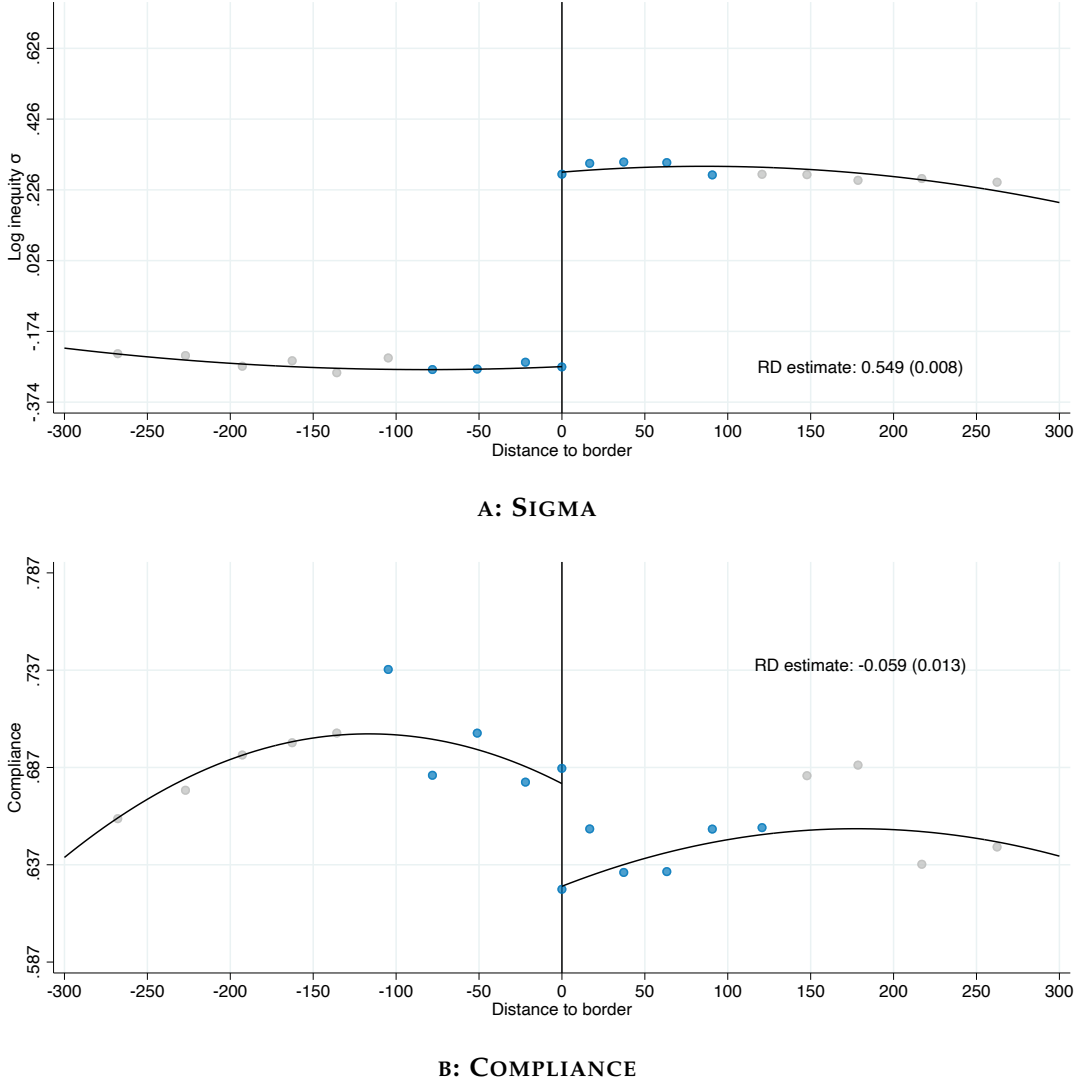
In the main analysis, we excluded properties located on neighborhood borders for the cross-sectional analysis but retained these properties for the tax reform analysis. In this subsection, we repeat the cross-sectional analysis while including properties located on neighborhood boundaries.

FIGURE E.1: OVERALL CHANGE IN COMPLIANCE AT TAX SECTOR BOUNDARIES



Notes: Panel A replicates the analysis from Panel B of Figure 4, and Panel B replicates the analysis from Figure 3, but additionally includes properties located on neighborhood boundaries. The figure shows the overall change in inequity (Panel A) and compliance (Panel B) at tax sector boundaries discussed in section 4.1. Specifically, we show the results of estimating the following equation for compliance and inequity (10): y_i by taxpayer i : $c_i = \lambda_{r(i)} + f(d_i) + \beta_0 HTS_i + h(d_i) \times HTS_i + \varepsilon_i$ where $\lambda_{r(i)}$ are boundary-segment fixed effects, HTS_i is an indicator for being on the high-tax side of the boundary ($d_i > 0$); $f_0(d_i)$ and $f_1(d_i)$ control for distance to the boundary on the low- and high-tax sides of the boundary, respectively; and ε_i is the residual. Overlaid on the figure, we show the point estimate of the discontinuity in compliance estimated using local linear distance controls, the MSE-minimizing bandwidth, and triangular kernel weights in distance. The dots in the figure show the coefficients from estimating (10) with fixed effects for decile-spaced bins of distance, using the same triangular kernel weights but censoring them at their tenth percentile to give non-zero weights to distances outside the optimal bandwidth. The bins in the optimal bandwidth are shown in blue while those outside are shown in grey. The black line is a global cubic polynomial fit in the same way.

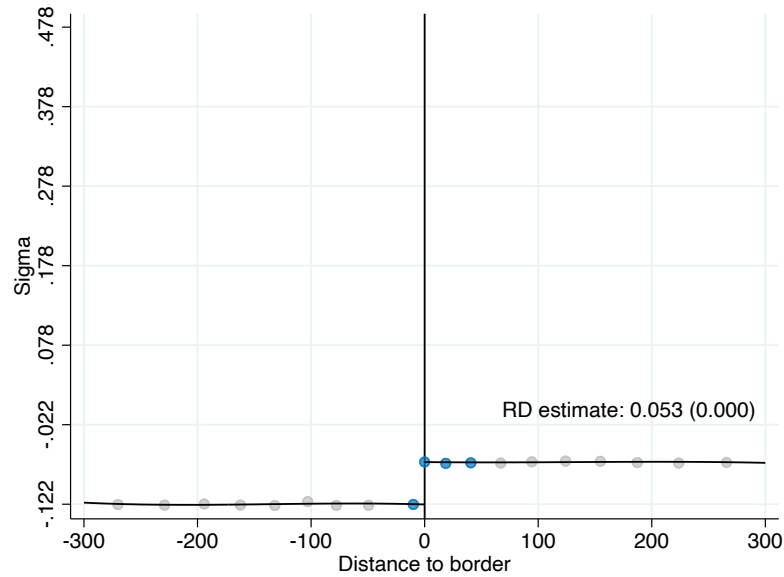
FIGURE E.2: AUGMENTED BOUNDARY DISCONTINUITY DESIGN



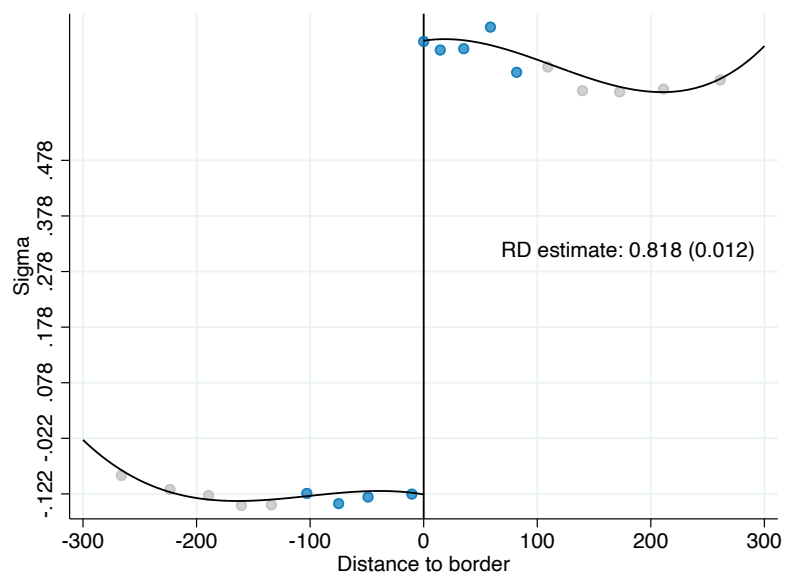
Notes: Panel A replicates the analysis from Figure 5, and Panel B replicates the analysis from Figure 6; however, both panels now also include properties located on neighborhood boundaries. The figure shows the impact on inequity and compliance in the augmented BDD discussed in section 5.1. Specifically, we show the results of estimation of equation (12): $y_i = \lambda_{r(i)} + g(\tau_i, e_i) + f(d_i) + \beta_0 HTS_i + h(d_i) \times HTS_i + \varepsilon_i$ using log-inequity σ as the outcome variable in panel A and compliance in panel B. $\lambda_{r(i)}$ are fixed effects for 500-meter segments along the boundaries to ensure we are comparing properties who are nearby each other; $g(\tau_i, e_i)$ are flexible controls for property i 's (log) tax liability τ_i and exposure to mistagging e_i (our baseline estimates use τ splines and exposure deciles); $f(d_i)$ and $h(d_i)$ control flexibly for distance to the boundary on the low- and high-tax sides of the boundary respectively; and HTS_i is an indicator for properties on the high-tax side of the boundary ($d_i > 0$). Overlaid on the figure, we show the point estimate of the discontinuity in inequity estimated using local linear distance controls, the MSE-minimizing bandwidth, and triangular kernel weights in distance. The dots in the figure show the coefficients from estimating (12) with fixed effects for decile-spaced bins of distance, using the same triangular kernel weights but censoring them at their tenth percentile to give non-zero weights to distances outside the optimal bandwidth. The bins in the optimal bandwidth are shown in blue while those outside are shown in gray. The black line is a global cubic polynomial fit in the same way.

FIGURE E.3: DIFFERENCE IN BOUNDARY DISCONTINUITY DESIGN: FIRST STAGE

PANEL A: LOW INEQUITY

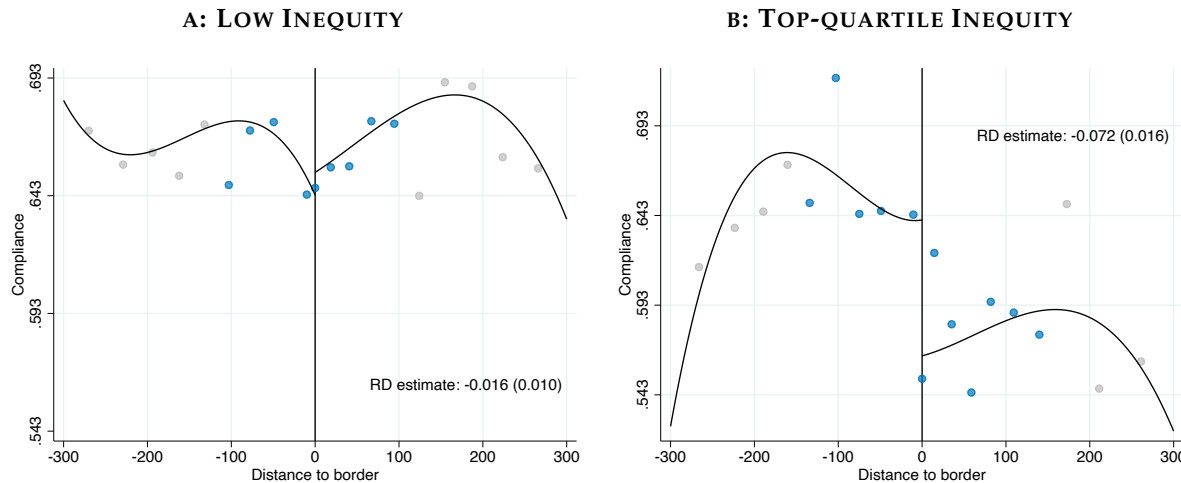


PANEL B: TOP-QUARTILE INEQUITY



Notes: This figure replicates the analysis from figure 8, but additionally includes properties located on neighborhood boundaries. The figure shows the results of estimating equation (12): $c_i = \lambda_{r(i)} + g(\tau_i, e_i) + f(d_i) + \beta_0 HTS_i + h(d_i) \times HTS_i + \varepsilon_i$ with inequity as the outcome variable, where terms are as defined in the notes to figure 6. Panel A shows the estimates in the subsample of properties facing low inequity (defined as being in the bottom 3 quartiles of inequity). Panel B shows the estimates in the subsample of properties facing top-quartile inequity.

FIGURE E.4: DIFFERENCE IN BOUNDARY DISCONTINUITY DESIGN: COMPLIANCE EFFECTS



Notes: This figure replicates the analysis from figure 9, but additionally includes properties located on neighborhood boundaries. The figure shows the results of estimating equation (12): $c_i = \lambda_{r(i)} + g(\tau_i, e_i) + f(d_i) + \beta_0 HTS_i + h(d_i) \times HTS_i + \varepsilon_i$ with compliance as the outcome variable, where terms are as defined in the notes to figure 6. Panel A shows the estimates in the subsample of properties facing low inequity (defined as being in the bottom 3 quartiles of inequity). Panel B shows the estimates in the subsample of properties facing top-quartile inequity.

TABLE E.3: DIFFERENCE IN BOUNDARY DISCONTINUITY DESIGN: COMPLIANCE EFFECTS

	(1)	(2)	(3)	(4)	(5)	(6)	(7)
1(high tax side)	0.00 (0.01)	0.00 (.)	0.00 (.)	0.00 (.)	0.08 (0.26)	0.07 (0.26)	0.00 (.)
1(high tax side) $\times \sigma $	-0.17*** (0.02)	-0.17*** (0.02)	-0.17*** (0.02)	-0.17*** (0.02)	-0.16*** (0.02)	-0.16*** (0.02)	-0.15*** (0.02)
R^2	0.108	0.108	0.107	0.108	0.110	0.109	0.111
Distance controls	✓	✓	✓	✓	✓	✓	✓
Segment fixed effects	✓	✓	✓	✓	✓	✓	✓
τ splines	✓	✓	✓	✗	✓	✓	✗
τ deciles	✗	✗	✗	✓	✗	✗	✓
Expansiveness splines	✗	✗	✓	✗	✗	✓	✗
Expansiveness deciles	✓	✓	✗	✓	✓	✗	✓
τ splines \times HTS	✗	✓	✓	✗	✓	✓	✗
τ deciles \times HTS	✗	✗	✗	✓	✗	✗	✓
τ splines \times exp deciles	✗	✗	✗	✗	✓	✗	✗
τ splines \times exp splines	✗	✗	✗	✗	✗	✓	✗
τ deciles \times exp deciles	✗	✗	✗	✗	✗	✗	✓
τ splines \times HTS \times exp deciles	✗	✗	✗	✗	✓	✗	✗
τ splines \times HTS \times exp splines	✗	✗	✗	✗	✗	✓	✗
τ deciles \times HTS \times exp deciles	✗	✗	✗	✗	✗	✗	✓
Elasticity	-0.263 0.025	-0.267 0.026	-0.273 0.026	-0.264 0.026	-0.245 0.028	-0.254 0.029	-0.238 0.028
N	53643	53643	53643	53643	53643	53643	53643

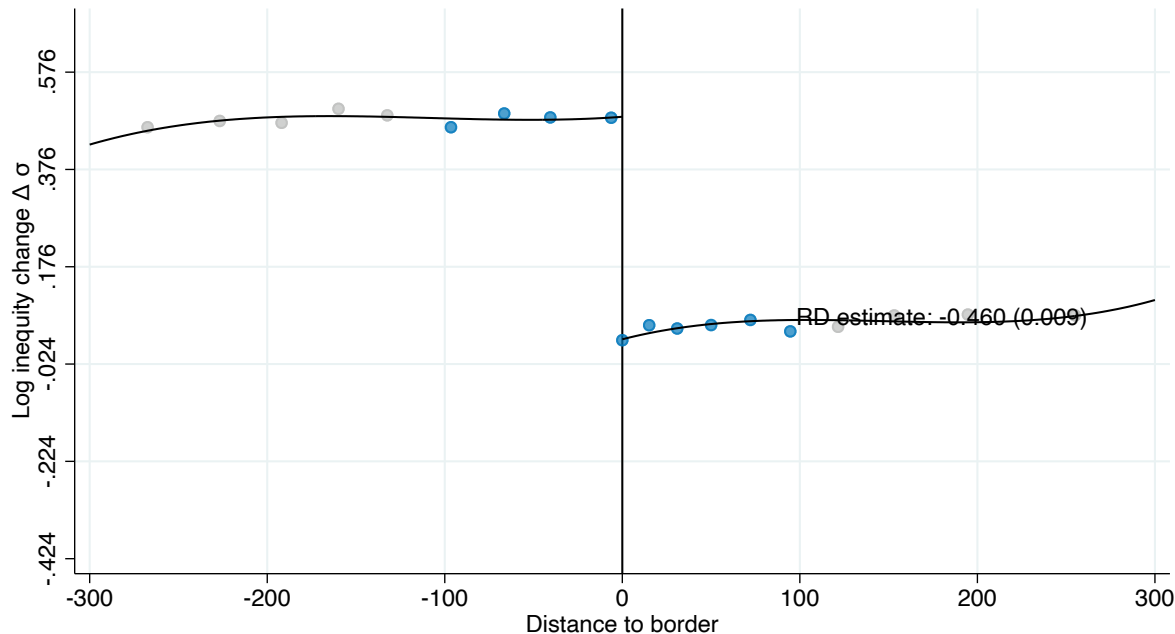
Notes: This table replicates the analysis from table 3, but additionally includes properties located on neighborhood boundaries. The table shows the results of estimation of equation (16): $c_i = \lambda_{r(i)} + g_0(\tau_i, e_i) + f(d_i) + HTS_i \times [\beta_0 + \eta \log(\sigma) + h(d_i) + g_1(\tau_i, e_i)] + \varepsilon_i$ where terms are as defined above in the notes to table E.13. In column (1), we control for cubic splines of the tax liability and fixed effects for deciles of the exposure distribution. In column (2) we control separately for the tax liability and exposure to mistagging on either side of the boundary. Column (3) replaces the exposure deciles with cubic splines in exposure while column (4) replaces the tax liability deciles with cubic splines. Columns (5)–(7) control for these separately on either side of the boundary.

E.2 Sample excluding properties on neighborhood borders

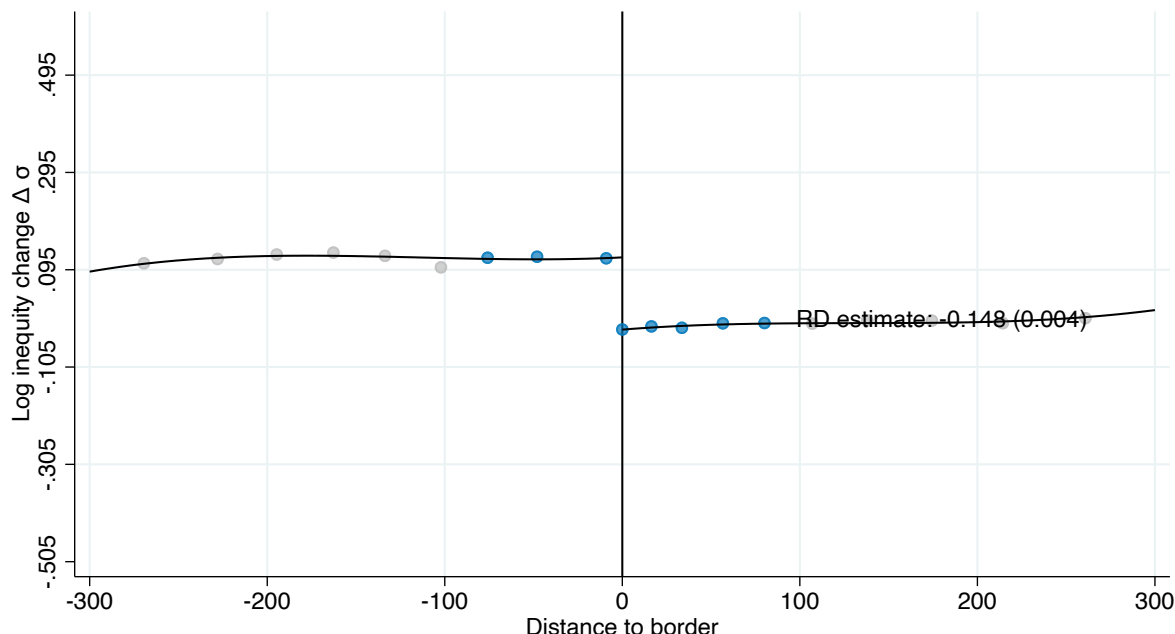
In the main analysis, we excluded properties located on neighborhood borders for the cross-sectional analysis but retained these properties for the tax reform analysis. In this subsection, we repeat the tax reform analysis while excluding properties located on neighborhood boundaries.

FIGURE E.5: DYNAMIC BOUNDARY DISCONTINUITY DESIGN: REMOVAL OF INEQUITY VS NO IMPROVEMENT

A: REMOVAL OF INEQUITY

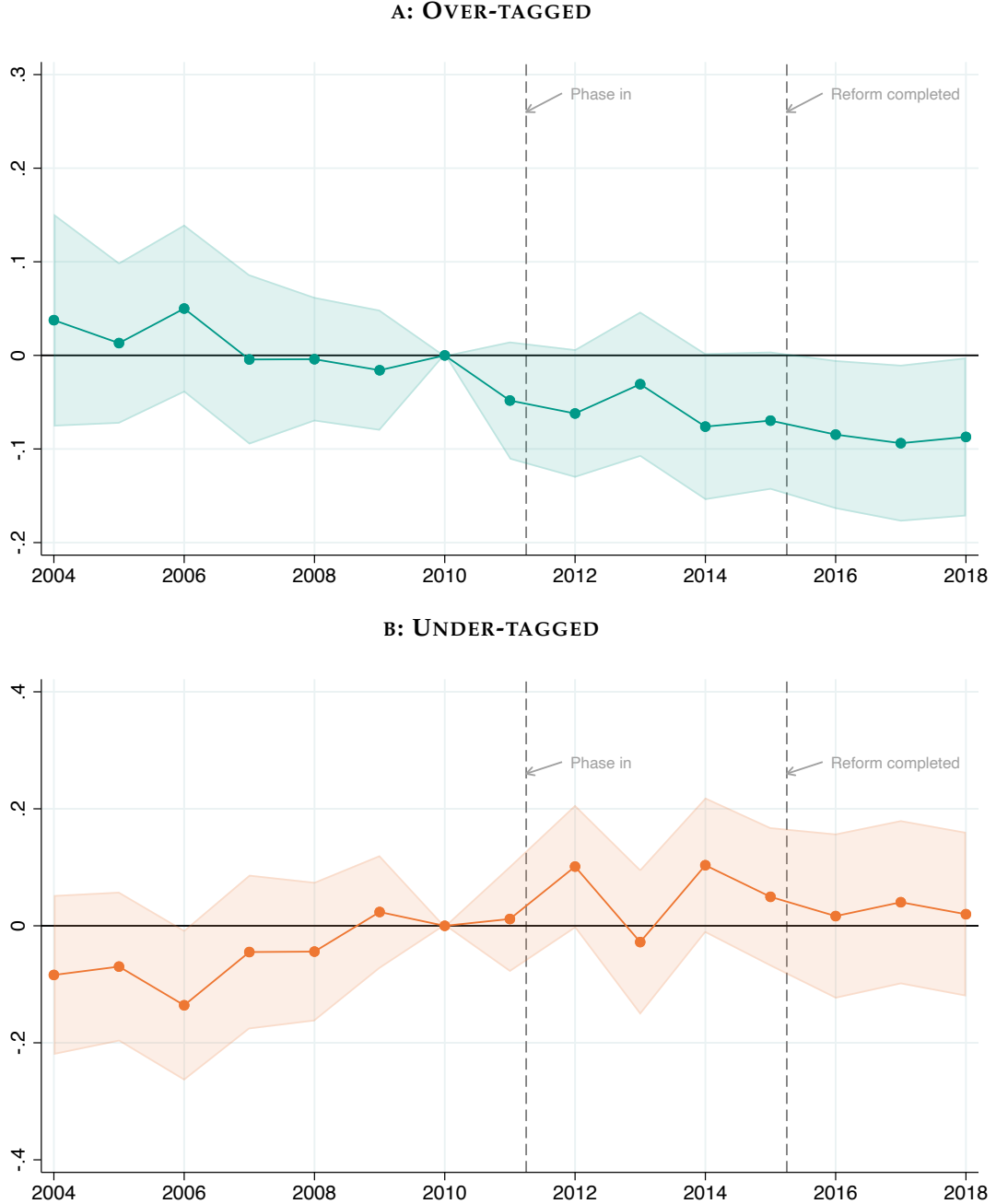


B: NO IMPROVEMENT



Notes: This figure replicates the analysis from figure 10, but additionally excludes properties located on neighborhood boundaries. The figure shows the results of estimating equation (17) $\Delta\sigma_i = \lambda_{r(i)} + g(\Delta\tau_i) + f_0(d_i) + HTS_i \times [\beta_0 + f_1(d_i)] + \varepsilon_i$ where the outcome variable is the change in inequity, $\lambda_{r(i)}$ are boundary-segment fixed effects, HTS_i is an indicator for being on the high-tax side of the boundary ($d_i > 0$); $f_0(d_i)$ and $f_1(d_i)$ control for distance to the boundary on the low- and high-tax sides of the boundary, respectively; and ε_i is the residual. $g(\Delta\tau_i)$ controls flexibly for changes in log tax liability, τ_i . Specifically, we control for splines of $\Delta\tau_i$. Panel A shows the estimates in the subsample of properties for whom the reform meaningfully reduced inequity. Panel B shows the estimates in the remaining subsample of properties.

FIGURE E.7: DIFFERENCE IN DIFFERENCE ESTIMATES OF OVERTAGGING AND UNDERTAGGING EFFECTS



Notes: This figure replicates the analysis from figure 12, but additionally excludes properties located on neighborhood boundaries. The figure shows the results of the estimation of equation (20) as discussed in section 6.3: $c_{iy} = \alpha_i + \lambda_{r(i)y} + \sum_{j \neq 2010} D_{jy} \times [f_{0j}(d_i) + \beta_{0j}\Delta\tau_i + \eta_{0j}\Delta\sigma_i + HTS_i \times (\delta_j + f_{1j}(d_i) + \beta_{1j}\Delta\tau_i + \eta_{1j}\Delta\sigma_i)] + \varepsilon_{iy}$, where $\lambda_{r(i)y}$ are segment-year fixed effects, $D_{jy} \equiv \mathbf{1}[y = j]$ are year dummies, and we include year-specific distance controls $f_{0j}(d_i)$ and $f_{1j}(d_i)$; and year-specific controls for property i 's tax liability change due to the reform. Panel A shows the estimated η_{1j} coefficients along with their 95% confidence intervals. Panel B shows the estimated η_{0j} coefficients along with their 95% confidence intervals.

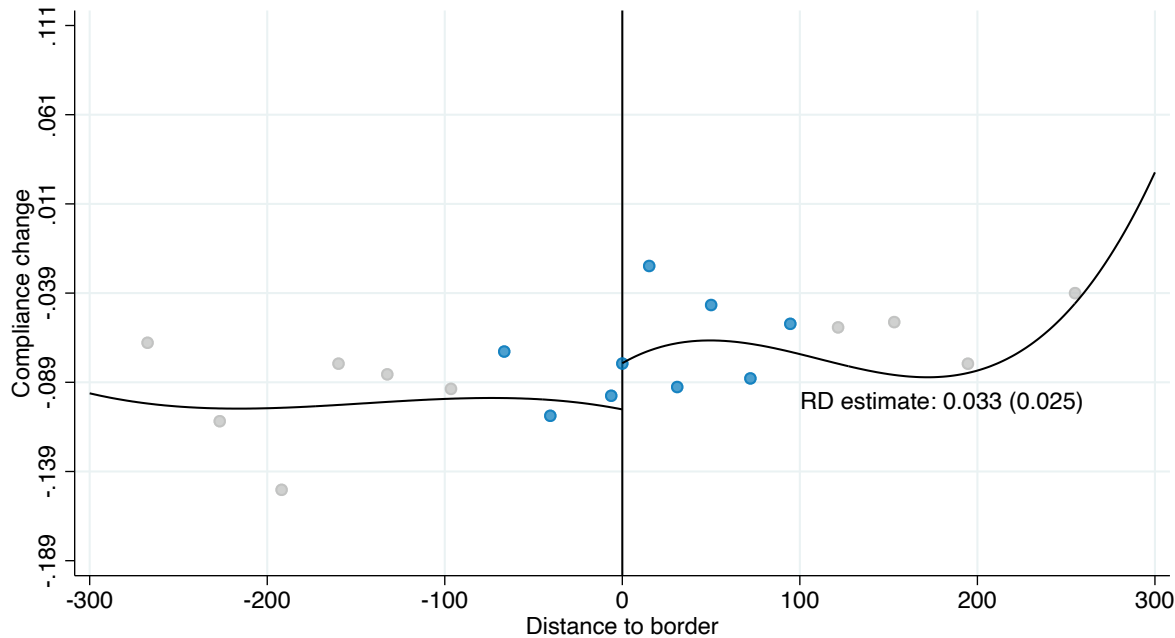
TABLE E.4: DYNAMIC DIFFERENCE IN BOUNDARY DISCONTINUITY DESIGN

	(1) Δ Compliance	(2) Δ Compliance	(3) Δ Compliance	(4) Δ Compliance
1(high tax side)	-0.013 (0.012)	-0.017 (0.032)	-0.010 (0.032)	-0.010 (0.024)
1(high tax side) X change in σ	-0.101*** (0.038)	-0.107*** (0.041)	-0.079* (0.044)	-0.111*** (0.040)
Distance controls	✓	✓	✓	✓
Segment FEs	✓	✓	✓	✓
τ splines	✓	✓	✓	✗
Expansiveness deciles	✓	✓	✗	✓
Interaction with HTS	✗	✓	✓	✓
τ splines \times expansiveness deciles	✗	✓	✗	✗
Expansiveness splines	✗	✗	✓	✗
τ splines \times expansiveness splines	✗	✗	✓	✗
τ deciles	✗	✗	✗	✓
τ deciles \times expansiveness deciles	✗	✗	✗	✓
Elasticity	0.157** (0.060)	0.166** (0.063)	0.122 (0.069)	0.172** (0.062)

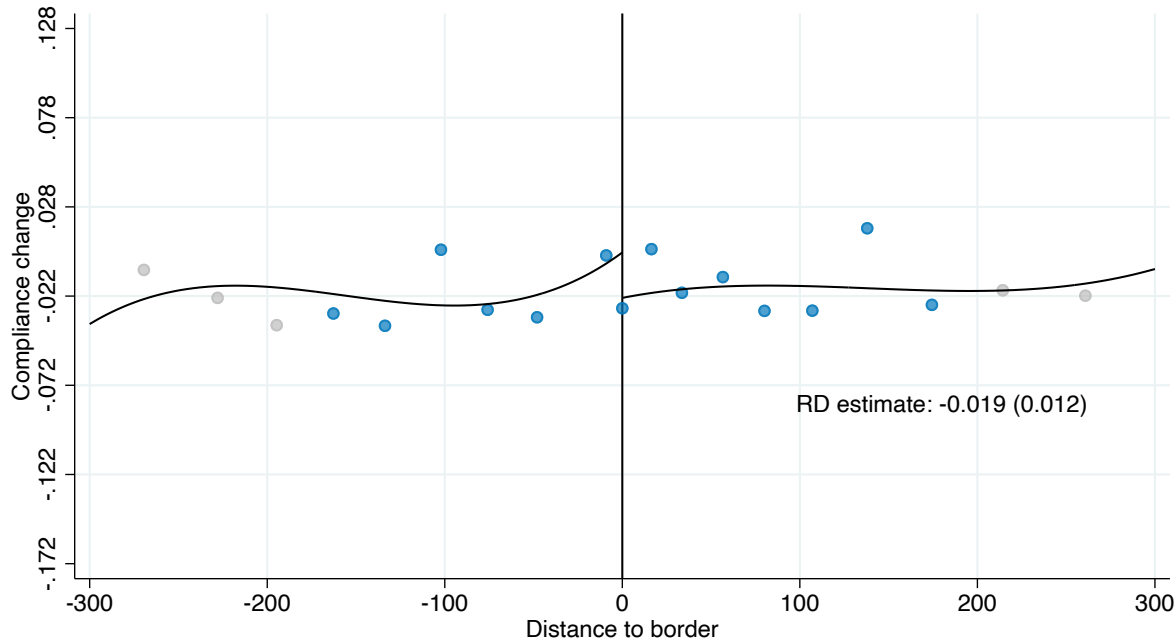
Notes: This table replicates the analysis from table 4, but additionally excludes properties located on neighborhood boundaries. This table shows the results of estimating equation (18) discussed in section 6.2: $\Delta c_i = \lambda_{r(i)} + g_0(\Delta\tau_i, e_i) + f_0(d_i) + HTS_i \times [\delta_0 + \eta \Delta \log(\sigma_i) + g_1(\Delta\tau_i, e_i) + f_1(d_i)] + \varepsilon_i$ where all terms are as defined above in the notes to table 2. Column (1) controls for cubic splines of the tax liability and fixed effects for deciles of the exposure distribution. Column (2) adds interactions between these controls and estimates them separately on either side of the boundary. Column (3) replaces the exposure deciles with splines, while column (4) replaces the tax liability splines with deciles of the tax liability distribution.

FIGURE E.6: DYNAMIC BOUNDARY DISCONTINUITY DESIGN: REMOVAL OF INEQUITY VS NO IMPROVEMENT

A: REMOVAL OF INEQUITY



B: NO IMPROVEMENT

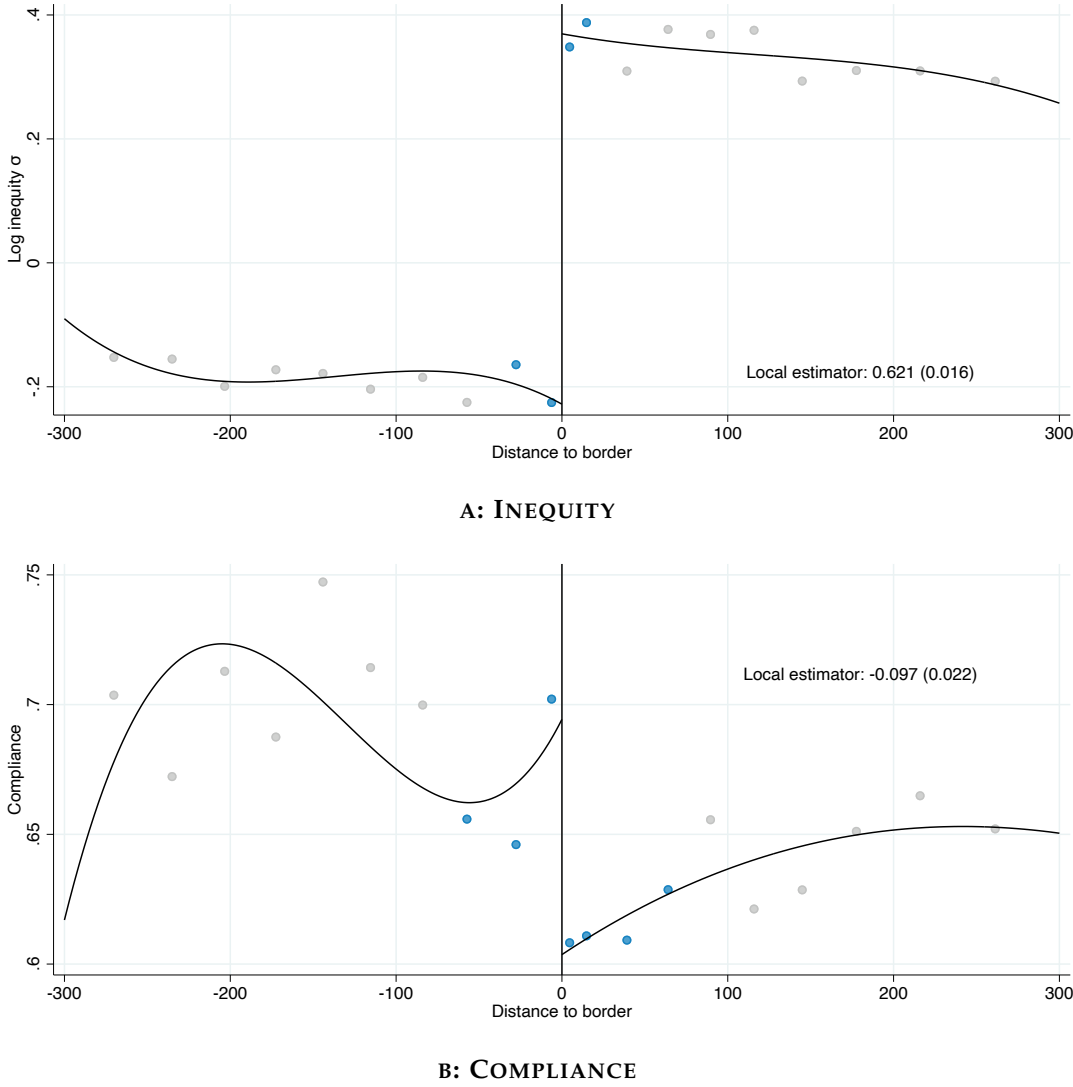


Notes: This figure replicates the analysis from figure 11, but additionally excludes properties located on neighborhood boundaries. The figure shows the results of estimating equation (17) $\Delta c_i = \lambda_{r(i)} + g(\Delta\tau_i) + f_0(d_i) + HTS_i \times [\beta_0 + f_1(d_i)] + \varepsilon_i$ where the outcome variable is the change in compliance, $\lambda_{r(i)}$ are boundary-segment fixed effects, HTS_i is an indicator for being on the high-tax side of the boundary ($d_i > 0$); $f_0(d_i)$ and $f_1(d_i)$ control for distance to the boundary on the low- and high-tax sides of the boundary, respectively; and ε_i is the residual. $g(\Delta\tau_i)$ controls flexibly for changes in log tax liability, τ_i . Specifically, we control for splines of $\Delta\tau_i$. Panel A shows the estimates in the subsample of properties for whom the reform meaningfully reduced inequity. Panel B shows the estimates in the remaining subsample of properties.

E.3 Sample with non-residential properties

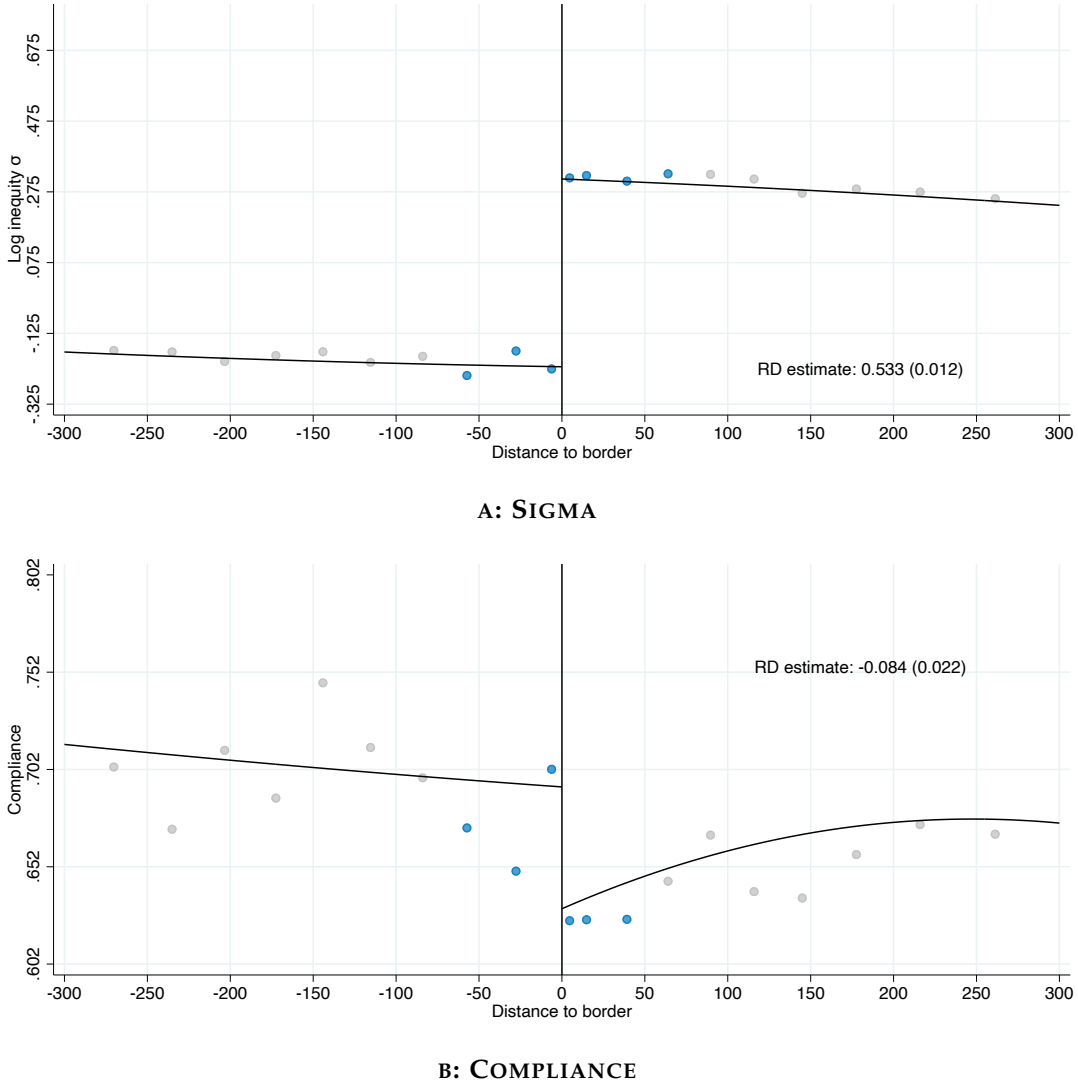
In the main text, we exclude non-residential properties. In this subsection, we repeat the main analysis while including the non-residential properties.

FIGURE E.8: OVERALL CHANGE IN COMPLIANCE AT TAX SECTOR BOUNDARIES



Notes: Panel A replicates the analysis from Panel B of Figure 4, and Panel B replicates the analysis from Figure 3, but additionally includes non-residential properties. The figure shows the overall change in inequity (Panel A) and compliance (Panel B) at tax sector boundaries discussed in section 4.1. Specifically, we show the results of estimating the following equation for compliance and inequity (10): y_i by taxpayer i : $c_i = \lambda_{r(i)} + f(d_i) + \beta_0 HTS_i + h(d_i) \times HTS_i + \varepsilon_i$ where $\lambda_{r(i)}$ are boundary-segment fixed effects, HTS_i is an indicator for being on the high-tax side of the boundary ($d_i > 0$); $f_0(d_i)$ and $f_1(d_i)$ control for distance to the boundary on the low- and high-tax sides of the boundary, respectively; and ε_i is the residual. Overlaid on the figure, we show the point estimate of the discontinuity in compliance estimated using local linear distance controls, the MSE-minimizing bandwidth, and triangular kernel weights in distance. The dots in the figure show the coefficients from estimating (10) with fixed effects for decile-spaced bins of distance, using the same triangular kernel weights but censoring them at their tenth percentile to give non-zero weights to distances outside the optimal bandwidth. The bins in the optimal bandwidth are shown in blue while those outside are shown in grey. The black line is a global cubic polynomial fit in the same way.

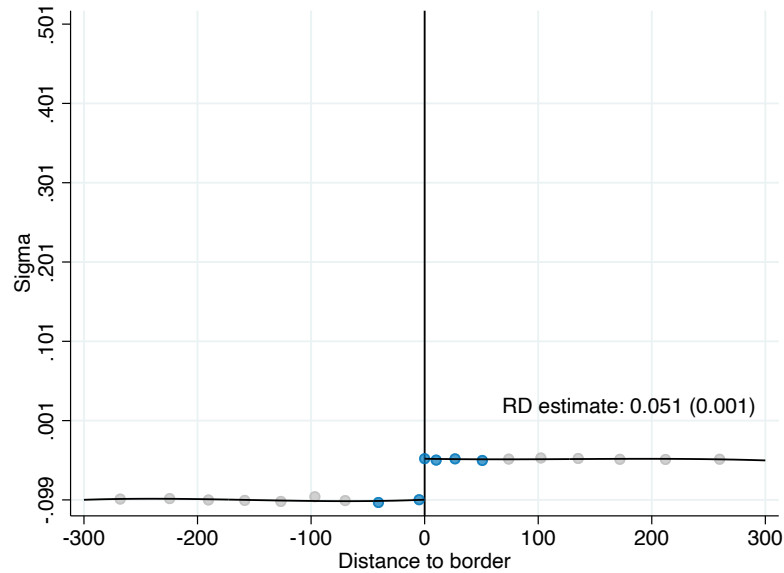
FIGURE E.9: AUGMENTED BOUNDARY DISCONTINUITY DESIGN



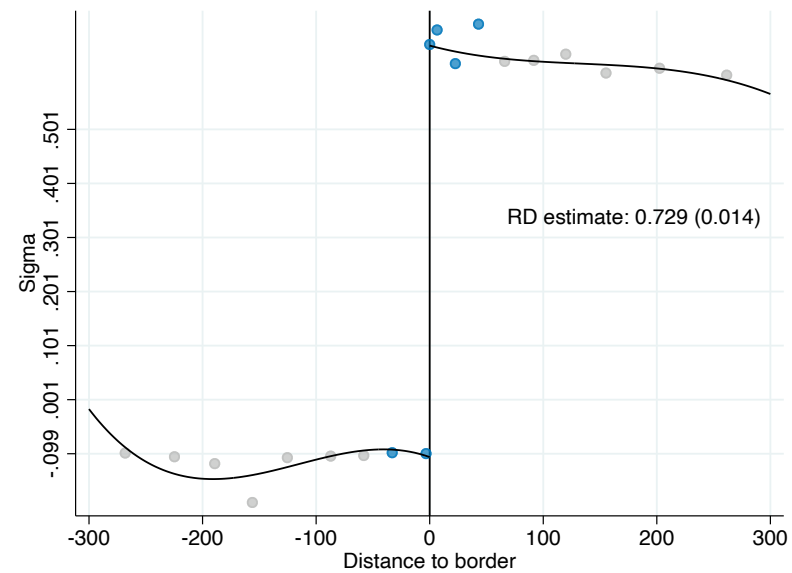
Notes: Panel A replicates the analysis from Figure 5, and Panel B replicates the analysis from Figure 6; however, both panels now also include non-residential properties. The figure shows the impact on inequity and compliance in the augmented BDD discussed in section 5.1. Specifically, we show the results of estimation of equation (12): $y_i = \lambda_{r(i)} + g(\tau_i, e_i) + f(d_i) + \beta_0 HTS_i + h(d_i) \times HTS_i + \varepsilon_i$ using log-inequity σ as the outcome variable in panel A and compliance in panel B. $\lambda_{r(i)}$ are fixed effects for 500-meter segments along the boundaries to ensure we are comparing properties who are nearby each other; $g(\tau_i, e_i)$ are flexible controls for property i 's (log) tax liability τ_i and exposure to mistagging e_i (our baseline estimates use τ splines and exposure deciles); $f(d_i)$ and $h(d_i)$ control flexibly for distance to the boundary on the low- and high-tax sides of the boundary respectively; and HTS_i is an indicator for properties on the high-tax side of the boundary ($d_i > 0$). Overlaid on the figure, we show the point estimate of the discontinuity in inequity estimated using local linear distance controls, the MSE-minimizing bandwidth, and triangular kernel weights in distance. The dots in the figure show the coefficients from estimating (12) with fixed effects for decile-spaced bins of distance, using the same triangular kernel weights but censoring them at their tenth percentile to give non-zero weights to distances outside the optimal bandwidth. The bins in the optimal bandwidth are shown in blue while those outside are shown in gray. The black line is a global cubic polynomial fit in the same way.

FIGURE E.10: DIFFERENCE IN BOUNDARY DISCONTINUITY DESIGN: FIRST STAGE

PANEL A: LOW INEQUITY

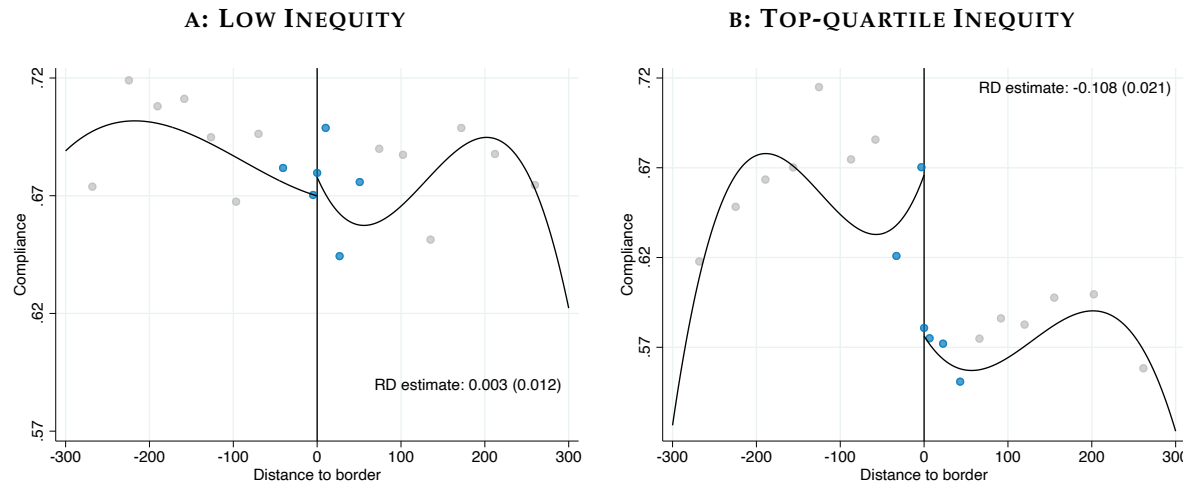


PANEL B: TOP-QUARTILE INEQUITY



Notes: This figure replicates the analysis from figure 8, but additionally includes non-residential properties. The figure shows the results of estimating equation (12): $c_i = \lambda_{r(i)} + g(\tau_i, e_i) + f(d_i) + \beta_0 HTS_i + h(d_i) \times HTS_i + \varepsilon_i$ with inequity as the outcome variable, where terms are as defined in the notes to figure 6. Panel A shows the estimates in the subsample of properties facing low inequity (defined as being in the bottom 3 quartiles of inequity). Panel B shows the estimates in the subsample of properties facing top-quartile inequity.

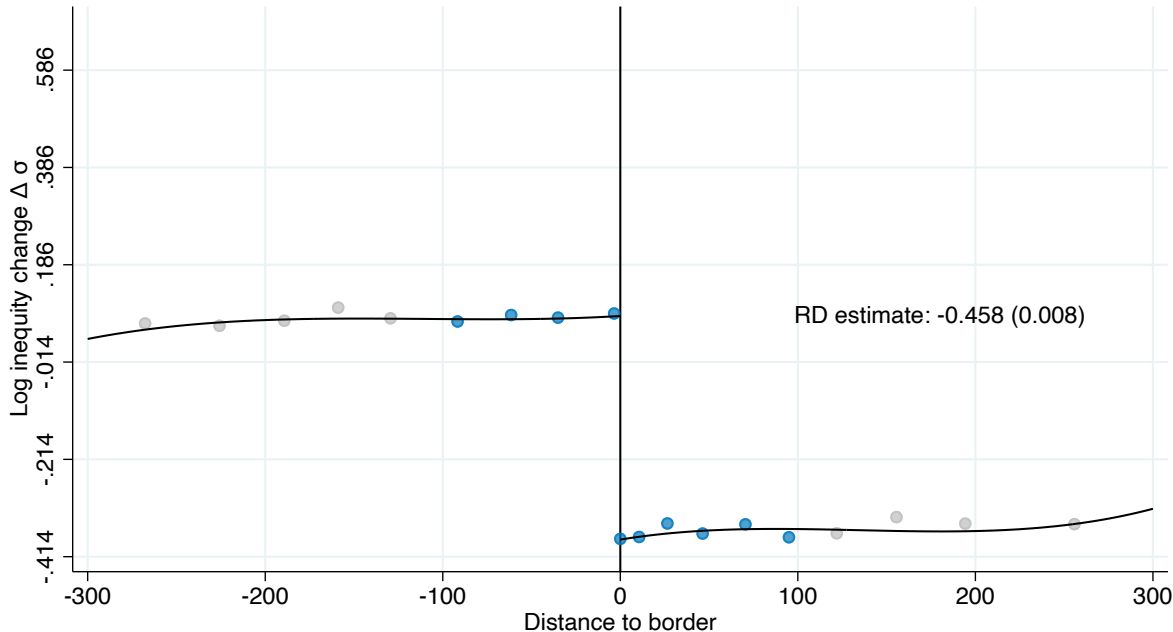
FIGURE E.11: DIFFERENCE IN BOUNDARY DISCONTINUITY DESIGN: COMPLIANCE EFFECTS



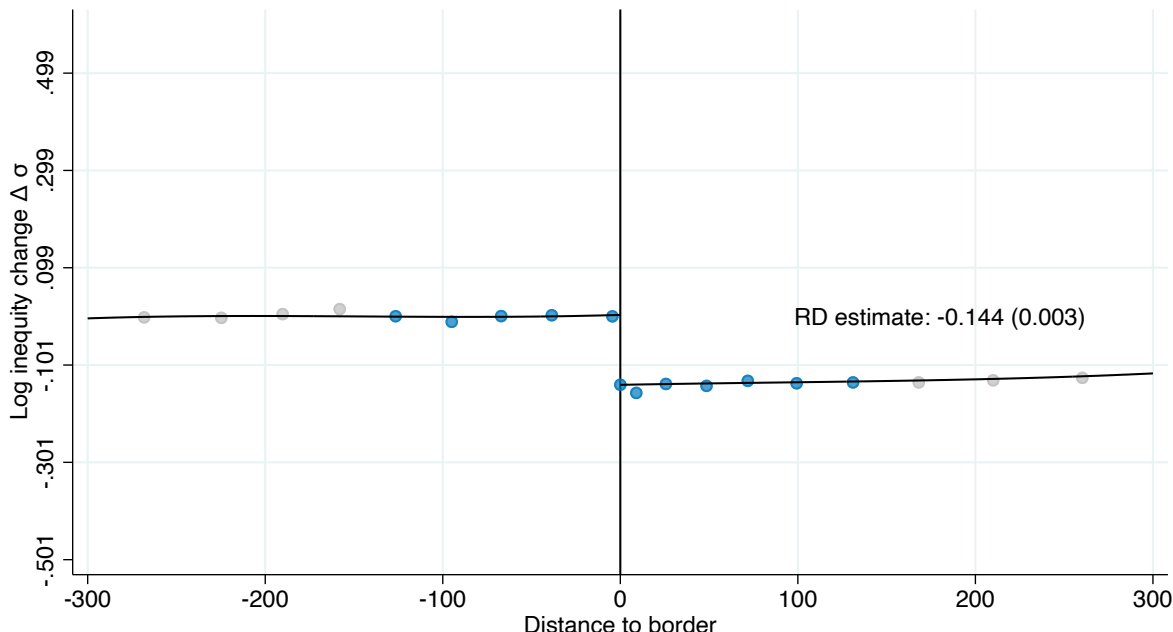
Notes: This figure replicates the analysis from figure 9, but additionally includes non-residential properties. The figure shows the results of estimating equation (12): $c_i = \lambda_{r(i)} + g(\tau_i, e_i) + f(d_i) + \beta_0 HTS_i + h(d_i) \times HTS_i + \varepsilon_i$ with compliance as the outcome variable, where terms are as defined in the notes to figure 6. Panel A shows the estimates in the subsample of properties facing low inequity (defined as being in the bottom 3 quartiles of inequity). Panel B shows the estimates in the subsample of properties facing top-quartile inequity.

FIGURE E.12: DYNAMIC BOUNDARY DISCONTINUITY DESIGN: REMOVAL OF INEQUITY VS NO IMPROVEMENT

A: REMOVAL OF INEQUITY

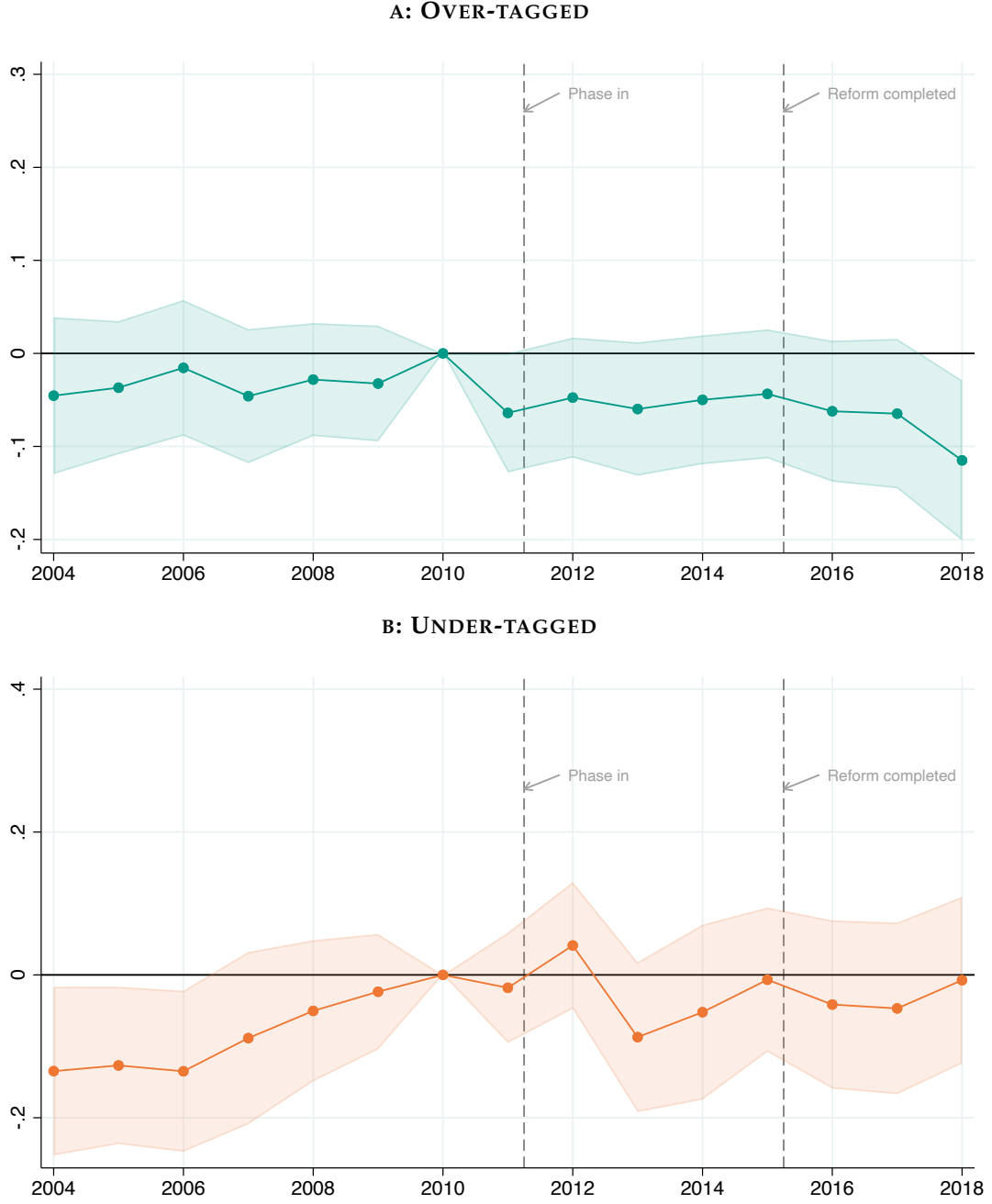


B: NO IMPROVEMENT



Notes: This figure replicates the analysis from figure 10, but additionally includes non-residential properties. The figure shows the results of estimating equation (17) $\Delta\sigma_i = \lambda_{r(i)} + g(\Delta\tau_i) + f_0(d_i) + HTS_i \times [\beta_0 + f_1(d_i)] + \varepsilon_i$ where the outcome variable is the change in inequality, $\lambda_{r(i)}$ are boundary-segment fixed effects, HTS_i is an indicator for being on the high-tax side of the boundary ($d_i > 0$); $f_0(d_i)$ and $f_1(d_i)$ control for distance to the boundary on the low- and high-tax sides of the boundary, respectively; and ε_i is the residual. $g(\Delta\tau_i)$ controls flexibly for changes in log tax liability, τ_i . Specifically, we control for splines of $\Delta\tau_i$. Panel A shows the estimates in the subsample of properties for whom the reform meaningfully reduced inequity. Panel B shows the estimates in the remaining subsample of properties.

FIGURE E.14: DIFFERENCE IN DIFFERENCE ESTIMATES OF OVERTAGGING AND UNDERTAGGING EFFECTS



Notes: This figure replicates the analysis from figure 12, but additionally includes non-residential properties. The figure shows the results of the estimation of equation (20) as discussed in section 6.3: $c_{iy} = \alpha_i + \lambda_{r(i)y} + \sum_{j \neq 2010} D_{jy} \times [f_{0j}(d_i) + \beta_{0j}\Delta\tau_i + \eta_{0j}\Delta\sigma_i + HTS_i \times (\delta_j + f_{1j}(d_i) + \beta_{1j}\Delta\tau_i + \eta_{1j}\Delta\sigma_i)] + \varepsilon_{iy}$, where $\lambda_{r(i)y}$ are segment-year fixed effects, $D_{jy} \equiv \mathbf{1}[y = j]$ are year dummies, and we include year-specific distance controls $f_{0j}(d_i)$ and $f_{1j}(d_i)$; and year-specific controls for property i 's tax liability change due to the reform. Panel A shows the estimated η_{1j} coefficients along with their 95% confidence intervals. Panel B shows the estimated η_{0j} coefficients along with their 95% confidence intervals.

TABLE E.5: AUGMENTED BOUNDARY DISCONTINUITY DESIGN: COMPLIANCE EFFECTS

	(1)	(2)	(3)	(4)	(5)	(6)
RD_Estimate	-0.08*** (0.02)	-0.08*** (0.01)	-0.08*** (0.01)	-0.08*** (0.02)	-0.08*** (0.01)	-0.08*** (0.01)
R^2						
Distance controls	✓	✓	✓	✓	✓	✓
Segment FEs	✓	✓	✓	✓	✓	✓
τ splines	✓	✓	✓	✓		
exp dec FEs	✓		✓			✓
τ decile FEs					✓	✓
exp splines		✓		✓		
τ splines \times exp dec FEs			✓			
τ splines \times exp splines				✓		
τ dec FEs \times exp dec FEs						✓
First-stage	0.555 (0.008)	0.542 (0.009)	0.557 (0.008)	0.542 (0.009)	0.555 (0.008)	0.556 (0.008)
fscoef_se						
Elasticity	-0.203 (0.037)	-0.199 (0.042)	-0.195 (0.037)	-0.203 (0.042)	-0.196 (0.036)	-0.185 (0.036)
elascoef_se						
N	12055	12054	12055	12054	12055	12055

Notes: This table replicates the analysis from table 2, but additionally includes non-residential properties. The table shows the results of estimating the augmented BDD equation (12): $c_i = \lambda_{r(i)} + g(\tau_i, e_i) + f_0(d_i) + \beta_0 HTS_i + f_1(d_i) \times HTS_i + \varepsilon_i$, where $\lambda_{r(i)}$ are fixed effects for 500-meter segments along the boundaries to ensure we are comparing properties who are nearby each other; $g(\tau_i, e_i)$ are flexible controls for property i 's (log) tax liability τ_i and exposure to mistagging e_i ; $f_0(d_i)$ and $f_1(d_i)$ control flexibly for distance to the boundary on the low- and high-tax sides of the boundary respectively; and HTS_i is an indicator for properties on the high-tax side of the boundary ($d_i > 0$). The columns use a variety of approaches to controlling flexibly for the tax liability and exposure to mistagging. In column (1) we control for cubic splines of the tax liability and fixed effects for deciles of exposure. In column (2) we replace the exposure deciles with cubic splines of exposure while column (3) replaces the splines of the tax liability with deciles. Columns (4)–(6) additionally interact the tax liability controls with the exposure controls.

TABLE E.6: DYNAMIC DIFFERENCE IN BOUNDARY DISCONTINUITY DESIGN

	(1) Δ Compliance	(2) Δ Compliance	(3) Δ Compliance	(4) Δ Compliance
1(high tax side)	0.006 (0.010)	0.007 (0.027)	0.009 (0.027)	-0.001 (0.021)
1(high tax side) X change in σ	-0.086*** (0.033)	-0.088** (0.035)	-0.083** (0.038)	-0.092*** (0.034)
Elasticity implied	-0.129	-0.132	-0.125	-0.138
Elasticity SE	0.050	0.053	0.056	0.052
Distance controls	✓	✓	✓	✓
Segment FEs	✓	✓	✓	✓
τ splines	✓	✓	✓	✗
Expansiveness deciles	✓	✓	✗	✓
Interaction with HTS	✗	✓	✓	✓
τ splines \times expansiveness deciles	✗	✓	✗	✗
Expansiveness splines	✗	✗	✓	✗
τ splines \times expansiveness splines	✗	✗	✓	✗
τ deciles	✗	✗	✗	✓
τ deciles \times expansiveness deciles	✗	✗	✗	✓

Notes: This table replicates the analysis from table 3, but additionally includes non-residential properties. This table shows the results of estimating equation (18) discussed in section 6.2:

$\Delta c_i = \lambda_{r(i)} + g_0(\Delta\tau_i, e_i) + f_0(d_i) + HTS_i \times [\delta_0 + \eta\Delta \log(\sigma_i) + g_1(\Delta\tau_i, e_i) + f_1(d_i)] + \varepsilon_i$ where all terms are as defined above in the notes to table 2. Column (1) controls for cubic splines of the tax liability and fixed effects for deciles of the exposure distribution. Column (2) adds interactions between these controls and estimates them separately on either side of the boundary. Column (3) replaces the exposure deciles with splines, while column (4) replaces the tax liability splines with deciles of the tax liability distribution.

TABLE E.7: DIFFERENCE IN BOUNDARY DISCONTINUITY DESIGN: COMPLIANCE EFFECTS

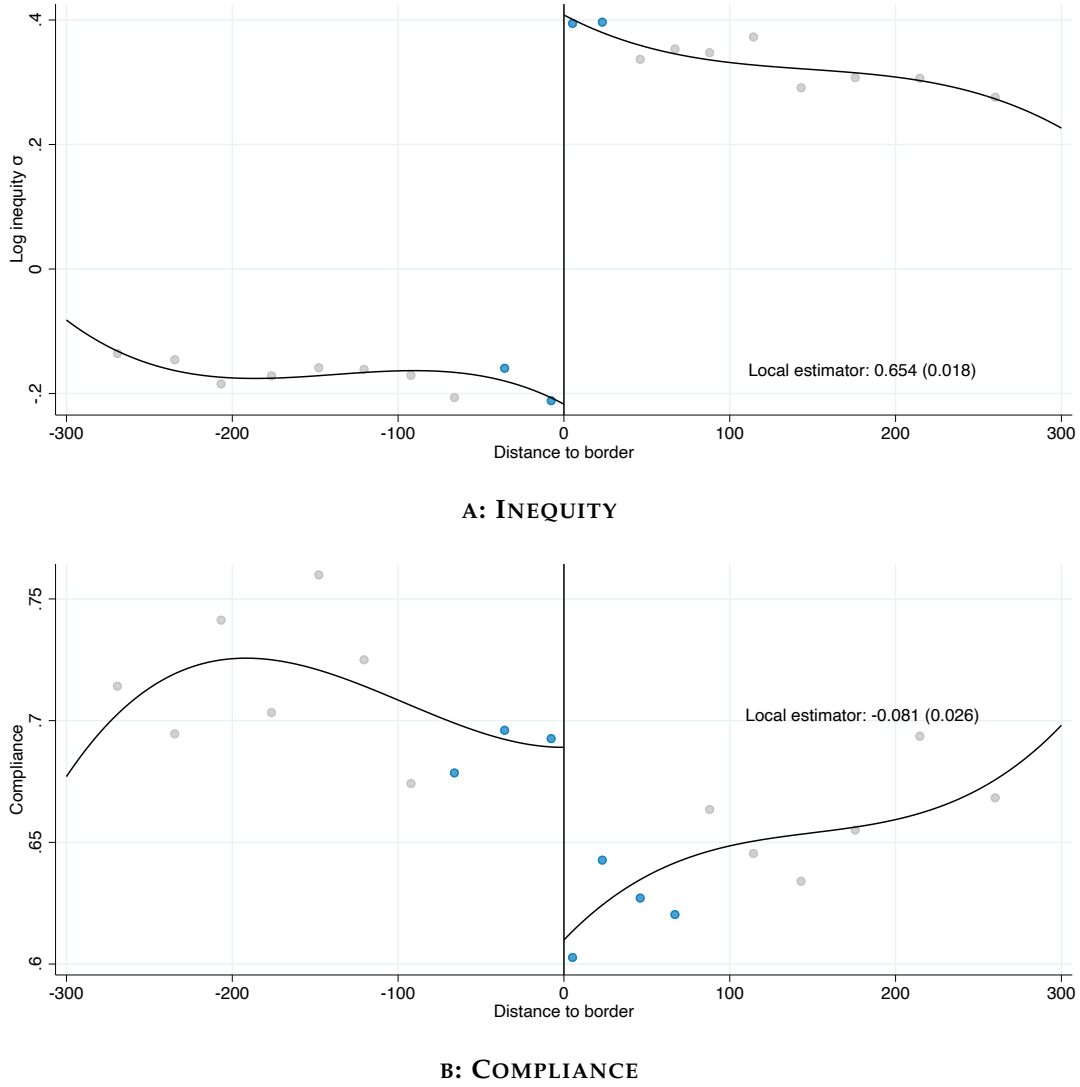
	(1)	(2)	(3)	(4)	(5)	(6)	(7)
1(high tax side)	-0.01 (0.01)	0.00 (.)	0.00 (.)	0.00 (.)	0.49 (0.30)	0.42 (0.30)	0.00 (.)
1(high tax side) $\times \sigma $	-0.16*** (0.02)	-0.16*** (0.02)	-0.17*** (0.02)	-0.16*** (0.02)	-0.14*** (0.02)	-0.15*** (0.02)	-0.14*** (0.02)
R^2	0.134	0.134	0.134	0.134	0.137	0.136	0.141
Distance controls	✓	✓	✓	✓	✓	✓	✓
Segment fixed effects	✓	✓	✓	✓	✓	✓	✓
τ splines	✓	✓	✓	✗	✓	✓	✗
τ deciles	✗	✗	✗	✓	✗	✗	✓
Expansiveness splines	✗	✗	✓	✗	✗	✓	✗
Expansiveness deciles	✓	✓	✗	✓	✓	✗	✓
τ splines \times HTS	✗	✓	✓	✗	✓	✓	✗
τ deciles \times HTS	✗	✗	✗	✓	✗	✗	✓
τ splines \times exp deciles	✗	✗	✗	✗	✓	✗	✗
τ splines \times exp splines	✗	✗	✗	✗	✗	✓	✗
τ deciles \times exp deciles	✗	✗	✗	✗	✗	✗	✓
τ splines \times HTS \times exp deciles	✗	✗	✗	✗	✓	✗	✗
τ splines \times HTS \times exp splines	✗	✗	✗	✗	✗	✓	✗
τ deciles \times HTS \times exp deciles	✗	✗	✗	✗	✗	✗	✓
Elasticity	-0.244 0.031	-0.243 0.031	-0.252 0.031	-0.242 0.031	-0.214 0.034	-0.232 0.035	-0.211 0.034
N	31587	31587	31587	31587	31587	31587	31587

Notes: This table replicates the analysis from table 4, but additionally includes non-residential properties. The table shows the results of estimation of equation (16): $c_i = \lambda_{r(i)} + g_0(\tau_i, e_i) + f_0(d_i) + HTS_i + [\beta_0 + \eta \log(\sigma) + f_1(d_i) + g_1(\tau_i, e_i)] + \varepsilon_i$ where terms are as defined above in the notes to table 2. In column (1), we control for cubic splines of the tax liability and fixed effects for deciles of the exposure distribution. In column (2) we control separately for the tax liability and exposure to mistagging on either side of the boundary. Column (3) replaces the exposure deciles with cubic splines in exposure while column (4) replaces the tax liability deciles with cubic splines. Columns (5)–(7) control for these separately on either side of the boundary.

E.4 Relaxed “large lots” Definition: Drop the top 0.1% in terms of land area

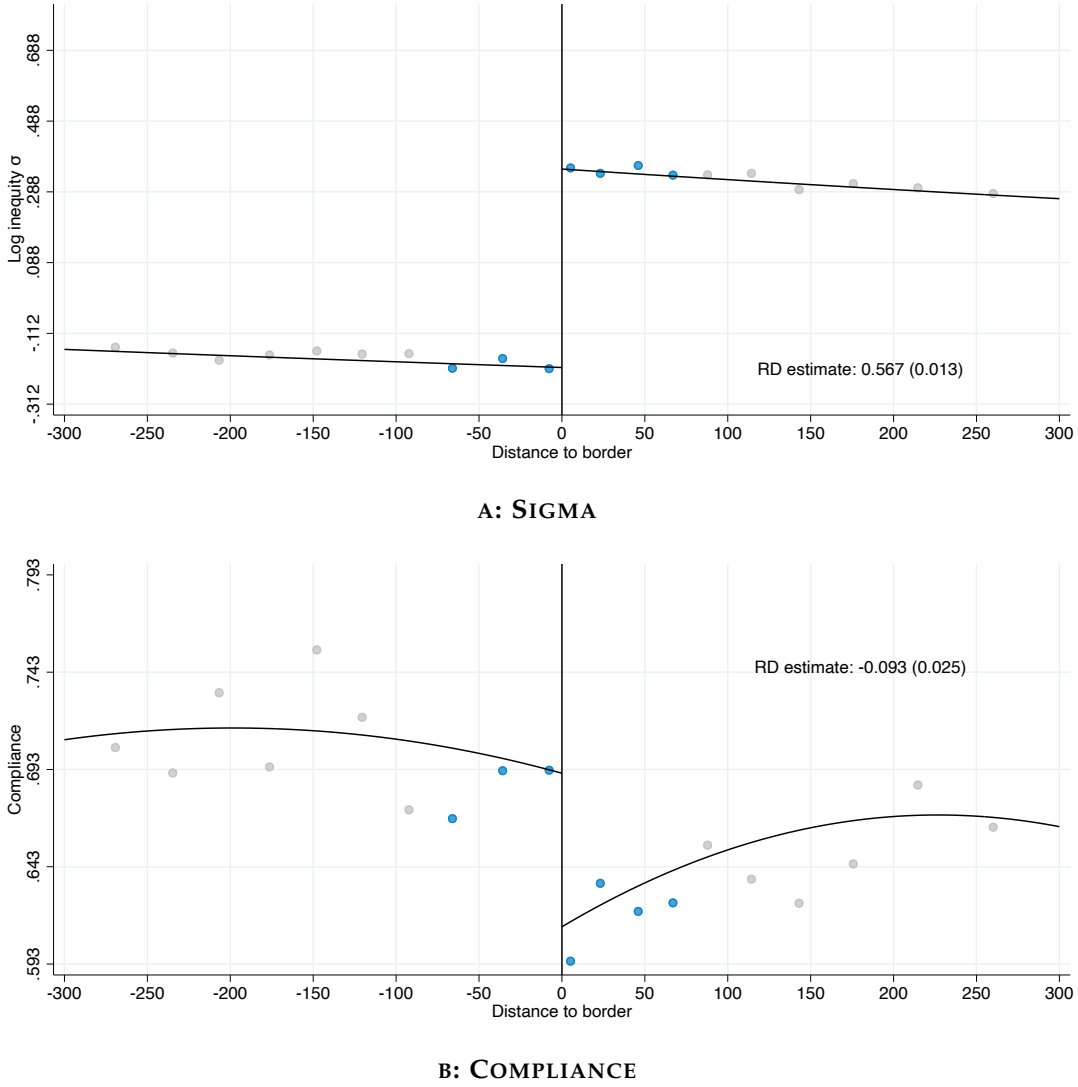
In the main text, we excluded “very large” lots because they introduce measurement error. We define “very large” lots as the top 0.5% in terms of land area. Here, we repeat the main analysis with a sample that excludes only the top 0.1% of lots in terms of land area.

FIGURE E.15: OVERALL CHANGE IN COMPLIANCE AT TAX SECTOR BOUNDARIES



Notes: Panel A replicates the analysis from Panel B of Figure 4, and Panel B replicates the analysis from Figure 3, but dropping only the top 0.1%, rather than 0.5%, of lots in terms of land area. The figure shows the overall change in inequity (Panel A) and compliance (Panel B) at tax sector boundaries discussed in section 4.1. Specifically, we show the results of estimating the following equation for compliance and inequity (10): y_i by taxpayer i : $c_i = \lambda_{r(i)} + f(d_i) + \beta_0 HTS_i + h(d_i) \times HTS_i + \varepsilon_i$ where $\lambda_{r(i)}$ are boundary-segment fixed effects, HTS_i is an indicator for being on the high-tax side of the boundary ($d_i > 0$); $f_0(d_i)$ and $f_1(d_i)$ control for distance to the boundary on the low- and high-tax sides of the boundary, respectively; and ε_i is the residual. Overlaid on the figure, we show the point estimate of the discontinuity in compliance estimated using local linear distance controls, the MSE-minimizing bandwidth, and triangular kernel weights in distance. The dots in the figure show the coefficients from estimating (10) with fixed effects for decile-spaced bins of distance, using the same triangular kernel weights but censoring them at their tenth percentile to give non-zero weights to distances outside the optimal bandwidth. The bins in the optimal bandwidth are shown in blue while those outside are shown in gray. The black line is a global cubic polynomial fit in the same way.

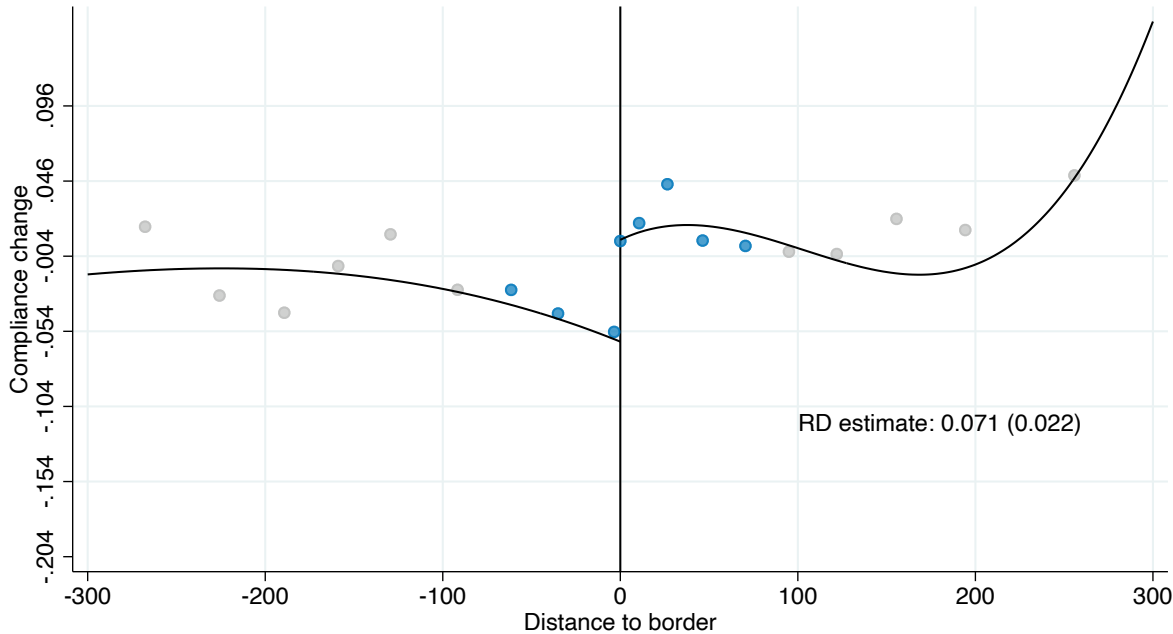
FIGURE E.16: AUGMENTED BOUNDARY DISCONTINUITY DESIGN



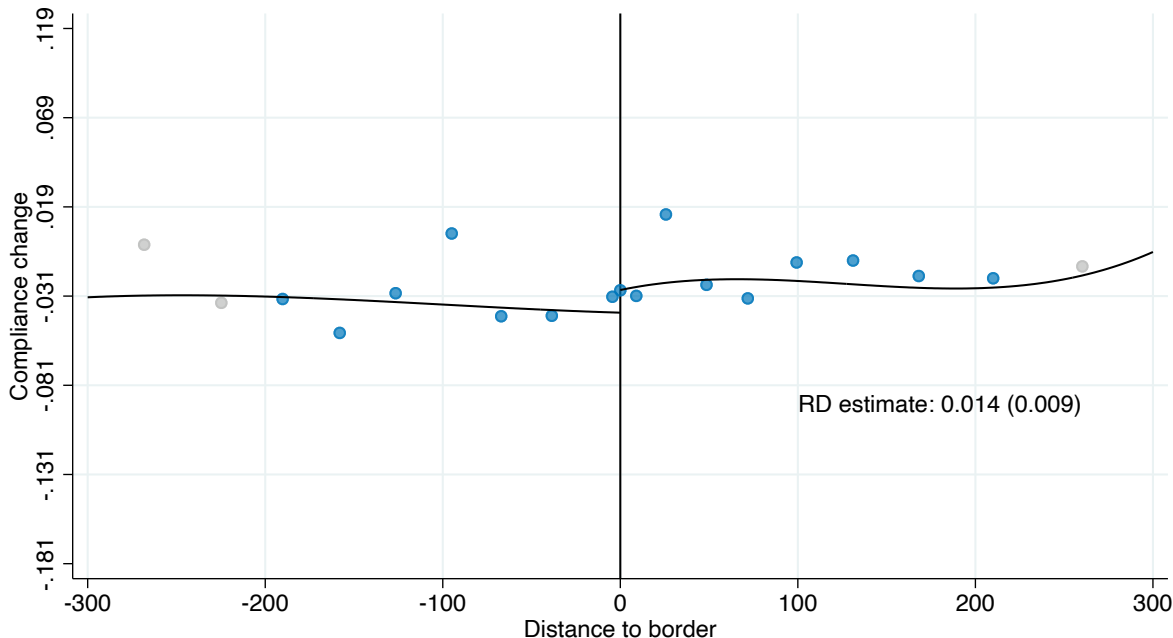
Notes: Panel A replicates the analysis from Figure 5, and Panel B replicates the analysis from Figure 6; however, both panels drop only the top 0.1%, rather than 0.5%, of lots in terms of land area. The figure shows the impact on inequity and compliance in the augmented BDD discussed in section 5.1. Specifically, we show the results of estimation of equation (12): $y_i = \lambda_{r(i)} + g(\tau_i, e_i) + f_0(d_i) + \beta_0 HTS_i + f_1(d_i) \times HTS_i + \varepsilon_i$ using log-inequity σ as the outcome variable in panel A and compliance in panel B. $\lambda_{r(i)}$ are fixed effects for 500-meter segments along the boundaries to ensure we are comparing properties who are nearby each other; $g(\tau_i, e_i)$ are flexible controls for property i 's (log) tax liability τ_i and exposure to mistagging e_i (our baseline estimates use τ splines and exposure deciles); $f_0(d_i)$ and $f_1(d_i)$ control flexibly for distance to the boundary on the low- and high-tax sides of the boundary respectively; and HTS_i is an indicator for properties on the high-tax side of the boundary ($d_i > 0$). Overlaid on the figure, we show the point estimate of the discontinuity in inequity estimated using local linear distance controls, the MSE-minimizing bandwidth, and triangular kernel weights in distance. The dots in the figure show the coefficients from estimating (12) with fixed effects for decile-spaced bins of distance, using the same triangular kernel weights but censoring them at their tenth percentile to give non-zero weights to distances outside the optimal bandwidth. The bins in the optimal bandwidth are shown in blue while those outside are shown in gray. The black line is a global cubic polynomial fit in the same way.

FIGURE E.13: DYNAMIC BOUNDARY DISCONTINUITY DESIGN: REMOVAL OF INEQUITY VS NO IMPROVEMENT

A: REMOVAL OF INEQUITY



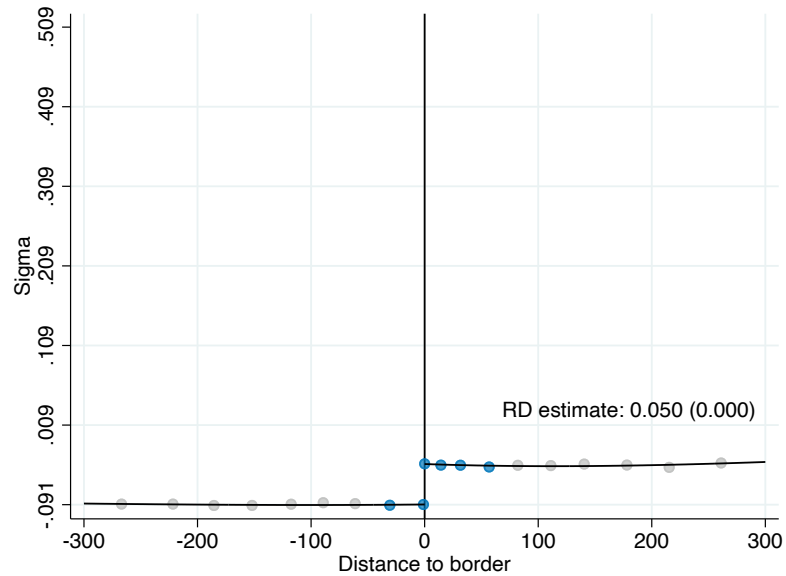
B: NO IMPROVEMENT



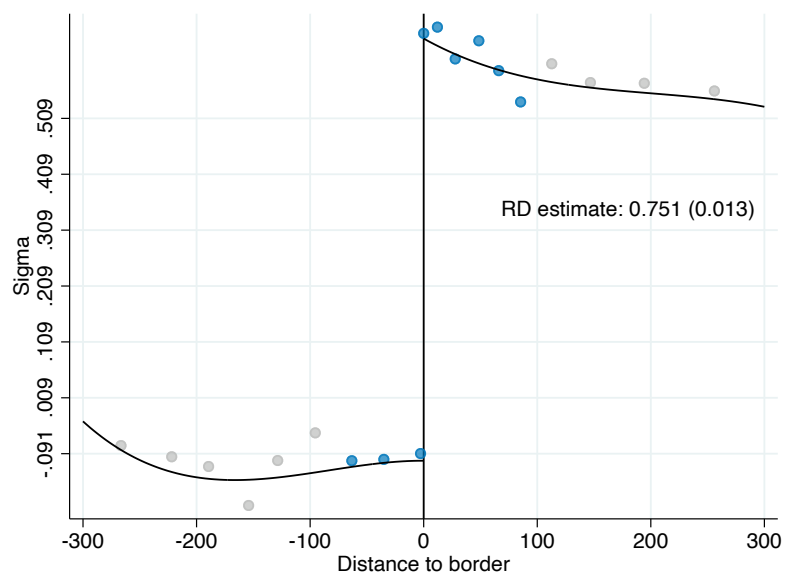
Notes: This figure replicates the analysis from figure 11, but additionally includes non-residential properties. The figure shows the results of estimating equation (17) $\Delta c_i = \lambda_{r(i)} + g(\Delta\tau_i) + f_0(d_i) + HTS_i \times [\beta_0 + f_1(d_i)] + \varepsilon_i$ where the outcome variable is the change in compliance, $\lambda_{r(i)}$ are boundary-segment fixed effects, HTS_i is an indicator for being on the high-tax side of the boundary ($d_i > 0$); $f_0(d_i)$ and $f_1(d_i)$ control for distance to the boundary on the low- and high-tax sides of the boundary, respectively; and ε_i is the residual. $g(\Delta\tau_i)$ controls flexibly for changes in log tax liability, τ_i . Specifically, we control for splines of $\Delta\tau_i$. Panel A shows the estimates in the subsample of properties for whom the reform meaningfully reduced inequity. Panel B shows the estimates in the remaining subsample of properties.

FIGURE E.17: DIFFERENCE IN BOUNDARY DISCONTINUITY DESIGN: FIRST STAGE

PANEL A: LOW INEQUITY

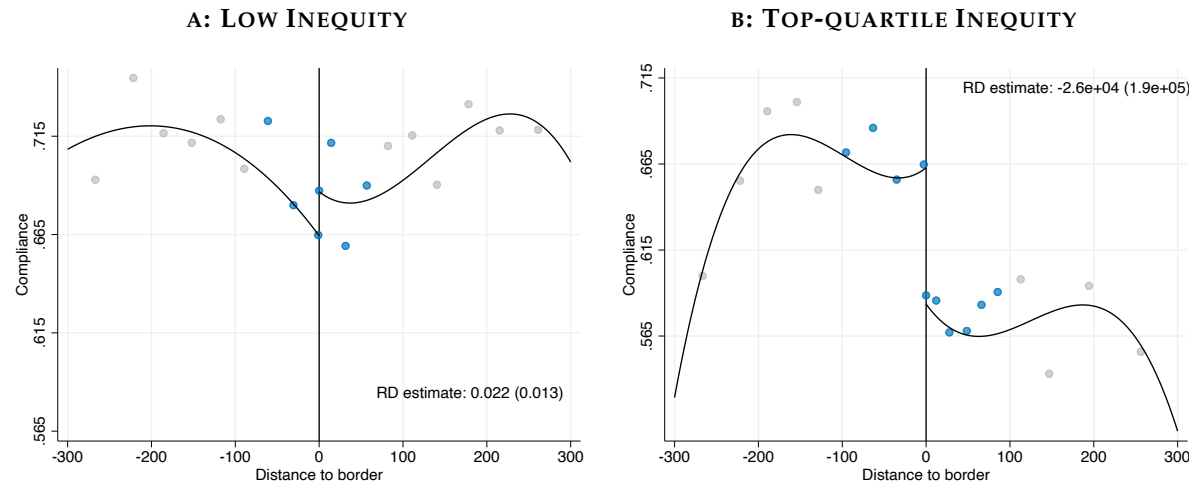


PANEL B: TOP-QUARTILE INEQUITY



Notes: This figure replicates the analysis from figure 8, but dropping only the top 0.1%, rather than 0.5%, of lots in terms of land area. The figure shows the results of estimating equation (12): $c_i = \lambda_{r(i)} + g(\tau_i, e_i) + f(d_i) + \beta_0 HTS_i + h(d_i) \times HTS_i + \varepsilon_i$ with inequity as the outcome variable, where terms are as defined in the notes to figure 6. Panel A shows the estimates in the subsample of properties facing low inequity (defined as being in the bottom 3 quartiles of inequity). Panel B shows the estimates in the subsample of properties facing top-quartile inequity.

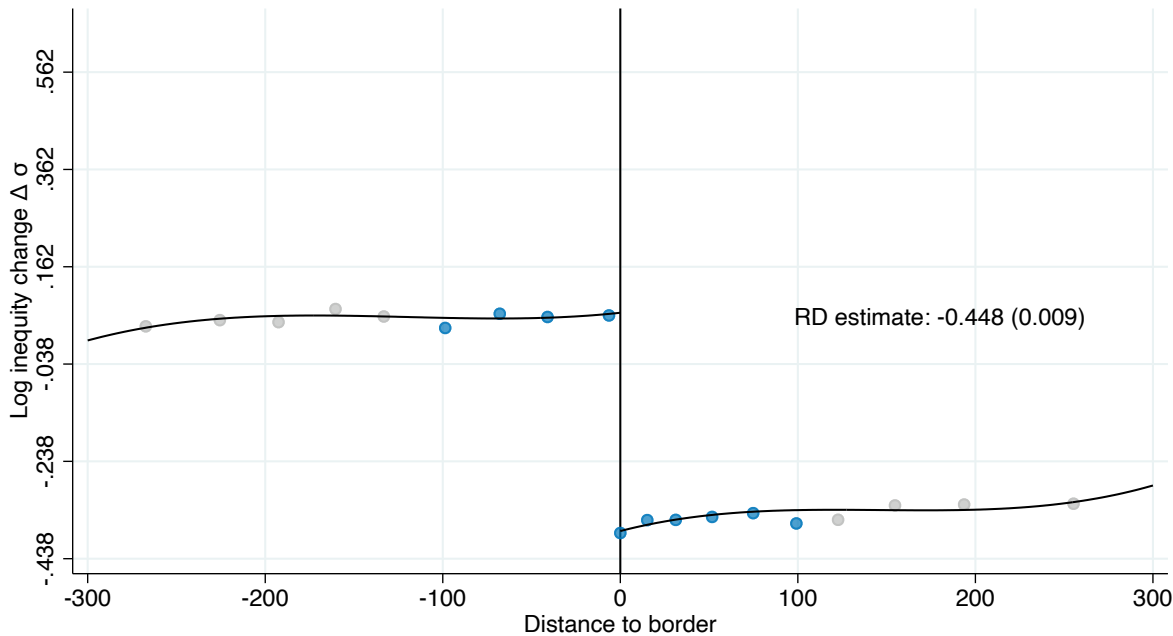
FIGURE E.18: DIFFERENCE IN BOUNDARY DISCONTINUITY DESIGN: COMPLIANCE EFFECTS



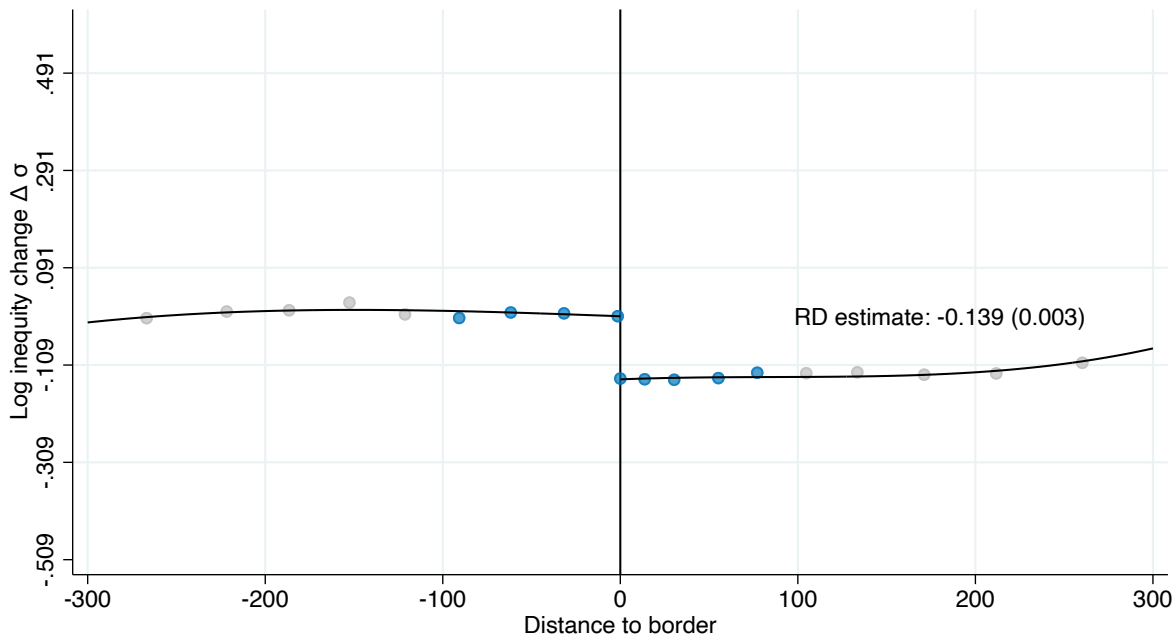
Notes: This figure replicates the analysis from figure 9, but dropping only the top 0.1%, rather than 0.5%, of lots in terms of land area. The figure shows the results of estimating equation (12): $c_i = \lambda_{r(i)} + g(\tau_i, e_i) + f_0(d_i) + \beta_0 HTS_i + f_1(d_i) \times HTS_i + \varepsilon_i$ with compliance as the outcome variable, where terms are as defined in the notes to figure 6. Panel A shows the estimates in the subsample of properties facing low inequity (defined as being in the bottom 3 quartiles of inequity). Panel B shows the estimates in the subsample of properties facing top-quartile inequity.

FIGURE E.19: DYNAMIC BOUNDARY DISCONTINUITY DESIGN: REMOVAL OF INEQUITY VS NO IMPROVEMENT

A: REMOVAL OF INEQUITY

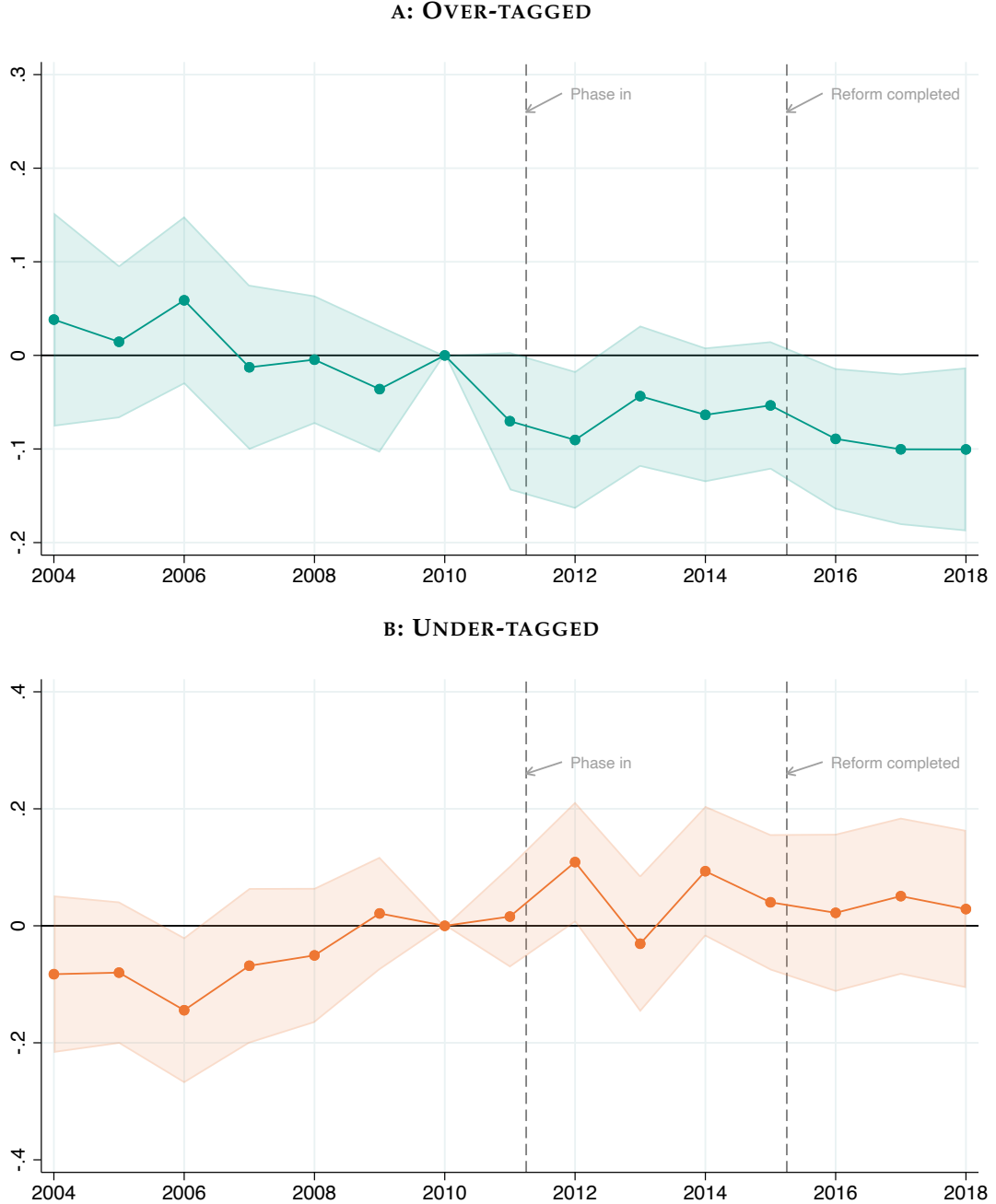


B: NO IMPROVEMENT



Notes: This figure replicates the analysis from figure 10, but dropping only the top 0.1%, rather than 0.5%, of lots in terms of land area. The figure shows the results of estimating equation (17) $\Delta\sigma_i = \lambda_{r(i)} + g(\Delta\tau_i) + f_0(d_i) + HTS_i \times [\beta_0 + f_1(d_i)] + \varepsilon_i$ where the outcome variable is the change in inequity, $\lambda_{r(i)}$ are boundary-segment fixed effects, HTS_i is an indicator for being on the high-tax side of the boundary ($d_i > 0$); $f_0(d_i)$ and $f_1(d_i)$ control for distance to the boundary on the low- and high-tax sides of the boundary, respectively; and ε_i is the residual. $g(\Delta\tau_i)$ controls flexibly for changes in log tax liability, τ_i . Specifically, we control for splines of $\Delta\tau_i$. Panel A shows the estimates in the subsample of properties for whom the reform meaningfully reduced inequity. Panel B shows the estimates in the remaining subsample of properties.

FIGURE E.21: DIFFERENCE IN DIFFERENCE ESTIMATES OF OVERTAGGING AND UNDERTAGGING EFFECTS



Notes: This figure replicates the analysis from figure 12, but dropping only the top 0.1%, rather than 0.5%, of lots in terms of land area. The figure shows the results of the estimation of equation (20) as discussed in section 6.3: $c_{iy} = \alpha_i + \lambda_{r(i)y} + \sum_{j \neq 2010} D_{jy} \times [f_{0j}(d_i) + \beta_{0j}\Delta\tau_i + \eta_{0j}\Delta\sigma_i + HTS_i \times (\delta_j + f_{1j}(d_i) + \beta_{1j}\Delta\tau_i + \eta_{1j}\Delta\sigma_i)] + \varepsilon_{iy}$, where $\lambda_{r(i)y}$ are segment-year fixed effects, $D_{jy} \equiv \mathbf{1}[y = j]$ are year dummies, and we include year-specific distance controls $f_{0j}(d_i)$ and $f_{1j}(d_i)$; and year-specific controls for property i 's tax liability change due to the reform. Panel A shows the estimated η_{1j} coefficients along with their 95% confidence intervals. Panel B shows the estimated η_{0j} coefficients along with their 95% confidence intervals.

TABLE E.8: AUGMENTED BOUNDARY DISCONTINUITY DESIGN: COMPLIANCE EFFECTS

	(1)	(2)	(3)	(4)	(5)	(6)
RD_Estimate	-0.08*** (0.02)	-0.06*** (0.02)	-0.08*** (0.02)	-0.06*** (0.02)	-0.08*** (0.02)	-0.08*** (0.02)
R^2						
Distance controls	✓	✓	✓	✓	✓	✓
Segment FEs	✓	✓	✓	✓	✓	✓
τ splines	✓	✓	✓	✓		
exp dec FEs	✓		✓			✓
τ decile FEs					✓	✓
exp splines		✓		✓		
τ splines \times exp dec FEs			✓			
τ splines \times exp splines				✓		
τ dec FEs \times exp dec FEs						✓
First-stage	0.553 (0.009)	0.497 (0.009)	0.564 (0.009)	0.526 (0.009)	0.552 (0.009)	0.566 (0.009)
fscoef_se						
Elasticity	-0.211 (0.045)	-0.171 (0.054)	-0.216 (0.044)	-0.162 (0.052)	-0.208 (0.045)	-0.223 (0.045)
elascoef_se						
N	9966	9965	9966	9965	9966	9966

Notes: This table replicates the analysis from table 2, but dropping only the top 0.1%, rather than 0.5%, of lots in terms of land area. The table shows the results of estimating the augmented BDD equation (12): $c_i = \lambda_{r(i)} + g(\tau_i, e_i) + f_0(d_i) + \beta_0 HTS_i + f_1(d_i) \times HTS_i + \varepsilon_i$, where $\lambda_{r(i)}$ are fixed effects for 500-meter segments along the boundaries to ensure we are comparing properties who are nearby each other; $g(\tau_i, e_i)$ are flexible controls for property i 's (log) tax liability τ_i and exposure to mistagging e_i ; $f_0(d_i)$ and $f_1(d_i)$ control flexibly for distance to the boundary on the low- and high-tax sides of the boundary respectively; and HTS_i is an indicator for properties on the high-tax side of the boundary ($d_i > 0$). The columns use a variety of approaches to controlling flexibly for the tax liability and exposure to mistagging. In column (1) we control for cubic splines of the tax liability and fixed effects for deciles of exposure. In column (2) we replace the exposure deciles with cubic splines of exposure while column (3) replaces the splines of the tax liability with deciles. Columns (4)–(6) additionally interact the tax liability controls with the exposure controls.

TABLE E.9: DIFFERENCE IN BOUNDARY DISCONTINUITY DESIGN: COMPLIANCE EFFECTS

	(1)	(2)	(3)	(4)	(5)	(6)	(7)
1(high tax side)	0.02 (0.01)	0.00 (.)	0.00 (.)	0.00 (.)	0.13 (0.34)	0.08 (0.33)	0.00 (.)
1(high tax side) $\times \sigma $	-0.17*** (0.02)	-0.17*** (0.02)	-0.17*** (0.02)	-0.17*** (0.02)	-0.15*** (0.03)	-0.16*** (0.03)	-0.15*** (0.03)
R^2	0.137	0.137	0.137	0.137	0.141	0.140	0.145
Distance controls	✓	✓	✓	✓	✓	✓	✓
Segment fixed effects	✓	✓	✓	✓	✓	✓	✓
τ splines	✓	✓	✓	✗	✓	✓	✗
τ deciles	✗	✗	✗	✓	✗	✗	✓
Expansiveness splines	✗	✗	✓	✗	✗	✓	✗
Expansiveness deciles	✓	✓	✗	✓	✓	✗	✓
τ splines \times HTS	✗	✓	✓	✗	✓	✓	✗
τ deciles \times HTS	✗	✗	✗	✓	✗	✗	✓
τ splines \times exp deciles	✗	✗	✗	✗	✓	✗	✗
τ splines \times exp splines	✗	✗	✗	✗	✗	✓	✗
τ deciles \times exp deciles	✗	✗	✗	✗	✗	✗	✓
τ splines \times HTS \times exp deciles	✗	✗	✗	✗	✓	✗	✗
τ splines \times HTS \times exp splines	✗	✗	✗	✗	✗	✓	✗
τ deciles \times HTS \times exp deciles	✗	✗	✗	✗	✗	✗	✓
Elasticity	-0.252 0.035	-0.253 0.035	-0.259 0.036	-0.254 0.035	-0.223 0.039	-0.242 0.040	-0.224 0.039
N	27968	27968	27968	27968	27968	27968	27968

Notes: This table replicates the analysis from table 3, but dropping only the top 0.1%, rather than 0.5%, of lots in terms of land area. The table shows the results of estimation of equation (16): $c_i = \lambda_{r(i)} + g_0(\tau_i, e_i) + f(d_i) + HTS_i \times [\beta_0 + \eta \log(\sigma) + h(d_i) + g_1(\tau_i, e_i)] + \varepsilon_i$ where terms are as defined above in the notes to table 2. In column (1), we control for cubic splines of the tax liability and fixed effects for deciles of the exposure distribution. In column (2) we control separately for the tax liability and exposure to mistagging on either side of the boundary. Column (3) replaces the exposure deciles with cubic splines in exposure while column (4) replaces the tax liability deciles with cubic splines. Columns (5)–(7) control for these separately on either side of the boundary.

TABLE E.10: DYNAMIC DIFFERENCE IN BOUNDARY DISCONTINUITY DESIGN

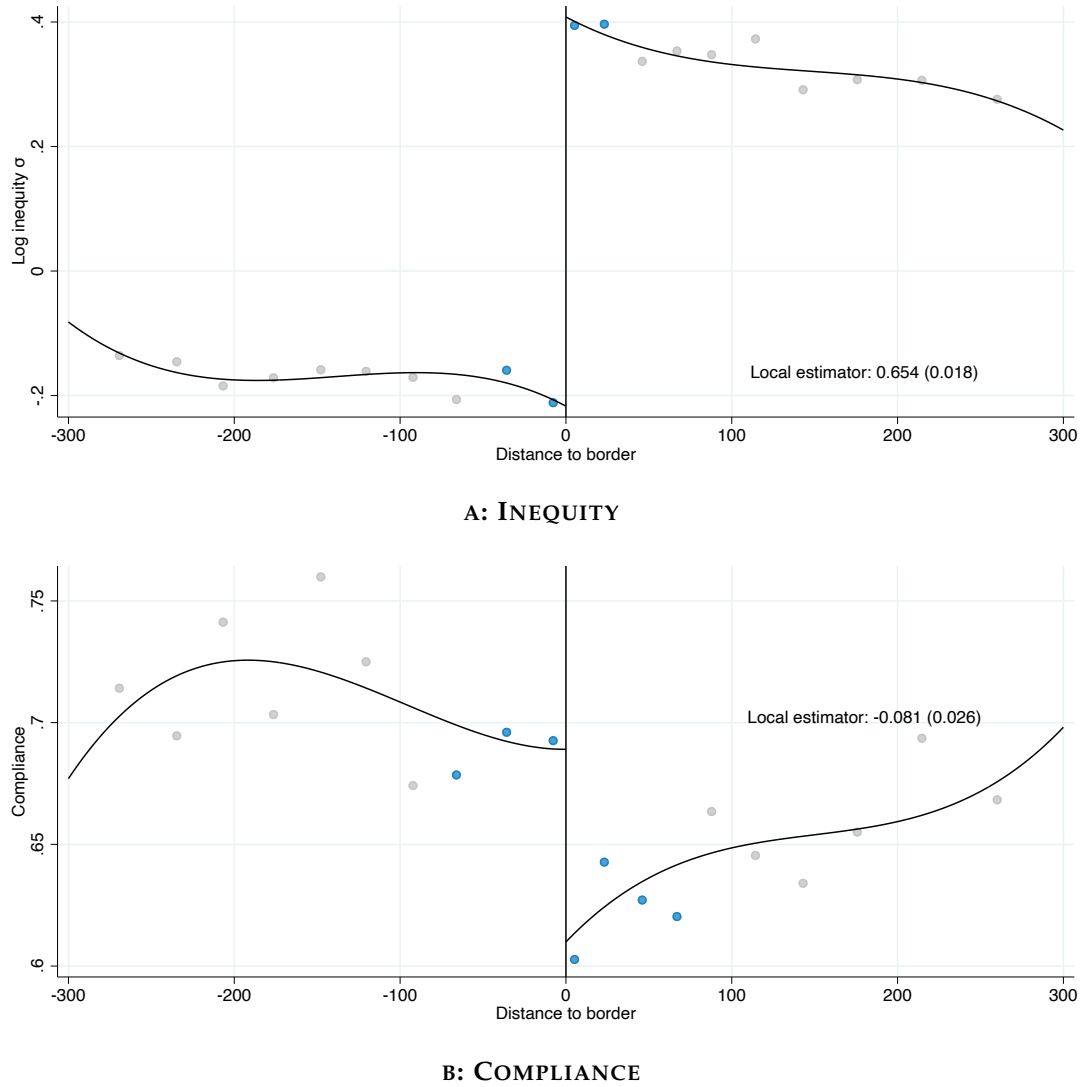
	(1) Δ Compliance	(2) Δ Compliance	(3) Δ Compliance	(4) Δ Compliance
1(high tax side)	-0.008 (0.011)	-0.009 (0.032)	-0.010 (0.031)	-0.008 (0.022)
1(high tax side) X change in σ	-0.091** (0.037)	-0.094** (0.040)	-0.088** (0.043)	-0.098** (0.039)
Elasticity implied	-0.138	-0.143	-0.133	-0.149
Elasticity SE	0.057	0.060	0.065	0.059
Distance controls	✓	✓	✓	✓
Segment FEs	✓	✓	✓	✓
τ splines	✓	✓	✓	✗
Expansiveness deciles	✓	✓	✗	✓
Interaction with HTS	✗	✓	✓	✓
τ splines \times expansiveness deciles	✗	✓	✗	✗
Expansiveness splines	✗	✗	✓	✗
τ splines \times expansiveness splines	✗	✗	✓	✗
τ deciles	✗	✗	✗	✓
τ deciles \times expansiveness deciles	✗	✗	✗	✓

Notes: This table replicates the analysis from table 4, but dropping only the top 0.1%, rather than 0.5%, of lots in terms of land area. This table shows the results of estimating equation (18) discussed in section 6.2: $\Delta c_i = \lambda_{r(i)} + g_0(\Delta\tau_i, e_i) + f_0(d_i) + HTS_i \times [\delta_0 + \eta\Delta \log(\sigma_i) + g_1(\Delta\tau_i, e_i) + f_1(d_i)] + \varepsilon_i$ where all terms are as defined above in the notes to table 2. Column (1) controls for cubic splines of the tax liability and fixed effects for deciles of the exposure distribution. Column (2) adds interactions between these controls and estimates them separately on either side of the boundary. Column (3) replaces the exposure deciles with splines, while column (4) replaces the tax liability splines with deciles of the tax liability distribution.

E.5 Stringent “large lots” Definition: Drop thee top 1% in terms of land area

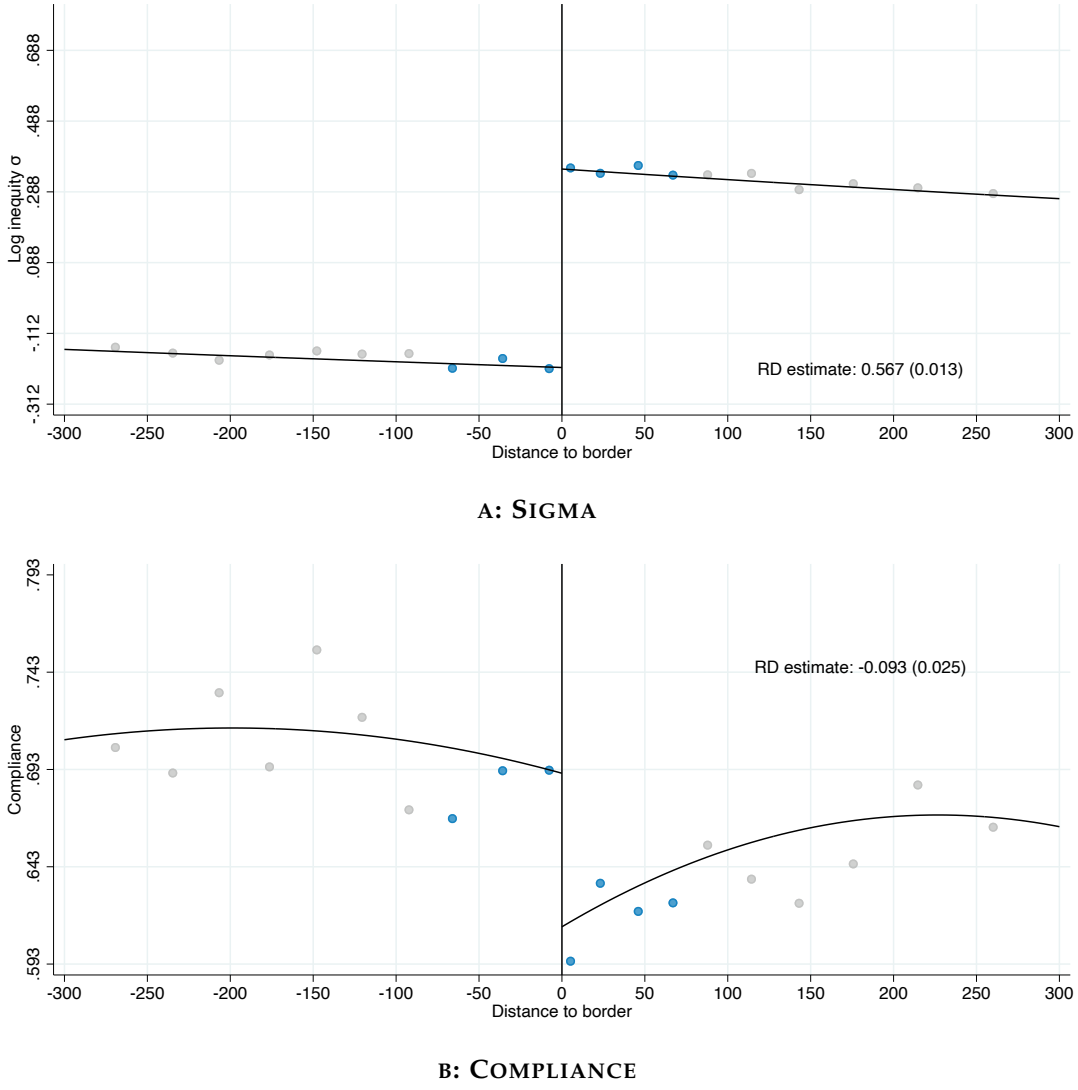
In the main text, we exclude “very large” lots because they introduce measurement error. We define “very large” lots as the top 0.5% in terms of land area. Here, we repeat the main analysis with a sample that excludes the top 1% of lots in terms of land area.

FIGURE E.22: OVERALL CHANGE IN COMPLIANCE AT TAX SECTOR BOUNDARIES



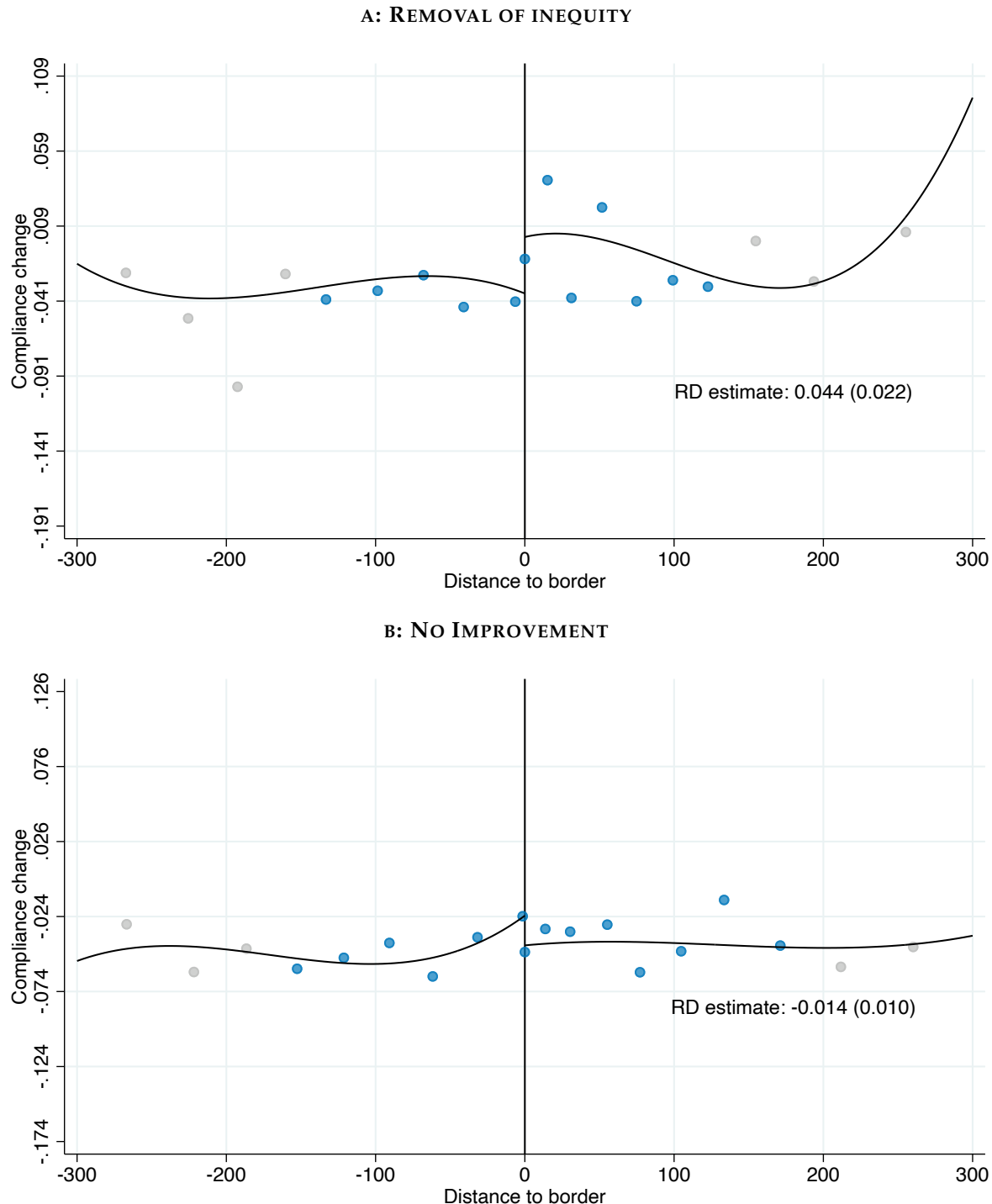
Notes: Panel A replicates the analysis from Panel B of Figure 4, and Panel B replicates the analysis from Figure 3, but dropping the top 1%, rather than 0.5%, of lots in terms of land area. The figure shows the overall change in inequity (Panel A) and compliance (Panel B) at tax sector boundaries discussed in section 4.1. Specifically, we show the results of estimating the following equation for compliance and inequity (10): y_i by taxpayer i : $c_i = \lambda_{r(i)} + f(d_i) + \beta_0 HTS_i + h(d_i) \times HTS_i + \varepsilon_i$ where $\lambda_{r(i)}$ are boundary-segment fixed effects, HTS_i is an indicator for being on the high-tax side of the boundary ($d_i > 0$); $f_0(d_i)$ and $f_1(d_i)$ control for distance to the boundary on the low- and high-tax sides of the boundary, respectively; and ε_i is the residual. Overlaid on the figure, we show the point estimate of the discontinuity in compliance estimated using local linear distance controls, the MSE-minimizing bandwidth, and triangular kernel weights in distance. The dots in the figure show the coefficients from estimating (10) with fixed effects for decile-spaced bins of distance, using the same triangular kernel weights but censoring them at their tenth percentile to give non-zero weights to distances outside the optimal bandwidth. The bins in the optimal bandwidth are shown in blue while those outside are shown in gray. The black line is a global cubic polynomial fit in the same way.

FIGURE E.23: AUGMENTED BOUNDARY DISCONTINUITY DESIGN



Notes: Panel A replicates the analysis from Figure 5, and Panel B replicates the analysis from Figure 6; however, both panels drop the top 1%, rather than 0.5%, of lots in terms of land area. The figure shows the impact on inequity and compliance in the augmented BDD discussed in section 5.1. Specifically, we show the results of estimation of equation (12): $y_i = \lambda_{r(i)} + g(\tau_i, e_i) + f_0(d_i) + \beta_0 HTS_i + f_1(d_i) \times HTS_i + \varepsilon_i$ using log-inequity σ as the outcome variable in panel A and compliance in panel B. $\lambda_{r(i)}$ are fixed effects for 500-meter segments along the boundaries to ensure we are comparing properties who are nearby each other; $g(\tau_i, e_i)$ are flexible controls for property i 's (log) tax liability τ_i and exposure to mistagging e_i (our baseline estimates use τ splines and exposure deciles); $f_0(d_i)$ and $f_1(d_i)$ control flexibly for distance to the boundary on the low- and high-tax sides of the boundary respectively; and HTS_i is an indicator for properties on the high-tax side of the boundary ($d_i > 0$). Overlaid on the figure, we show the point estimate of the discontinuity in inequity estimated using local linear distance controls, the MSE-minimizing bandwidth, and triangular kernel weights in distance. The dots in the figure show the coefficients from estimating (12) with fixed effects for decile-spaced bins of distance, using the same triangular kernel weights but censoring them at their tenth percentile to give non-zero weights to distances outside the optimal bandwidth. The bins in the optimal bandwidth are shown in blue while those outside are shown in gray. The black line is a global cubic polynomial fit in the same way.

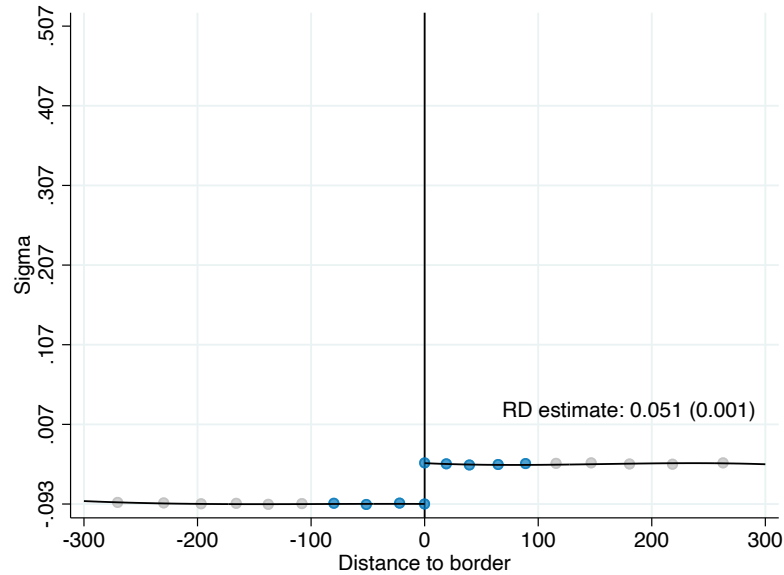
FIGURE E.20: DYNAMIC BOUNDARY DISCONTINUITY DESIGN: REMOVAL OF INEQUITY VS NO IMPROVEMENT



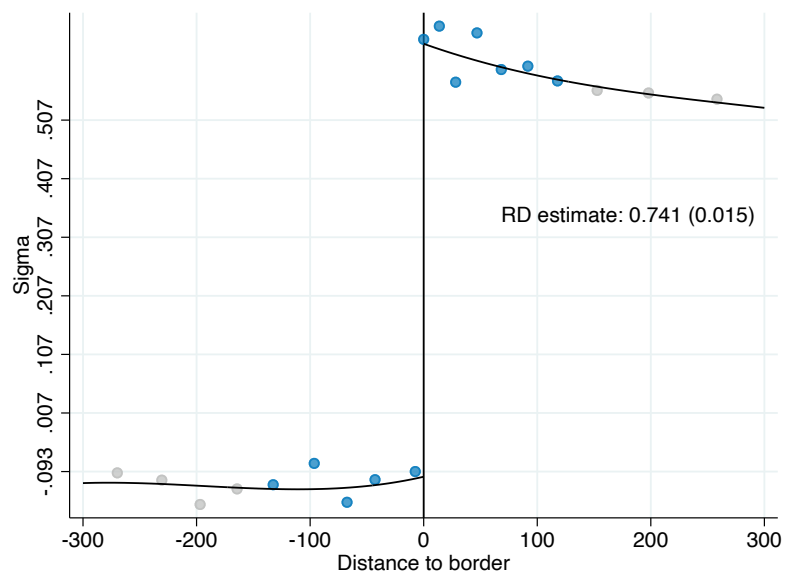
Notes: This figure replicates the analysis from figure 11, but dropping only the top 0.1%, rather than 0.5%, of lots in terms of land area. The figure shows the results of estimating equation (17) $\Delta c_i = \lambda_{r(i)} + g(\Delta\tau_i) + f_0(d_i) + HTS_i \times [\beta_0 + f_1(d_i)] + \varepsilon_i$ where the outcome variable is the change in compliance, $\lambda_{r(i)}$ are boundary-segment fixed effects, HTS_i is an indicator for being on the high-tax side of the boundary ($d_i > 0$); $f_0(d_i)$ and $f_1(d_i)$ control for distance to the boundary on the low- and high-tax sides of the boundary, respectively; and ε_i is the residual. $g(\Delta\tau_i)$ controls flexibly for changes in log tax liability, τ_i . Specifically, we control for splines of $\Delta\tau_i$. Panel A shows the estimates in the subsample of properties for whom the reform meaningfully reduced inequity. Panel B shows the estimates in the remaining subsample of properties.

FIGURE E.24: DIFFERENCE IN BOUNDARY DISCONTINUITY DESIGN: FIRST STAGE

PANEL A: LOW INEQUITY

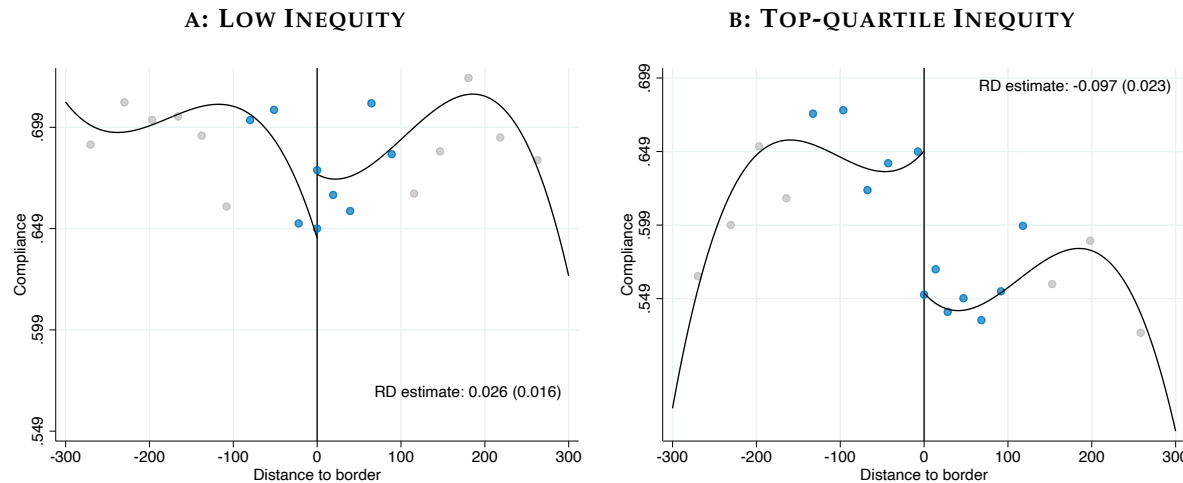


PANEL B: TOP-QUARTILE INEQUITY



Notes: This figure replicates the analysis from figure 8, but dropping the top 1%, rather than 0.5%, of lots in terms of land area. The figure shows the results of estimating equation (12): $c_i = \lambda_{r(i)} + g(\tau_i, e_i) + f_0(d_i) + \beta_0 HTS_i + f_1(d_i) \times HTS_i + \varepsilon_i$ with inequity as the outcome variable, where terms are as defined in the notes to figure 6. Panel A shows the estimates in the subsample of properties facing low inequity (defined as being in the bottom 3 quartiles of inequity). Panel B shows the estimates in the subsample of properties facing top-quartile inequity.

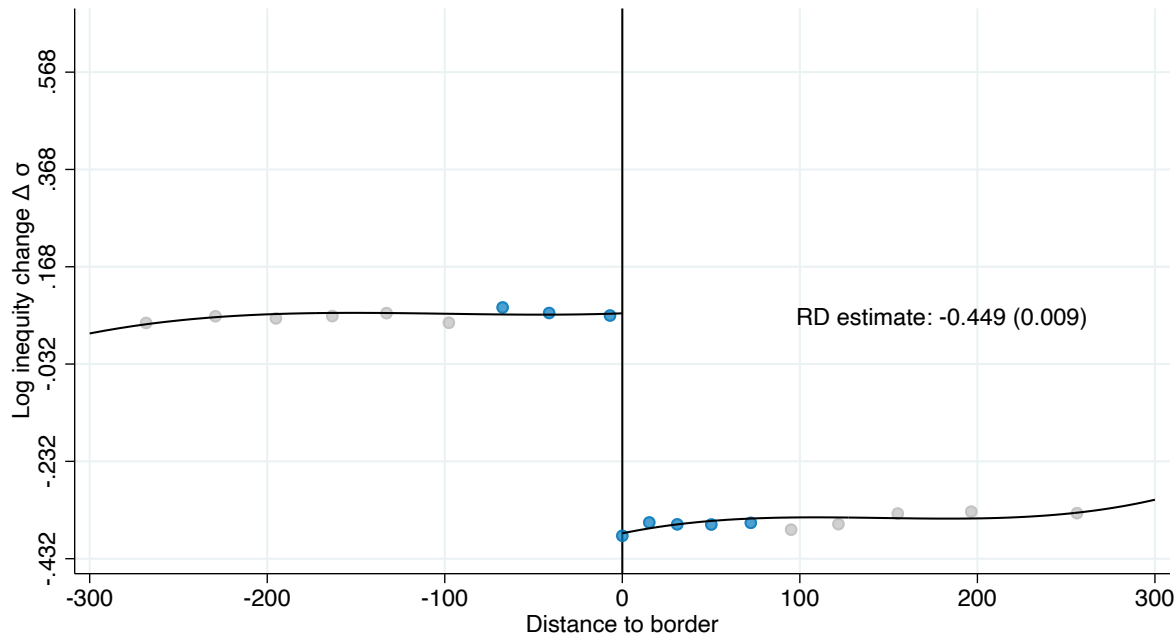
FIGURE E.25: DIFFERENCE IN BOUNDARY DISCONTINUITY DESIGN: COMPLIANCE EFFECTS



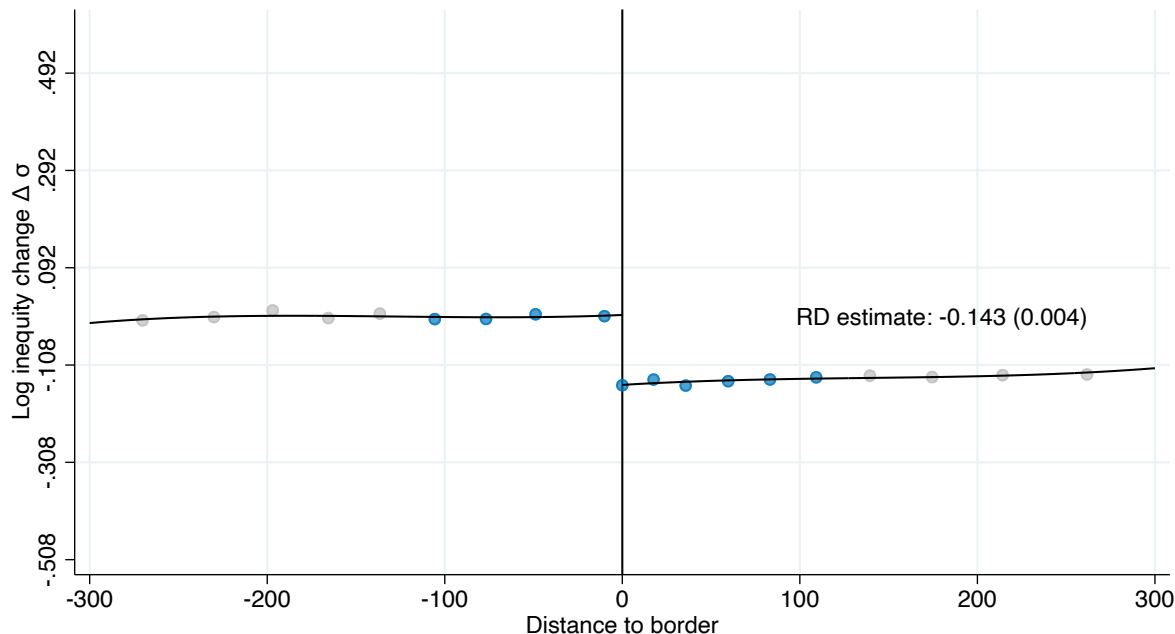
Notes: This figure replicates the analysis from figure 9, but dropping the top 1%, rather than 0.5%, of lots in terms of land area. The figure shows the results of estimating equation (12): $c_i = \lambda_{r(i)} + g(\tau_i, e_i) + f(d_i) + \beta_0 HTS_i + h(d_i) \times HTS_i + \varepsilon_i$ with compliance as the outcome variable, where terms are as defined in the notes to figure 6. Panel A shows the estimates in the subsample of properties facing low inequity (defined as being in the bottom 3 quartiles of inequity). Panel B shows the estimates in the subsample of properties facing top-quartile inequity.

FIGURE E.26: DYNAMIC BOUNDARY DISCONTINUITY DESIGN: REMOVAL OF INEQUITY VS NO IMPROVEMENT

A: REMOVAL OF INEQUITY

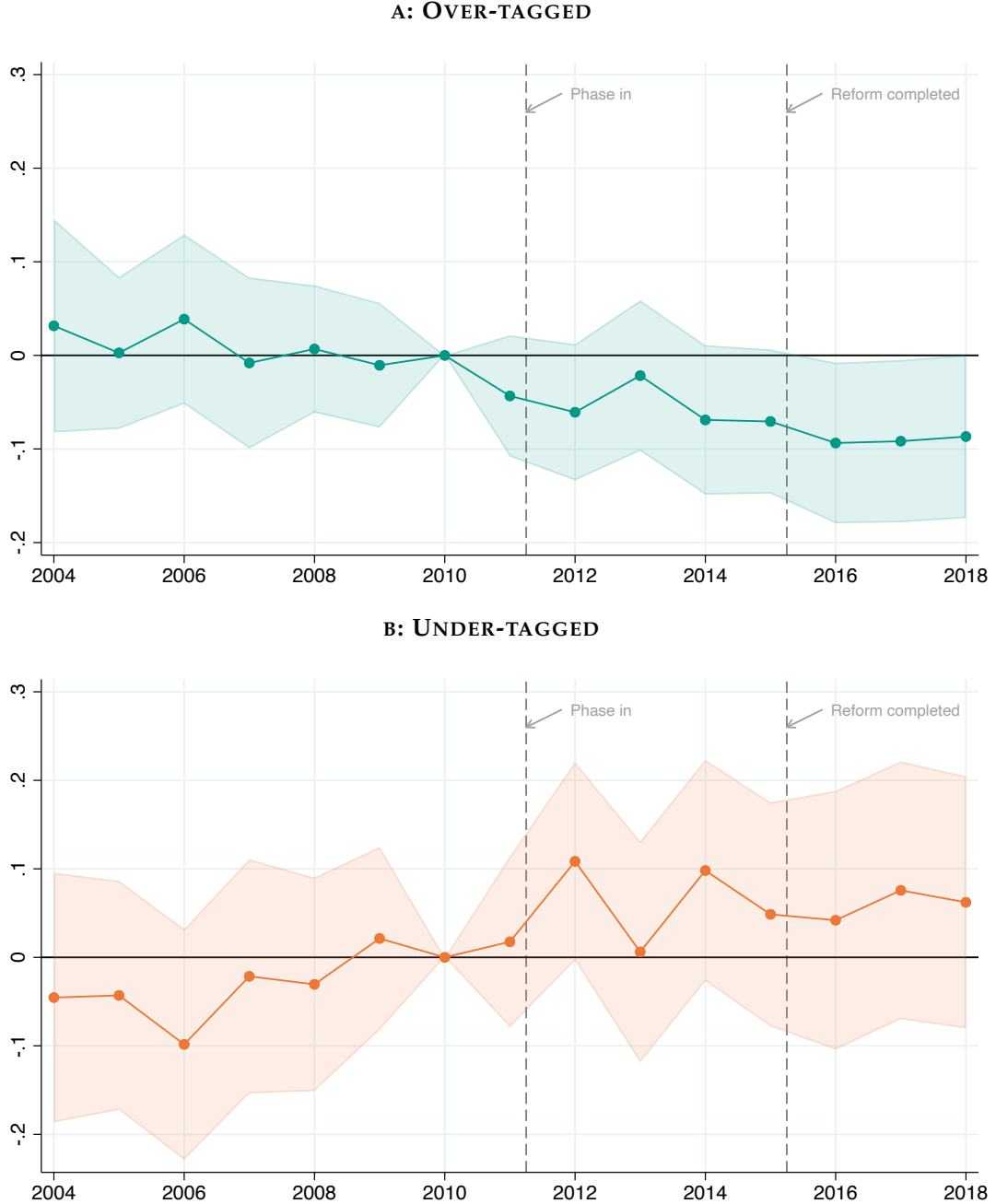


B: NO IMPROVEMENT



Notes: This figure replicates the analysis from figure 10, but dropping the top 1%, rather than 0.5%, of lots in terms of land area. The figure shows the results of estimating equation (17) $\Delta\sigma_i = \lambda_{r(i)} + g(\Delta\tau_i) + f_0(d_i) + HTS_i \times [\beta_0 + f_1(d_i)] + \varepsilon_i$ where the outcome variable is the change in inequity, $\lambda_{r(i)}$ are boundary-segment fixed effects, HTS_i is an indicator for being on the high-tax side of the boundary ($d_i > 0$); $f_0(d_i)$ and $f_1(d_i)$ control for distance to the boundary on the low- and high-tax sides of the boundary, respectively; and ε_i is the residual. $g(\Delta\tau_i)$ controls flexibly for changes in log tax liability, τ_i . Specifically, we control for splines of $\Delta\tau_i$. Panel A shows the estimates in the subsample of properties for whom the reform meaningfully reduced inequity. Panel B shows the estimates in the remaining subsample of properties.

FIGURE E.28: DIFFERENCE IN DIFFERENCE ESTIMATES OF OVERTAGGING AND UNDERTAGGING EFFECTS



Notes: This figure replicates the analysis from figure 12, but dropping the top 1%, rather than 0.5%, of lots in terms of land area. The figure shows the results of the estimation of equation (20) as discussed in section 6.3: $c_{iy} = \alpha_i + \lambda_{r(i)y} + \sum_{j \neq 2010} D_{jy} \times [f_{0j}(d_i) + \beta_{0j}\Delta\tau_i + \eta_{0j}\Delta\sigma_i + HTS_i \times (\delta_j + f_{1j}(d_i) + \beta_{1j}\Delta\tau_i + \eta_{1j}\Delta\sigma_i)] + \varepsilon_{iy}$, where $\lambda_{r(i)y}$ are segment-year fixed effects, $D_{jy} \equiv \mathbf{1}[y = j]$ are year dummies, and we include year-specific distance controls $f_{0j}(d_i)$ and $f_{1j}(d_i)$; and year-specific controls for property i 's tax liability change due to the reform. Panel A shows the estimated η_{1j} coefficients along with their 95% confidence intervals. Panel B shows the estimated η_{0j} coefficients along with their 95% confidence intervals.

TABLE E.11: AUGMENTED BOUNDARY DISCONTINUITY DESIGN: COMPLIANCE EFFECTS

	(1)	(2)	(3)	(4)	(5)	(6)
RD_Estimate	-0.09*** (0.02)	-0.08*** (0.02)	-0.10*** (0.02)	-0.08*** (0.02)	-0.09*** (0.02)	-0.10*** (0.02)
<i>R</i> ²						
Distance controls	✓	✓	✓	✓	✓	✓
Segment FEs	✓	✓	✓	✓	✓	✓
τ splines	✓	✓	✓	✓		
exp dec FEs	✓		✓			✓
τ decile FEs					✓	✓
exp splines		✓		✓		
τ splines \times exp dec FEs			✓			
τ splines \times exp splines				✓		
τ dec FEs \times exp dec FEs						✓
First-stage	0.519 (0.011)	0.499 (0.011)	0.531 (0.011)	0.513 (0.010)	0.518 (0.011)	0.535 (0.011)
fscoef_se						
Elasticity	-0.252 (0.059)	-0.228 (0.067)	-0.264 (0.056)	-0.238 (0.065)	-0.253 (0.059)	-0.260 (0.056)
elascoef_se						
<i>N</i>	8800	8799	8800	8799	8800	8800

Notes: This table replicates the analysis from table 2, but dropping the top 1%, rather than 0.5%, of lots in terms of land area. The table shows the results of estimating the augmented BDD equation (12): $c_i = \lambda_{r(i)} + g(\tau_i, e_i) + f_0(d_i) + \beta_0 HTS_i + f_1(d_i) \times HTS_i + \varepsilon_i$, where $\lambda_{r(i)}$ are fixed effects for 500-meter segments along the boundaries to ensure we are comparing properties who are nearby each other; $g(\tau_i, e_i)$ are flexible controls for property i 's (log) tax liability τ_i and exposure to mistagging e_i ; $f_0(d_i)$ and $f_1(d_i)$ control flexibly for distance to the boundary on the low- and high-tax sides of the boundary respectively; and HTS_i is an indicator for properties on the high-tax side of the boundary ($d_i > 0$). The columns use a variety of approaches to controlling flexibly for the tax liability and exposure to mistagging. In column (1) we control for cubic splines of the tax liability and fixed effects for deciles of exposure. In column (2) we replace the exposure deciles with cubic splines of exposure while column (3) replaces the splines of the tax liability with deciles. Columns (4)–(6) additionally interact the tax liability controls with the exposure controls.

TABLE E.12: DIFFERENCE IN BOUNDARY DISCONTINUITY DESIGN: COMPLIANCE EFFECTS

	(1)	(2)	(3)	(4)	(5)	(6)	(7)
1(high tax side)	0.00 (0.02)	0.00 (.)	0.00 (.)	0.00 (.)	0.23 (0.38)	0.21 (0.37)	0.00 (.)
1(high tax side) $\times \sigma $	-0.17*** (0.02)	-0.17*** (0.03)	-0.18*** (0.03)	-0.17*** (0.02)	-0.15*** (0.03)	-0.19*** (0.03)	-0.15*** (0.03)
R^2	0.124	0.124	0.124	0.124	0.127	0.126	0.131
Distance controls	✓	✓	✓	✓	✓	✓	✓
Segment fixed effects	✓	✓	✓	✓	✓	✓	✓
τ splines	✓	✓	✓	✗	✓	✓	✗
τ deciles	✗	✗	✗	✓	✗	✗	✓
Expansiveness splines	✗	✗	✓	✗	✗	✓	✗
Expansiveness deciles	✓	✓	✗	✓	✓	✗	✓
τ splines \times HTS	✗	✓	✓	✗	✓	✓	✗
τ deciles \times HTS	✗	✗	✗	✓	✗	✗	✓
τ splines \times exp deciles	✗	✗	✗	✗	✓	✗	✗
τ splines \times exp splines	✗	✗	✗	✗	✗	✓	✗
τ deciles \times exp deciles	✗	✗	✗	✗	✗	✗	✓
τ splines \times HTS \times exp deciles	✗	✗	✗	✗	✓	✗	✗
τ splines \times HTS \times exp splines	✗	✗	✗	✗	✗	✓	✗
τ deciles \times HTS \times exp deciles	✗	✗	✗	✗	✗	✗	✓
Elasticity	-0.261 0.039	-0.262 0.039	-0.282 0.040	-0.263 0.039	-0.229 0.043	-0.300 0.050	-0.235 0.043
N	23868	23868	23868	23868	23868	23868	23868

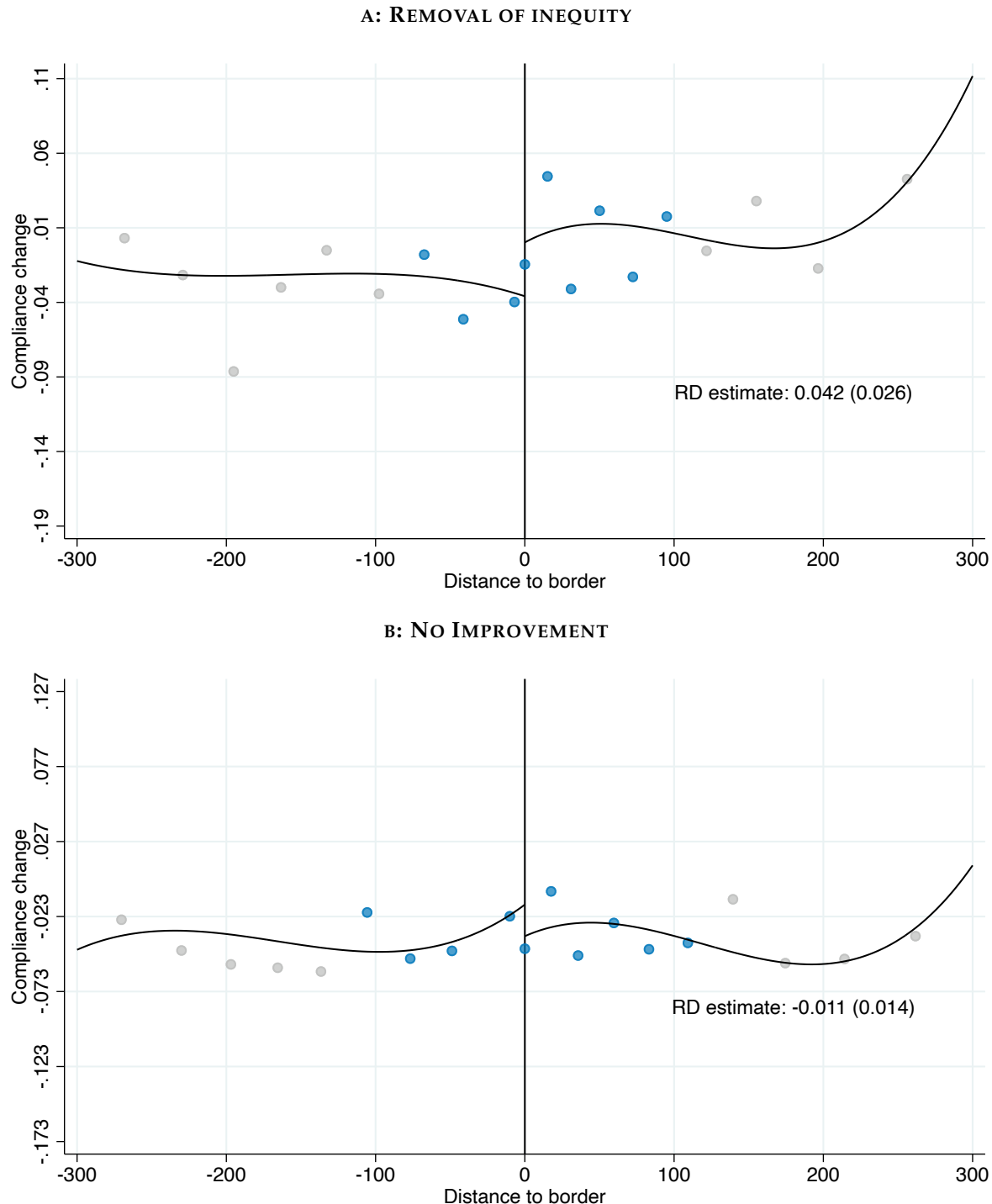
Notes: This table replicates the analysis from table 3, but dropping the top 1%, rather than 0.5%, of lots in terms of land area. The table shows the results of estimation of equation (16): $c_i = \lambda_{r(i)} + g_0(\tau_i, e_i) + f_0(d_i) + HTS_i \times [\beta_0 + \eta \log(\sigma) + f_1(d_i) + g_1(\tau_i, e_i)] + \varepsilon_i$ where terms are as defined above in the notes to table 2. In column (1), we control for cubic splines of the tax liability and fixed effects for deciles of the exposure distribution. In column (2) we control separately for the tax liability and exposure to mistagging on either side of the boundary. Column (3) replaces the exposure deciles with cubic splines in exposure while column (4) replaces the tax liability deciles with cubic splines. Columns (5)–(7) control for these separately on either side of the boundary.

TABLE E.13: DYNAMIC DIFFERENCE IN BOUNDARY DISCONTINUITY DESIGN

	(1) Δ Compliance	(2) Δ Compliance	(3) Δ Compliance	(4) Δ Compliance
1(high tax side)	-0.005 (0.012)	-0.012 (0.033)	-0.009 (0.032)	-0.005 (0.025)
1(high tax side) X change in σ	-0.088** (0.040)	-0.097** (0.042)	-0.086* (0.047)	-0.104** (0.041)
Elasticity implied	-0.139	-0.153	-0.135	-0.163
Elasticity SE	0.062	0.066	0.074	0.065
Distance controls	✓	✓	✓	✓
Segment FEs	✓	✓	✓	✓
τ splines	✓	✓	✓	✗
Expansiveness deciles	✓	✓	✗	✓
Interaction with HTS	✗	✓	✓	✓
τ splines \times expansiveness deciles	✗	✓	✗	✗
Expansiveness splines	✗	✗	✓	✗
τ splines \times expansiveness splines	✗	✗	✓	✗
τ deciles	✗	✗	✗	✓
τ deciles \times expansiveness deciles	✗	✗	✗	✓

Notes: This table replicates the analysis from table 4, but dropping the top 1%, rather than 0.5%, of lots in terms of land area. This table shows the results of estimating equation (18) discussed in section 6.2: $\Delta c_i = \lambda_{r(i)} + g_0(\Delta\tau_i, e_i) + f_0(d_i) + HTS_i \times [\delta_0 + \eta\Delta \log(\sigma_i) + g_1(\Delta\tau_i, e_i) + f_1(d_i)] + \varepsilon_i$ where all terms are as defined above in the notes to table 2. Column (1) controls for cubic splines of the tax liability and fixed effects for deciles of the exposure distribution. Column (2) adds interactions between these controls and estimates them separately on either side of the boundary. Column (3) replaces the exposure deciles with splines, while column (4) replaces the tax liability splines with deciles of the tax liability distribution.

FIGURE E.27: DYNAMIC BOUNDARY DISCONTINUITY DESIGN: REMOVAL OF INEQUITY VS NO IMPROVEMENT



Notes: This figure replicates the analysis from figure 11, but dropping the top 1%, rather than 0.5%, of lots in terms of land area. The figure shows the results of estimating equation (17) $\Delta c_i = \lambda_{r(i)} + g(\Delta\tau_i) + f_0(d_i) + HTS_i \times [\beta_0 + f_1(d_i)] + \varepsilon_i$ where the outcome variable is the change in compliance, $\lambda_{r(i)}$ are boundary-segment fixed effects, HTS_i is an indicator for being on the high-tax side of the boundary ($d_i > 0$); $f_0(d_i)$ and $f_1(d_i)$ control for distance to the boundary on the low- and high-tax sides of the boundary, respectively; and ε_i is the residual. $g(\Delta\tau_i)$ controls flexibly for changes in log tax liability, τ_i . Specifically, we control for splines of $\Delta\tau_i$. Panel A shows the estimates in the subsample of properties for whom the reform meaningfully reduced inequity. Panel B shows the estimates in the remaining subsample of properties.

E.6 Alternative Definitions of Non-Trivial Degree of Inequity

In sections 4.2 and 5.1.2, we restrict our sample to properties that face a non-trivial degree of inequity, defined as having $|\sigma_i| > 0.05$. In this appendix, we assess the robustness of our results by varying the threshold used to define a “non-trivial degree of inequity.” We then repeat our main estimations from both sections for each alternative threshold definition.

In section 4.2, we develop a boundary discontinuity design that estimates the overall effect on compliance from facing a tax schedule based on a high land-price assessment rather than a lower-priced schedule. Specifically, we estimate the equation for compliance c_i :

$$c_i = \lambda_{r(i)} + f_0(d_i) + \beta_0 HTS_i + f_1(d_i) \times HTS_i + \varepsilon_i \quad (\text{E.1})$$

where $\lambda_{r(i)}$ are boundary-segment fixed effects, HTS_i is an indicator for being on the high-tax side of the boundary ($d_i > 0$); $f_0(d_i)$ and $f_1(d_i)$ control for distance to the boundary on the low- and high-tax sides of the boundary, respectively; and ε_i is the residual.

Figure E.29 presents robustness checks in which we systematically vary the definition of the “non-trivial degree of inequity” threshold. For each alternative cutoff of $|\sigma_i|$, we re-estimate equation (E.1). The vertical axis plots the estimated discontinuity in compliance (β_0) as a solid blue line, along with its corresponding 95% confidence interval (shaded area). The horizontal axis shows the chosen threshold for “non-trivial inequity.” Gray bars indicate the proportion of properties retained in each estimation. The figure demonstrates that the results from figure 3 remain broadly stable for thresholds ranging between 0.02 and 0.2.

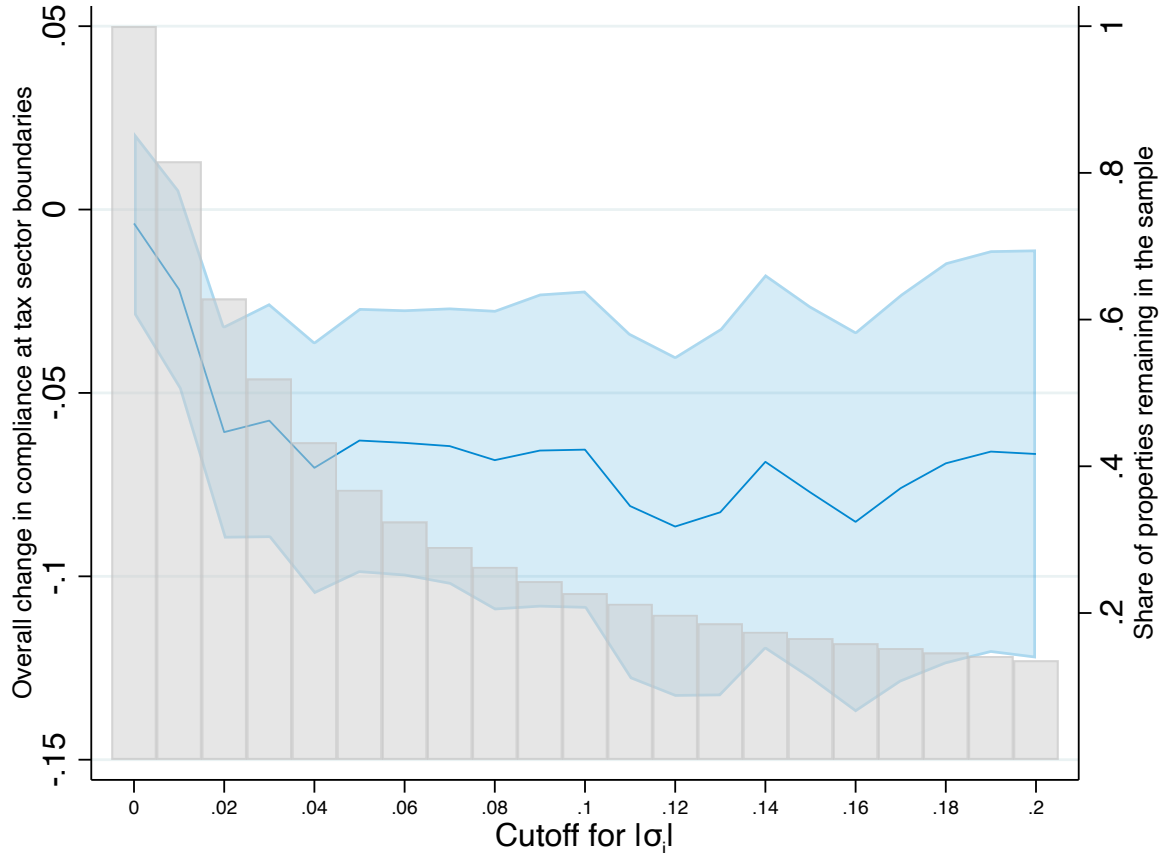
Similarly, Figure E.30 provides analogous robustness checks for the augmented boundary discontinuity design introduced in Section 5.1.2, which explicitly conditions on properties’ tax liabilities (τ) and exposure to mistagging (e) to isolate the discontinuous change in inequity at the boundary. For each alternative cutoff, we re-estimate the following equation

$$c_i = \lambda_{r(i)} + g(\tau_i, e_i) + f_0(d_i) + \beta_0 HTS_i + f_1(d_i) \times HTS_i + \varepsilon_i \quad (\text{E.2})$$

where $\lambda_{r(i)}$ are fixed effects for 500-meter segments along the boundaries to ensure we are comparing properties who are nearby each other; $g(\tau_i, e_i)$ spline controls for τ and decile indicators for exposure; $f_0(d_i)$ and $f_1(d_i)$ control flexibly for distance to the boundary on the low- and high-tax sides of the boundary respectively; and HTS_i is an indicator for properties on the high-tax side of the boundary ($d_i > 0$).

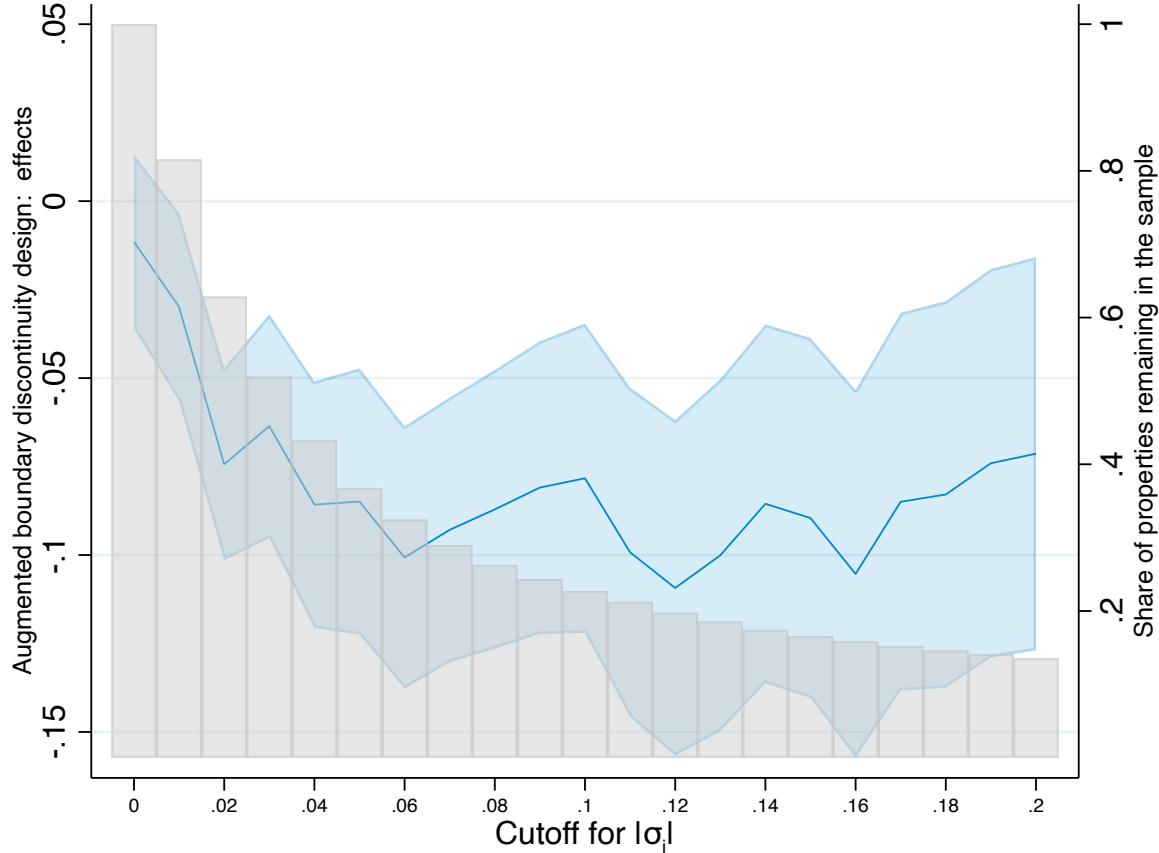
As before, the vertical axis shows the estimated discontinuity in compliance along with its 95% confidence interval, while the horizontal axis displays the threshold defining “non-trivial inequity,” and gray bars indicate the proportion of properties retained in each estimation. The findings from figure 6 also remain robust across thresholds between 0.02 and 0.2.

FIGURE E.29: OVERALL CHANGE IN COMPLIANCE AT TAX SECTOR BOUNDARIES



Notes: This figure replicates the analysis from Figure 3, varying the threshold of $|\sigma_i|$ used to define a non-trivial degree of inequity for sample inclusion. Specifically, we repeatedly estimate the following equation for compliance (E.1): c_i by taxpayer i : $c_i = \lambda_{r(i)} + f_0(d_i) + \beta_0 HTS_i + f_1(d_i) \times HTS_i + \varepsilon_i$ where $\lambda_{r(i)}$ are boundary-segment fixed effects, HTS_i is an indicator for being on the high-tax side of the boundary ($d_i > 0$); $f_0(d_i)$ and $f_1(d_i)$ control for distance to the boundary on the low- and high-tax sides of the boundary, respectively; and ε_i is the residual. The estimation is repeated twenty-one times, each with a different cutoff defining “non-trivial inequity.” The vertical axis plots the estimated discontinuity in compliance (β_0) as a solid blue line, along with its corresponding 95% confidence interval (shaded area). The horizontal axis shows the chosen threshold for “non-trivial inequity.” Gray bars indicate the proportion of properties retained in each estimation. The figure demonstrates that the results from figure 3 remain broadly stable for thresholds ranging between 0.02 and 0.2.

FIGURE E.30: AUGMENTED BOUNDARY DISCONTINUITY DESIGN: COMPLIANCE EFFECTS



Notes: This figure replicates the analysis from Figure 6, varying the threshold of $|\sigma_i|$ used to define a non-trivial degree of inequity for sample inclusion. Specifically, we repeatedly estimate the following equation for compliance (E.2): $c_i = \lambda_{r(i)} + g(\tau_i, e_i) + f_0(d_i) + \beta_0 HTS_i + f_1(d_i) \times HTS_i + \varepsilon_i$ where $\lambda_{r(i)}$ are fixed effects for 500-meter segments along the boundaries to ensure we are comparing properties who are nearby each other; $g(\tau_i, e_i)$ are splines for property i 's (log) tax liability τ_i and exposure to mistagging e_i deciles; $f_0(d_i)$ and $f_1(d_i)$ control flexibly for distance to the boundary on the low- and high-tax sides of the boundary respectively; and HTS_i is an indicator for properties on the high-tax side of the boundary ($d_i > 0$). The estimation is repeated twenty-one times, each with a different cutoff defining “non-trivial inequity.” The vertical axis plots the estimated discontinuity in compliance (β_0) as a solid blue line, along with its corresponding 95% confidence interval (shaded area). The horizontal axis shows the chosen threshold for “non-trivial inequity.” Gray bars indicate the proportion of properties retained in each estimation. The figure demonstrates that the results from figure 6 remain broadly stable for thresholds ranging between 0.02 and 0.2.

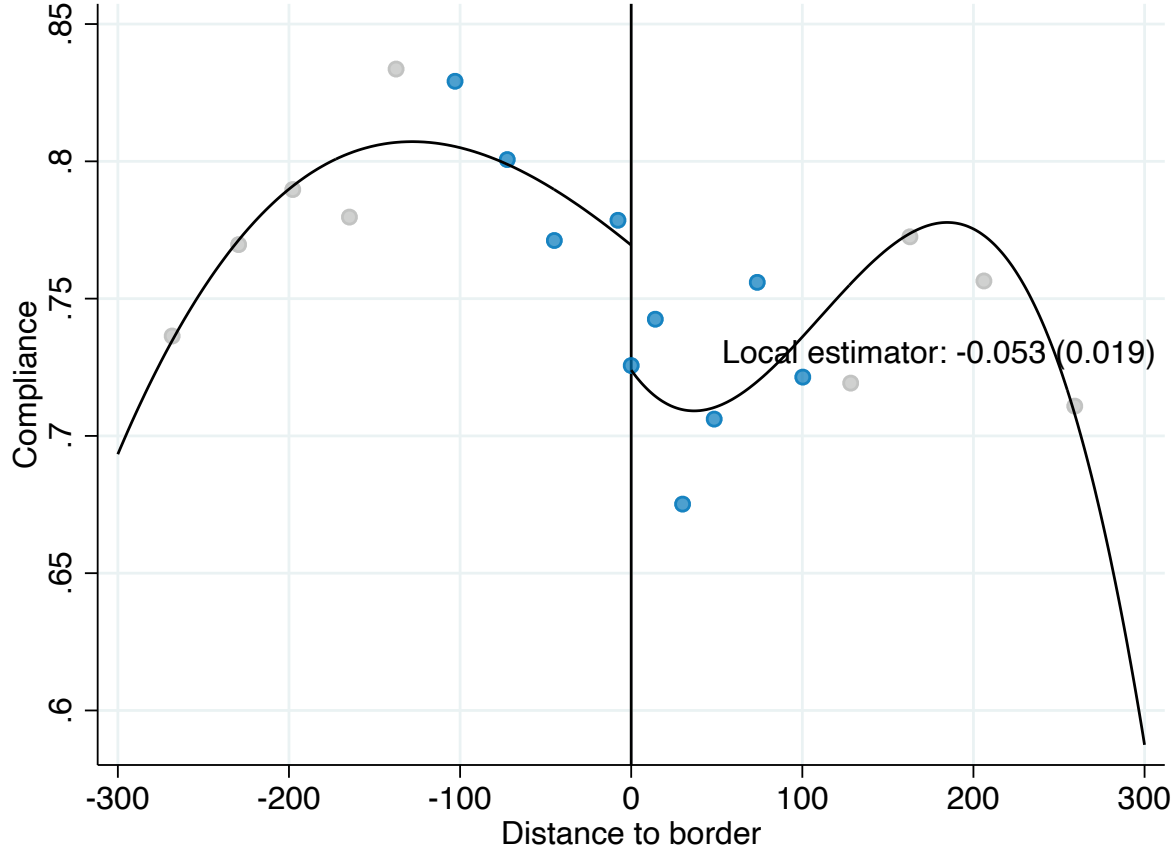
F Robustness to Alternative Definitions of Compliance

In section 2.3, we introduced compliance—defined as the proportion of a household’s IPTU bill paid within 18 months of issuance—as our main outcome for analyzing behavioral responses to mistagging. In this appendix, we revisit our core analyses while adjusting two key choices related to our outcome variable. First, we explore the extensive margin response to mistagging. Second, we vary the payment time frame used in our compliance definition.

F.1 Extensive Margin Response

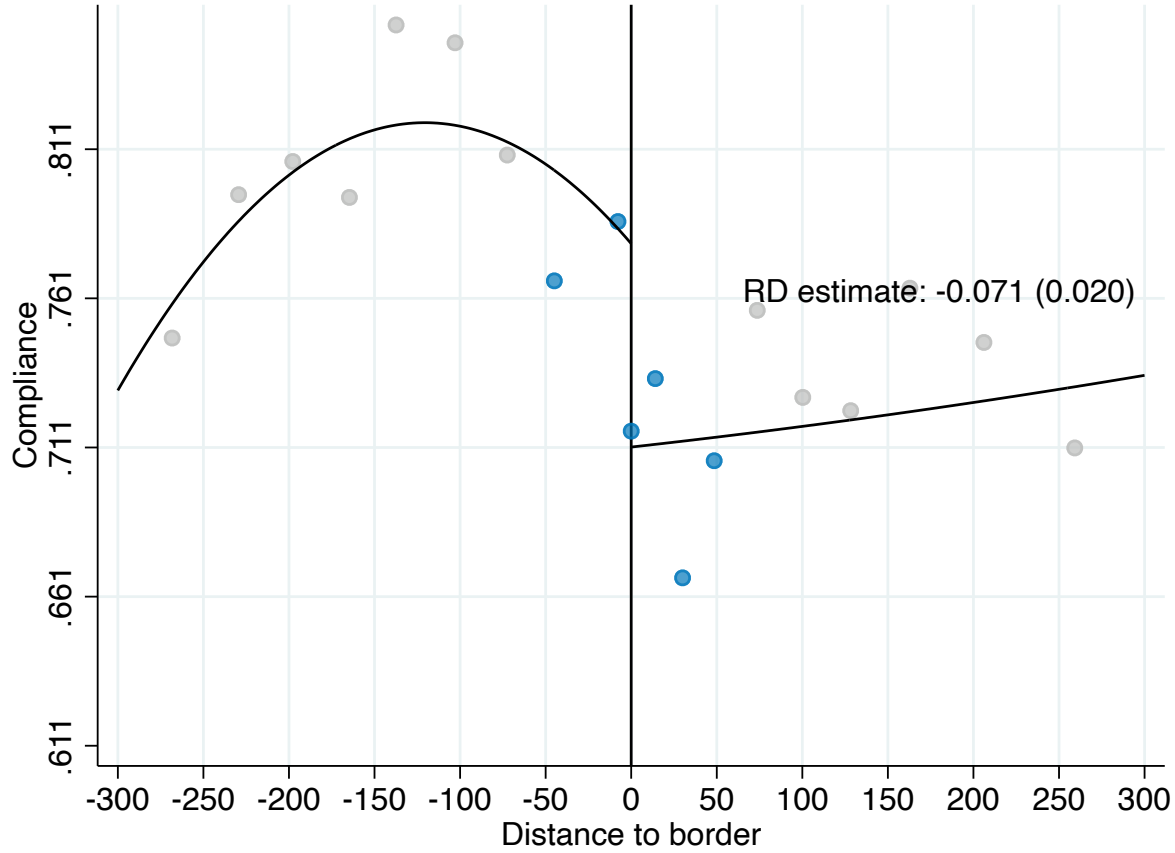
In the main text, we combine both extensive and intensive margin behavioral responses to mistagging in our definition of compliance. Figure A.3 illustrates that compliance is driven almost entirely on the extensive margin, with households typically settling their entire IPTU bill when they choose to pay. In this section, we refine our analysis by focusing solely on the extensive margin of compliance. Specifically, we redefine our outcome variable such that it equals one if a household makes any payment within 18 months of receiving their bill, and zero otherwise. The figures and tables below reproduce the main analyses with this new outcome variable. Each figure and table references the corresponding result from the main sections of the paper.

FIGURE F.1: OVERALL CHANGE IN COMPLIANCE AT TAX SECTOR BOUNDARIES



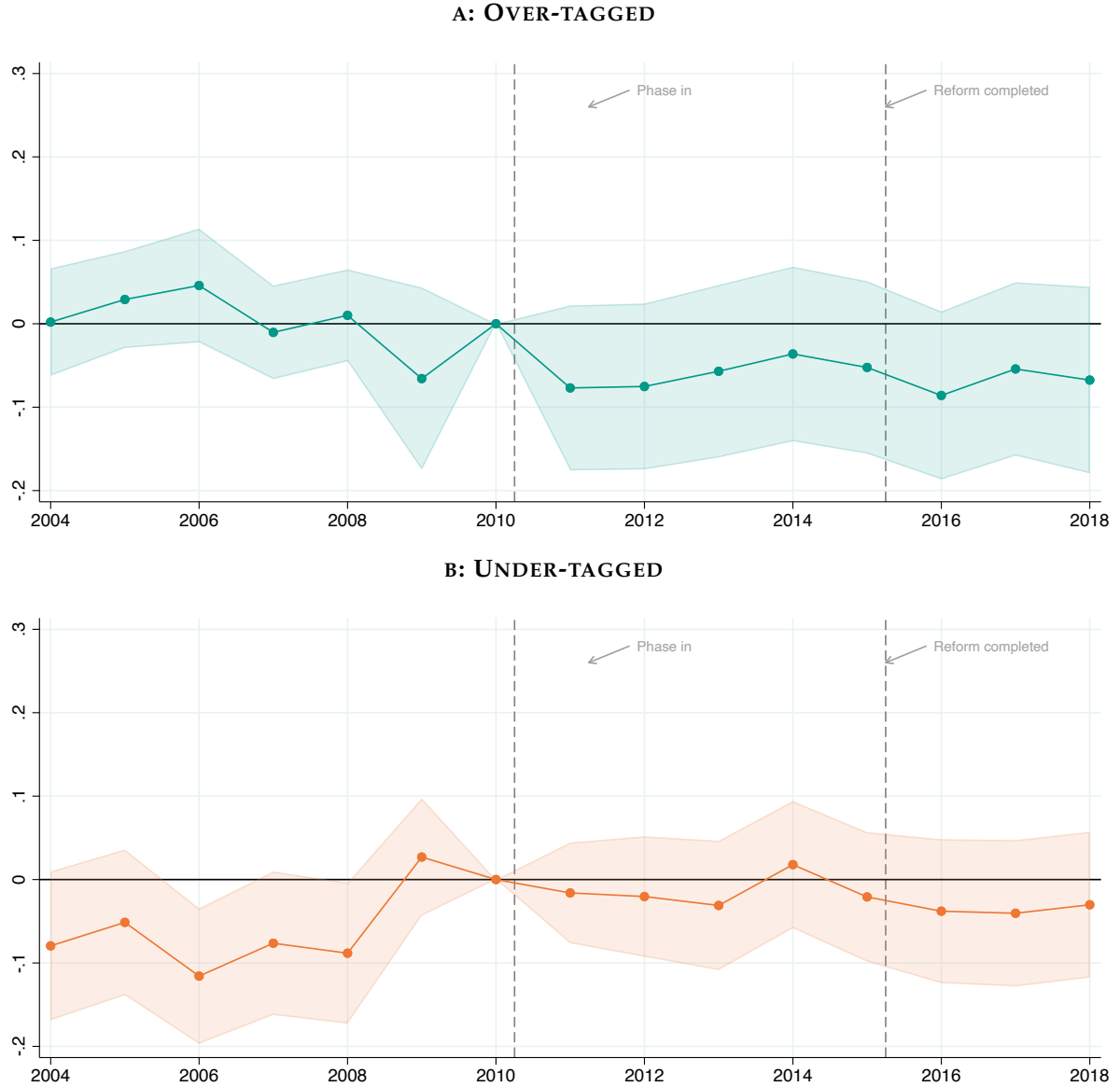
Notes: This figure presents the same analysis as depicted in Figure 3, but focuses on the extensive margin response of compliance. The figure shows the extensive margin change in compliance at tax sector boundaries discussed in section 4.1. Specifically, we show the results of estimating the following equation for extensive margin of compliance c_i by taxpayer i : (10) $c_i = \lambda_{r(i)} + f(d_i) + \beta_0 HTS_i + h(d_i) \times HTS_i + \varepsilon_i$ where $\lambda_{r(i)}$ are boundary-segment fixed effects, HTS_i is an indicator for being on the high-tax side of the boundary ($d_i > 0$); $f_0(d_i)$ and $f_1(d_i)$ control for distance to the boundary on the low- and high-tax sides of the boundary, respectively; and ε_i is the residual. Overlaid on the figure, we show the point estimate of the discontinuity in compliance estimated using local linear distance controls, the MSE-minimizing bandwidth, and triangular kernel weights in distance. The dots in the figure show the coefficients from estimating (10) with fixed effects for decile-spaced bins of distance, using the same triangular kernel weights but censoring them at their tenth percentile to give non-zero weights to distances outside the optimal bandwidth. The bins in the optimal bandwidth are shown in blue while those outside are shown in gray. The black line is a global cubic polynomial fit in the same way.

FIGURE F.2: AUGMENTED BOUNDARY DISCONTINUITY DESIGN: COMPLIANCE EFFECTS



Notes: This figure presents the same analysis as depicted in Figure 6, but focuses on the extensive margin response of compliance. The figure shows the first stage impact on inequity in the augmented BDD discussed in section 5.1. Specifically, we show the results of estimation of equation (12): $c_i = \lambda_{r(i)} + g(\tau_i, e_i) + f(d_i) + \beta_0 HTS_i + h(d_i) \times HTS_i + \varepsilon_i$ using the extensive margin of compliance as the outcome variable, where $\lambda_{r(i)}$ are fixed effects for 500-meter segments along the boundaries to ensure we are comparing properties who are nearby each other; $g(\tau_i, e_i)$ are flexible controls for property i 's (log) tax liability τ_i and exposure to mistagging e_i (our baseline estimates use τ splines and exposure deciles); $f(d_i)$ and $h(d_i)$ control flexibly for distance to the boundary on the low- and high-tax sides of the boundary respectively; and HTS_i is an indicator for properties on the high-tax side of the boundary ($d_i > 0$). Overlaid on the figure, we show the point estimate of the discontinuity in inequity estimated using local linear distance controls, the MSE-minimizing bandwidth, and triangular kernel weights in distance. The dots in the figure show the coefficients from estimating (12) with fixed effects for decile-spaced bins of distance, using the same triangular kernel weights but censoring them at their tenth percentile to give non-zero weights to distances outside the optimal bandwidth. The bins in the optimal bandwidth are shown in blue while those outside are shown in gray. The black line is a global cubic polynomial fit in the same way.

FIGURE F.3: DIFFERENCE IN DIFFERENCE ESTIMATES OF OVERTAGGING AND UNDERTAGGING EFFECTS



Notes: This figure presents the same analysis as depicted in Figure 12, but focuses on the extensive margin response of compliance. The figure shows the results of the estimation of equation (20) as discussed in section 6.3: $c_{iy} = \alpha_i + \lambda_{r(i)y} + \sum_{j \neq 2010} D_{jy} \times [f_{0j}(d_i) + \beta_{0j}\Delta\tau_i + \eta_{0j}\Delta\sigma_i + HTS_i \times (\delta_j + f_{1j}(d_i) + \beta_{1j}\Delta\tau_i + \eta_{1j}\Delta\sigma_i)] + \varepsilon_{iy}$, where $\lambda_{r(i)y}$ are segment-year fixed effects, $D_{jy} \equiv 1 [y = j]$ are year dummies, and we include year-specific distance controls $f_{0j}(d_i)$ and $f_{1j}(d_i)$; and year-specific controls for property i 's tax liability change due to the reform. Panel A shows the estimated η_{1j} coefficients along with their 95% confidence intervals. Panel B shows the estimated η_{0j} coefficients along with their 95% confidence intervals.

TABLE F.1: DIFFERENCE IN BOUNDARY DISCONTINUITY DESIGN: COMPLIANCE EFFECTS

	(1)	(2)	(3)	(4)	(5)	(6)	(7)
1(high tax side)	0.01 (0.02)	0.00 (.)	0.00 (.)	0.00 (.)	0.34 (0.36)	0.32 (0.36)	0.00 (.)
1(high tax side) $\times \sigma $	-0.17*** (0.02)	-0.17*** (0.02)	-0.19*** (0.02)	-0.17*** (0.02)	-0.16*** (0.03)	-0.17*** (0.03)	-0.15*** (0.03)
R^2	0.132	0.132	0.131	0.132	0.135	0.133	0.139
Distance controls	✓	✓	✓	✓	✓	✓	✓
Segment fixed effects	✓	✓	✓	✓	✓	✓	✓
τ splines	✓	✓	✓	✗	✓	✓	✗
τ deciles	✗	✗	✗	✓	✗	✗	✓
Expansiveness splines	✗	✗	✓	✗	✗	✓	✗
Expansiveness deciles	✓	✓	✗	✓	✓	✗	✓
τ splines \times HTS	✗	✓	✓	✗	✓	✓	✗
τ deciles \times HTS	✗	✗	✗	✓	✗	✗	✓
τ splines \times exp deciles	✗	✗	✗	✗	✓	✗	✗
τ splines \times exp splines	✗	✗	✗	✗	✗	✓	✗
τ deciles \times exp deciles	✗	✗	✗	✗	✗	✗	✓
τ splines \times HTS \times exp deciles	✗	✗	✗	✗	✓	✗	✗
τ splines \times HTS \times exp splines	✗	✗	✗	✗	✗	✓	✗
τ deciles \times HTS \times exp deciles	✗	✗	✗	✗	✗	✗	✓
Elasticity	-0.258 0.036	-0.259 0.036	-0.283 0.036	-0.260 0.036	-0.235 0.040	-0.260 0.043	-0.232 0.040
N	25060	25060	25060	25060	25060	25060	25060

Notes: This table presents the same analysis as depicted in table 3, but focuses on the extensive margin response of compliance. It shows the results of estimation of equation (16): $c_i = \lambda_{r(i)} + g_0(\tau_i, e_i) + f(d_i) + HTS_i \times [\beta_0 + \eta \log(\sigma) + h(d_i) + g_1(\tau_i, e_i)] + \varepsilon_i$ where $\lambda_{r(i)}$ are fixed effects for 500-meter segments along the boundaries to ensure we are comparing properties who are nearby each other; $g(\tau_i, e_i)$ are flexible controls for property i 's (log) tax liability τ_i and exposure to mistagging e_i ; $f(d_i)$ and $h(d_i)$ control flexibly for distance to the boundary on the low- and high-tax sides of the boundary respectively; and HTS_i is an indicator for properties on the high-tax side of the boundary ($d_i > 0$). In column (1), we control for cubic splines of the tax liability and fixed effects for deciles of the exposure distribution. In column (2) we control separately for the tax liability and exposure to mistagging on either side of the boundary. Column (3) replaces the exposure deciles with cubic splines in exposure while column (4) replaces the tax liability deciles with cubic splines. Columns (5)–(7) control for these separately on either side of the boundary.

TABLE F.2: DYNAMIC DIFFERENCE IN BOUNDARY DISCONTINUITY DESIGN

	(1) Δ Compliance	(2) Δ Compliance	(3) Δ Compliance	(4) Δ Compliance
1(high tax side)	-0.004 (0.008)	0.005 (0.021)	0.000 (0.020)	0.003 (0.016)
1(high tax side) X change in σ	-0.078*** (0.026)	-0.084*** (0.027)	-0.095*** (0.028)	-0.085*** (0.027)
Elasticity implied	-0.118	-0.128	-0.144	-0.129
Elasticity SE	0.039	0.041	0.043	0.040
Distance controls	✓	✓	✓	✓
Segment FEs	✓	✓	✓	✓
τ splines	✓	✓	✓	✗
Expansiveness deciles	✓	✓	✗	✓
Interaction with HTS	✗	✓	✓	✓
τ splines \times expansiveness deciles	✗	✓	✗	✗
Expansiveness splines	✗	✗	✓	✗
τ splines \times expansiveness splines	✗	✗	✓	✗
τ deciles	✗	✗	✗	✓
τ deciles \times expansiveness deciles	✗	✗	✗	✓

Notes: This table presents the same analysis as depicted in table 4, but focuses on the extensive margin response of compliance. It shows the results of estimating equation (18) discussed in section 6.2: $\Delta c_i = \lambda_{\tau(i)} + g_0(\Delta\tau_i, e_i) + f_0(d_i) + HTS_i \times [\delta_0 + \eta\Delta \log(\sigma_i) + g_1(\Delta\tau_i, e_i) + f_1(d_i)] + \varepsilon_i$ where all terms are as defined above in the notes to table F.1. Column (1) controls for cubic splines of the tax liability and fixed effects for deciles of the exposure distribution. Column (2) adds interactions between these controls and estimates them separately on either side of the boundary. Column (3) replaces the exposure deciles with splines, while column (4) replaces the tax liability splines with deciles of the tax liability distribution.

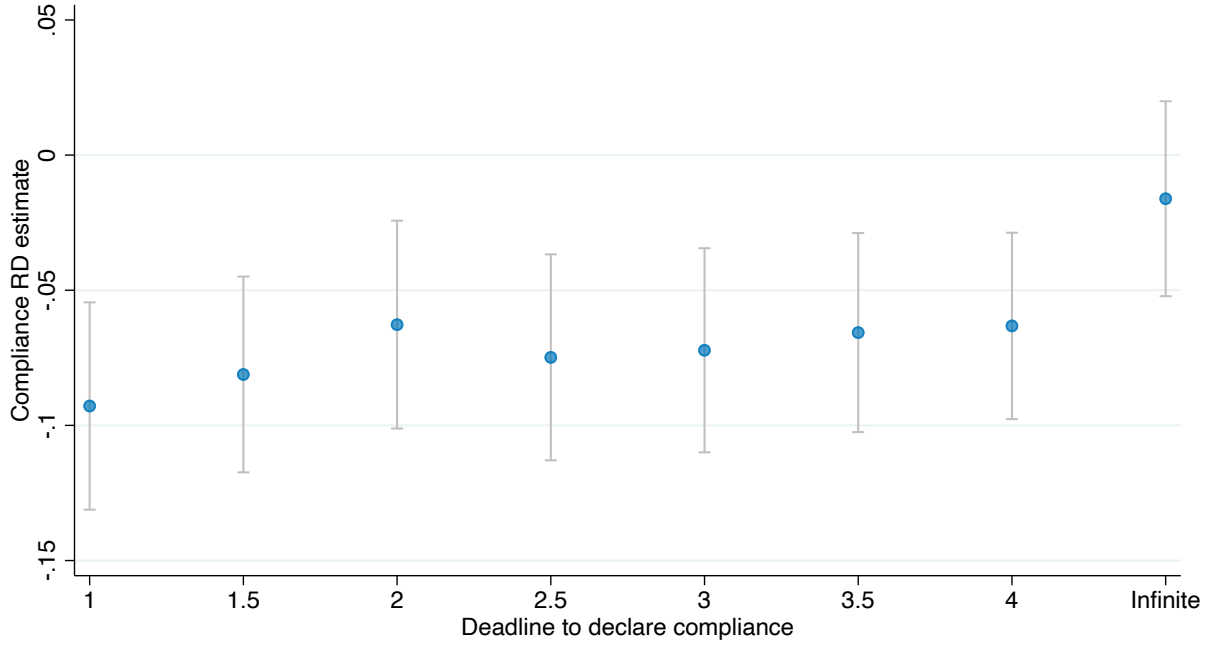
F.2 Timeframe for Payments in the Definition of Compliance

In section 2.3, we introduced compliance—defined as the proportion of a household’s IPTU bill paid within 18 months of issuance—as our main outcome for analyzing behavioral responses to mistagging. In this appendix, we vary the time frame considered for payments in the definition of compliance, and replicate the main analyses with each definition.

When evaluating the results presented in this section, two considerations are worth noting. First, our payments data is complete only up to the year 2020. Therefore, time frames extending beyond four years should be approached with caution when analyzing compliance data from 2016 onward. Second, there are constant amnesties of debt, which incentivize back payments. Consequently, time frames extending multiple years should also be treated with caution for any year.

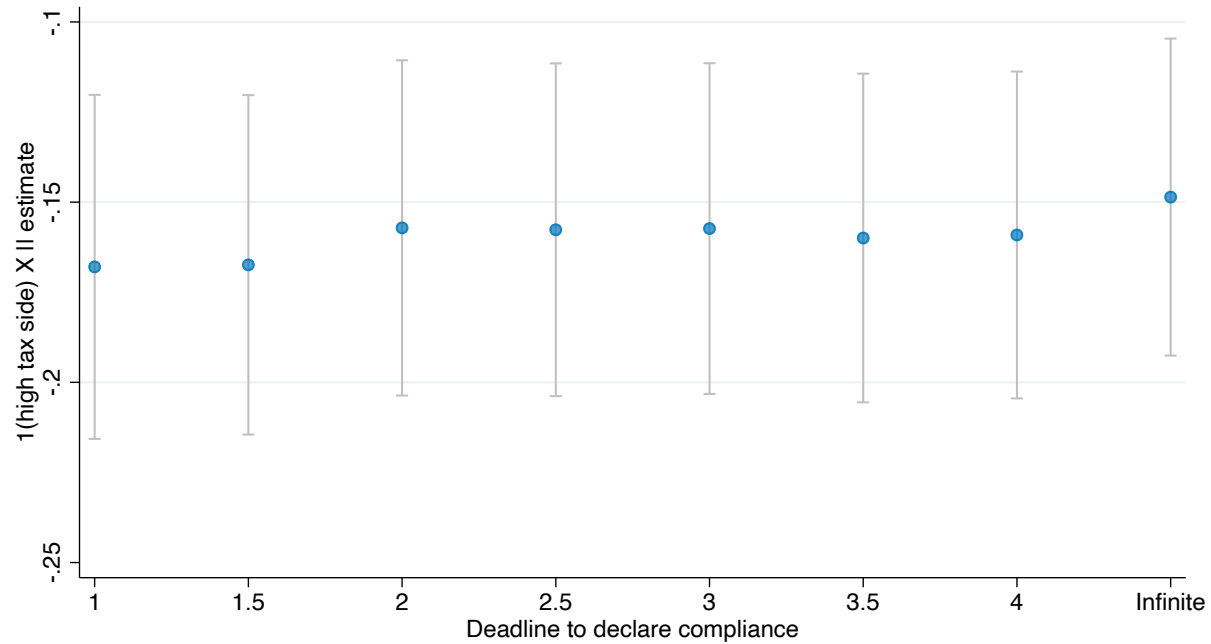
The figures below reproduce three of the main analyses, repeating each exercise eight times. In each time, we vary the time horizon considered to define compliance. We then plot on the vertical coordinate the estimated parameter of interest of each analysis, and in the horizontal coordinate the time horizon considered for payments. Each figure references the corresponding result from the main sections of the paper.

FIGURE F.4: AUGMENTED BOUNDARY DISCONTINUITY DESIGN: COMPLIANCE EFFECTS



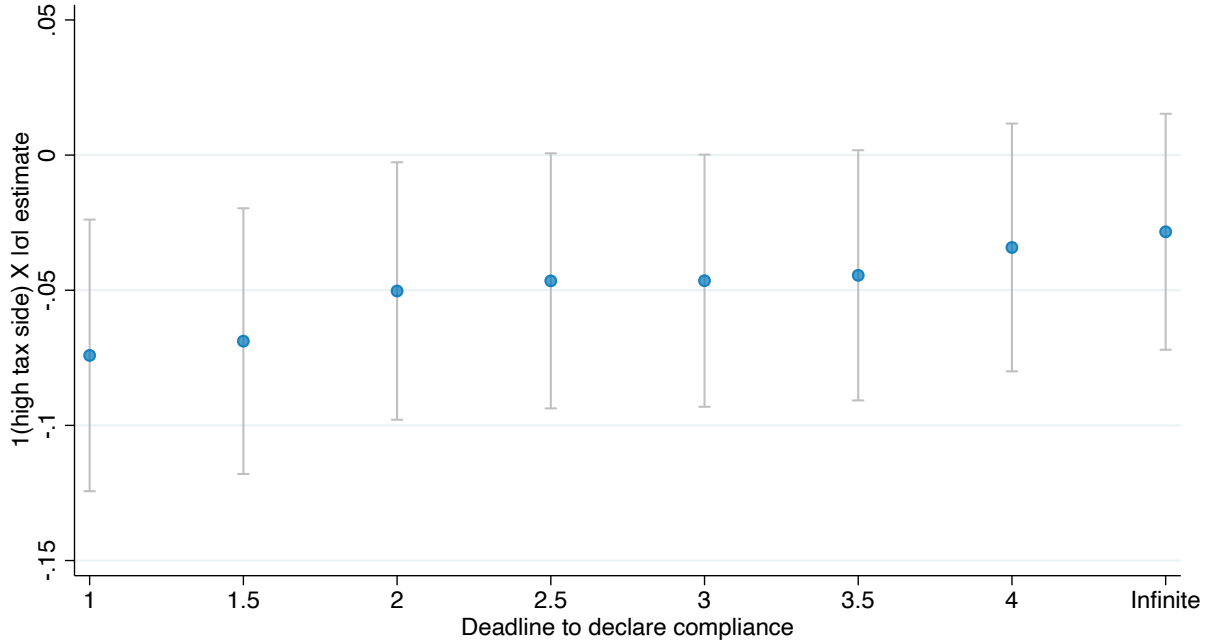
Notes: This figure presents the same analysis as depicted in column one of table 2, but varies the timeline we consider of payments for the definition of compliance. The figure shows the results of estimating the augmented BDD equation (12): $c_i = \lambda_{r(i)} + g(\tau_i, e_i) + f_0(d_i) + \beta_0 HTS_i + f_1(d_i) \times HTS_i + \varepsilon_i$, where $\lambda_{r(i)}$ are fixed effects for 500-meter segments along the boundaries to ensure we are comparing properties who are nearby each other; $g(\tau_i, e_i)$ are cubic splines of the (log) tax liability τ_i and fixed effects for deciles of exposure to mistagging e_i ; $f(d_i)$ and $h(d_i)$ control flexibly for distance to the boundary on the low- and high-tax sides of the boundary respectively; and HTS_i is an indicator for properties on the high-tax side of the boundary ($d_i > 0$). We estimate (12) separately eight times, where we vary the time horizon considered to define compliance. The vertical coordinate of each dot and the vertical gray bars show the estimated impact on compliance and its 95% confidence interval. The horizontal coordinate of each dot shows the time horizon considered.

FIGURE F.5: DIFFERENCE IN BOUNDARY DISCONTINUITY DESIGN: COMPLIANCE EFFECTS



Notes: This figure presents the same analysis as depicted in column one of table 3, but varies the timeline we consider of payments for the definition of compliance. The figure shows the results of estimation of equation (16): $c_i = \lambda_{r(i)} + g_0(\tau_i, e_i) + f_0(d_i) + HTS_i \times [\beta_0 + \eta \log(\sigma) + f_1(d_i) + g_1(\tau_i, e_i)] + \varepsilon_i$ where terms are as defined above in the notes to table 2. We estimate (16) separately eight times, where we vary the time horizon considered to define compliance. The vertical coordinate of each dot and the vertical gray bars show the estimated η and its 95% confidence interval. The horizontal coordinate of each dot shows the time horizon considered.

FIGURE F.6: DYNAMIC DIFFERENCE IN BOUNDARY DISCONTINUITY DESIGN



Notes: This figure presents the same analysis as depicted in column one of table 4, but varies the timeline we consider of payments for the definition of compliance. The figure shows the results of estimating equation (18) discussed in section 6.2: $\Delta c_i = \lambda_{r(i)} + g_0(\Delta\tau_i, e_i) + f_0(d_i) + HTS_i \times [\delta_0 + \eta \Delta \log(\sigma_i) + g_1(\Delta\tau_i, e_i) + f_1(d_i)] + \varepsilon_i$ where all terms are as defined above in the notes to table 2. We estimate (18) separately eight times, where we vary the time horizon considered to define compliance. The vertical coordinate of each dot and the vertical gray bars show the estimated η and its 95% confidence interval. The horizontal coordinate of each dot shows the time horizon considered.

G Salience of inequity

In this appendix, we describe our methodology for constructing a measure of the salience of tax inequity faced by each property. We then use this measure in figure 7, discussed in section 5.1.3, to argue that our results are driven by households for whom the inequity of the IPTU is salient.

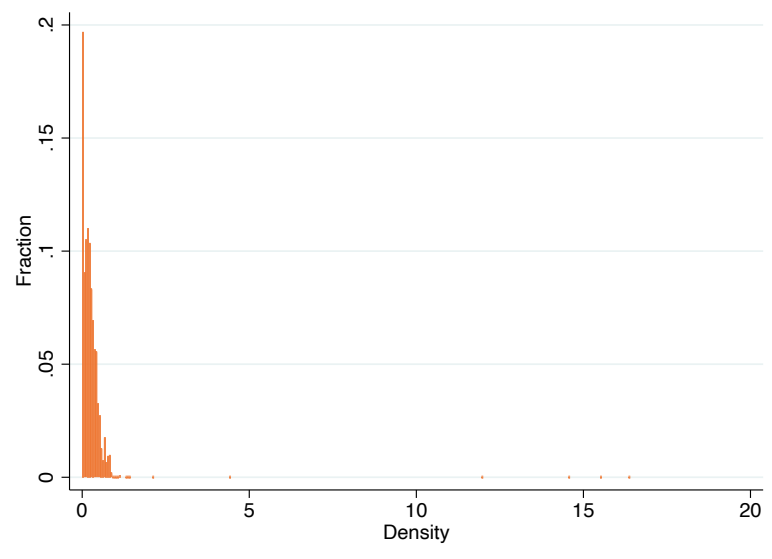
We build on the notions of similarity used in [Auerbach & Hassett \(2002\)](#) to study horizontal inequity of taxation among similar taxpayers. Intuitively, salience is higher when a property's counterfactual tax liability is similar to the actual tax liability of properties located immediately across the tax boundary. Specifically, for each property i , we first calculate a counterfactual tax liability, $\hat{\tau}_i$. We then define our salience measure as the density of $\hat{\tau}_i$ evaluated in the distribution of tax liabilities of properties situated directly on the opposite side of the boundary they face.

To construct our salience measure, we take the following steps:

1. Calculate the counterfactual tax liability ($\hat{\tau}_i$) for every property in 2010.
2. For each street segment $r \in R$ and tax-side $h \in 0, 1$:
 - Identify properties located directly across the boundary (on the opposite tax side within the same street segment).
 - If there are fewer than two properties on the opposite side, assign a salience value of zero to all properties on side h within segment r .
 - Otherwise, for properties on side h within segment r , denote the set of their counterfactual tax liabilities by V .
 - Estimate the kernel density (using an Epanechnikov kernel) of each value in V , based on the distribution of observed tax liabilities on the opposite side of the boundary within the same segment.
 - Assign the estimated density to each corresponding property as its salience measure.

Figure G.1 displays the resulting distribution of our constructed salience measure across properties:

FIGURE G.1: DISTRIBUTION OF OUR MEASURE OF SALIENCE



Lastly, we divide our sample into five groups according to the quintiles of the salience measure distribution. Within each quintile group, we estimate the BDD specification controlling flexibly for tax liability (τ_i) and exposure to mistagging (e_i):

$$c_i = \lambda_{r(i)} + g(\tau_i, e_i) + f_0(d_i) + \beta_0 HTS_i + f_1(d_i) \times HTS_i + \varepsilon_i$$

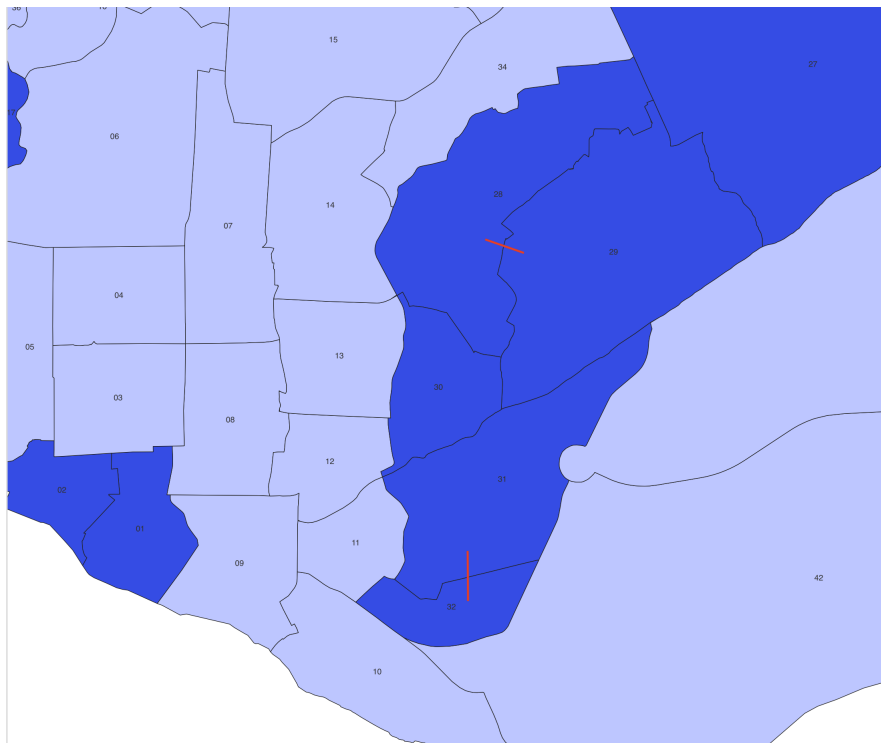
where $g(\tau_i, e_i)$ includes splines for τ_i and decile indicators for e_i . Figure 7 summarizes the estimated results, displaying the implied elasticity of compliance with respect to inequity in each quintile. The figure shows that our results are increasing in the salience of the property tax. In the bottom quintile the estimated effect is zero, but the elasticity is positive in the higher quintiles of salience.

H Placebo Test for Difference in Boundary Discontinuities Design

In Section 5.2, we introduce a Difference-in-Boundary Discontinuities Design that permits discontinuities in the untreated potential outcomes, G_0 , and allows for the distribution of unobservables, ν_0 , to vary discontinuously at sector boundaries. Specifically, our design accommodates the possibility that the left and right limits of the conditional expectation $\mathbb{E} [G_0(t, d, \nu_0) | \tau = t, D = d]$ at $D = 0$ differ. However, we assume that this discontinuity remains constant across potential treatment intensities σ_z . That is, we assume that while households on the high-tax side may be differentially compliant to households on the low-tax side, this difference is constant across households with different levels of exposure to mistagging.

To empirically assess the validity of this assumption, we implement a placebo test using boundaries separating sectors with identical rates, where no actual tax difference exists ($\sigma_i = 0$ for all properties). We construct a placebo dataset by pairing properties along such boundaries with properties located at the nearest boundary with a different sector rate. For example, in Figure H.1, the boundary between sectors 31-32 is matched to the boundary between sectors 28-29.⁵⁶ We classify each boundary as either a “high-tax boundary” or a “low-tax boundary,” based on their relative sector rates. In the given example, sectors 31-32 form the “low-tax boundary” (sector rate 0.02), while sectors 28-29 form the “high-tax boundary” (sector rate 0.03).

FIGURE H.1: ILLUSTRATION OF BOUNDARY MATCHING FOR PLACEBO TEST



This approach enables us to construct simulated values of σ that represent placebo tax-rate differences faced by each property if it were located at the paired boundary:

⁵⁶We avoid linking sectors 31-32 with sectors 30-31 because both share the same sector rate of 0.02.

$$\tilde{\sigma}_i = \frac{T_h}{T_l} = \frac{1 + p_{d(i)} \frac{a_i}{b_i}}{1 + \hat{p}_{d(i)} \frac{a_i}{b_i}} \quad (\text{H.1})$$

where $d(i)$ denotes the boundary segment of property i , $p_{d(i)}$ represents the sector rate at the actual boundary $d(i)$, and $\hat{p}_{d(i)}$ denotes the sector rate at the matched placebo boundary. Importantly, the true inequity measure, σ_i , remains zero for all properties, since genuine inequities are defined within actual boundaries rather than across matched placebo boundaries. Using this simulated variable, we estimate the following placebo Difference-in-Boundary Discontinuities specification:

$$c_i = \gamma_{b(i)} + g_0(\tau_i, e_i) + f(d_i) + HTS_i \times [\beta_0 + \eta \log(\tilde{\sigma}) + h(d_i) + g_1(\tau_i, e_i)] + \varepsilon_i \quad (\text{H.2})$$

where $\gamma_{b(i)}$ are fixed effects for the placebo boundary matches; $g(\tau_i, e_i)$ are flexible controls for property i 's (log) tax liability τ_i and exposure to mistagging e_i (our baseline estimates use τ splines and exposure deciles); $f(d_i)$ and $h(d_i)$ control flexibly for distance to the true boundary on the low- and high-tax sides of the boundary respectively; and HTS_i is an indicator for properties on the high-tax side of the boundary match ($d_i > 0$).

Table H.1 summarizes the estimated results. Reassuringly, none of the specifications show evidence that compliance gaps are correlated with exposure to mistagging as measured through the placebo tax-rate differences, providing support for our identifying assumption.

TABLE H.1: DIFFERENCE IN BOUNDARY DISCONTINUITY DESIGN: COMPLIANCE EFFECTS AND PLACEBO INEQUITY

	(1)	(2)	(3)	(4)	(5)	(6)	(7)
1(high tax side)	-0.03 (0.02)	0.00 (.)	0.00 (.)	0.00 (.)	-2.56** (0.95)	-1.64* (0.82)	0.00 (.)
1(high tax side) $\times \sigma $	-0.05 (0.07)	-0.04 (0.07)	0.10 (0.12)	-0.05 (0.07)	0.03 (0.08)	-0.04 (0.16)	0.03 (0.08)
R^2	0.044	0.045	0.045	0.046	0.056	0.048	0.071
Distance controls	✓	✓	✓	✓	✓	✓	✓
Segment fixed effects	✓	✓	✓	✓	✓	✓	✓
τ splines	✓	✓	✓	✗	✓	✓	✗
τ deciles	✗	✗	✗	✓	✗	✗	✓
Expansiveness splines	✗	✗	✓	✗	✗	✓	✗
Expansiveness deciles	✓	✓	✗	✓	✓	✗	✓
τ splines \times HTS	✗	✓	✓	✗	✓	✓	✗
τ deciles \times HTS	✗	✗	✗	✓	✗	✗	✓
τ splines \times exp deciles	✗	✗	✗	✗	✓	✗	✗
τ splines \times exp splines	✗	✗	✗	✗	✗	✓	✗
τ deciles \times exp deciles	✗	✗	✗	✗	✗	✗	✓
τ splines \times HTS \times exp deciles	✗	✗	✗	✗	✓	✗	✗
τ splines \times HTS \times exp splines	✗	✗	✗	✗	✗	✓	✗
τ deciles \times HTS \times exp deciles	✗	✗	✗	✗	✗	✗	✓
Elasticity	-0.080 0.125	-0.076 0.126	0.184 0.210	-0.089 0.124	0.046 0.136	-0.067 0.284	0.046 0.135
<i>N</i>	12304	12304	12304	12304	12304	12304	12304

Notes: This table replicates the analysis from table 3, but using placebo boundaries and inequities $\tilde{\sigma}$ rather than true inequities σ . The table shows the results of estimation of equation (H.2): $c_i = \gamma_{b(i)} + g_0(\tau_i, e_i) + f(d_i) + HTS_i \times [\beta_0 + \eta \log(\tilde{\sigma}) + h(d_i) + g_1(\tau_i, e_i)] + \varepsilon_i$ where $\gamma_{b(i)}$ are fixed effects for the placebo boundary matches; $g(\tau_i, e_i)$ are flexible controls for property i 's (log) tax liability τ_i and exposure to mistagging e_i ; $f(d_i)$ and $h(d_i)$ control flexibly for distance to the true boundary on the low- and high-tax sides of the boundary respectively; and HTS_i is an indicator for properties on the high-tax side of the boundary match ($d_i > 0$). In column (1), we control for cubic splines of the tax liability and fixed effects for deciles of the exposure distribution. In column (2) we control separately for the tax liability and exposure to mistagging on either side of the boundary. Column (3) replaces the exposure deciles with cubic splines in exposure while column (4) replaces the tax liability deciles with cubic splines. Columns (5)–(7) control for these separately on either side of the boundary.

I Tax Enforcement

This appendix provides some additional background on the way that the IPTU is enforced to assist in interpreting our findings. We touch upon these issues briefly in describing the context in section 2 and raise the potential issue of differential enforcement on either side of the tax sector boundaries in section 4.1. Here we expand upon the tax enforcement procedures in place and investigate empirically whether there is evidence that tax enforcement is indeed less stringent on the high-tax side.

In contrast to many low- and middle-income countries, tax enforcement in Manaus is predominantly automated and involves minimal discretion. The municipal finance and technology authority (SEMEF; *Secretaria Municipal de Finanças e Tecnologia da Informação*) notifies households of their tax liabilities by mail in mid-January each tax year. These tax notices contain the tax liability calculated automatically by a computer using the statutory formula and the properties' data in the cadaster.

If a household does not settle its IPTU bill, fines and interest are automatically applied, and legal actions may be initiated. The application of these fines and interest occurs automatically for any household that remains delinquent as of January 1 of the year following the IPTU issuance, without any discretion on the part of SEMEF officials.⁵⁷

While the fines and interest are automatically applied and carry the force of law, if the debt remains unpaid, the municipality must actively pursue it in order to collect the debt. Under federal law N. 6.830, municipalities are required to secure a “certification of debt” prior to pursuing judicial enforcement. This raises the possibility that SEMEF, internalizing the inequity of the jump in tax liabilities at the sector boundaries, may pursue delinquent taxpayers on the high-tax side of the tax sector boundaries less aggressively than cases on the low-tax side, and that it is this difference in enforcement that accounts, at least in part, for the jump in compliance at the boundaries.

To explore this concern empirically, we use the same sample of properties used in the analysis of the overall compliance responses in section 4.1, focusing on properties that remained delinquent on their 2010 tax bills by the end of 2011. We then tracked whether these properties had received a “certified debt” status by the end of 2011. Of these, 62% were certified, while 38% were not. To determine if the likelihood of certification varied according to tax side, we applied the same BDD model used in Equation (10), reformulated as follows to assess certification status:

$$1[\text{debt certified}]_i = \lambda_{r(i)} + f_0(d_i) + \beta_0 HTS_i + f_1(d_i) \times HTS_i + \varepsilon_i \quad (\text{I.1})$$

where $\lambda_{r(i)}$ are boundary-segment fixed effects, HTS_i is an indicator for being on the high-tax side of the boundary ($d_i > 0$); $f(d_i)$ and $h(d_i)$ control for distance to the boundary on the low- and high-tax sides of the boundary, respectively; and ε_i is the residual.

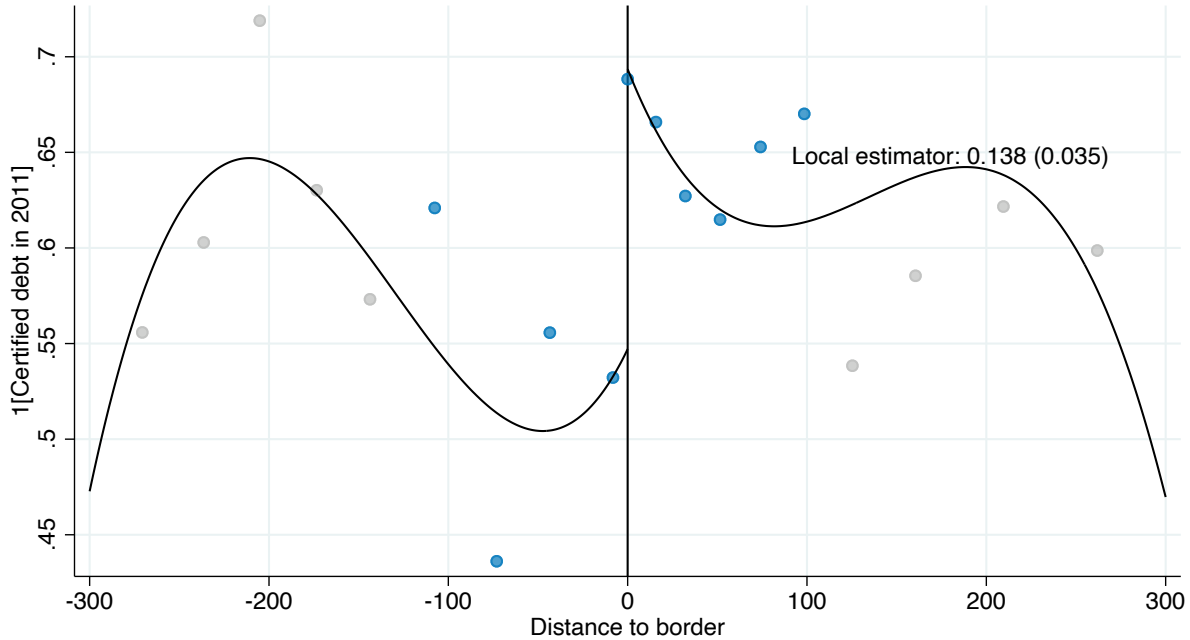
Figure I.1 displays the outcomes of estimating Equation (I.1). This figure provides our point estimate for the change in the probability of having debt certified at the boundary, calculated using local linear controls for distance, the MSE-minimizing bandwidth, and triangular weighting kernels (Calonico *et al.*, 2014, 2018, 2019, 2020). To help visualize the design, the figure also shows an estimated conditional expectation over the full -300 meter – +300 meter window, estimated using decile-spaced bins of distance on either side of the boundary and the triangular kernel used to estimate the point estimate, censoring the kernel at its tenth percentile to still give positive weight to observations outside the MSE-optimal bandwidth. Bins containing the

⁵⁷See <https://www.manaus.am.gov.br/pgm/divida-ativa-servico/>, accessed 2025-03-12.

optimal bandwidth are shown in blue while bins outside the optimal bandwidth are shown in gray.

The results indicate a 13.8 percentage point *higher* likelihood of certification on the high-tax side of the boundary. Moreover, the jump is precisely estimated, allowing us to very confidently reject the possibility that enforcement is weaker on the high-tax side of the boundaries. As a result, we interpret our BDD results as, if anything, lower bounds on the effects of inequity.

FIGURE I.1: CHANGE IN DEBT CERTIFICATION PROBABILITY AT TAX SECTOR BOUNDARIES



Notes: The figure shows the change in the probability of having a debt certified at tax sector boundaries. Specifically, we show the results of estimating the following equation (I.1): $1[\text{debt certified}]_i = \lambda_{r(i)} + f(d_i) + \beta_0 HTS_i + h(d_i) \times HTS_i + \varepsilon_i$ where $\lambda_{r(i)}$ are boundary-segment fixed effects, HTS_i is an indicator for being on the high-tax side of the boundary ($d_i > 0$); $f(d_i)$ and $h(d_i)$ control for distance to the boundary on the low- and high-tax sides of the boundary, respectively; and ε_i is the residual. Overlaid on the figure, we show the point estimate of the discontinuity in the probability to be certified estimated using local linear distance controls, the MSE-minimizing bandwidth, and triangular kernel weights in distance. The dots in the figure show the coefficients from estimating (I.1) with fixed effects for decile-spaced bins of distance, using the same triangular kernel weights but censoring them at their tenth percentile to give non-zero weights to distances outside the optimal bandwidth. The bins in the optimal bandwidth are shown in blue while those outside are shown in gray. The black line is a global cubic polynomial fit in the same way. The results indicate a 13.8 percentage point higher likelihood of certification on the high-tax side of the boundary, which allows us to confidently dismiss the possibility of lesser enforcement on the high-tax side. Consequently, we interpret our main BDD results as lower bounds on the effect with identical enforcement on each side.

J House Prices and IPTU: Evidence from Property Listings

As we discuss in section 2.5, capitalization of the IPTU into house prices may dampen the inequity taxpayers feel when making tax compliance decisions. In Section 3.3.2 and Appendix P, we introduce a modified model that allows households to select properties based on their preferences, which includes a consideration of tax differences and a distaste for tax inequities. This model suggests that, beyond compliance elasticities, a critical sufficient statistic for assessing welfare and shaping optimal policy is $\kappa \equiv -\partial p_{L\phi}/\partial T_\phi$. This parameter represents the degree to which property taxes are reflected in house prices. In this appendix, we empirically explore the extent of this tax capitalization.

We gathered data on housing market asking prices by scraping the online real estate platform [Viva Real](#), collecting details such as addresses and property features (e.g., number of rooms). To merge these market prices with our administrative data, research assistants manually overlaid SEFAZ's geographic map of Manaus onto Google Maps addresses. Through manual inspection, the RAs matched properties between the two sources and rated their confidence in each match. This exercise yielded a dataset comprising 2,553 properties, with asking prices, tax liabilities, and other attributes. Figure J.1 presents a scatter plot of log tax liability against log asking price for these properties, indicating that assessed property values serve only as an approximate proxy for actual market values.

To investigate the extent to which property taxes are capitalized into house prices, we perform two exercises. First, using the properties where the match was classified as "confident" by the RAs, we estimated the following equation:

$$\log(p)_i = e_\kappa \tau_i + \beta X_i + \varepsilon_i \quad (\text{J.1})$$

where $\log(p)_i$ is the log of the asking market price for property i , τ_i is the log of tax liability, X_i are several characteristics of the property collected, and ε_i is the residual. We estimated this equation using a double-selection lasso linear regression. Our coefficient of interest is $e_\kappa = \kappa \frac{T_i}{p_i}$, the elasticity of the asking price with respect to the tax liability.

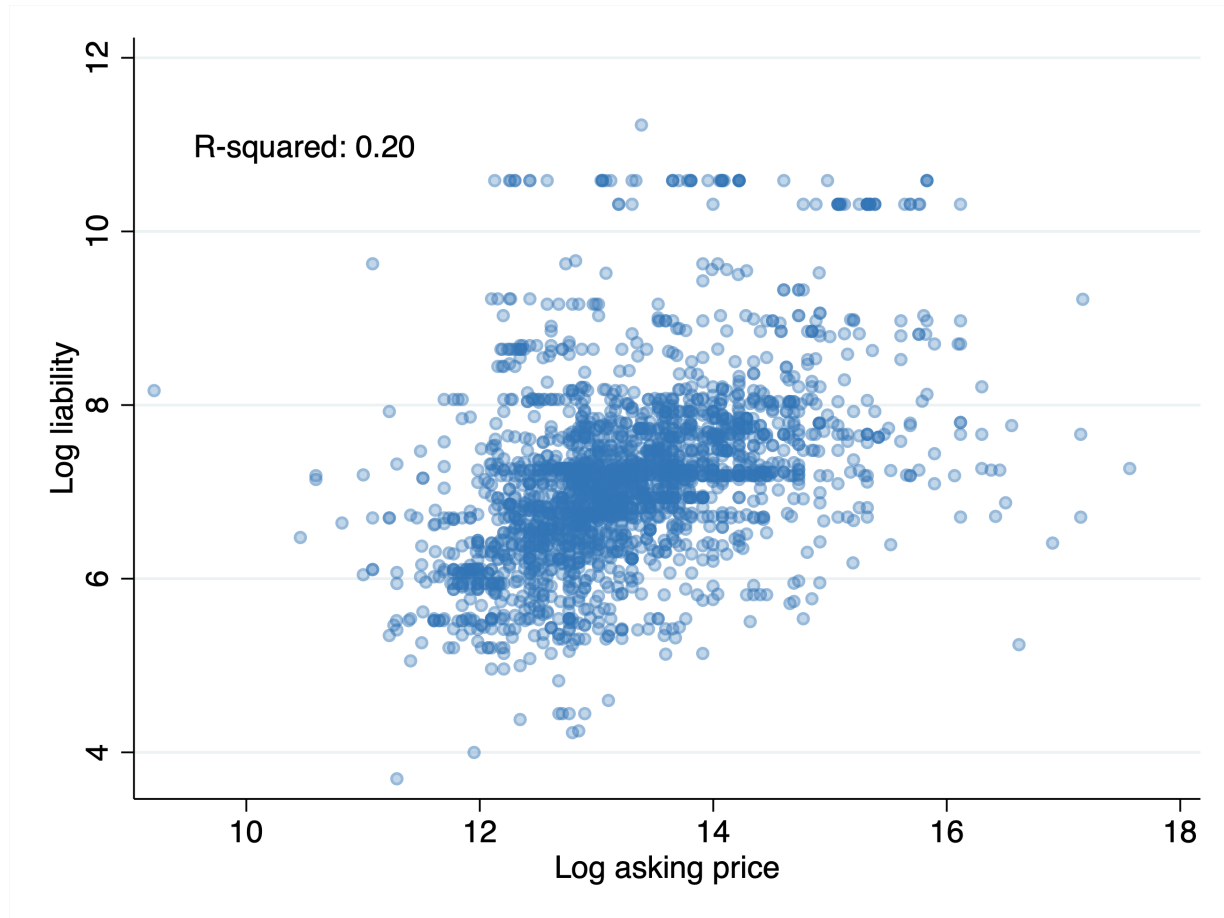
Next, we used a boundary discontinuity design akin to section 4.1. Specifically, we estimated the equation

$$y_i = \gamma_{b(i)} + f(d_i) + \beta_0 HTS_i + h(d_i) \times HTS_i + \varepsilon_i \quad (\text{J.2})$$

where $\gamma_{b(i)}$ are boundary fixed effects, HTS_i is an indicator for being on the high-tax side of the boundary ($d_i > 0$); $f(d_i)$ and $h(d_i)$ control for distance to the boundary on the low- and high-tax sides of the boundary, respectively; and ε_i is the residual. The outcome variable, y_i , is the log of tax liability for property i in the first stage, and the log of the asking market price for property i in the reduced form. Both stages are estimated using local linear controls for distance, the same MSE minimizing bandwidth, and triangular weighting kernels ([Calonico et al., 2014, 2018, 2019, 2020](#)).

The results of both exercises are displayed in table J.1. The results show no evidence of any meaningful capitalization of the IPTU into listing prices.

FIGURE J.1: DISTRIBUTION OF LOG LIABILITY AND LOG ASKING PRICE



Notes: The figure shows the scatter plot of the log liability and the log asking price. We gathered data on housing market asking prices by scraping the online real estate platform [Viva Real](#), collecting details such as addresses. To integrate these market prices with our administrative data, research assistants overlaid SEFAZ's geographic map of Manaus onto Google Maps addresses and matched properties between the two sources. This exercise yielded a dataset comprising 2,553 properties, with asking prices, tax liabilities, and other attributes.

TABLE J.1: HOUSING PRICE RESPONSE TO PROPERTY TAXES

	(1)	(2)
Elasticity estimate	0.04 (0.05)	-0.06 (0.18)
Admin controls	✓	✗
VivaReal controls	✓	✗
RD specification	✗	✓
<i>N</i>	930	1014

Notes: The table shows estimates of the elasticity of the asking price of properties with respect to the tax liability. Column (1) shows the results of estimating equation (J.1): $\log(P)_i = e_\kappa \tau_i + \beta X_i + \varepsilon_i$ where $\log(p)_i$ is the log of the asking market price for property i , τ_i is the log of tax liability, X_i are several characteristics of the property collected, and ε_i is the residual. Column (2) shows the implied elasticity from estimating the first stage and the reduced form from equation (J.2): $y_i = \gamma_{b(i)} + f(d_i) + \beta_0 HTS_i + h(d_i) \times HTS_i + \varepsilon_i$ where $\gamma_{b(i)}$ are boundary fixed effects, HTS_i is an indicator for being on the high-tax side of the boundary ($d_i > 0$); $f(d_i)$ and $h(d_i)$ control for distance to the boundary on the low- and high-tax sides of the boundary, respectively; and ε_i is the residual. The outcome variable, y_i , is the log of tax liability for property i in the first stage, and the log of the asking market price for property i in the reduced form.

K Optimal Tax Simulations

This appendix performs a series of simulations of our conceptual framework in section 3. To calibrate the model, we need to make a parametric assumption about compliance rates. In particular, we will assume that compliance takes the iso-elastic form

$$c_{\theta\phi} = c_0 \left(\frac{T_\phi}{y_\theta} \right)^{-\varepsilon} \sigma^{-\eta} \quad (\text{K.1})$$

K.1 Comparative Statics

The baseline model has a number of parameters. Table K.1 lists the parameters, what they are, and the values we set them to. We also display the range of the parameters over which we perform comparative statics. For the social marginal welfare weights, our comparative statics exercises hold the average social marginal weight fixed at its baseline value $\frac{1}{2}(0.475 + \frac{0.475}{1.6})$, and then vary the ratio of the social marginal welfare weights g_L/g_H between 1.3 and 1.9. Similarly when studying wealth inequality we hold the average wealth fixed at its baseline value $\frac{1}{2}(6,630.8 + 4,911.5)$ and vary the ratio y_H/y_L between 1.1 and 1.6. Figure K.1 shows the results of these comparative statics exercises. The figures confirm the comparative statics highlighted in proposition 2 and add new comparative statics also.

K.2 Share of Overall Response from Inequity

As discussed in section 7, the model can be used to study the implications for tax policy of different decompositions of the overall compliance response at the tax sector boundaries into the part that comes from responses to inequity and the part that comes from responses to the tax liability. Figure 13 shows the results of that calibration.

Here, we also study how the results about the progressivity of the tax schedule change when we use different welfare weights. To do this, we hold the welfare weight on the occupants of low-value houses, g_L , fixed and vary the ratio g_L/g_H between 1.4 and 1.8. Figure K.2 shows the optimal tax schedule's progressivity as a function of the share of the overall response due to inequity for the different values of g_L/g_H . For each of these, we compute the progressivity of the optimal tax schedule with our baseline estimate of the share of the overall response due to inequity — 46.5% relative to the progressivity of the optimal tax schedule with no responses to inequity. Our baseline calibration suggests that the progressivity at our baseline estimates is 44% of the progressivity absent inequity responses. This ratio ranges from 41% when $g_L/g_H = 1.8$ to 48% when $g_L/g_H = 1.4$, suggesting that this result is quite insensitive to the strength of redistributive preferences used.

K.3 Simulations of Extensions to the Model

Mistagging of Both Types of Houses In section 3.3.1 and Appendix O we extend the model to allow for both the $\theta = L$ and the $\theta = H$ types of houses to be mistagged. We present two sets of simulations to explore how these forces may affect the optimal tax schedule. First, in panel A of figure K.3, we hold fixed the extent of mistagging of both house types $\psi_{Lh} = \psi_{Hl} = 0.1$ and the strength of the behavioral response to overtagging $\eta_{Lh} = 0.12$ and vary the strength of the behavioral response to undertagging $\eta_{Hl} \in [-0.05, 0.15]$. In Panel B we hold fixed the strength of the behavioral response to mistagging $\eta_{Lh} = \eta_{Hl} = 0.12$ and the extent of overtagging $\psi_{Lh} = 0.1$

and vary the extent of undertagging $\psi_{Hl} \in [0, 0.15]$. The conclusions of our baseline model with only overtagging are robust to the inclusion of (responses to) undertagging.

Location Choice and Endogenous House Prices We now turn to simulating the optimal tax schedule in the extended model that allows for location choice and endogenous house prices discussed in section 3.3.2 and Appendix P. The key additional sufficient statistic is now $\kappa \equiv -dp_{\theta\phi}/dT_\phi$. Our analysis in Appendix J finds no evidence in support of a non-zero value for κ , but nevertheless we consider a wide range of values for κ between -0.15 and 0.15. Figure K.4 shows the results, suggesting that one needs to see quite substantial amounts of capitalization before the progressivity of the tax schedule is very much affected.

TABLE K.1: BASELINE MODEL PARAMETERS

Parameter	Value	Justification	Simulation Range
ε	0.33	consistency with reduced form: $-\frac{dc}{c} = \varepsilon \frac{dT}{T} + \eta \frac{d\sigma}{\sigma}$ and $\hat{\eta} = 0.12$	0.2 – 0.5
η	0.12	Dynamic boundary discontinuity design	0.05 – 0.2
ψ	0.1	$\sim 10\%$ of properties are near boundaries	0 – 0.2
ρ	3	Standard in literature (Elminejad et al., 2025)	1.5 – 4.5
λ	1	Normalization	
g_H	0.475/1.6	baseline	
g_L	0.475	baseline	$g_L/g_H \in [1.3, 1.9]$
y_H	6,630.8	$E[T LTS] = 172.4$ and 2.6% of income	
y_L	4,911.5	$E[T HTS] = 127.7$ and 2.6% of income	$y_H/y_L \in [1.1, 1.6]$
c_0	0.211	Make baseline compliance of 0.7 consistent with y_H, y_L , baseline taxes and equation (K.1).	

FIGURE K.1: SIMULATIONS OF BASELINE MODEL COMPARATIVE STATICS

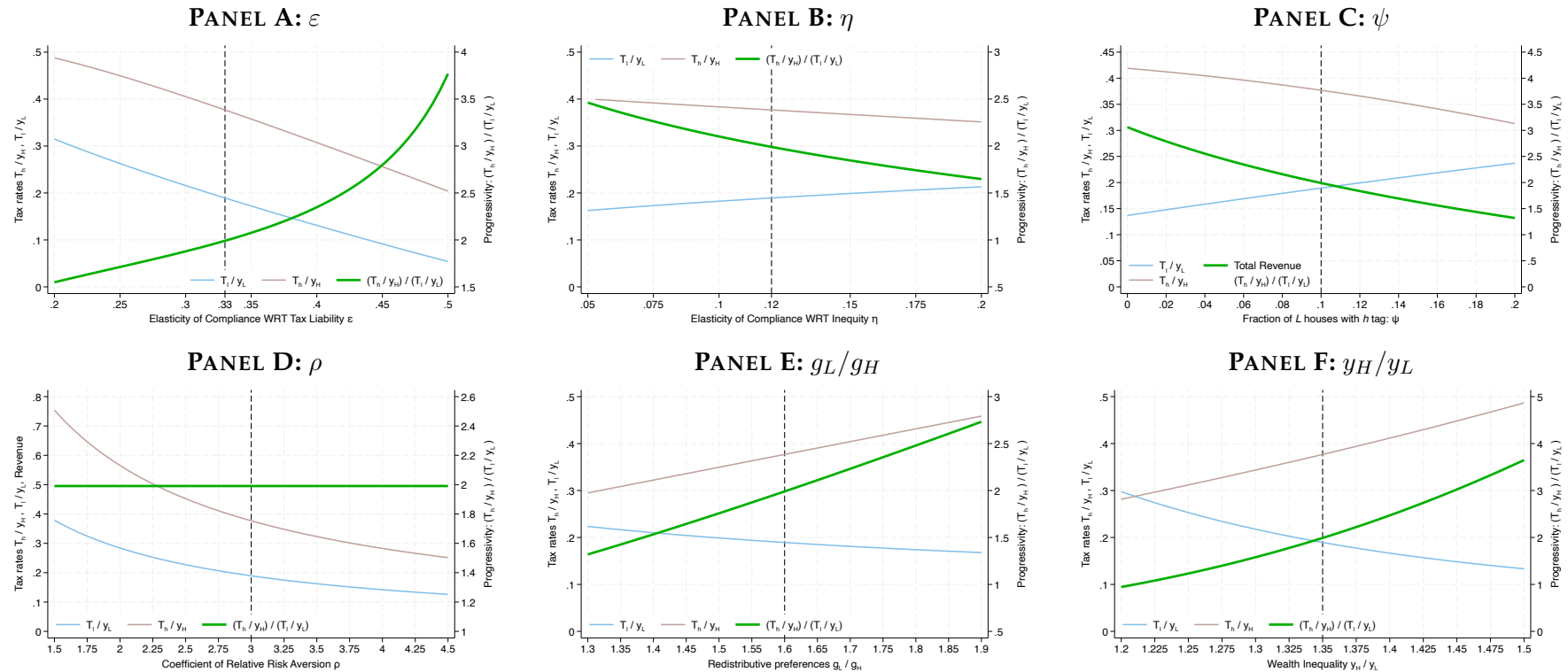
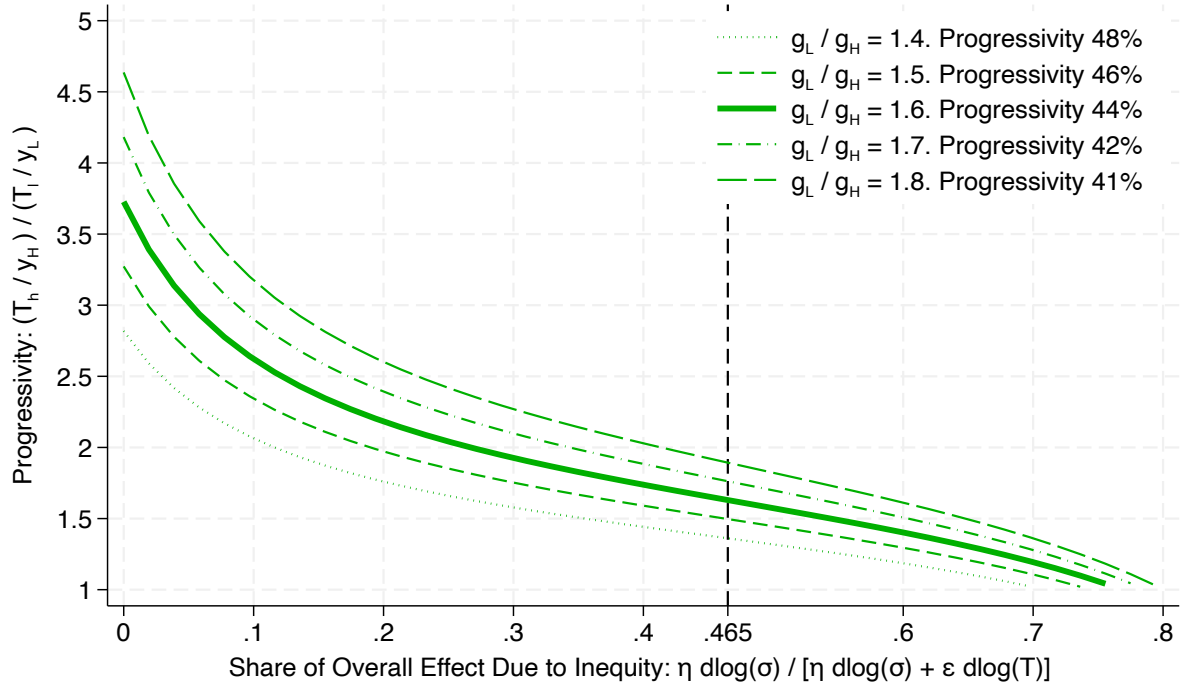


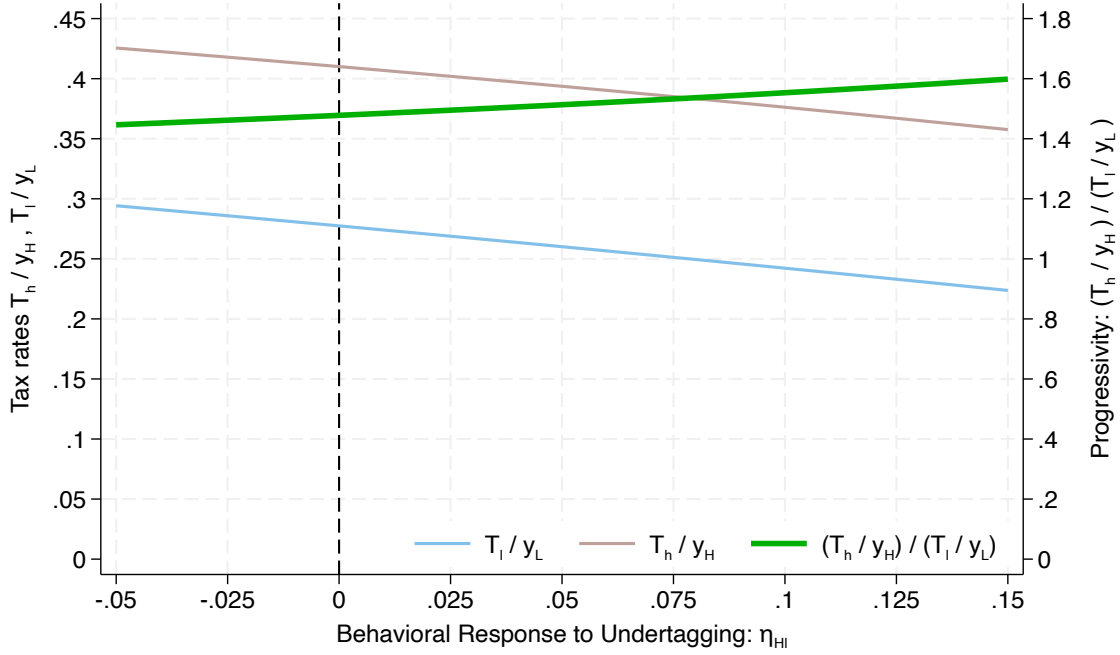
FIGURE K.2: INEQUITY AND PROGRESSIVITY UNDER DIFFERENT REDISTRIBUTIVE PREFERENCES



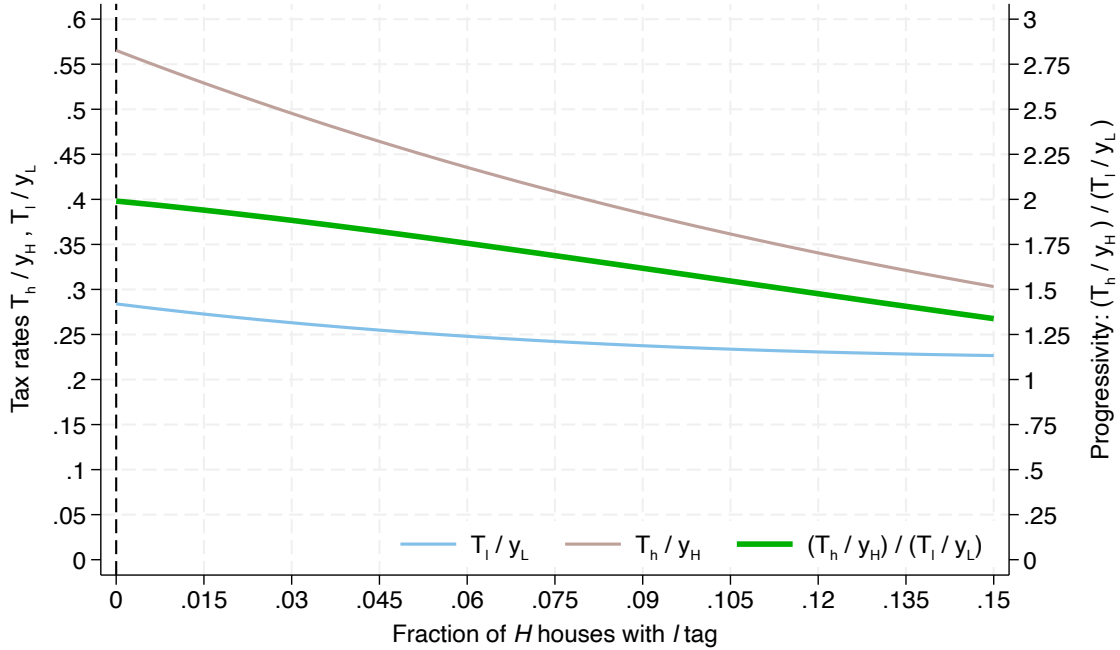
Notes: The figure shows the progressivity of the optimal tax schedule in proposition 2 as a function of the share of the overall response at the tax sector boundaries that is driven by responses to inequity. Each line is drawn for a different strength of redistributive preferences g_L/g_H between 1.4 and 1.8 (our baseline value is 1.6). For each simulation, we compute the progressivity of the tax schedule at our baseline estimates (which suggest that inequity responses account for 46.5% of the overall response) relative to the progressivity of the optimal tax schedule absent inequity responses.

FIGURE K.3: OPTIMAL TAX SCHEDULE WITH MISTAGGING OF BOTH HOUSE TYPES

PANEL A: BEHAVIORAL RESPONSE TO UNDERTAGGING: η_{Hl}

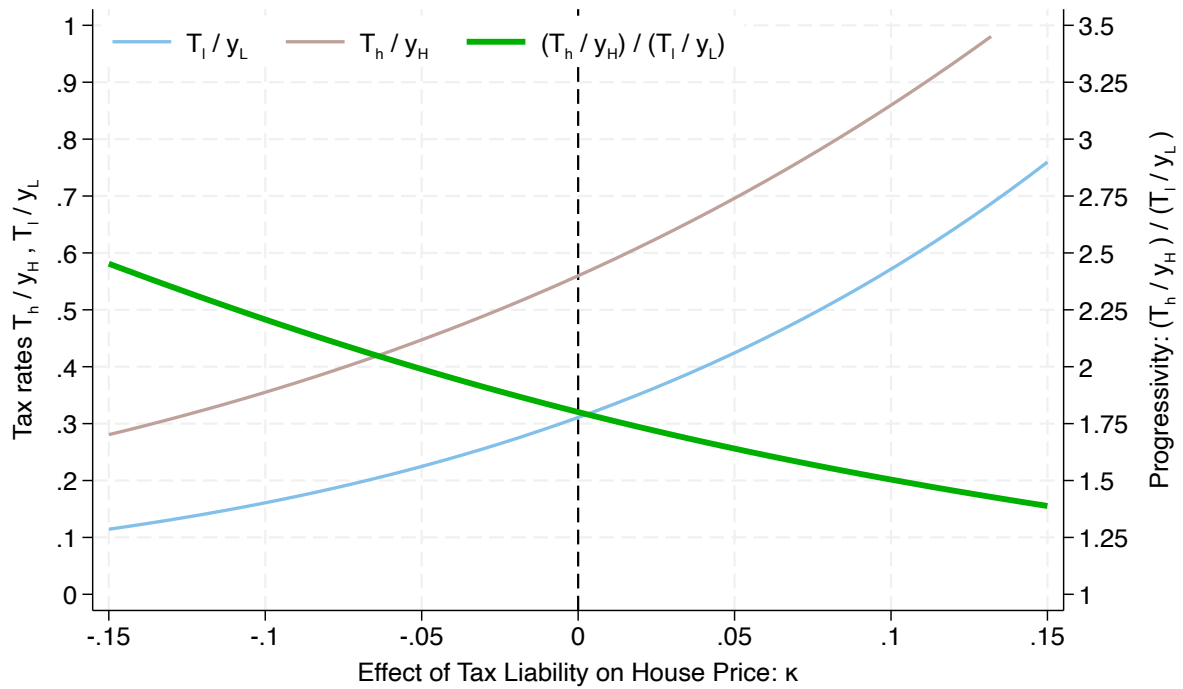


PANEL B: EXTENT OF UNDERTAGGING: ψ_{Hl}



Notes: The figure shows the optimal tax schedule in the extended model allowing for mistagging of both types of households, discussed in section 3.3.1 and Appendix O. In Panel A we hold fixed the extent of mistagging of both house types $\psi_{Lh} = \psi_{Ll} = 0.1$ and the strength of the behavioral response to overtagging $\eta_{Lh} = 0.12$ and vary the strength of the behavioral response to undertagging $\eta_{Hl} \in [-0.05, 0.15]$. In Panel B we hold fixed the strength of the behavioral response to mistagging $\eta_{Lh} = \eta_{Hl} = 0.12$ and the extent of overtagging $\psi_{Lh} = 0.1$ and vary the extent of undertagging $\psi_{Hl} \in [0, 0.15]$.

FIGURE K.4: OPTIMAL TAX SCHEDULE WITH ENDOGENOUS HOUSE PRICES



Notes: The figure shows the optimal tax schedule in the extended model allowing for location choices and endogenous house prices, discussed in section 3.3.2 and Appendix P. We vary the responsiveness of house prices to property taxes $\kappa = -dp_{\theta\phi}/dT_\phi$ between -0.15 and 0.15.

L Fiscal Capacity Counterfactuals

As discussed in Section 7, the finding that taxpayers respond strongly to inequities in the tax schedule implies substantial returns to investments in fiscal capacity—specifically, the ability to differentiate between high- and low-value properties. In this appendix, we use data on housing market asking prices from the online real estate platform [Viva Real](#) to quantify the potential gains from three counterfactual improvements in the property assessment system that would enable more accurate valuations.

As a benchmark, we first measure the implied assessed market price from the current presumptive formula, highlighting that assessed values often diverge substantially from market asking prices. We then consider three counterfactual improvements to the assessment system. First, we recalibrate the coefficients in the existing tax formula using the asking price data. Second, we evaluate a more flexible estimation of assessed values based on the same set of attributes currently used in the presumptive formula. Third, we assess the gains from incorporating additional property characteristics available in the Viva Real data but not presently observed by the tax authority.

We collected data on housing market asking prices by scraping the online real estate platform [Viva Real](#), which includes property addresses and physical characteristics (e.g., number of rooms). To link this data to the administrative tax records, research assistants manually georeferenced properties by overlaying SEFAZ's cadastral maps onto Google Maps and matching properties across the two sources. This process yielded 2,553 properties with matched asking prices, tax liabilities, and physical attributes. To ensure consistency across counterfactual exercises, we restrict the sample to the 1,659 properties with complete information in both the administrative cadaster and the Viva Real dataset.

As a benchmark, we compute the implied assessed market value for each property based on its tax liability. Since all properties in our sample are subject to a uniform tax rate of 0.9%, the assessed market value, \hat{y}_i , is given by

$$\hat{y}_i = \frac{T_i}{0.009} = [b_i + p_{s(i)}a_i]$$

where T_i is the IPTU liability for property i , b_i is the assessed building value, a_i is the land value, and $p_{s(i)}$ is the sector-specific price per unit of land. To evaluate the prediction accuracy of the assessed market value, we calculate the mean squared error (MSE) between \hat{y}_i and the observed asking price y_i , the root mean squared error (RMSE), and the mean absolute error (MAE). Table L.1 shows the corresponding results. Given that the average asking price is 856,322.34, the RMSE and the MAE are quite large, which imply that the current formula frequently mistakes the market price.

We next evaluate how recalibrating the coefficients in the existing property tax formula improves prediction accuracy relative to market prices. The IPTU presumptive formula can be expressed as a nonlinear function of property characteristics and administrative coefficients. Specifically, note that the assessed market value of property i is given by

$$a_i = \text{land area}_i \times \text{share constructed}_i \prod_{A_j \in A} \alpha_j^{1[A_j]_i}$$

where while $A_j \in A$ denote binary attributes with associated coefficients α_j . For example, consider a property with 100 square meters of land, of which 50 percent is constructed. Suppose the property is located on a corner ($A_1 = 1$ with $\alpha_1 = 1.1$), has flat topography ($A_7 = 0$ with

$\alpha_7 = 1$), and normal pedology ($A_{11} = 1$ with $\alpha_{11} = 1$). The assessed land value in this case is given by $10000 \times 0.5 \times 1.1 = 5500$.

Similarly, both the sector-specific land price $p_{s(i)}$ and the assessed building value are determined as functions of binary property attributes with associated coefficients. In total, the presumptive formula contains 371 coefficients, which are estimable with sufficiently data. Given our limited sample from Viva Real, we estimate 51 of the coefficients from the presumptive using nonlinear least squares estimation. The remaining coefficients correspond to attributes that are either universally zero in the sample or exhibit insufficient variation (e.g., sectors with a single observation), in which case we aggregate them with related categories where appropriate. Using the recalibrated formula, we predict the associated asking prices. The results show that, relative to the current formula, we are able to improve the MSE, the RMSE and the MAE by 37%, 21%, and 32% respectively.

We next evaluate how much the government could improve assessment accuracy using a more flexible, yet readily implementable, prediction model. Specifically, we estimate a random forest model to predict asking prices based on the same set of property attributes used in the presumptive IPTU formula. We conduct a grid search over hyperparameters—the number of features considered at each split and the number of trees in the forest—and select the combination that minimizes the out-of-bag (OOB) mean squared error (MSE). Model performance is evaluated by predicting asking prices and computing the same accuracy measures used in previous exercises. As shown in Table L.1, the random forest achieves substantial improvements relative to the current presumptive formula: MSE declines by 65 percent, RMSE by 41 percent, and MAE by 55 percent.

Finally, we analyze what would be the benefits of also incorporating additional property attributes available in the Viva Real data but not in the cadaster. We repeat the same exercise to train the random forest model and we use it to predict the asking prices. The results highlight the large returns to investing in fiscal capacity. Relative to the current presumptive formula, we are able to improve the MSE, the RMSE and the MAE by 92%, 73%, and 82% respectively.

TABLE L.1: PREDICTION ACCURACY ACROSS MODELS

Model	Accuracy Measure	Prediction Error
Current presumptive formula	MSE	1,853,381,626,281.09
Updated formula	MSE	1,159,854,055,479.57
Random forest	MSE	648,280,875,973
Random forest with additional attributes	MSE	139,635,236,188
Current presumptive formula	RMSE	1,361,389.59
Updated formula	RMSE	1,076,965.20
Random forest	RMSE	805,158.90
Random forest with additional attributes	RMSE	373,678.00
Current presumptive formula	MAE	735,637.21
Updated formula	MAE	500,677.70
Random forest	MAE	329,301.60
Random forest with additional attributes	MAE	128,935.80

M Proof of Proposition 1

Proof. To see that the optimal property tax satisfies (2) and (3), note that without mistagging, social welfare is

$$W = \omega_L V_{Ll} + \omega_H V_{Hh} + B(r) \quad (\text{M.1})$$

The government chooses T_l and T_h to maximize W subject to its constraint that $r = c_L T_l + c_H T_h$. Without inequity, household compliance decisions depend only on the tax that they face and so the (normalized) social marginal welfare effects of changes in the two taxes are

$$\begin{aligned} \frac{dW}{dT_l} \frac{1}{b(r)} &= \frac{\omega_L}{b(r)} \frac{\partial V_{Ll}}{\partial T_l} + \frac{dr}{dT_l} = 0 \\ \frac{dW}{dT_h} \frac{1}{b(r)} &= \frac{\omega_H}{b(r)} \frac{\partial V_{Hh}}{\partial T_h} + \frac{dr}{dT_h} = 0 \end{aligned}$$

with marginal revenue effects

$$\begin{aligned} \frac{dr}{dT_l} &= c_{Ll} + \frac{dc_{Ll}}{dT_l} T_l = c_{Ll} (1 - \varepsilon) \\ \frac{dr}{dT_h} &= c_{Hh} + \frac{dc_{Hh}}{dT_h} T_h = c_{Hh} (1 - \varepsilon) \end{aligned}$$

The marginal private welfare effects are

$$\frac{\partial V_{\theta\phi}}{\partial T_\phi} = -c_{\theta\phi} u'(y_\theta - T_\phi) \simeq -c_{\theta\phi} u'(y_\theta) \left(1 + \rho \frac{T_\phi}{y_\theta} \right) \quad (\text{M.2})$$

where we approximate marginal utility using $u'(y_\theta - T_\phi) \simeq u'(y_\theta) (1 + \rho T_\phi / y_\theta)$, where $\rho \equiv -u''(x) x / u'(x)$ is the coefficient of relative risk aversion (Chetty, 2006). Combining these elements, the optimal property taxes satisfy the first order conditions

$$\frac{dW}{dT_l} \frac{1}{b(r)} = -g_L \left(1 + \rho \frac{T_l}{y_L} \right) c_L + c_L (1 - \varepsilon) = 0 \quad (\text{M.3})$$

$$\frac{dW}{dT_h} \frac{1}{b(r)} = -g_H \left(1 + \rho \frac{T_h}{y_H} \right) c_H + c_H (1 - \varepsilon) = 0 \quad (\text{M.4})$$

Solving equations (M.3) and (M.4) yields expressions (2) and (3) in Lemma 1.

To see that the level of taxation is lower the stronger are behavioral responses, note that differentiation of (2) and (3) shows that both taxes are lower when ε is higher. Since the private marginal welfare effects are strictly negative, the optimum is on the increasing side of the Laffer curve and so tax revenues also decrease.

To see that the progressivity of the tax is increasing in the relative welfare weights, combine (2) and (3) and rearrange so that we can relate the progressivity of the tax schedule to the ratio of the welfare weights:

$$\frac{g_L}{g_H} = \frac{1 + \rho T_h / y_H}{1 + \rho T_l / y_L}$$

Similarly, we can combine (2) and (3) to relate the progressivity of the tax schedule to the com-

pliance elasticity:

$$\frac{T_h/y_H}{T_l/y_L} = 1 + \frac{\left(\frac{g_L}{g_H} - 1\right)(1 - \varepsilon)}{1 - \varepsilon - g_L}$$

Differentiating with respect to ε shows that the progressivity of the optimal tax schedule is increasing in the compliance elasticity. \square

N Proof of Proposition 2

Proof. Social welfare with mistagging is

$$W = \psi\omega_L V_{Lh} + (1 - \psi)\omega_L V_{Ll} + \omega_H V_{Hh} + B(r) \quad (\text{N.1})$$

where the private welfare of the θ -types with the ϕ tag is

$$V_{\theta\phi} = \int_{-\infty}^{\gamma_{\theta\phi}^*} (u(y_\theta) - \gamma) dF(\gamma) + \int_{\gamma_{\theta\phi}^*}^{\infty} (u(y_\theta - T_\phi) - d(\sigma)) dF(\gamma) \quad (\text{N.2})$$

The optimal tax schedule satisfies $dW/dT_l = dW/dT_h = 0$.

Starting with the government's budget, total revenue is

$$r = \psi c_{L,h} T_h + (1 - \psi) c_{L,l} T_l + c_{H,h} T_h$$

and the effects of changes in taxes on tax revenue are:

$$\begin{aligned} \frac{dr}{dT_h} &= \psi \left(c_{L,h} + \frac{dc_{L,h}}{dT_h} T_h \right) + c_{H,h} + \frac{dc_{H,h}}{dT_h} T_h \\ &= \psi c_{L,h} (1 - \varepsilon - \eta) + c_{H,h} (1 - \varepsilon) \\ \frac{dr}{dT_l} &= \psi \frac{dc_{L,h}}{dT_l} T_h + (1 - \psi) \left(c_{L,l} + \frac{dc_{L,l}}{dT_l} T_l \right) \\ &= \psi c_{L,h} \eta \sigma + (1 - \psi) c_{L,l} (1 - \varepsilon) \end{aligned}$$

For the $\{Ll\}$ and the $\{Hh\}$ types, the marginal private welfare effects of a small change in the tax liability are as in equation (M.2) in the proof of lemma 1 in appendix M. However, for the $\{Lh\}$ types we now have marginal welfare effects

$$\begin{aligned} \frac{dV_{Lh}}{dT_l} &= \int_{\gamma_{Lh}^*}^{\infty} -d'(\sigma) \frac{\partial \sigma}{\partial T_l} dF = c_{L,h} d'(\sigma) \frac{T_h}{T_l^2} \\ &\simeq c_{L,h} u'(y_L - T_h) \frac{\eta}{\varepsilon} \frac{T_h}{T_l} \simeq c_{L,h} u'(y_L) \left[1 + \rho \frac{T_l}{y_L} \right] \frac{\eta}{\varepsilon} \sigma \\ \frac{dV_{Lh}}{dT_h} &= \int_{\gamma_{Lh}^*}^{\infty} \left[-u'(y_L - T_h) - d'(\sigma) \frac{\partial \sigma}{\partial T_h} \right] = -c_{Lh} \left[u'(y_L - T_h) + d'(\sigma) \frac{\partial \sigma}{\partial T_h} \right] \\ &\simeq -c_{Lh} u'(y_L - T_h) \left(1 + \frac{\eta}{\varepsilon} \right) \simeq -c_{L,h} u'(y_L) \left[1 + \rho \frac{T_l}{y_L} \right] \left(1 + \frac{\eta}{\varepsilon} \right) \end{aligned}$$

where we have approximated marginal utility around y_L using $u'(y) \simeq u'(y_L) \left(1 - \rho \frac{y - y_L}{y_L} \right)$. We also follow Allcott & Taubinsky (2015) and Brockmeyer *et al.* (2023) to express the marginal

disutility of inequity in money-metric terms. To see this, note that

$$\begin{aligned}\varepsilon &\equiv -\frac{\partial c_{Lh}}{\partial T_h} \frac{T_h}{c_{Lh}} = \frac{f(\gamma_{Lh}^*)}{1 - F(\gamma_{Lh}^*)} \frac{\partial \gamma_{Lh}^*}{\partial T_h} T_h = \frac{f(\gamma_{Lh}^*)}{1 - F(\gamma_{Lh}^*)} u'(y_L - T_h) T_h \\ \eta &\equiv -\frac{\partial c_{Lh}}{\partial \sigma} \frac{\sigma}{c_{Lh}} = \frac{f(\gamma_{Lh}^*)}{1 - F(\gamma_{Lh}^*)} \frac{\partial \gamma_{Lh}^*}{\partial \sigma} \sigma = \frac{f(\gamma_{Lh}^*)}{1 - F(\gamma_{Lh}^*)} d'(\sigma) \sigma \\ &\Leftrightarrow d'(\sigma) = \frac{\eta}{\varepsilon} u'(y_L - T_h) T_h\end{aligned}$$

Mistagged households have higher marginal utility for two reasons. First, they face higher taxes, reducing consumption and raising marginal utility T_h/y_L (the $\rho \frac{T_l}{y_L} \sigma$ term in the square brackets). Second, they experience disutility from inequity, with money-metric equivalent $(\eta/\varepsilon) u' T_l$. Increases in T_h aggravate both of these forces, so $dV_{Lh}/dT_h < 0$. However, even though mistagged households don't face the tax T_l , increases in T_l reduce inequity σ , improving their welfare: $dV_{Lh}/dT_l > 0$.

Combining these elements, we can see that the (normalized) marginal social welfare effects are:

$$\begin{aligned}\frac{dW}{dT_l} \frac{1}{b(r)} &= \frac{\omega_L}{b(r)} \psi \frac{dV_{L,h}}{dT_l} + \frac{\omega_L}{b(r)} (1 - \psi) \frac{dV_{L,l}}{dT_l} + \frac{dr}{dT_l} \\ &\simeq g_L \psi c_{L,h} \left[1 + \rho \frac{T_l}{y_L} \sigma \right] \frac{\eta}{\varepsilon} \sigma - g_L (1 - \psi) c_{L,l} \left[1 + \rho \frac{T_l}{y_L} \right] + [\psi c_{L,h} \eta \sigma + (1 - \psi) c_{L,l} (1 - \varepsilon)]\end{aligned}\tag{N.3}$$

$$\begin{aligned}\frac{dW}{dT_h} \frac{1}{b(r)} &= \frac{\omega_L}{b(r)} \psi \frac{dV_{L,h}}{dT_h} + \frac{\omega_H}{b(r)} \frac{dV_{H,h}}{dT_h} + \frac{dr}{dT_h} \\ &\simeq -g_L \psi c_{L,h} \left[1 + \rho \frac{T_h}{y_L} \right] \left(1 + \frac{\eta}{\varepsilon} \right) - g_H c_{H,h} \left[1 + \rho \frac{T_h}{y_H} \right] + [\psi c_{L,h} (1 - \varepsilon - \eta) + c_{H,h} (1 - \varepsilon)]\end{aligned}\tag{N.4}$$

Dividing (N.3) and (N.4) by the number of taxpayers of each tax, these can be written as

$$\frac{dW}{dT_l} \frac{1}{b(r)} \frac{1}{(1 - \psi) c_{Ll}} \simeq g_L \varphi_l \left[1 + \rho \frac{T_l}{y_L} \sigma \right] \frac{\eta}{\varepsilon} \sigma - g_L \left[1 + \rho \frac{T_l}{y_L} \right] + \varphi_l \eta \sigma + (1 - \varepsilon) = 0\tag{N.5}$$

$$\begin{aligned}\frac{dW}{dT_h} \frac{1}{b(r)} \frac{1}{\psi c_{Lh} + c_{Hh}} &\simeq -g_L \varphi_h \left[1 + \rho \frac{T_h}{y_L} \right] \left(1 + \frac{\eta}{\varepsilon} \right) - g_H (1 - \varphi_h) \left[1 + \rho \frac{T_h}{y_H} \right] \\ &\quad + \varphi_h (1 - \varepsilon - \eta) + (1 - \varphi_h) (1 - \varepsilon) = 0\end{aligned}\tag{N.6}$$

where $\varphi_l = \psi c_{Lh} / (1 - \psi) c_{Ll}$ is the number of mistagged L households relative to the number of l -tax taxpayers; and $\varphi_h = \psi c_{Lh} / (\psi c_{Lh} + c_{Hh})$ is the number of mistagged L households relative to the number of h -tax taxpayers.

Rearranging (N.5) and (N.6) yields the expressions (6) and (7) for the optimal tax schedule in proposition 2. Applying the implicit function theorem to the system of equations (N.5) and (N.6) yields the comparative static statements in proposition 2. \square

O Model with Undertagging and Overtagging

This appendix presents the details of the model briefly discussed in section 3.3.1. We generalize the model in section 3.2 in two ways. First, we allow for a fraction $\psi_{Hl} \geq 0$ of H -type households to be undertagged with the l tag (in addition to the fraction ψ_{Lh} of overtaged L -types). This creates a fourth group of households whose compliance and marginal welfare effects we need to incorporate into the analysis. Second, we allow undertagged and overtaged households to have different elasticities of compliance with respect to inequity. Undertagged households' elasticity is η_{Hl} while overtaged households' elasticity is η_{Lh} . This is important since our empirical evidence in section 6.3 suggests that undertagged households do not respond to inequity, only overtaged households do.

Undertagged households' compliance responds to both the high-tag tax T_h and the low-tag tax T_l . Specifically,

$$\begin{aligned}\frac{dc_{Hl}}{dT_h} &= \frac{\partial c_{Hl}}{\partial \sigma_{Hl}} \frac{\partial \sigma_{Hl}}{\partial T_h} = \frac{c_{Hl}}{\sigma_{Hl}} \eta_{Hl} \frac{T_l}{T_h^2} = \frac{c_{Hl}}{T_h} \eta_{Hl} \\ \frac{dc_{Hl}}{dT_l} &= \frac{\partial c_{Hl}}{\partial T_l} + \frac{\partial c_{Hl}}{\partial \sigma_{Hl}} \frac{\partial \sigma_{Hl}}{\partial T_l} = -\varepsilon \frac{c_{Hl}}{T_l} - \eta_{Hl} \frac{c_{Hl}}{\sigma_{Hl}} \frac{1}{T_h} = -\frac{c_{Hl}}{T_l} (\varepsilon + \eta_{Hl})\end{aligned}$$

We can also connect the marginal disutility of inequity and the marginal utility of consumption for this fourth group:

$$\begin{aligned}\gamma_{Hl}^* &= u(y_H) - u(y_H - T_l) + d(\sigma_{Hl}) & \frac{\partial \gamma_{Hl}^*}{\partial T_l} &= u'(y_H - T_l) & \frac{\partial \gamma_{Hl}^*}{\partial \sigma_{Hl}} &= d'(\sigma_{Hl}) \\ \varepsilon &\equiv -\frac{\partial c_{Hl}}{\partial T_l} \frac{T_l}{c_{Hl}} = \frac{f(\gamma_{Hl}^*)}{1 - F(\gamma_{Hl}^*)} \frac{\partial \gamma_{Hl}^*}{\partial T_l} T_l & \eta_{Hl} &\equiv -\frac{\partial c_{Hl}}{\partial \sigma_{Hl}} \frac{\sigma_{Hl}}{c_{Hl}} \frac{f(\gamma_{Hl}^*)}{1 - F(\gamma_{Hl}^*)} \frac{\partial \gamma_{Hl}^*}{\partial \sigma_{Hl}} \sigma_{Hl} \\ \leftrightarrow d'(\sigma_{Hl}) &= \frac{\eta_{Hl}}{\varepsilon} u'(y_H - T_l) T_h\end{aligned}$$

Incorporating the undertagged households, the revenue from taxation now becomes:

$$r = \psi_{Lh} c_{Lh} T_h + (1 - \psi_{Lh}) c_{Ll} T_l + \psi_{Hl} c_{Hl} T_l + (1 - \psi_{Hl}) c_{Hh} T_h$$

the effects of tax changes are:

$$\begin{aligned}\frac{dr}{dT_h} &= \psi_{Lh} \left(c_{Lh} + \frac{dc_{Lh}}{dT_h} T_h \right) + \psi_{Hl} \frac{dc_{Hl}}{dT_h} T_l + (1 - \psi_{Hl}) \left(c_{Hh} + \frac{dc_{Hh}}{dT_h} T_h \right) \\ &= \psi_{Lh} c_{Lh} (1 - \varepsilon - \eta_{Lh}) + \psi_{Hl} c_{Hl} \eta_{Hl} \frac{1}{\sigma} + (1 - \psi_{Hl}) c_{Hh} (1 - \varepsilon) \\ \frac{dr}{dT_l} &= \psi_{Lh} \frac{dc_{Lh}}{dT_l} T_h + (1 - \psi_{Lh}) \left(c_{Lh} + \frac{dc_{Lh}}{dT_l} T_l \right) + \psi_{Hl} \left(c_{Hl} + \frac{dc_{Hl}}{dT_l} T_l \right) \\ &= \psi_{Lh} c_{Lh} \eta_{Lh} + (1 - \psi_{Lh}) c_{Ll} (1 - \varepsilon) + \psi_{Hl} c_{Hl} (1 - \varepsilon - \eta_{Hl})\end{aligned}$$

where $\sigma = T_h/T_l$ is the extent of inequity (but note that $\sigma_{Hl} = 1/\sigma$ while $\sigma_{Lh} = \sigma$).

The undertagged H -type households have private welfare

$$V_{Hl} = \int_{-\infty}^{\gamma_{Hl}^*} [u(y_H) - \gamma] dF(\gamma) + \int_{\gamma_{Hl}^*}^{\infty} [u(y_H - T_l) - d(\sigma_{Hl})] dF(\gamma)$$

with marginal welfare effects

$$\begin{aligned} \frac{dV_{Hl}}{dT_l} &= \int_{\gamma_{Hl}^*}^{\infty} \left[-u' (y_H - T_l) - d' (\sigma_{Hl}) \frac{\partial \sigma_{Hl}}{\partial T_l} \right] dF(\gamma) = -c_{Hl} \left[u' (y_H - T_l) + d' (\sigma_{Hl}) \frac{1}{T_h} \right] \\ &\simeq -c_{Hl} u' (y_H - T_l) \left(1 + \frac{\eta_{Hl}}{\varepsilon} \right) \simeq -c_{Lh} u' (y_H) \left[1 + \rho \frac{T_l}{y_H} \right] \left(1 + \frac{\eta_{Hl}}{\varepsilon} \right) \\ \frac{dV_{Hl}}{dT_h} &= \int_{\gamma_{Hl}^*}^{\infty} -d' (\sigma_{Hl}) \frac{\partial \sigma_{Hl}}{\partial T_h} dF(\gamma) = c_{Hl} d' (\sigma_{Hl}) \frac{T_l}{T_h^2} \\ &\simeq c_{Hl} u' (y_H - T_l) \frac{\eta_{Hl}}{\varepsilon} \frac{T_l}{T_h} \simeq c_{Hl} u' (y_H) \left[1 + \rho \frac{T_l}{y_H} \right] \frac{\eta_{Hl}}{\varepsilon} \frac{1}{\sigma} \end{aligned}$$

Combining these elements, we can see that the marginal social welfare effects are:

$$\begin{aligned} W &= \omega_L \psi_{Lh} V_{Lh} + \omega_L (1 - \psi_{Lh}) V_{Ll} + \omega_H \psi_{Hl} V_{Hl} + \omega_H (1 - \psi_{Hl}) V_{Hh} + B(r) \\ \frac{dW}{dT_l} \frac{1}{b(r)} &= \omega_L \psi_{Lh} \frac{dV_{Lh}}{dT_l} + \omega_L (1 - \psi_{Lh}) \frac{dV_{Ll}}{dT_l} + \omega_H \psi_{Hl} \frac{dV_{Hl}}{dT_l} + \frac{dr}{dT_l} \\ &\simeq g_L \psi_{Lh} c_{Lh} \left[1 + \rho \frac{T_h}{y_L} \right] \frac{\eta_{Lh}}{\varepsilon} \sigma - g_L (1 - \psi_{Lh}) c_{Ll} \left(1 + \rho \frac{T_l}{y_L} \right) \\ &\quad - g_H \psi_{Hl} c_{Hl} \left[1 + \rho \frac{T_l}{y_H} \right] \left(1 + \frac{\eta_{Hl}}{\varepsilon} \right) \\ &\quad + [\psi_{Lh} c_{Lh} \eta_{Lh} \sigma + (1 - \psi_{Lh}) c_{Ll} (1 - \varepsilon) + \psi_{Hl} c_{Hl} (1 - \varepsilon - \eta_{Hl})] \\ \frac{dW}{dT_h} \frac{1}{b(r)} &= \omega_L \psi_{Lh} \frac{dV_{Lh}}{dT_h} + \omega_H \psi_{Hl} \frac{dV_{Hl}}{dT_h} + \omega_H (1 - \psi_{Hl}) \frac{dV_{Hh}}{dT_h} + \frac{dr}{dT_h} \\ &\simeq -g_L \psi_{Lh} c_{Lh} \left[1 + \rho \frac{T_h}{y_L} \right] \left(1 + \frac{\eta_{Lh}}{\varepsilon} \right) + g_H \psi_{Hl} c_{Hl} \left[1 + \rho \frac{T_l}{y_H} \right] \frac{\eta_{Hl}}{\varepsilon} \frac{1}{\sigma} \\ &\quad - g_H (1 - \psi_{Hl}) c_{Hh} \left(1 + \rho \frac{T_h}{y_H} \right) \\ &\quad + [\psi_{Lh} c_{Lh} (1 - \varepsilon - \eta_{Lh}) + \psi_{Hl} c_{Hl} \eta_{Hl} \frac{1}{\sigma} + (1 - \psi_{Hl}) c_{Hh} (1 - \varepsilon)] \end{aligned}$$

Rearranging these yields the expressions for the optimal tax schedule in section 3.3.1:

$$\begin{aligned} \frac{T_l}{y_L} &= \frac{1 - \varepsilon - \bar{g}_l + \varphi_{Ll} \frac{\eta_{Lh}}{\varepsilon} \sigma (g_L + \varepsilon) - \varphi_{Hl} \frac{\eta_{Hl}}{\varepsilon} (g_H + \varepsilon)}{\rho \left(\bar{g}_l + g_H \varphi_{Hl} \left[\left(1 + \frac{\eta_{Hl}}{\varepsilon} \right) \frac{y_L}{y_H} - 1 \right] - g_L \varphi_{Ll} \frac{\eta_{Lh}}{\varepsilon} \sigma^2 \right)} \\ \frac{T_h}{y_H} &= \frac{1 - \varepsilon - \bar{g}_h + \varphi_{Hh} \frac{\eta_{Hl}}{\varepsilon} \frac{1}{\sigma} (g_H + \varepsilon) - \varphi_{Lh} \frac{\eta_{Lh}}{\varepsilon} (g_L + \varepsilon)}{\rho \left(\bar{g}_h + g_L \varphi_{Lh} \left[\left(1 + \frac{\eta_{Lh}}{\varepsilon} \right) \frac{y_H}{y_L} - 1 \right] - g_H \varphi_{Hh} \frac{\eta_{Hl}}{\varepsilon} \frac{1}{\sigma^2} \right)} \end{aligned}$$

P Model with Location Choice and Endogenous House Prices

This appendix presents the details of the model briefly discussed in section 3.3.2. In section P.1 we present a micro-founded model of residential location choice, while in section P.2 we study the welfare implications and optimal policy.

P.1 Location Choice

We consider an extension of the model presented in section 3.2 in which households first choose where to live and then whether to pay the corresponding property tax. Households are characterized by three traits: First, they have an evasion cost γ that governs how much utility they lose from evading the tax, as in section 3.2. Second, they have idiosyncratic preferences for the houses on the high side of the boundary ξ_h and the low side ξ_l . Third, they are either high or low-income $y_H \gg y_L$. For simplicity, we will assume that H -type houses are sufficiently expensive that high-income households are never willing to live in an L -type house, so that we can focus only on the choice of low-income households between L -type houses in the low-tax sector and L -type houses in the high-tax sector.

A household living in a house tagged ϕ that pays its property tax receives utility

$$u_{L\phi}^{\text{pay}} = u(v_L - p_{L\phi} - T_\phi) - d(\tilde{\sigma}) + \xi_\phi \quad (\text{P.1})$$

where v_L is the value of the housing services the house provides and $p_{L\phi}$ is the (annualized) market price of a house of type L with a tag of ϕ . Note that this price does not depend on whether taxes are paid, it is a market price for that type of house. Of course, households who anticipate not paying their property taxes would have a higher willingness to pay for the house than those who plan to evade. The disutility from inequity now reflects only the portion of inequity that is not capitalized into house prices: $\tilde{\sigma} = (T_h + p_{Lh} - p_{Ll}) / T_l$. At the extreme, when tax differences are fully capitalized into house prices, $p_{Lh} - p_{Ll} = T_h - T_l$ and $\tilde{\sigma} = 1$, so households no longer experience inequity. However, whenever tax differences are less than fully capitalized into house prices, mistagging still generates inequity and shapes optimal policy schedules.

If, on the other hand, households don't pay their property tax, they receive utility

$$u_{L\phi}^{\text{evade}} = u(v_L - p_{L\phi}) - \gamma + \xi_\phi \quad (\text{P.2})$$

Households pay their property tax whenever this makes them better off:

$$\begin{aligned} u_{Ll}^{\text{pay}} > u_{Ll}^{\text{evade}} &\leftrightarrow \gamma > \gamma_l^* = u(v_L - p_{Ll}) - u(v_L - p_{Ll} - T_l) \\ u_{Lh}^{\text{pay}} > u_{Lh}^{\text{evade}} &\leftrightarrow \gamma > \gamma_h^* = u(v_L - p_{Lh}) - u(v_L - p_{Lh} - T_h) + d(\tilde{\sigma}) \end{aligned}$$

Assuming there is no over-capitalization of taxes into house prices (i.e. that $p_{Ll} - p_{Lh} \leq T_h - T_l$), we can also see that this means that $\gamma_h^* > \gamma_l^*$.

The thresholds γ_l^*, γ_h^* define three types of households, and we can characterize the location choice of each type in turn.

First, for households with $\gamma > \gamma_h^*$, who pay their taxes regardless of which location they

choose, they prefer the high-tax side to the low-tax side whenever

$$\begin{aligned} u(v_L - p_{Lh} - T_h) - d(\tilde{\sigma}) + \xi_h &> u(v_L - p_{Ll} - T_l) + \xi_l \\ \Delta\xi = \xi_h - \xi_l &> u(v_L - p_{Ll} - T_l) - u(v_L - p_{Lh} - T_h) + d(\tilde{\sigma}) = \xi_{hh}^* \geq 0 \end{aligned} \quad (\text{P.3})$$

Second, for households with $\gamma < \gamma_l^*$, who evade the tax regardless of which location they choose, they prefer the high-tax side whenever

$$\begin{aligned} u(v_L - p_{Lh}) + \xi_h &> u(v_L - p_{Ll}) + \xi_l \\ \Delta\xi = \xi_h - \xi_l &> u(v_L - p_{Ll}) - u(v_L - p_{Lh}) = \xi_{hl}^* \leq 0 \end{aligned} \quad (\text{P.4})$$

Finally, the third, intermediate group has $\gamma_l^* < \gamma \leq \gamma_h^*$. These households evade on the high-tax side, but pay property tax on the low-tax side. They prefer to live on the high-tax side (and evade the property tax) whenever

$$\begin{aligned} u(v_L - p_{Lh}) - \gamma + \xi_h &> u(v_L - p_{Ll} - T_l) + \xi_l \\ \gamma < u(v_L - p_{Lh}) - u(v_L - p_{Ll} - T_l) + \xi_h - \xi_l &= \bar{\gamma}(\Delta\xi) \end{aligned} \quad (\text{P.5})$$

Combining conditions (P.3), , and we can characterize all households' location and evasion decisions. Household i chooses location ϕ and compliance $\in \{\text{pay}, \text{evade}\}$ according to:

$$\{\phi^i, \text{compliance}^i\} = \begin{cases} \{l, \text{evade}\}, & \text{if } \gamma^i \leq \gamma_l^* \& \Delta\xi^i \leq \xi_{hl}^*; \\ \{l, \text{pay}\}, & \text{if } (\gamma^i > \gamma_l^* \& \Delta\xi^i \leq \xi_{hl}^*) \text{ or } (\gamma^i > \bar{\gamma}(\Delta\xi^i) \& \xi_{hl}^* < \Delta\xi^i \leq \xi_{hh}^*); \\ \{h, \text{evade}\}, & \text{if } (\gamma^i \leq \bar{\gamma}(\Delta\xi^i) \& \xi_{hl}^* < \Delta\xi^i \leq \xi_{hh}^*) \text{ or } (\gamma^i > \gamma_h^* \& \Delta\xi^i > \xi_{hh}^*); \\ \{h, \text{pay}\}, & \text{if } \gamma^i > \gamma_h^* \& \Delta\xi^i > \xi_{hh}^*. \end{cases} \quad (\text{P.6})$$

Figure P.1 illustrates the four types of households and the boundaries dividing them.

Equation P.6 characterizes households' decisions taking taxes T_ϕ and house prices $p_{L\phi}$ as given. To pin down prices, we need the demand for each type of house to equal the supply. If the joint distribution of $\gamma, \Delta\xi$ is given by $J(\gamma, \Delta\xi)$, then the demand for houses on the low-tax side is

$$Q_l^D = \int_{-\infty}^{\xi_{hl}^*} \int_{-\infty}^{\infty} j(\gamma, \Delta\xi) d\gamma d\Delta\xi + \int_{\xi_{hl}^*}^{\xi_{hh}^*} \int_{\bar{\gamma}(\Delta\xi)}^{\infty} j(\gamma, \Delta\xi) d\gamma d\Delta\xi$$

Similarly demand for houses on the high-tax side is

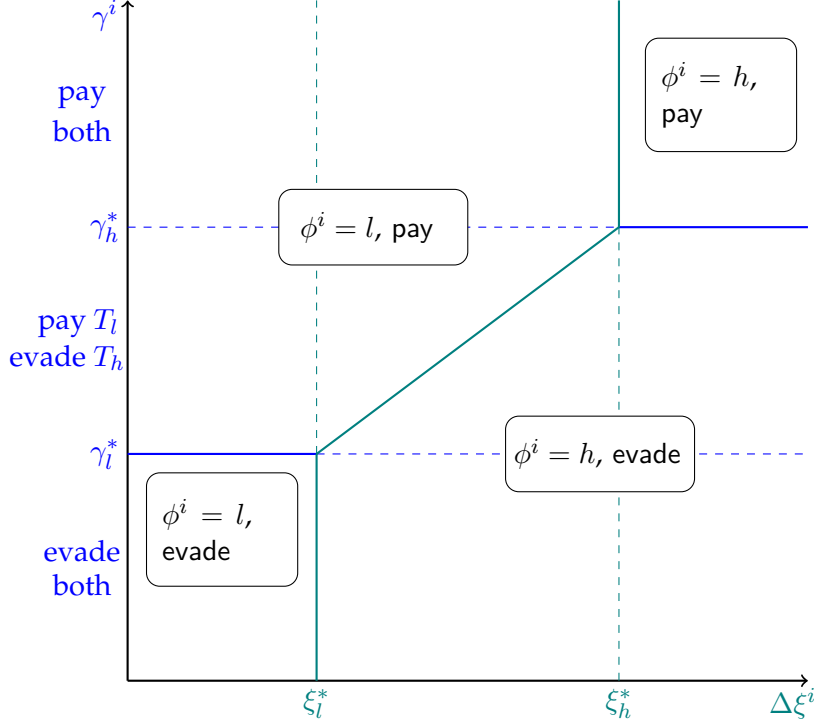
$$Q_h^D = \int_{\xi_{hh}^*}^{\xi_{hh}^*} \int_{-\infty}^{\bar{\gamma}(\xi_h)} j(\gamma, \xi) d\gamma d\xi_h + \int_{\xi_{hh}^*}^{\infty} \int_{-\infty}^{\infty} j(\gamma, \xi_h) d\gamma d\xi_h$$

And prices adjust to equilibrate the market such that

$$Q_l^D = Q_l^S = 1 - \psi \quad \& \quad Q_h^D = Q_h^S = \psi \quad (\text{P.7})$$

These pin down the equilibrium prices and hence define the cutoffs $\gamma_l^*, \gamma_h^*, \xi_{hl}^*, \xi_{hh}^*$ and the

FIGURE P.1: LOCATION AND COMPLIANCE CHOICES



function $\bar{\gamma}(\Delta \xi)$. Given these, the compliance rates are given by

$$c_{Ll} = \frac{1}{1-\psi} \left(\int_{-\infty}^{\xi_l^*} \int_{\gamma_l^*}^{\infty} j(\gamma, \Delta \xi) d\gamma d\Delta \xi + \int_{\xi_h^*}^{\xi_h^*} \int_{\bar{\gamma}(\Delta \xi)}^{\infty} j(\gamma, \Delta \xi) d\gamma d\Delta \xi \right) \quad (\text{P.8})$$

$$c_{Lh} = \frac{1}{\psi} \int_{\xi_h^*}^{\infty} \int_{\bar{\gamma}(\Delta \xi)}^{\infty} j(\gamma, \Delta \xi) d\gamma d\Delta \xi \quad (\text{P.9})$$

In this model, changes in taxes affect compliance through three channels. Consider, for example, a small increase in the high tax T_h . This affects compliance through

1. A direct effect: A higher T_h leads to a higher γ_h (holding house prices fixed), reducing compliance.
2. A mobility effect: A higher T_h (holding house prices fixed) makes living in the high-tax sector less attractive (to those who pay it), raising ξ_h^* and causing a set of compliant households in the high-tax sector to move to the low-tax sector.
3. A house-price effect: A higher T_h reduces demand for houses in the high-tax sector. To equilibrate demand and supply, the price of houses in the high-tax sector, p_{Lh} falls, and this affects compliance decisions by lowering the marginal utility of consumption of paying taxes, and dampening the increase in effective inequity $\tilde{\sigma}$ from the increase in T_h .

Our empirical analysis captures the combination of these three mechanisms. For small changes in taxes, the effect of taxes on location choices causes no first-order welfare effects by the envelope theorem, but the overall effects of tax changes on compliance capture the full fiscal externality that is relevant for welfare, and so our empirical analysis captures the relevant

empirical quantities. However, as the model above shows, house price changes have first-order effects on households' welfare, and these can affect the welfare effects of tax policy and the shape of the optimal tax schedule. The next section explores these issues in more detail.

P.2 Welfare and Optimal Policy

As described above, incorporating mobility into the model creates two new channels through which taxes affect compliance: a mobility effect and a house-price effect. However, by the envelope theorem, only the house-price effect has first-order effects on households' welfare. What does matter for policy design is the size of the fiscal externality, and for this we want to capture the net of the three effects.

To achieve this, we generalize the model slightly and instead of committing to a specific model of household residential choice we capture the reduced form effect of taxes on prices through the expression $p_\theta(T_\phi) = p_\theta^0 - \kappa T_\phi$ where the parameter κ governs the degree of capitalization of taxes into house prices. We also continue to consider reduced-form elasticities of compliance ε and η that allow for all channels through which taxes affect compliance.

In this model, the private welfare of the three types of households is given by⁵⁸

$$\begin{aligned} V_{Ll} &= \int_{-\infty}^{\gamma_{Ll}^*} [u(v_L - p_L(T_l)) - \gamma] dF(\gamma) + \int_{\gamma_{Ll}^*}^{\infty} [u(v_L - p_L(T_l) - T_l)] dF(\gamma) \\ V_{Lh} &= \int_{-\infty}^{\gamma_{Lh}^*} [u(v_L - p_L(T_h)) - \gamma] dF(\gamma) + \int_{\gamma_{Lh}^*}^{\infty} [u(v_L - p_L(T_h) - T_h) - d(\tilde{\sigma})] dF(\gamma) \\ V_{Hh} &= \int_{-\infty}^{\gamma_{Hh}^*} [u(v_H - p_H(T_h)) - \gamma] dF(\gamma) + \int_{\gamma_{Hh}^*}^{\infty} [u(v_H - p_H(T_h) - T_h)] dF(\gamma) \end{aligned}$$

Starting with the correctly tagged households, the marginal private welfare effects are now

$$\begin{aligned} \frac{\partial V_L}{\partial T_l} &= (1 - c_{Ll}) u'(y_L(T_l)) \kappa - c_{Ll} u'(y_L(T_l) - T_l) (1 - \kappa) \\ &\simeq (1 - c_L) u'(y_L(T_l)) \kappa - c_{Ll} u'(y_L(T_l)) \left(1 + \rho \frac{T_l}{y_L(T_l)}\right) (1 - \kappa) \\ &= \kappa u'(y_L(T_l)) \left(1 + c_{Ll} \rho \frac{T_l}{y_L(T_l)}\right) - c_{Ll} u'(y_L(T_l)) \left(1 + \rho \frac{T_l}{y_L(T_l)}\right) \end{aligned} \quad (\text{P.10})$$

$$\frac{\partial V_H}{\partial T_h} = \kappa u'(y_H(T_h)) \left(1 + c_{Hh} \rho \frac{T_h}{y_H(T_h)}\right) - c_{Hh} u'(y_H(T_h)) \left(1 + \rho \frac{T_h}{y_H(T_h)}\right) \quad (\text{P.11})$$

where we introduced the notation that $y_\theta(T_\phi) = v_\theta - p_\theta(T_\phi)$ and we used the approximation to marginal utility that $u'(y_\theta(T_\phi) + x) \simeq u'(y_\theta(T_\phi)) \left(1 - \rho \frac{x}{y_\theta(T_\phi)}\right)$.

We get two extra effects:

1. All households have higher utility from the capitalization of tax liabilities into house prices. This is the $u'(\tilde{y}_{\theta\phi})\kappa \times 1$ term. Note, this applies also to the households that don't pay the tax since we assume it affects the market price of houses and that there is no price discrimination by tax evasion.

⁵⁸In the specific model of household mobility outlined above, the expressions below hold conditional on location taste $\Delta\xi^i$, and the overall welfare integrates across location tastes to yield expressions like the ones below.

2. Households who do pay the tax enjoy even higher utility since they pay the tax on top of gaining utility from the lower house price. That is, the higher house price dampens the utility loss from paying the tax due to the concavity of the utility function (governed by ρ). This is the $u'(\tilde{y}_{\theta\phi})\kappa \times c_{\theta\phi}\rho \frac{T_\phi}{\tilde{y}_{\theta\phi}}$ term.

Turning to the mistagged households, as before, we will want to express their marginal disutility from inequity $d'(\tilde{\sigma})$ in dollar terms and we use the responsiveness of compliance to inequity and the tax liability to do so. To do this, we use the definitions of the reduced-form elasticities ε and η :

$$\eta \equiv -\frac{\partial c}{\partial \sigma} \frac{\sigma}{c} = \frac{\partial c}{\partial \gamma^*} \frac{\partial \gamma^*}{\partial \sigma} \frac{\sigma}{c} = (1 - \kappa) d'(\tilde{\sigma}) \frac{f(\gamma^*)}{1 - F(\gamma^*)} \sigma \quad (\text{P.12})$$

$$\begin{aligned} \varepsilon &\equiv -\frac{\partial c}{\partial T_\phi} \frac{T_\phi}{c} = \frac{\partial c}{\partial \gamma^*} \frac{\partial \gamma^*}{\partial T_\phi} \frac{T_\phi}{c} \\ &= \left[-u'(y_\theta(T_\phi)) \frac{\partial p_\theta(T_\phi)}{\partial T_\phi} + u'(y_\theta(T_\phi) - T_\phi) \left(1 + \frac{\partial p_\theta(T_\phi)}{\partial T_\phi} \right) \right] \frac{f(\gamma^*)}{1 - F(\gamma^*)} T_\phi \\ &= [u'(y_\theta(T_\phi)) \kappa + u'(y_\theta(T_\phi) - T_\phi) (1 - \kappa)] \frac{f(\gamma^*)}{1 - F(\gamma^*)} T_\phi \end{aligned} \quad (\text{P.13})$$

Where we see that now the elasticity with respect to the tax liability will be stronger since $u(\cdot)$ is strictly concave and $y' < 0$.

It also changes how we use the relationship between the two elasticities to express $d(\tilde{\sigma})$ in terms of elasticities: Combining (P.12) and (P.13), gives us

$$d'(\tilde{\sigma}) = \frac{\eta}{\varepsilon} \left[u'(y_L(T_h) - T_h) + u'(y_L(T_h)) \frac{\kappa}{1 - \kappa} \right] T_l \quad (\text{P.14})$$

Combining these expressions we can see that the effect of marginal changes in the low-type tax T_l is

$$\begin{aligned} \frac{\partial V_{Lh}}{\partial T_l} &= \int_{\gamma_{Lh}^*}^{\infty} -d'((1 - \kappa)\sigma)(1 - \kappa) \frac{\partial \sigma}{\partial T_l} dF(\gamma) = c_{Lh} d'(\tilde{\sigma})(1 - \kappa) \frac{\sigma}{T_l} \\ &= c_{Lh} \frac{\eta}{\varepsilon} \sigma [u'(y_L(T_h) - T_h)(1 - \kappa) + \kappa u'(y_L(T_h))] \\ &\simeq c_{L,h} \frac{\eta}{\varepsilon} \sigma u'(y_L(T_l)) \left(1 + \rho [\kappa(1 - \sigma) + \sigma(1 - \kappa)] \frac{T_l}{y_L(T_l)} \right) \end{aligned} \quad (\text{P.15})$$

while the effect of a marginal change in the high-type tax T_h is

$$\begin{aligned}
\frac{\partial V_{Lh}}{\partial T_h} &= \int_{-\infty}^{\gamma_{Lh}^*} u'(y_L(T_h)) \frac{\partial y_L}{\partial T_h} dF(\gamma) + \int_{\gamma_{Lh}^*}^{\infty} \left[u'(y_L(T_h) - T_h) \left(\frac{\partial p_L}{\partial T_h} - 1 \right) - d'(\tilde{\sigma})(1 - \kappa) \frac{\partial \sigma}{\partial T_h} \right] dF(\gamma) \\
&= (1 - c_{Lh}) u'(y_L(T_h)) \kappa + c_{Lh} \left[u'(y_L(T_h) - T_h) (\kappa - 1) - d'(\tilde{\sigma})(1 - \kappa) \frac{1}{T_l} \right] \\
&= (1 - c_{Lh}) u'(y_L(T_h)) \kappa - c_{Lh} u'(y_L(T_h) - T_h) (1 - \kappa) \\
&\quad - c_{Lh} (1 - \kappa) \frac{\eta}{\varepsilon} \left[u'(y_L(T_h) - T_h) + u'(y_L(T_h)) \frac{\kappa}{1 - \kappa} \right] \\
&= u'(y_L(T_h)) \kappa \left[1 - c_{Lh} \left(1 + \frac{\eta}{\varepsilon} \right) \right] - c_{Lh} u'(y_L(T_h) - T_h) (1 - \kappa) \left(1 + \frac{\eta}{\varepsilon} \right) \\
&\simeq u'(y_L(T_l)) \left[1 - \rho \kappa \left(1 - \frac{1}{\sigma} \right) \frac{y_H}{y_L} \frac{T_h}{y_L(T_l)} \right] \kappa \left[1 - c_{Lh} \left(1 + \frac{\eta}{\varepsilon} \right) \right] \\
&\quad - c_{Lh} u'(y_L(T_l)) \left[1 + \rho \frac{y_H}{y_L} \left[1 - \kappa \left(1 - \frac{1}{\sigma} \right) \right] \frac{T_h}{y_H(T_h)} \right] (1 - \kappa) \left(1 + \frac{\eta}{\varepsilon} \right) \\
&= u'(y_L(T_l)) \kappa \left[1 - \rho \kappa \left(1 - \frac{1}{\sigma} \right) \frac{y_H}{y_L} \frac{T_h}{y_H(T_h)} \right] \\
&\quad - c_{Lh} u'(y_L(T_l)) \left[1 + \rho \left[(1 - \kappa) - \left(1 - \frac{1}{\sigma} \right) \kappa \right] \frac{y_H}{y_L} \frac{T_h}{y_H(T_h)} \right] \left(1 + \frac{\eta}{\varepsilon} \right)
\end{aligned} \tag{P.16}$$

Marginal Welfare Effects and Optimal Taxes Turning to the social welfare effects and optimal taxation, the equations get uglier, but the intuition is very much the same. Social welfare, as before, is given by

$$W = \omega_L [\psi V_{Lh} + (1 - \psi) V_{Ll}] + \omega_H V_{Hh} + B(r) \tag{P.17}$$

This means that the normalized marginal welfare effect of the low-type tax T_l is

$$\begin{aligned}
\frac{\partial W}{\partial T_l} \frac{1}{b(r)} &= \frac{\omega_L}{b(r)} \left[\psi \frac{\partial V_{Lh}}{\partial T_l} + (1 - \psi) \frac{\partial V_{Ll}}{\partial T_l} \right] + \frac{\omega_H}{b(r)} \frac{\partial V_{Hh}}{\partial T_l} + \frac{\partial r}{\partial T_l} \\
&= \psi g_L c_{Lh} \frac{\eta}{\varepsilon} \sigma \left(1 + \rho [(1 - \sigma) \kappa + \sigma (1 - \kappa)] \frac{T_l}{y_L(T_l)} \right) \\
&\quad + (1 - \psi) g_L \left[\kappa \left(1 + c_{Ll} \rho \frac{T_l}{y_L(T_l)} \right) - c_{Ll} \left(1 + \rho \frac{T_l}{y_L(T_l)} \right) \right] + \psi c_{Lh} \eta \sigma + (1 - \psi) c_{Ll} (1 - \varepsilon)
\end{aligned} \tag{P.18}$$

and the normalized marginal welfare effect of the high-type tax T_h is

$$\begin{aligned}
\frac{\partial W}{\partial T_h} \frac{1}{b(r)} &= \frac{\omega_L}{b(r)} \left[\psi \frac{\partial V_{Lh}}{\partial T_h} + (1 - \psi) \frac{\partial V_{Ll}}{\partial T_h} \right] + \frac{\omega_H}{b(r)} \frac{\partial V_{Hh}}{\partial T_h} + \frac{\partial r}{\partial T_h} \\
&= \psi g_L \left(\kappa \left[1 - \rho \kappa \left(1 - \frac{1}{\sigma} \right) \frac{y_H}{y_L} \frac{T_h}{y_H} \right] + c_{Lh} \left[1 + \rho \left[(1 - \kappa) - \left(1 - \frac{1}{\sigma} \right) \kappa \right] \frac{y_H}{y_L} \frac{T_h}{y_H} \right] \left(1 + \frac{\eta}{\varepsilon} \right) \right) \\
&\quad - g_H \left[\kappa \left(1 + c_{Hl} \rho \frac{T_h}{y_H} \right) - c_H \left(1 + \rho \frac{T_h}{y_H} \right) \right] + \psi c_{Lh} (1 - \varepsilon - \eta) + c_{Hh} (1 - \varepsilon)
\end{aligned} \tag{P.19}$$

Setting (P.18) and (P.19) to zero and rearranging, the modified optimal tax formulas are given

by equations (8) and (9):

$$\frac{T_l}{\tilde{y}_{Ll}} = \frac{1 - \varepsilon - g_L + \varphi_l \frac{\eta}{\varepsilon} \sigma (g_L + \varepsilon) + \kappa \frac{g_L}{c_{Ll}}}{\rho g_L (1 - \kappa) [1 - \varphi_l \frac{\eta}{\varepsilon} \sigma^2 (1 - \tilde{\kappa})]} \quad (\text{P.20})$$

$$\frac{T_h}{\tilde{y}_{Hh}} = \frac{1 - \varepsilon - \bar{g}_h - \varphi_h \frac{\eta}{\varepsilon} (g_L + \varepsilon) + \kappa \frac{\tilde{g}_h}{\tilde{c}_h}}{\rho (1 - \kappa) \left[\bar{g}_h + \varphi_h g_L \left(\frac{\tilde{y}_{Hh}}{\tilde{y}_{Ll}} (1 + \frac{\eta}{\varepsilon}) (1 - \tilde{\kappa}) - 1 \right) + \varphi_h g_L \frac{\kappa}{c_{Lh}} \tilde{\kappa} \frac{\tilde{y}_{Hh}}{\tilde{y}_{Ll}} \right]} \quad (\text{P.21})$$

where $\tilde{\kappa} = \frac{\kappa}{1-\kappa} (1 - \frac{1}{\sigma})$ measures the increase in marginal utility from the loss in house value from being taxed at T_h rather than T_l ; $\tilde{g}_h = (g_H + \phi g_L) / (1 + \phi)$ is the average marginal social welfare weight of those asked to pay the h tax (note this is not the same as the average social marginal welfare weight of those who *do* pay the h -tax \bar{g}_h); and $\tilde{c}_h = (c_{Hh} + \psi c_{Lh}) / (1 + \phi)$ is the fraction of those asked to pay the h tax who comply.

The equations look much as before, but with some new terms. In the numerators we have the $\kappa g/c$ terms. These account for the fact that all households gain house value when taxes increase, benefiting them. The $(1 - \kappa)$ term in the denominators is similarly there to account for the decrease in marginal utility of consumption coming from the loss of home value. The $(1 - \tilde{\kappa})$ terms in the denominator account for the lower marginal disutility from paying taxes, dampened by the additional house-price loss experienced by the overtagged compliant households. Finally, the final term in the denominator in (P.21) accounts for the lower marginal utility of all overtagged households from their higher house prices.

Notably, these effects interact with the channels highlighted for mistagging: The $(1 - \tilde{\kappa})$ terms dampen (but do not eliminate) the forces that made the mistagging make taxes less progressive.

Q Proof of Proposition 3

The proof of proposition 3 is a relatively straightforward application of theorem 1 in Dong *et al.* (2023). We proceed in three steps. First, we show that potential changes in inequity when $D \rightarrow 0$ are independent of ν . Second, we show that the reduced form effect of crossing the boundary is identified. And third, we combine these results to show the proposition.

Our first lemma shows that crossing the boundary can be thought of as an excludable instrument conditional on the mistagging exposure rank U and the tax liability τ :

Lemma 5 (Excludability). *Let Assumptions 1, 2 & 3 hold. Then for any $u \in [0, 1]$,*

$$\lim_{d \rightarrow 0^-} f_{\nu|\sigma,\tau,D}(v, q_0(d, u, t), t, d) = \lim_{d \rightarrow 0^+} f_{\nu|\sigma,\tau,D}(v, q_1(d, u, t), t, d) = \lim_{d \rightarrow 0} f_{\nu|U,\tau,D}(v, u, t, d) \quad (\text{Q.1})$$

for $v \in \mathcal{V}$ and $\tau \in \mathcal{T}$

Proof. By Bayes' rule, assumption 3, that $U_0|(\nu, D = 0, \tau = t) \sim U_1|(\nu, D = 0, \tau = t)$, where we now make explicit the conditioning on distance $D = 0$ and tax liability τ , implies that $\nu|(U_0 = u, D = 0, \tau = t) \sim \nu|(U_1 = u, D = 0, \tau = t)$, i.e. that $f_{\nu|U_1,D,\tau} = f_{\nu|U_0,D,\tau}$. By invoking our smoothness assumption 2 and the definition relating observed to potential exposure ranks $U \equiv U_1 \mathbf{1}[D > 0] + U_0 \mathbf{1}[D < 0]$, we can show that their limits are the same from both sides:

$$\lim_{D \rightarrow 0^+} f_{\nu|U_1,D,\tau}(\nu, u, t) = \lim_{D \rightarrow 0^-} f_{\nu|U_0,D,\tau}(\nu, u, t) = \lim_{D \rightarrow 0} f_{\nu|U,D,\tau}(\nu, u, t)$$

Finally, we exploit the fact that under Assumption 1, for a given $D = d$ and $\tau = t$, whenever $d > 0$ there is a one-to-one mapping between u and $q_1(d, u, t)$ and whenever $d < 0$ there is a one-to-one mapping between u and $q_0(d, u, t)$ so that the same limits apply to the distributions conditional on inequity levels as the distributions conditional on exposure ranks

$$\lim_{D \rightarrow 0^+} f_{\nu|\sigma,D,\tau}(\nu, q_1(d, u, t), t) = \lim_{D \rightarrow 0^-} f_{\nu|\sigma,D,\tau}(\nu, q_0(d, u, t), t) = \lim_{D \rightarrow 0} f_{\nu|U,D,\tau}(\nu, u, t)$$

□

Lemma 5 thus show that given an exposure rank $U = u$ and a tax liability $\tau = t$, all potential changes in inequity σ when $D \rightarrow 0$ are independent of the unobservables ν . Our second lemma shows that the reduced-form impact of crossing the boundary on compliance is identified:

Lemma 6. *Let Assumptions 1, 2 & 3 hold. Then for any $u \in [0, 1]$,*

$$\begin{aligned} & \lim_{d \rightarrow 0^+} \mathbb{E}[C|U = u, \tau = t, D = d] - \lim_{d \rightarrow 0^-} \mathbb{E}[C|U = u, \tau = t, D = d] \\ &= \int (G(\sigma_1(u, t), t, 0, v) - G(\sigma_0(u, t), 0, t, v)) F_{\nu|U,\tau,D}(dv, u, t, 0) \end{aligned} \quad (\text{Q.2})$$

Proof. By assumption 1, we can map from the exposure quantiles U to the treatment levels one-to-one:

$$\begin{aligned} & \lim_{D \rightarrow 0^+} \mathbb{E}[C|U = u, D = d, \tau = t] - \lim_{D \rightarrow 0^-} \mathbb{E}[C|U = u, D = d, \tau = t] \\ &= \lim_{D \rightarrow 0^+} \mathbb{E}[C|\sigma = q_1(d, u, t), U_1 = u, D = d, \tau = t] - \lim_{D \rightarrow 0^-} \mathbb{E}[C|\sigma = q_0(d, u, t), U_0 = u, D = d, \tau = t] \end{aligned}$$

And we can substitute in the definition of the potential outcome $C = G(\sigma, \tau, D, \nu)$

$$\begin{aligned} & \lim_{D \rightarrow 0^+} \mathbb{E}[C | \sigma = q_1(d, u, t), U_1 = u, D = d, \tau = t] - \lim_{D \rightarrow 0^-} \mathbb{E}[C | \sigma = q_0(d, u, t), U_0 = u, D = d, \tau = t] \\ &= \lim_{D \rightarrow 0^+} \mathbb{E}[G(q_1(d, u, t), t, d, \nu) | \sigma = q_1(d, u, t), U_1 = u, D = d, \tau = t] \\ &\quad - \lim_{D \rightarrow 0^-} \mathbb{E}[G(q_0(d, u, t), t, d, \nu) | \sigma = q_0(d, u, t), U_0 = u, D = d, \tau = t] \end{aligned}$$

By the smoothness assumption 2 and the compact support of ν , we can exchange the order of the limit and the expectation integral and the expectation above is continuous in D so that

$$\begin{aligned} & \lim_{D \rightarrow 0^+} \mathbb{E}[G(q_1(d, u, t), t, d, \nu) | \sigma = q_1(d, u, t), U_1 = u, D = d, \tau = t] \\ &\quad - \lim_{D \rightarrow 0^-} \mathbb{E}[G(q_0(d, u, t), t, d, \nu) | \sigma = q_0(d, u, t), U_0 = u, D = d, \tau = t] \\ &= \mathbb{E}[G(\sigma_1(u), t, 0, \nu) | U_1 = u, D = 0, \tau = t] - \mathbb{E}[G(\sigma_0(u), t, 0, \nu) | U_0 = u, D = 0, \tau = t] \end{aligned}$$

Finally, by assumption 3 and lemma 5 the two expectations are integrating over the same distribution f_ν so we have that

$$\begin{aligned} & \mathbb{E}[G(\sigma_1(u), t, 0, \nu) | U_1 = u, D = 0, \tau = t] - \mathbb{E}[G(\sigma_0(u), t, 0, \nu) | U_0 = u, D = 0, \tau = t] \\ &= \int (G(\sigma_1(u), t, 0, v) - G(\sigma_0(u), t, 0, v)) F_{\nu|U,\tau,D}(dv, u, t, 0) \end{aligned}$$

□

For the third step to complete the proof of proposition 3, note that by definition $\sigma = q(d, t, u) = q_0(d, t, u)(1 - Z) + q_1(d, t, u)Z$. Assumption 2 implies that $q_z(d, t, u)$, $z = 0, 1$ is smooth and so the right and left limits at $D = 0$ exist: $\lim_{D \rightarrow 0^+} q(d, t, u) = q_1(0, t, u) \equiv \sigma_1(t, u)$ and $\lim_{D \rightarrow 0^-} q(d, t, u) = q_0(0, t, u) \equiv \sigma_0(t, u)$. Combining this with lemmas 5 and 6 shows that equation (11) holds.

To see that the weighted W-LATE also holds note three things. First, the Q τ -LATEs $\eta(u, t)$ are identified. Second, the weighting function $w(t, u)$ is assumed to be known or estimable. Third, the set $\mathcal{U} \equiv \{u \in [0, 1] : |\sigma_1(u) - \sigma_0(u)| > 0\}$ is identified given that the potential treatments $q_z(d, t, u)$, $z = 0, 1$ are identified (and in fact correspond to the quantiles such that $F_{E_z|t,d}^{-1}(u) > 0$).

R Proof of Proposition 4

Our proof proceeds similarly to the proof of proposition 4. We proceed in five steps.

First, note that our relaxed assumptions still allow us to apply 5 to the distribution of ν_1 and so we have that

$$\lim_{d \rightarrow 0^-} f_{\nu_1|\sigma,\tau,D}(v_1, q_0(d, u, t), t, d) = \lim_{d \rightarrow 0^+} f_{\nu_1|\sigma,\tau,D}(v_1, q_1(d, u, t), t, d) = \lim_{d \rightarrow 0} f_{\nu_1|U,\tau,D}(v_1, u, t, d) \quad (\text{R.1})$$

for $v_1 \in \mathcal{V}_1$ and $\tau \in \mathcal{T}$

Second, our relaxed assumptions mean that we cannot apply 5 to the distribution of ν_0 . Instead, the limits are given by the following lemma:

Lemma 7 (ν_0 Limits). *Let Assumptions 1 & 4 hold. Then for any $u \in [0, 1]$, The limiting conditional distributions of ν_0 as $D \rightarrow 0$ from above and from below exist and are given by*

$$\begin{aligned} \lim_{D \rightarrow 0^+} f_{\nu_0|\sigma,\tau,D}(v_0, q_1(d, u, t), t, d) &= \lim_{d \rightarrow 0^+} f_{\nu_0|U_1,\tau,D}(v_0, u, t, d) = f_1(v_0, t) \\ \lim_{D \rightarrow 0^-} f_{\nu_0|\sigma,\tau,D}(v_0, q_0(d, u, t), t, d) &= \lim_{d \rightarrow 0^-} f_{\nu_0|U_0,\tau,D}(v_0, u, t, d) = f_0(v_0, t) \end{aligned}$$

Proof. The proof proceeds in two steps. First, by Assumption 1, we can relate observed treatment σ to the potential exposure rank U_z on either side of the boundary. For a given $D = d$ and $\tau = t$, whenever $d > 0$ there is a one-to-one mapping between U_1 and $q_1(d, U_1, t)$ and whenever $d < 0$ there is a one-to-one mapping between U_0 and $q_0(d, U_0, t)$ so that for any $d > 0$, $f_{\nu_0|U_1,\tau,D}(v_0, u, t, d) = f_{\nu_0|\sigma,\tau,D}(v_0, q_1(d, u, t), t, d)$ and for any $d < 0$, $f_{\nu_0|U_0,\tau,D}(v_0, u, t, d) = f_{\nu_0|\sigma,\tau,D}(v_0, q_0(d, u, t), t, d)$.

Second, note that by Assumption 4, the distribution of ν_0 is independent of a taxpayer's potential mistagging exposure rank, and has both left- and right-limits at $D = 0$, though they need not be the same, as indicated by the subscripts at the end of the equalities. \square

Third, we establish the limiting values of the conditional expectations of compliance.

Lemma 8 (Compliance Limits). *Let Assumptions 1, 4, & 5 hold. Then, for any $u \in [0, 1]$,*

$$\begin{aligned} \lim_{d \rightarrow 0^+} \mathbb{E}[C|U = u, \tau = t, D = d] &= \int_{\mathcal{V}_0} G_0(t, 0, v_0) dF_1(dv_0, t) \\ &\quad + \int_{\mathcal{V}_1} G_1(\sigma_1(u, t), t, 0, v_1) F_{\nu_1|U,\tau,D}(dv_1, u, t, 0) \\ &= m_0^+(t) + m_1^+(u, t) \end{aligned} \quad (\text{R.2})$$

$$\begin{aligned} \lim_{d \rightarrow 0^-} \mathbb{E}[C|U = u, \tau = t, D = d] &= \int_{\mathcal{V}_0} G_0(t, 0, v_0) dF_0(dv_0, t) \\ &\quad + \int_{\mathcal{V}_1} G_1(\sigma_1(u, t), t, 0, v_1) F_{\nu_1|U,\tau,D}(dv_1, u, t, 0) \\ &= m_0^-(t) + m_1^-(u, t) \end{aligned} \quad (\text{R.3})$$

(R.4)

Proof. We present the proof for the limit from above in equation (R.2). Exactly analogous steps establish the statement for the limit from below in equation (R.3). By assumption 1, we can map

from the exposure quantiles U to the treatment levels one-to-one:

$$\lim_{D \rightarrow 0^+} \mathbb{E}[C|U = u, D = d, \tau = t] = \lim_{D \rightarrow 0^+} \mathbb{E}[C|\sigma = q_1(d, u, t), U_1 = u, D = d, \tau = t]$$

And we can substitute in the definition of the potential outcome $C = G(\sigma, \tau, D, \nu) = G_0(D, \tau, \nu_0) + G_1(\sigma, \tau, D, \nu_1)$

$$\begin{aligned} & \lim_{D \rightarrow 0^+} \mathbb{E}[C|\sigma = q_1(d, u, t), U_1 = u, D = d, \tau = t] \\ &= \lim_{D \rightarrow 0^+} \mathbb{E}[G_0(d, t, \nu_0) + G_1(q_1(d, u, t), t, d, \nu_1) | \sigma = q_1(d, u, t), D = d, \tau = t] \end{aligned}$$

By the smoothness in Assumption 4 with the compact supports of ν_1 and ν_2 , we can exchange the order of the limit and the expectation and the expectation has a right-limit in D at $D = 0$ so that

$$\begin{aligned} & \lim_{D \rightarrow 0^+} \mathbb{E}[G_0(D, \tau, \nu_0) + G_1(\sigma, \tau, D, \nu_1) | \sigma = q_1(d, u, t), D = d, \tau = t] \\ &= \mathbb{E}_{\nu_0}[G_0(0, t, \nu_0) | D = 0, \tau = t] + \mathbb{E}_{\nu_1}[G_1(\sigma_1(u), t, 0, \nu_1) | U_1 = u, D = 0, \tau = t] \end{aligned}$$

Finally, applying lemmas 5 and 7, these are

$$\begin{aligned} & \mathbb{E}_{\nu_0}[G_0(0, t, \nu_0) | D = 0, \tau = t] + \mathbb{E}_{\nu_1}[G_1(\sigma_1(u), t, 0, \nu_1) | U_1 = u, D = 0, \tau = t] \\ &= \int_{\mathcal{V}_0} G_0(t, 0, \nu_0) F_{\nu_0|U_1, \tau, D}(dv_1, u, t, 0) + \int_{\mathcal{V}_1} G_1(\sigma_1(u, t), t, 0, \nu_1) F_{\nu_1|U_1, \tau, D}(dv_1, u, t, 0) \\ &= \int_{\mathcal{V}_0} G_0(t, 0, \nu_0) F_1(dv_0, t) + \int_{\mathcal{V}_1} G_1(\sigma_1(u, t), t, 0, \nu_1) F_{\nu_1|U, \tau, D}(dv_1, u, t, 0) \end{aligned}$$

□

Fourth, we combine these elements to establish equation (15). For the denominator, note that by definition $\sigma = q(d, t, u) = q_0(d, t, u)(1 - Z) + q_1(d, t, u)Z$. Assumption 2 implies that $q_z(d, t, u)$, $z = 0, 1$ is smooth and so the right and left limits at $D = 0$ exist: $\lim_{D \rightarrow 0^+} q(d, t, u) = q_1(0, t, u) \equiv \sigma_1(t, u)$ and $\lim_{D \rightarrow 0^-} q(d, t, u) = q_0(0, t, u) \equiv \sigma_0(t, u)$. Applying lemma 6 to the terms in the numerator, we have

$$\begin{aligned} \lim_{d \rightarrow 0^+} \mathbb{E}[C|U = \bar{u}, \tau = t, D = d] &= m_0^+(t) + m_1^+(\bar{u}, t) \\ \lim_{d \rightarrow 0^-} \mathbb{E}[C|U = \bar{u}, \tau = t, D = d] &= m_0^-(t) + m_1^-(\bar{u}, t) \\ \lim_{d \rightarrow 0^+} \mathbb{E}[C|U = \underline{u}, \tau = t, D = d] &= m_0^+(t) + m_1^+(\underline{u}, t) \\ \lim_{d \rightarrow 0^-} \mathbb{E}[C|U = \underline{u}, \tau = t, D = d] &= m_0^-(t) + m_1^-(\underline{u}, t) \end{aligned}$$

And inserting these into the definition of $\eta(\underline{u}, \bar{u}, t)$ completes the proof.

Fifth, to see that the weighted WDD-LATE is also identified, note three things. First, the $Q\tau$ DD-LATEs $\eta(\underline{u}, \bar{u}, t)$ are identified. Second, the weighting function $w(\underline{u}, \bar{u}, t)$ is assumed to be known or estimable. Third, the set $\mathcal{U} \equiv \{u \in [0, 1] : |\sigma_1(u) - \sigma_0(u)| > 0\}$ is identified given that the potential treatments $q_z(d, t, u)$, $z = 0, 1$ are identified (and in fact correspond to the quantiles such that $F_{E_z|t, d}^{-1}(u) > 0$).